

A General Wear Algorithm for Wear Predictions in Total Hip Replacements

Shawn Toh Ming Song

A Thesis Submitted in Partial Fulfilment of The Requirements of Liverpool John Moores University for The Degree of Doctor of Philosophy

January 2023

Abstract

Total hip replacements are known to be one of the most successful orthopaedic interventions of all time when the hip joint becomes damaged due to disease or trauma. Currently, these hip prostheses have a lifespan of approximately 15 years, however, according to the National Joint Registry (NJR) in for England, Wales, Northern Ireland, and the Isle of Man for 2021, 8% of implanted prostheses fail prematurely with wear being one of the main reasons for these failures. Wear occurs at the contacting surfaces of the hip prosthesis and is inevitable due to the surfaces being in constant contact throughout its lifespan.

Current experimental methods to assess wear at the contacting surfaces are expensive, time-consuming and complicated. Computational wear modelling is an alternative method which is faster and cheaper compared to experimental methods and can be used to improve prosthesis design and increase overall longevity. The focus of this research is to develop a wear algorithm which can accurately predict wear at both the bearing surface and taper junction, including linear and volumetric wear damage.

In this research, a new computational method, to predict wear at the articulating bearing surface and the taper junction surfaces of total hip prosthesis, is proposed. The method incorporates wear laws into a commercial finite element package to predict wear at the articulating bearing surface and the taper junction. The assessment of wear in this research is based on wear at the bearing surface and fretting wear at the taper junction as the primary mechanism causing surface damage. This method is unique in that it simulates both the articulating bearing surface wear and taper junction fretting wear within the same analysis with individual surface characteristics. The method is capable of modelling the fixation of the femoral head onto the femoral stem during surgery.

This method has been used to investigate different design, and clinical recommendations with results consistent with wear damage observed within current literature. This research has investigated the impact of body weight on the wear of the contacting surfaces of the THR prosthesis. The results showed that a reduction in body weight from 140kg to 100kg would decrease wear up to 30% and significantly improve the longevity of the prosthesis. The impact of adding bicycling on the wear at the contacting surfaces of the THR prosthesis was also investigated. By adding bicycling up to 80km per week, the results show that there was a significant increase in the amount of wear observed, however, the health benefits may outweigh the risks. These studies will allow for clinical recommendations post-THR to help patients return to an active lifestyle.

The method has also investigated different design parameters, such as the different femoral head sizes on the wear on the contacting surfaces on the THR prosthesis. Four different femoral head sizes (22mm, 28mm, 32mm and 36mm) were investigated. The results showed that increasing the femoral head size would increase the volumetric wear at the bearing surface; however, the risk of dislocation decreased. This study would allow for further design modifications to further increase the lifespan of the THR prosthesis.

The results obtained from the computational method were found to be consistent with wear damage observed within current literature and the method is able to model the wear evolution effectively. The computational method here can be used in conjunction with experimental testing to create a longer lasting hip prosthesis through design, materials and surgical approaches.

Acknowledgements

The journey to completing this research has been long and full of uphill battles, which I would never have been able to complete without the help, support and contributions of the following people and organizations. I would like to take this opportunity to express my deepest gratitude to them.

Firstly, this research would not have been possible without the continued guidance and support of my supervisory team, Dr Ariyan Ashkanfar, Dr Russell English, and Dr Glynn Rothwell. I have been extremely lucky to have a supervisory team who cared so much about my work and always provided prompt feedback even during the busiest of times. No words can express how grateful I am to them. Without their guidance, I would have surely been at odds. I would like to give them my deepest and most sincere gratitude for everything they have done for me.

This project has been funded and supported by the School of Engineering, Liverpool John Moores University, Liverpool, UK. I wish to thank them for the support provided by the scholarship, conferences, travel and experimental costs. Without the scholarship, I would not have been able to achieve this feat.

I would like to specially thank Professor Thomas Joyce from Newcastle University, Dr David Langton and Dr Andrew Naylor for their continued support, guidance and invaluable advice throughout this research. I would also like to thank Professor James Ren for the wonderful opportunities given to me during my research.

I would like to thank Mr Clint Davies Taylor, from Dassault Systems, Simulia Ltd, Warrington, UK for his indispensable knowledge on the software used for this research.

I am also grateful to my colleagues for their editing help, late-night feedback sessions and moral support. Thanks should also go to the research admin team and librarians, whom without, I would still be stuck in admin documents.

Lastly, I would be remiss in not mentioning my family, especially my parents and grandparents. Their belief in me has kept my spirits and motivation high during my research. I would also like to acknowledge myself for continuing to push forward with the research and never giving up especially during the tough times.

Shawn Toh Ming Song

Contents

Abstract	iii
Acknowledgements	v
Table of Figures	x
Table of Tables	xi
Table of Algorithms	xii
Nomenclature	xiii
Glossary and Abbreviation	xv
1. Introduction	17
1.1. Background	17
1.2. Aims and Objectives	18
1.3. Scope of the thesis	19
1.4. Outline of the thesis	20
1.5. Publications resulting from this thesis	23
2. Background – A review	24
2.1. Introduction	24
2.2. Hip Joint	25
2.3. Total Hip Replacements	33
2.3.1. Total hip replacement procedure	37
2.3.2. Failure in THRs	39
2.4. Wear in THRs	42
2.5. Wear assessment	48
2.5.1. Wear Laws	49
2.5.2. Wear Coefficient	51
2.5.3. Wear Fraction	56
2.5.4. Experimental Methods for measuring wear	57
2.5.5. Computational method for predicting wear	66
2.6. Discussion and rationale	79
2.7. Conclusion	82
3. Computational method of wear prediction at contacting surfaces in total hip replacements	83
3.1. Introduction	83
3.2. Theoretical Wear Calculation	84
3.2.1. Dissipated Energy Wear Law	84
3.2.2. Archard’s Wear Law	86

3.3.	Wear implementation	87
3.4.	Finite Element Implementation	90
3.4.1.	Material Properties and Interaction Behaviour	90
3.4.2.	Wear Fraction.....	91
3.4.3.	Finite Element Models	91
3.4.4.	Impaction Load.....	92
3.4.5.	Loading and Boundary Conditions	93
3.4.6.	Applying wear onto the geometry	95
3.5.	Computational Framework	96
3.6.	Algorithms	98
3.6.1.	Input requested from user	100
3.6.2.	Main Algorithm	101
3.6.3.	Pre-processing data.....	102
3.6.4.	Getting initial surface nodes in contact	103
3.6.5.	Extract data from ODB file	103
3.6.6.	Pairing nodes in contact.....	104
3.6.7.	Create a total wear.....	105
3.6.8.	Wear depth calculation.....	106
3.6.9.	Writing results into the ABAQUS output databases (*.odb format)	108
3.6.10.	Updating the geometry	110
3.6.11.	Submitting the jobs	110
3.6.12.	Volumetric Wear	111
3.7.	Computational Cost.....	111
3.8.	Results Convergence	112
3.8.1.	Finite element mesh study.....	112
3.8.2.	Mesh study for wear modelling.....	113
3.8.3.	Scaling factor	114
3.9.	Summary and Conclusions	116
4.	Technical Results and Validation of Methodology	118
4.1.	Introduction.....	118
4.2.	Wear Analysis Input.....	119
4.3.	Results and discussion	120
4.4.	Conclusion	128
5.	Impact of the human body weight on THR prosthesis wear	130
5.1.	Introduction.....	130

5.2.	Wear Analysis Input.....	131
5.3.	Results and Discussion	133
5.4.	Discussion	140
5.5.	Conclusion	142
6.	Impact of different femoral head sizes on THR wear	143
6.1.	Introduction.....	143
6.2.	Wear Analysis Input.....	144
6.3.	Results	146
6.4.	Discussion	152
6.5.	Conclusion	156
7.	Impact of bicycling on the wear of THR prostheses	158
7.1.	Introduction.....	158
7.2.	Methodology	159
7.3.	Wear Analysis Input.....	162
7.4.	Results and Discussion	164
7.5.	Conclusion	170
8.	Conclusion and future work.....	172
8.1.	Conclusion	172
8.2.	Future work	174
	References.....	176
	Appendices.....	188
	Appendix I: Graphical user interface of the wear algorithm.....	189
	Appendix II: Publication.....	191
	Appendix III: Poster Presentations	216

Table of Figures

Figure 1-1: Thesis structure and research track	22
Figure 2-1: Natural hip joint	25
Figure 2-2: Ligaments of the hip joint a) Image taken from Drake, Vogl et al. (2009) b) Image taken from Gray (1878)	26
Figure 2-3: Natural hip joint movements a) flexion-extension, b) abduction-adduction and c) internal-external Image from Drake, Vogl et al. (2009)	27
Figure 2-4: Modern total hip prosthesis	35
Figure 3-1: 1-to-3 node pairing implementation	89
Figure 3-2: 1-to-1 node pairing implementation	89
Figure 3-3: a) Assembled FE model b) Mesh assigned on 3D FE model	91
Figure 3-4: Impaction assembly load-time history	92
Figure 3-5: 3-dimensional hip joint loadings during a walking cycle	93
Figure 3-6: 3-dimensional hip joint rotations during a walking cycle	93
Figure 3-7: Loading and boundary conditions assigned onto the 3D FE model	94
Figure 3-8: Visualisation of resultant nodal vector	95
Figure 3-9: Applied wear depth direction	96
Figure 3-10: Flowchart illustrating method for wear prediction	97
Figure 3-11: Graphical user interface (GUI) of the wear algorithm	98
Figure 3-12: Mesh independence study	112
Figure 3-13: Wear modelling mesh convergence for bearing surface	113
Figure 3-14: Wear modelling mesh convergence for taper junction	114
Figure 3-15: Effect of different scaling factors on simulation time and accuracy	115
Figure 3-16: Effect of scaling factor on the wear occurring in the analysis	116
Figure 4-1: a) Variation of contact shear stresses, b) Variation of relative displacement during a walking cycle, c) Wear depth values at the end of 100,000 cycles	121
Figure 4-2: Variation in wear depth over 5 million walking cycles	122
Figure 4-3: Variation in a) cumulative volumetric wear, b) volumetric wear rate with respect to n^{th} million cycles	123
Figure 4-4: a) Maximum linear wear of XLPE liner at every million cycles, b) linear wear rate at each million load cycles	124
Figure 4-5: Variation of contact pressure (CPRESS) a) at the first gait cycle, b) at the end of 5 million cycle	124
Figure 4-6: Comparison of wear pattern between this study and conventional UHMWPE	126
Figure 5-1: Evolution of wear pattern on the XLPE bearing liner during wear analysis for different patient's weights	134
Figure 5-2: Evolution of wear pattern on the femoral head taper surface during wear analysis for different patient's weight	134
Figure 5-3: XLPE liner a) total volumetric wear b) volumetric wear rates over 5 million cycles	135
Figure 5-4: Femoral head bearing surface a) total volumetric wear, b) volumetric wear rates over 5 million cycles	136
Figure 5-5: Femoral Head taper junction a) total volumetric wear, b) volumetric wear rates over 5 million cycles	136
Figure 5-6: Femoral stem a) total volumetric wear b) volumetric wear rates over 5 million cycles	138
Figure 5-7: Percentage of wear between the bearing surface and taper surface at the femoral ball at 5 million cycles	138
Figure 5-8: Total metallic volumetric wear at 5 million cycles	139
Figure 6-1: Evolution of wear pattern over 10 years at XLPE bearing liner for different head sizes	147
Figure 6-2: Evolution of wear pattern over 10 years at femoral head taper surface	147
Figure 6-3: Cumulative Volumetric Wear and Volumetric Wear Rate of a) XLPE bearing liner, b) Femoral head bearing surface, c) Femoral head taper surface, d) Femoral stem trunnion	150
Figure 6-4: Evolution of maximum linear wear and linear wear rate at the XLPE bearing liner	151
Figure 7-1: a) FE model of hip prosthesis assembled for walking, b) Loadings and rotations for walking cycle, c) FE model of hip prosthesis assembled for bicycling cycle, d) Loadings and rotations for bicycling cycle ...	160

<i>Figure 7-2: Flowchart detailing the modified wear algorithm</i>	<i>161</i>
<i>Figure 7-3: Comparison of wear patterns between walking and bicycling up to 5 years of XLPE liner</i>	<i>164</i>
<i>Figure 7-4: Evolution of wear patterns of the XLPE bearing liner, femoral head bearing surface, femoral head taper surface, femoral stem surface for walking and bicycling up to 5 years.....</i>	<i>165</i>
<i>Figure 7-5: Total volumetric wear and volumetric wear rates for a) XLPE bearing liner, b) Femoral head, c) Femoral stem.....</i>	<i>167</i>

Table of Tables

<i>Table 2-1: Common modes of THR failure as reported in the NJR</i>	<i>41</i>
<i>Table 2-2: Values of wear coefficient for different material combinations of review wear models on bearing and taper surfaces.....</i>	<i>55</i>
<i>Table 2-3: Volumetric wear for bearing surfaces in current literature.....</i>	<i>64</i>
<i>Table 2-4: Volumetric wear for taper surfaces in current literature</i>	<i>65</i>
<i>Table 2-5: Summary of computational analysis for bearing surfaces in THRs</i>	<i>75</i>
<i>Table 2-6: Summary of computational analysis for taper surfaces in THRs.....</i>	<i>77</i>
<i>Table 3-1: Material Properties for THR</i>	<i>90</i>
<i>Table 3-2: Friction coefficient based on contacting surfaces</i>	<i>90</i>
<i>Table 3-3: Wear fraction specified for individual contacting surfaces</i>	<i>91</i>
<i>Table 4-1: Input parameters for wear analysis in chapter 4</i>	<i>119</i>
<i>Table 4-2: Linear and volumetric wear rates of XLPE and UHMWPE in literature.</i>	<i>125</i>
<i>Table 5-1: Input parameters for wear analysis in chapter 5</i>	<i>132</i>
<i>Table 5-2: Volumetric wear rates of XLPE liner in contact with CoCr femoral via radiography</i>	<i>140</i>
<i>Table 5-3: Volumetric wear rates of femoral head taper surface in literature</i>	<i>141</i>
<i>Table 6-1: Input parameters for wear analysis in chapter 8</i>	<i>145</i>
<i>Table 6-2: Volumetric wear rates of XLPE liner in current study vs literature</i>	<i>153</i>
<i>Table 7-1: Input parameters for wear analysis in chapter 7</i>	<i>163</i>
<i>Table 7-2: Volumetric wear rates of XLPE liner in current study vs literature</i>	<i>168</i>
<i>Table 7-3: Volumetric wear rate between walking and bicycling up to 5 years.....</i>	<i>169</i>

Table of Algorithms

<i>Function 1: inputRequest</i>	100
<i>Function 2: MainAlgorithm</i>	101
<i>Function 3: Preprocessing</i>	102
<i>Function 4: GetInteractionNodes</i>	103
<i>Function 5: ExtractValues</i>	104
<i>Function 6: PairingNodes</i>	105
<i>Function 7: WearTotal</i>	105
<i>Function 8: WearFunc</i>	107
<i>Function 9: writeOdb</i>	108
<i>Function 10: writeInp</i>	110
<i>Function 11: Submit</i>	110
<i>Function 12: VolumetricWear</i>	111

Nomenclature

V	volume of material loss
W_v	total volume of the material removed
L	sliding distance
A_r	real area of contact of the friction couple
F_n	Normal applied force
H	Material hardness
k	Dimensionless wear coefficient
A_w	worn area
n	Number of wear debris generated
N	Number of asperities mated at contact
V_p	surface of a worn area
K	Archard wear coefficient
s	Sliding distance or slip
α	Energy wear coefficient
E	Accumulated dissipated energy
Q	Tangential force
μ	Friction coefficient
q	Frictional shear stress
p	Normal applied force
i	Time interval
j	Analysis stage
τ	surface contact shear stress
τ_i	Surface Contact Shear Stress at time interval, i

$\tau_{i,j}$	Surface Contact Shear Stress at time interval, i at analysis stage, j
s_i	Relative displacement at time interval, i
$s_{i,j}$	Relative displacement at time interval, i at analysis stage, j
P	Contact pressure
$P_{i,j}$	Contact pressure at time interval, i at analysis stage, j
W_c	Cyclic wear depth
F	Contact force
W_d	Linear wear depth
<i>CSHEAR1</i>	Contact shear stress in direction 1
<i>CSHEAR2</i>	Contact shear stress in direction 2
<i>CSLIP1</i>	Contact displacement in direction 1
<i>CSLIP2</i>	Contact displacement in direction 2
$\overrightarrow{CTANDIR}$	Resultant nodal contact tangent direction vector
$\overrightarrow{CTANDIR1}$	Nodal contact tangent direction vector in direction 1
$\overrightarrow{CTANDIR2}$	Nodal contact tangent direction vector in direction 2
<i>CWD</i>	Cyclic wear depth
CWD_i	Cyclic wear depth at time interval, i

Glossary and Abbreviation

FE	Finite Element
NHS	National Health Service of the United Kingdom
NSAIDs	Non-steroidal anti-inflammatory drugs
MoP	Metal-on-Polyethylene
CoP	Ceramic-on-Polyethylene
CoC	Ceramic -on- Ceramic
MoM	Metal -on- Metal
XLPE	Highly crossed linked polyethylene
UHMWPE	Ultra-high molecular weight polyethylene
CoCrMo	Cobalt-Chrome-Molybdenum
Ti	Titanium
THR	Total Hip Replacement
ARMD	Adverse reactions to metal debris
POD	Pin-on-disk
SEM	Scanning electron microscope
GUI	Graphical User Interface
CMM	Coordinate Measuring Machine
Arthroplasty	The surgical reconstruction or replacement of a joint (Oxford Dictionary)
Metallosis	A condition caused by the build-up of metallic particles
Tribology	The science of interacting surfaces in relative motion (Oxford Dictionary)
NJR	National Joint Registry of England, Wales, Northern Ireland, the Isle of Man and Guernsey
*.odb	Results output file

*.inp	Input file for finite element analysis
WM	Wear Method
PT	Pairing Type

Chapter 1

Introduction

1.1. Background

A hip joint is one of the most important joints in a human body as it supports the weight of the body in both static and dynamic postures in everyday activities. When the hip joint becomes damaged, it causes the body to lose mobility and increases pain. The hip joint can become damaged in numerous ways such as through disease or trauma. If the joint has become severely damaged and treatments along with medications have not helped in improving mobility, the damaged joint may be removed and replaced with a prosthesis.

This procedure is known as total hip arthroplasty and is one of the most successful surgeries performed since the 1960s and restores patients to an active lifestyle.

Approximately 100,000 hip replacement procedures were recorded in the National Joint Registry (NJR) for England, Wales, Northern Ireland, and the Isle of Man in 2021 with numbers increasing every year by approximately 3000 cases (NJR 2022) with the

exemption of COVID-19 impacted years of 2020 and 2021. Typically, an implanted hip prosthesis has a lifespan of approximately 15 years with some prematurely failing. Wear has been found to be responsible for many of these failures.

Wear is known as the gradual removal of material on contacting surfaces under relative movement and different types of wear can occur depending on their relative motions. It is an inevitable phenomenon occurring when two or more surfaces are mated together while subjected to load and sliding/rolling. Within the body, debris generated through wear causes a biological response within the surrounding tissues which drives the process towards periprosthetic tissue destruction, implant loosening and ultimately prosthesis failure. The wear debris accumulated may also act as an abrasive which would cause further amounts of wear.

Within a hip prosthesis, wear can occur between the bearing surfaces and the taper junction. The wear between the bearing surfaces is caused by the surfaces articulating against each other causing the transfer of materials while the wear at the taper junction is known as fretting wear, where the transfer of materials is caused by very small relative movements (micromotion) of solid surfaces in contact.

1.2. Aims and Objectives

The aim of this work is to develop a computational tool to predict wear that could occur in THRs. The study proposes a methodological tool to predict the wear depth, volumetric wear, and surface wear damage occurring over time in a hip prosthesis. This method can also be used as a general tool to predict wear in other prosthetic designs or even other prosthetic devices.

In order to achieve this aim, a commercial model of a hip prosthesis is used, to illustrate the wider principles of wear process and wear modelling. Then, the study developed a new wear model using a programming language (Python) and finite element (FE) analysis (ABAQUS) by investigating and considering parameters in the prediction of wear.

A significant goal is to develop and generalise the algorithm with a graphical user interface for any 3D FE analysis within the FE package (ABAQUS) as a user plug-in to accurately predict linear and volumetric wear rates while observing the evolution of wear patterns throughout the analysis.

1.3. Scope of the thesis

There are many mechanical failures which can occur within an engineering component which produce different forms of mechanical failures. Some types of mechanical failures are ductile and brittle fracture, creep, fatigue, corrosion, and wear. This research focuses on wear as the main mechanical failure within THR prostheses. Wear as a mechanical failure can occur through several mechanisms, such as adhesive, abrasive, corrosive, erosive, surface fracture and fatigue wear.

Adhesive and fretting wear (alongside the surface damage occurring due to wear) is known as a complex phenomenon to investigate, measure and predict. Being able to predict the extent of wear that could occur within mechanical components over time in service is vital to improving future designs. This research will focus on the extent of wear within THR prostheses to aid in increasing the lifespan of these devices.

The work presented in this research focuses solely on the mechanical wear (bearing surface and fretting) as being the primary mechanism causing damage on the contacting surfaces due to the repeated mechanical loading and frictional forces causing the surfaces

to gradually wear down over time. The method presented has been used to predict both bearing and taper surface wear of THR prostheses and could be used for different applications in the future.

1.4. Outline of the thesis

The whole structure of the thesis is outlined in Figure 1-1.

The first chapter of this thesis presents an introduction to the thesis, the aim of the research and the outline of the research. Chapter 1 also contains a brief description of the motivation for this research.

In Chapter 2, an extensive background review was conducted to provide and establish a suitable background for the chapters which follow. This includes an in-depth background on the hip joint, the need for total hip replacement, problems with current THRs, a suitable background on wear, wear characteristics, wear within THRs and a review of the current wear modelling available within the literature.

In Chapter 3, the methodology for this research is detailed and establishes the basis for the rest of this research. An FE model of a commercial hip prosthesis was modelled, and a developed wear algorithm is applied onto the FE model to predict the wear occurring at the contacting surfaces of the hip prosthesis.

The methodology presented in Chapter 3 is then used for different studies with the findings detailed between Chapters 4 and 7. The results are discussed in separate discussion sections within the individual chapters.

A full description of the 3D results based on the realistic loading conditions and rotations from the wear analysis is detailed in Chapter 4. In this chapter, the results from the wear

algorithm are validated against current literature by volumetric wear rates while the wear pattern has been validated against wear patterns from a similar material.

In Chapter 5, the method described in Chapter 3 is used to investigate the effect of body weight on the wear in THR prostheses. The results from this chapter can be used for clinical recommendations to further improve the longevity of THR prostheses.

In Chapter 6, the effect of different femoral head sizes on the wear on THR prostheses is investigated. As there are many choices with modular THR prostheses, different femoral head sizes were investigated for increased wear with larger femoral head sizes. The results from this chapter can be used for design recommendations to improve the longevity of THR prostheses.

In Chapter 7, the effect of adding cycling to the daily life on the wear on THRs is investigated. This chapter investigated the increase in the amount of wear by including bicycling for commute alongside walking for up to 5 years of activity. The results from this chapter can also be used for clinical recommendations to further improve the longevity of THR prostheses.

Lastly, a complete conclusion to the research and possible future work are provided in Chapter 8.

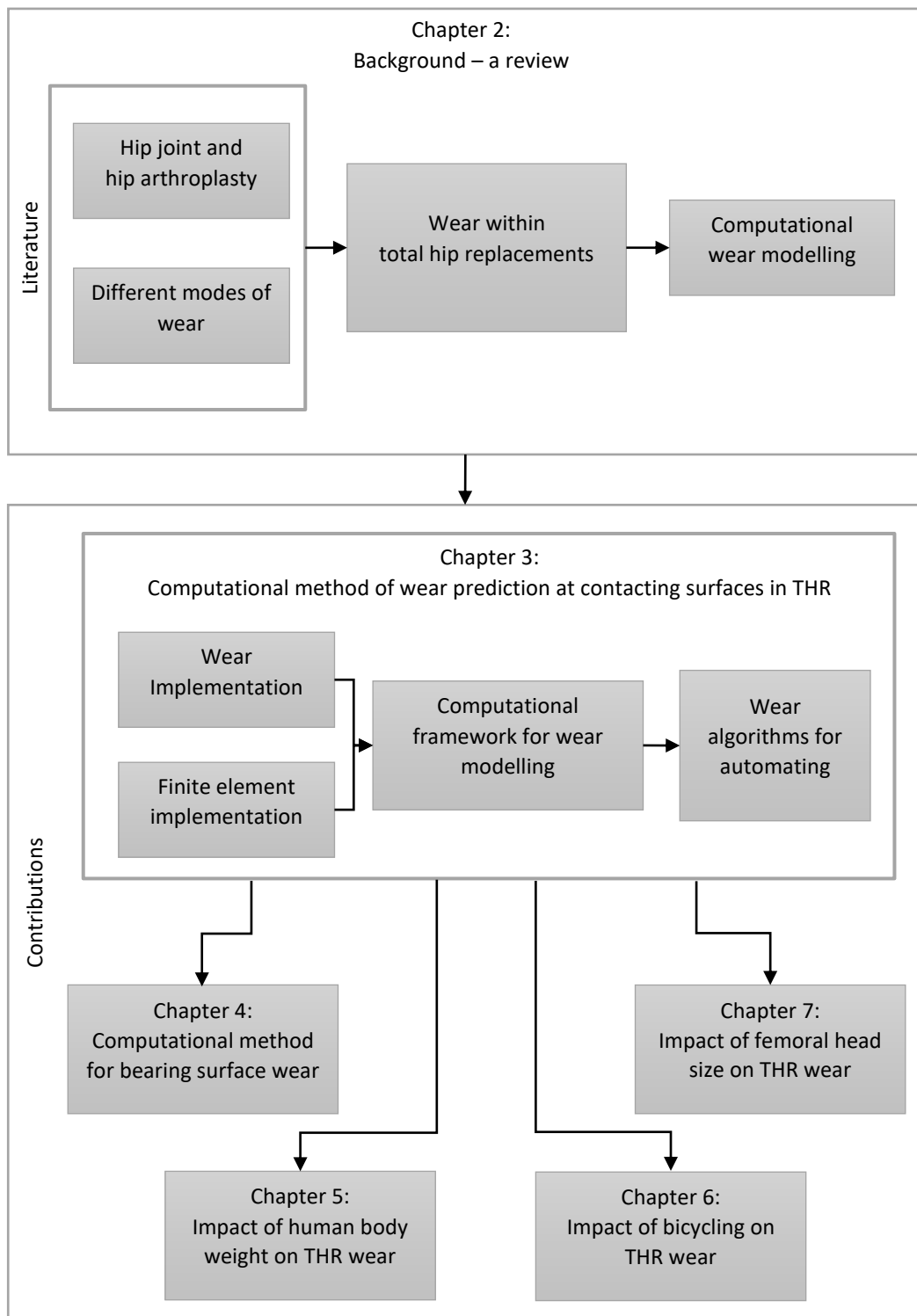


Figure 1-1: Thesis structure and research track

1.5. Publications resulting from this thesis

1. "Development of a wear algorithm using finite element analysis to investigate design variations on the wear rates in total hip replacement." Simulia RUM Conference 2019.
2. Toh, S. M. S., A. Ashkanfar, R. English and G. Rothwell (2021). "Computational method for bearing surface wear prediction in total hip replacements." Journal of the Mechanical Behavior of Biomedical Materials 119: 104507.
3. Toh, S. M. S., A. Ashkanfar, R. English and G. Rothwell (2022). "The relation between body weight and wear in Total Hip Prosthesis: A finite element study." Computer Methods and Programs in Biomedicine Update: 100060.
4. Toh, S. M. S., A. Ashkanfar, R. English, G. Rothwell, D. J. Langton and T. Joyce (2022). "How Does Bicycling Affect the Longevity of Total Hip Arthroplasty? A Finite Element Wear Analysis." Journal of the Mechanical Behavior of Biomedical Materials 139: 105673.

In-Preparation Journal Papers

5. Ashkanfar, A., S. M. S. Toh, R. English, D. J. Langton and T. Joyce (2022). "The impact of femoral head size on the longevity of total hip arthroplasty prostheses: A finite element analysis." The Journal of Arthroplasty.
6. The impact of losing weight on the wear in Total Hip Prosthesis.
7. The effect of different taper designs on the wear in Total Hip Prosthesis.

Chapter 2

Background – A review

2.1. Introduction

The purpose of this chapter is to present a complete review of current literature and a summary of existing fundamental knowledge on wear as a suitable background for the chapters which follow. In this chapter, firstly, a brief explanation on the anatomy of the natural hip joint, with the causes and treatment of hip disorders, is discussed in detail. This will be followed by a comprehensive literature review of total hip replacements with the combination of materials used. The cause of THR prostheses' failure is then discussed in depth. Wear within THR prostheses is discussed along with current methods for wear assessment. A review of current experimental and computational methods of measuring wear is provided.

2.2. Hip Joint

A hip joint, scientifically referred to as the acetabulofemoral joint, is a ball-and-socket joint between the head of the femur and acetabulum of the pelvis. It is one of the most important joints in the body as it supports the weight of the body in both static and dynamic postures in everyday activities. The acetabulum is a cup-like depression located on the pelvis while the head of the femur is hemispherical and fits completely into the concavity of the acetabulum (Figure 2-1). The strength of the hip is provided due to its reinforcement by strong ligaments and musculature, providing a relatively stable joint. These ligaments also provide stability and prevent excessive movement of the hip joint, allowing for normal movement and function.

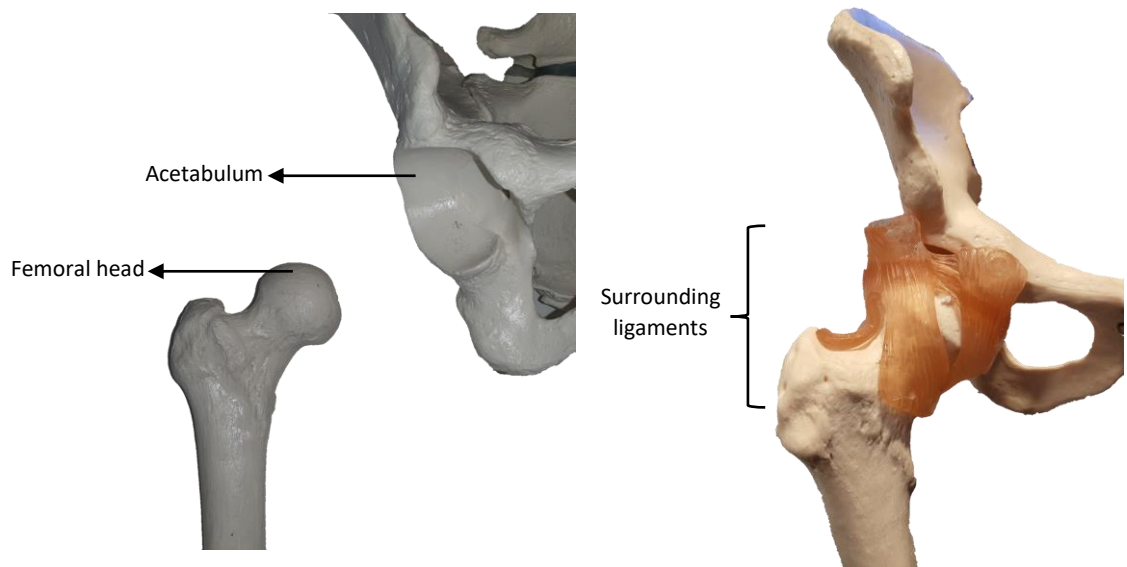


Figure 2-1: Natural hip joint

These ligaments include the following (see Figure 2-2):

- Iliofemoral ligament – The strongest and most important ligament of the hip joint. It is located on the front of the hip joint and prevents excessive flexion of the hip.
- Pubofemoral ligament - This ligament is located on the front and inner side of the hip joint and prevents excessive adduction and internal rotation of the hip.

- Ischiofemoral ligament - This ligament is located on the back and inner side of the hip joint and prevents excessive extension and external rotation of the hip.
- Ligamentum teres - This ligament is located in the centre of the hip joint and helps to maintain stability.

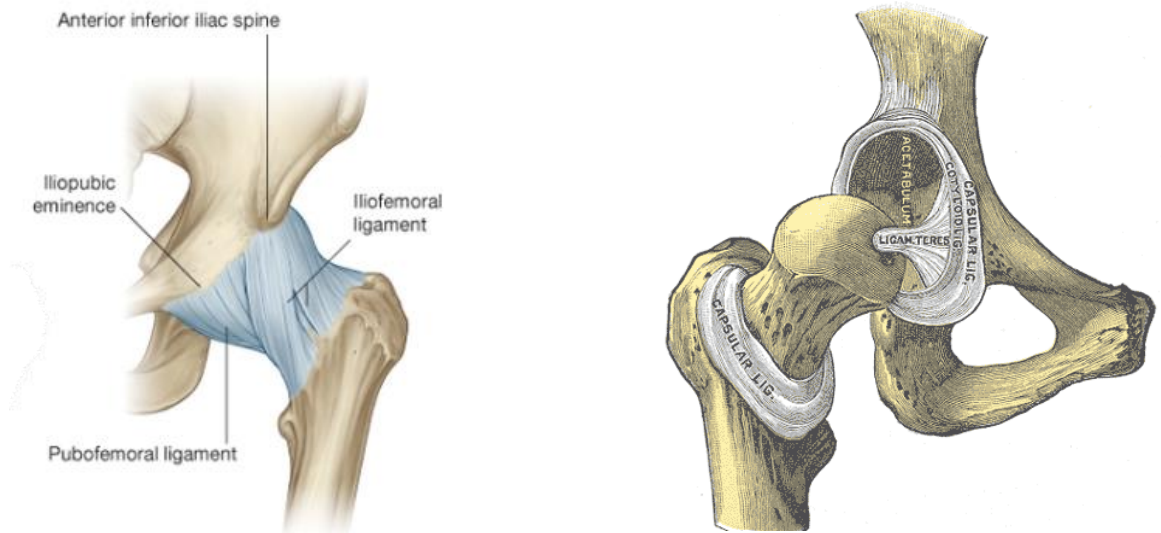


Figure 2-2: Ligaments of the hip joint a) Image taken from Drake, Vogl et al. (2009) b) Image taken from Gray (1878)

The natural hip joint allows movements in multiple directions, which include flexion-extension, abduction-adduction and internal-external (see Figure 2-3). The hip movements are explained below (Mulholland and Wyss 2001, Davis, Ritter et al. 2007, Hallaçeli, Uruç et al. 2014, Charbonnier, Chagué et al. 2015):

- Flexion: This is the movement of bringing the thigh towards the chest. The normal range of motion for hip flexion is approximately 120-130 degrees (see Figure 2-3a).
- Extension: This is the movement of straightening the leg. The normal range of motion for hip extension is approximately 0-30 degrees (see Figure 2-3a).

- Abduction: This is the movement of moving the leg away from the midline of the body. The normal range of motion for hip abduction is approximately 45-60 degrees (see Figure 2-3b).
- Adduction: This is the movement of moving the leg towards the midline of the body. The normal range of motion for hip adduction is approximately 20-30 degrees (see Figure 2-3b).
- External rotation: This is the movement of rotating the leg outward. The normal range of motion for hip external rotation is approximately 30-50 degrees (see Figure 2-3c).
- Internal rotation: This is the movement of rotating the leg inward. The normal range of motion for hip internal rotation is approximately 30-50 degrees (see Figure 2-3c).

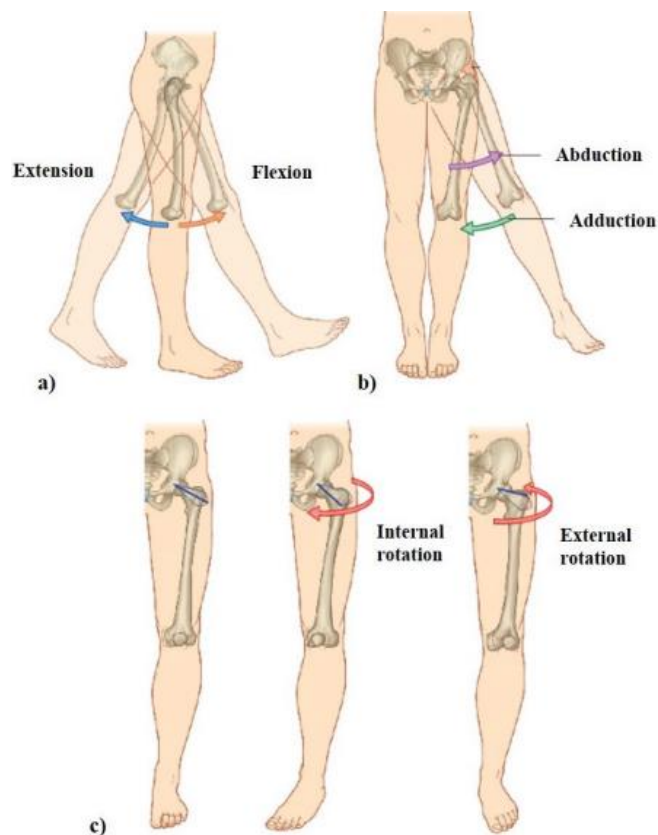


Figure 2-3: Natural hip joint movements a) flexion-extension, b) abduction-adduction and c) internal-external

Image from Drake, Vogl et al. (2009)

The loads experienced by the natural hip joint are high, where they can exceed several times body weight during normal day-to-day activities such as walking, sitting, climbing stairs, running, or standing (Byrne, Mulhall et al. 2010, Varady, Glitsch et al. 2015). The acetabular labrum is tasked with distributing and supporting the loads to reduce the loads acting in the hip joint (Ferguson, Bryant et al. 2000, Ferguson, Bryant et al. 2000, Ferguson, Bryant et al. 2003). The acetabular labrum is a thick, crescent-shaped band cartilage of type II collagen with a layer of collagen type I that is typically 2-3mm thick and surrounds the edge of the acetabulum, or socket, in the pelvis. It has several important functions in the hip joint, including:

- Deepening the socket: The labrum helps to deepen the acetabulum, which allows the head of the thighbone (femur) to fit securely into the socket. This increases the stability of the hip joint and allows for a greater range of motion.
- Providing stability: The labrum helps to keep the femur securely in place within the acetabulum. It acts as a barrier to prevent the femur from slipping out of the socket.
- Lubricating the joint: The labrum is rich in synovial fluid, which lubricates the hip joint and allows the bones to move smoothly against each other.
- Absorbing shock: The labrum helps to absorb shock and distribute forces across the hip joint. This can reduce wear and tear on the joint and prevent damage to the cartilage.

If the acetabulum labrum were to become damaged, it would cause the two hard bony surfaces of the joint to act upon each other causing high stresses with high friction making the joint stiff and painful which would be detrimental to the performance in the joint and the patient.

There are many ways in which a hip joint may become damaged or lose its functionality due to diseases such as:

- **Arthritis** – A common condition which many people develop as they age which causes the swelling and tenderness of joint. The cartilage in the hip joint gradually wears over time and it becomes frayed and rough. This can cause severe pain, stiffness, and immobility. According to the UK National Health Service, approximately 10 million people are affected by arthritis in the UK (NHS 2022). Osteoarthritis and rheumatoid arthritis are the 2 most common types of arthritis.
 - **Osteoarthritis** – Osteoarthritis is caused by the mechanical wear and tear on the joints. This causes cartilage to break down and subsequently cause pain, stiffness, tenderness, and loss of flexibility (Buckwalter, Saltzman et al. 2004, Arden and Nevitt 2006, Sinusas 2012). The exact cause of osteoarthritis is still unknown and involves many pathophysiological processes which coincide with an inflammatory response (Wieland, Michaelis et al. 2005, Goldring and Otero 2011, Sinusas 2012). Currently, there is no cure for osteoarthritis, but there are treatments which can help slow the condition (NHS 2022). Osteoarthritis was found to be responsible for 88% of primary hip replacements as per the National Joint Registry in 2021 (NJR 2022).
 - **Rheumatoid arthritis** – Rheumatoid arthritis is a chronic, inflammatory, systemic autoimmune disease in which a person's immune system attacks the lining of joints throughout the body (Bullock, Rizvi et al. 2018). Unlike osteoarthritis, which is a degenerative joint disease, rheumatoid arthritis is

a systemic disease that can affect many different parts of the body. It occurs when the immune system mistakenly attacks healthy tissue, leading to swelling, stiffness, and pain in the joints (NHS 2022, Smith and Berman 2022). The exact cause of RA is unknown, but it is thought to be a combination of genetic and environmental factors. Treatment for RA typically involves a combination of medications and other therapies to control inflammation and relieve symptoms. Early diagnosis and treatment can help prevent joint damage and disability.

- **Psoriatic arthritis** – Psoriatic arthritis is an autoimmune disease which affects people with the skin condition, psoriasis and causes inflammation within both small and large joints (Day, Nam et al. 2012, Krakowski, Gerkowicz et al. 2019). Some symptoms of Psoriatic arthritis include, swelling of joints, scaly patches of skin, joint stiffness and pain, and excessive fatigue.
- **Hip fracture** – Fractured neck of the femur was found to be responsible for approximately 5% of primary hip replacements as per the National Joint Registry in 2021 (NJR 2022). The most common reason for fracture is osteoporosis which is characterised by the deterioration of the bone due to age and it increases the fragility of the bone (Lin and Lane 2004, Ginaldi, Di Benedetto et al. 2005, Rachner, Khosla et al. 2011). Internal fixation devices such as bone screws are typically used for femoral head neck fractures, however complicated fractures are treated with total hip replacements.

- **Avascular necrosis** – A condition caused by disruption to the blood supply to the head of the femur which causes severe pain and immobility and can lead to the death of bone tissue (Edgar and Einhorn 2014). Avascular necrosis was responsible for 2% of primary hip replacements as per the National Joint Registry in 2021 (NJR 2022). The common risk factors of avascular necrosis are alcoholism, use of steroids, chemotherapy, and sickle cell anaemia (Lamb, Holton et al. 2019).
- **Others** – Other hip joint disorders as an indication of total hip replacement surgery consist of trauma, hip bursitis, ankylosing spondylitis and snapping hip syndrome.

Treatments for hip joint disease will depend on the specific condition and the severity of the symptoms. Some common treatments for hip joint diseases include the following (Koo, Kim et al. 1995, Castro and Barrack 2000, Steinberg, Larcom et al. 2001, Wang, Sun et al. 2010, Sinusas 2012, Kim, Oh et al. 2017, NHS 2022):

1. **Medications** - Nonsteroidal anti-inflammatory drugs (NSAIDs) can be used to reduce pain and swelling in the hip joint.
2. **Physical therapy** - Exercises and stretching can help to improve mobility and strength in the hip joint.
3. **Injections** - Corticosteroid injections can be used to reduce inflammation and pain in the hip joint.
4. **Alternative treatments** - Some patients may find relief from hip joint pain using alternative treatments such as acupuncture, massage, or herbal remedies.

The treatments listed above are used to manage symptoms from hip joint disorders, however in severe cases, a hip surgery may be necessary to remove the damaged bone

and cartilage and replace it with a metal or plastic implant. There are several types of hip surgery, including:

1. **Hip resurfacing** – A surgical procedure to repair the damaged surface of the hip joint. Usually recommended for individuals with early stages of osteoarthritis or other hip diseases who are not candidates for total hip replacement surgery. In this surgery, the damaged surface of the hip joint is removed and replaced with a smooth artificial surface (Siguier, Siguier et al. 2001, Mont, Ragland et al. 2006, McMinn, Daniel et al. 2011).
2. **Partial hip replacement** – A surgical procedure in which the damaged or diseased portion of the femoral head is replaced with an artificial implant, either with metal or ceramic. Usually performed to relieve pain and improve mobility in individuals with a damaged or diseased femoral head. (Shebubakar, Hutagalung et al. 2009, Grammatico-Guillon, Perreau et al. 2017)
3. **Total hip replacement** – A surgical procedure in which both the hip socket and femoral head is replaced with an artificial prosthesis, either with metal, ceramic or plastic. It is usually recommended for individuals with advanced osteoarthritis, or other hip disorders with severe hip pain and disability which has not responded to other treatment options such as medications and physical therapy. (Crawford and Murray 1997, Learmonth, Young et al. 2007)

2.3. Total Hip Replacements

Total Hip Replacements are one of the most successful orthopaedic interventions of the last few generations (Learmonth, Young et al. 2007). Prof. Themistocles Glück made the first attempt to replace a damaged hip joint of a patient using an ivory ball and socket joint in Germany in 1891 (Szostakowski, Jagiello et al. 2017). In 1925, Smith Petersen trialled creating a THR out of glass due to its smooth surface (Knight, Aujla et al. 2011), and while it was biocompatible, it could not withstand the forces going through a hip joint. They later moved to trial stainless steel to create the first total hip replacement which was fitted onto the bone with bolts and screws.

Since the creation of the hip prosthesis in 1891, many combinations of materials and techniques have been trialled to find the combination that would yield the fewest complications and the best long-term survival. Earlier designs of THRs prostheses were manufactured as two components, an acetabular cup and a femoral component which consisted of a femoral head and femoral stem as a single component known as a monolithic prosthesis. As the design in THRs progressed, it was found beneficial to use two separate components to allow for flexibility intra-operatively, based on the requirements of different patients. This was known as modular THR. The main advantages of modular THRs are:

- Decreased implant inventory
- Ability to remove femoral head at revision surgery to improve exposure or change head size without component removal.
- Better adjustment of head sizes, leg length offset, neck length
- Use of different materials for components
- Self-locking mechanism

Subsequent clinical experience, however, has witnessed significant drawbacks associated with modularity:

- Corrosion
- Implant fracture below the head and neck taper joint
- Reduced range of motion
- Dissociation of implant, possible loosening of components
- Increased wear

In the early 1960's, Sir John Charnley introduced three major contributions to the evolution of the total hip replacement: 1) the idea of low friction torque arthroplasty; 2) use of acrylic cement to fix components to living bone; and 3) introduction of high-density polyethylene as a bearing material. The prosthesis designed by Sir John Charnley in the early 1960s is identical, in principle, to the modern prostheses used today.

A modern total hip prosthesis generally consists of a ball and socket joint comprising of three components, an acetabular cup, a femoral head, and femoral stem. Different sizes of components are available based on the requirements of the anatomy of the patients.

- **Acetabular cup** – Fitted into the pelvic acetabulum and typically manufactured with a metallic material, normally of Titanium. Other designs may incorporate ceramic (such as alumina or zirconia) or to a lesser extent, cobalt-chrome alloy. Depending on the type of hip prosthesis, there may be an additional liner made of polyethylene, either Ultra-High-Molecular-Weight Polyethylene or highly cross-linked polyethylene which has low friction, high toughness, good impact resistance and good biocompatibility (the capability of the material implanted to exist in harmony with tissue without causing negative effects).

- **Femoral head** – The femoral head replaces the top of the natural femur. Femoral heads are typically made of cobalt chrome or ceramic and are produced in varying diameters and neck lengths to fit the patient’s anatomy.
- **Femoral stem** – The femoral stem is inserted into the femur and can either be cemented or press-fitted. The stem consists of a trunnion, neck, and a stem. Made of metals such as cobalt-chrome, or titanium.

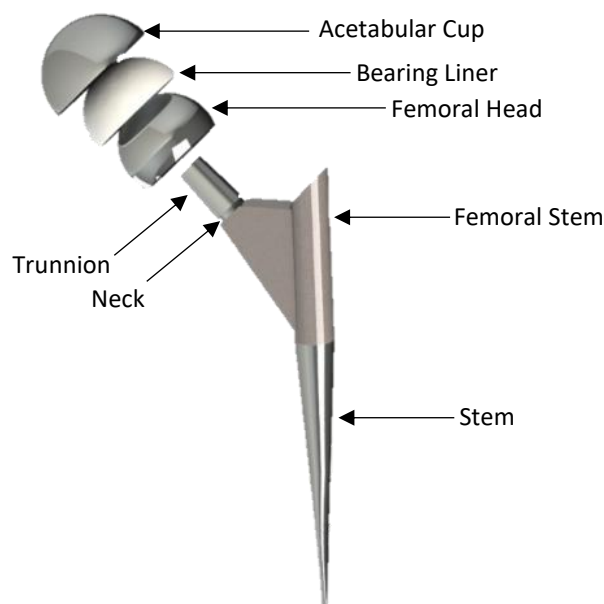


Figure 2-4: Modern total hip prosthesis

The types of THR used are named after the material combinations used between the articulating surface of the THR. There are several different combinations of materials for THRs, such as, Metal-on-Plastic (MoP), Ceramic-on-Plastic (CoP), Ceramic-on-Ceramic (CoC), and Metal-on-Metal (MoM). The naming convention of these THRs is: material of femoral head on material of acetabular cup.

- **MoP and CoP** – MoP/CoP THRs consists of a metal/ceramic femoral head on a polyethylene bearing liner. Polyethylene is chosen for its high wear resistance;

however, it has a high wear rate when compared to metal or ceramic components. Early MoP bearings initially had high failure rates due to softer polyethylene materials, however modern highly cross-linked polyethylene (XLPE) is more resistant than the early materials.

- **CoC** – CoC THRs consist of using a ceramic acetabular cup and a ceramic femoral head, usually with alumina (Al_2O_3) or zirconia (ZrO_2). CoC THRs provides low friction and resistance to major scratches which would make the bearing surface less vulnerable to wear. CoC THRs also exhibit decreased and less bioactive particulate than polyethylene or metal bearings (Jenabzadeh, Pearce et al. 2012). Previously CoC THRs had a high rate of breakage, however, with newer manufacturing techniques such as hot isostatic pressing, spark plasma sintering, alongside with advanced ceramic materials, coupled with higher testing has virtually eliminated this and should not be a relevant argument against its use. Squeaking of the prosthesis has also been widely reported which is unpleasant for patients (Walter, O'Toole et al. 2007).
- **MoM** – MoM THRs consist of using a metallic acetabular cup and a metallic femoral head, usually with Cobalt-chromium alloy ($CoCrMo$), or Titanium (Ti). MoM THRs initially gained popularity as they were developed to provide less wear, less bone resorption with fewer risks of dislocation, however, it was later found that there were extremely high revision rates just after 10 years at 18.2% (Ferguson, Palmer et al. 2018). Since 2011, MoM hip prostheses have accounted for less than 1% of all hip prostheses. Failure of the MoM hip prosthesis is due to the metal ion debris generated at the bearing surface which triggers adverse

immunological reactions, resulting in localised bone destruction and soft tissue necrosis (Salem, Lindner et al. 2019).

Currently, a wide range of prosthetic devices are available commercially which vary by design, type, and materials. Some of the main joint replacement manufacturers are Stryker Corp, DePuy Syntheses, Zimmer Biomet, and Smith & Nephew.

2.3.1. Total hip replacement procedure

Total hip replacements are performed in a hospital or surgery centre, which involves the replacement of the whole hip joint with an artificial prosthesis. The surgery is performed under anaesthesia, either whole-body or below-the-waist, depending on the recommendation of the surgeons.

The surgeon would make an incision to access the hip joint. The femoral bone will be dislocated from the socket and the femoral head would be removed with an opening created at the top of the femur. The femoral stem would then be placed into the opening in the femur and fixed using a cement mantel (typically Plexiglas) or biological growth that allows the bone to grow into and onto the femoral stem surface coated with a porous or rough material.

The damaged cartilage from the acetabulum would be removed and a perfect hemispherical bone socket, matched with the external shape of the acetabular cup, would be made in the pelvis acetabulum and the acetabular cup is placed. A trial femoral head is placed onto the femoral stem to inspect the size and adequacy of the hip motion. When an appropriate head size is found, the actual head would be placed on the stem trunnion and fixed with impaction. The layers of tissue would be then closed with

dissolvable stitches and the patient could usually head home to recover within the same day, depending on the condition.

During the surgery, the assembly of the femoral head onto the femoral stem during the surgery is via impaction. To apply the impaction on the femoral head, a polymer tipped impactor instrument and a mallet is used to avoid damaging the prosthesis. The amount of impaction force used during assembly is important for implant fixation and longevity. The strength of the fixation can also be attributed to other factors such as taper design, condition of taper surfaces, mismatch angle, angle of impaction, taper environment, and number of impactions (Pennock, Schmidt et al. 2002, Heiney, Battula et al. 2009, Rehmer, Bishop et al. 2012, English, Ashkanfar et al. 2016, Ashkanfar, Langton et al. 2017, Ashkanfar, Langton et al. 2017, Grosso, Jang et al. 2018, Panagiotidou, Cobb et al. 2018, Haschke, Konow et al. 2019). Maximum fixation is crucial in minimizing taper problems such as corrosion, fretting, micromotion, and unintended disassembly.

The positive correlation between the magnitude of the assembly force and the taper fixation connection strength has been investigated in several studies with the taper “pull-off” force being used as the measure to assess taper strength. The magnitude of assembly impaction force was initially determined by surgeons who were required to apply an impact typical of that used intra-operatively to assemble the femoral head onto the stem. The measured forces found were approximately between 1600N to 5000N (Pennock, Schmidt et al. 2002, Heiney, Battula et al. 2009, Lavernia, Baerga et al. 2009). It was found that the femoral head pull-off force increased linearly with the peak assembly force when the femoral head was impacted onto the stem (Rehmer, Bishop et al. 2012, Danoff, Longaray et al. 2018, Grosso, Jang et al. 2018, Krull, Morlock et al. 2018, Scholl, Pierre et al. 2018). The same relationship is also true when the femoral head is quasi-statically

pressed onto the stem (Rehmer, Bishop et al. 2012, Ramoutar, Crosnier et al. 2017, Scholl, Pierre et al. 2018, Pierre, Swaminathan et al. 2019, Chaudhary, Boruah et al. 2020). Ouellette, Mali et al. (2019) and Panagiotidou, Cobb et al. (2018) have both reported that a higher assembly force would result in significantly reduced fretting corrosion. English, Ashkanfar et al. (2016) investigated the effect of assembly forces on taper fretting wear and found that an increased assembly force would result in a reduction in fretting wear. Surgeons are provided with general guidelines and training by hip prostheses manufacturers on the technique of femoral head assembly; however, the guidelines are vague for the force required during impaction, using statements such as 'slightly' or 'firmly' to describe the magnitude of impaction force. In reality, the magnitude of impaction force is based on the surgeons' preference, experience, type of femoral head prosthesis, and quality of the patients' bone stock.

2.3.2. Failure in THRs

Modern THRs currently have an expected lifespan of 10 to 15 years with a small cohort surpassing 15 years, however, approximately 8% of these prostheses have failed prematurely. Recent data from the National Joint Registry of the UK (NJR), indicates that approximately 100,000 THRs are performed every year with the number increasing every year. In the UK alone, the number of THR procedures performed has increased by 43% in the last decade while the average age of patients receiving THRs is decreasing. As such, there is a need to increase the longevity of these devices further to accommodate their more active lifestyle.

The most common modes of failure reported in the NJR are aseptic loosening, dislocation, adverse reaction to particulate debris, periprosthetic fracture, infection, and pain (see Table 2-1). The NJR have reported aseptic loosening as the most common reason for THR

failure (46.1%). Aseptic loosening refers to the loosening of the prosthesis that may result from wear debris or inadequate fixation during surgery. Various theories have been presented to explain aseptic loosening based on observational, experimental, and clinical studies (Jiang, Jia et al. 2013). The main mechanism seems to be the excess production of wear particles which triggers a pro-inflammatory reaction leading to increased osteoclast differentiation, macrophage production, linear or focal osteolysis. Patient susceptibility to aseptic loosening may be affected by host-, genetic-, surgical-, and implant-related factors (Sundfeldt, V Carlsson et al. 2006, Electricwala, Narkbunnam et al. 2016, Karachalios, Komnos et al. 2018)

Dislocation is reported to be the second most common reason for THR failure (16.6%). Dislocation of the femoral head from within the acetabular component is the most common early complication after THR with the majority occurring within the first year (Amlie, Høvik et al. 2010). To reduce the risk of dislocations, larger femoral heads have been introduced to increase the distance required for dislocation, however, they have been limited in the past due to their association with larger amounts of wear in conventional UHMWPE liners (Livermore, Ilstrup et al. 1990). With the development of newer and advanced materials such as XLPE, the use of larger femoral heads may be the key to reduce the risk of dislocations.

Adverse reaction to particulate debris is also reported as one of the most common modes of THR failure (15.2%). The generation of wear debris from any part of the prosthesis is unavoidable and induces an extensive biological cascade of adverse cellular responses, where macrophages are the main cellular type involved in this hostile inflammatory process (Howie, Rogers et al. 1993, Bitar and Parvizi 2015). The resultant of this complex contribution of the generated wear debris and mechanical instability of the prosthetic

components is called osteolysis. Osteolysis is defined as the process of progressive destruction of periprosthetic bony tissue. Macrophages cause osteolysis indirectly by releasing numerous chemotactic inflammatory mediators, and directly by resorbing bone with their membrane microstructures.

The other common modes of THR failures are pain (15.8%), periprosthetic fracture (12.4%), and infection (5.1%). Other less common reasons reported in the NJR are malalignment, implant fracture, head-socket size mismatch, implant wear, and others. When a failure occurs, a revision surgery is needed to replace the failed implant. Revisions are less successful than primary surgeries due to the much more complex procedure and the reduction in bone quality. It is also much more costly than primary surgery with more discomfort and pain for patients. THR failures vary via type, design, and brand of prosthesis.

Table 2-1: Common modes of THR failure as reported in the NJR

Mode of failure	% of failure
Aseptic Loosening	46.1%
Dislocation	16.6%
Adverse reaction to particulate debris	10.7%
Pain	15.8%
Periprosthetic Fracture	12.4%
Infection	5.1%

The NJR have reported that MoM THRs showed a high overall risk of revision with currently minimal usage of these prostheses. The high risk of revision can be attributed to the adverse reactions to metal debris (ARMD). Langton, Joyce et al. (2011) introduced ARMD as an umbrella term to describe joint failure secondary to surface wear of the bearing surface or corrosion debris in the absence of any other obvious explanation. This includes metallosis, pseudotumor, and aseptic lymphocyte-dominated vasculitis-associated lesion. Initially, ARMD related failures were reported for MoM bearing surfaces(Kwon, Glyn-Jones et al. 2010, Langton, Jameson et al. 2010), however, further

research has shown that this type of failure could also arise from the taper junction of MoP THRs (Cipriano, Issack et al. 2008, Langton, Sidaginamale et al. 2012, Bishop, Witt et al. 2013, Oliveira, Candelária et al. 2015, Hunter, Hsu et al. 2019).

From the modes of failures, wear contributes to many of the different modes of failures, such as aseptic loosening, adverse reaction to particulate debris, infection. Consequently, an understanding of all clinical failures (mainly wear for this research) at all interfaces is needed to reduce the number of revisions, increase longevity, and provide more comfort for patients.

2.4. Wear in THRs

Wear is known as the gradual removal of material on solid contacting surfaces under relative movement. Wear and friction must be exactly related with each other in each state of contact within a system, although a comprehensive simple relationship should not be expected (Kato 2000). Wear is associated with timely and costly mechanical failure, whereas friction results in energy loss due to shearing and ploughing. Generally, lubrication is used to separate contacting surfaces from each other resulting in reduced wear and frictional forces.

Types of wear can be identified by their relative motions such as:

- **Adhesive wear** – Occurs when two bodies slide over or are pressed into each other, which material is then removed by fracture.
- **Abrasive wear** – Occurs when a hard rough surface slides across a softer surface, resulting in the deformation or cutting of the material.
- **Fatigue** – Occurs when the material is weakened by cyclic loading, forming micro-cracks which grow and propagate forming wear particles.

- **Fretting wear** – Occurs during cycling rubbing between two surfaces.
- **Erosive wear** – Occurs during the impact of particles of solid or liquid against the surface of a material, which gradually removes material from the surface through repeated deformations and cutting actions.
- **Corrosive wear** – Occurs when a layer of film is formed due to chemical reactions between the worn material and corroding medium.

Wear at the contacting surfaces in a hip prosthesis is inevitable due to the cyclic load that occurs. The most common mechanisms of wear debris generation in THR prostheses are often categorized as abrasive wear, adhesive wear, and third-body wear. This wear debris would interact with the surrounding tissues which the body would react to.

The biological response to particle wear debris is complex and drives the process towards periprosthetic tissue destruction and implant loosening, leading to prosthesis failure (Hu and Yoon 2018). Furthermore, the accumulation of wear particles released into the joint cavity can act as an abrasive and increase wear. Metallic particles released can lead to blackish metal deposits in the periprosthetic known as metallosis (Korovessis, Petsinis et al. 2006, Rony, Lancigu et al. 2018). Polyethylene particles released are nondegradable and can lead to inflammation leading to aseptic loosening of the prosthesis (Schmalzried, Jasty et al. 1992, Massin and Achour 2017) (CHAPPARD, RONY et al. 2021).

- **Wear between femoral head and acetabular cup surfaces**

Adverse consequences of bearing wear can either be catastrophic implant failure or local host biological responses resulting in osteolysis or soft-tissue reactions (A., D. et al. 2014). Implant failure can be associated with component malpositioning, impingement, or polyethylene oxidation. Host biological reactions to wear debris and particle-driven aseptic loosening remain the most frequent cause of revision (NJR 2021). Factors which

affect the bearing surface wear are the bearing couple, which affects both the amount of volumetric wear and the biological responses of the wear debris, and the effect of femoral head size, which affect the amount of volumetric wear generated.

The ideal bearing surface in a THR prosthesis would have the following features (H., H. et al. 1998):

- Low coefficient of friction
- Small volume of wear particle generation
- Low tissue reaction to wear particles
- High resistance to third body wear
- Enough deformation of articular surfaces to permit adequate film lubrication.

- **Hard-on-soft couples**

Hard-on-soft bearing couples consists of a metallic or ceramic femoral head on a polyethylene (conventional UHMWPE or highly cross-linked polyethylene) bearing liner. UHMWPE was first introduced in 1962 as the bearing for the Charnley hip prosthesis for its material properties such as low friction, low density, and fine biocompatibility (Charnley 1961, Lewis 1997, Schmidig, Patel et al. 2010). However, the high wear rates of UHMWPE have led to the premature failure of these prostheses (Harms and Kansen 2018). Revell, Weightman et al. (1978) and Mirra, Marder et al. (1982) were among the first to associate UHMWPE debris with osteolysis and aseptic loosening in the late 1970s and early 1980s respectively. Furthermore, conventional UHMWPE which were sterilized by gamma irradiation produced free radicals that are oxidised in contact with air (Hopper, Young et al. 2003). Oxidation decreases the resistance of the UHMWPE resulting in the

degradation and increased brittleness of the UHMWPE, and thus may increase wear (McKellop, Shen et al. 2000).

To decrease polyethylene wear, highly cross-linked polyethylene (XLPE) was developed to improve the material properties of UHMWPE. The first generation XLPE materials which used irradiation doses between 50 and 105kGy, were introduced in the late 1990s and early 2000s (Kurtz and Patel 2016)

- **Hard-on-hard couples**

Hard-on-hard bearing couples consist of a metallic or ceramic femoral head on a metallic or ceramic acetabular cup. Generally, the bearing couples would be MoM or CoC bearing couples.

MoM bearing couples were first introduced in the 1960s (Zahiri, Schmalzried et al. 1999) with second generation designs introduced in the late 1980s (Dorr, Wan et al. 2000).

These were popularized in recognition of the low volumetric wear rate and increased stability with larger femoral head sizes (Williams, Royle et al. 2009). Although the volumetric wear was found to be extremely low compared to MoP or CoP bearing couples, the number of wear particles generated was found to be 13 – 500 times greater and was found to be more biologically active (Doorn, Campbell et al. 1998). These generated metallic wear particles can cause metallosis and increased incidence of pseudotumor formation (Bosker, Ettema et al. 2015). Patients with MoM bearing couples have been shown to have increased metal ions levels at long term follow-ups which are known to be genotoxic (Engh, MacDonald et al. 2014). In-vitro analysis has shown the potential for cobalt and chromium ions to induce DNA damage directly through disruption at the level of the nucleus and indirectly through the formation of reactive oxygen species (Raghunathan, Devey et al. 2013). A recall of the MoM bearing couple by

DePuy Orthopaedics was issued in 2010 due to a high rate of revision in the registry data. According to the National Joint Registry for England and Wales, it was found that there was a revision rate of 13.6% for MoM bearing couples while general hip implants were between 3.3% and 4.9% (Cohen 2011). Since the recall, the use of large femoral head MoM bearing couples has sharply fallen from 20% in 2005 to <1% in 2021 (NJR 2022). CoC bearing couples were developed in the early 1970s (Boutin, Christel et al. 1988) in the form of an all alumina acetabular cup and an alumina ceramic femoral ball glued to a cemented metal stem (Jenabzadeh, Pearce et al. 2012). The acetabular cup was implanted either with cement or as a press-fit (Griss and Heimke 1981, Mittelmeier and Heisel 1992). The fixation, however, proved to be insufficient with aseptic loosening being the predominant cause of failure (Boutin, Christel et al. 1988, Garcia-Cimbrello, Martinez-Sayanes et al. 1996). High rates of fracture were also reported (Griss and Heimke 1981) which was predominantly due to the material of large grain size, the presence of inclusions and grain boundaries, and poor tolerances for taper designs which mated ceramics to the implants (Jenabzadeh, Pearce et al. 2012). Advances in ceramic materials have led to improved bearing design and taper designs providing excellent biocompatibility, improved mechanical strength and superior wear characteristics (Hannouche, Hamadouche et al. 2005, Tateiwa, Clarke et al. 2008, Greene, Malkani et al. 2009, Napier and Shimmin 2016).

- **Wear between femoral head taper surface and femoral stem trunnion**

Modular hip prosthesis was developed to have increased advantages such as adjustment of the patient's leg length during surgery, decreased inventory size, decreased cost, simplified revision procedures (Lieberman, Rimnac et al. 1994, Hallab, Messina et al. 2004, Rieker, Schön et al. 2005, Witzleb, Ziegler et al. 2006, Paleochorlidis, Badras et al.

2009). A significant problem of the modular hip prosthesis comes from the additional contact interface between the femoral head and stem which may increase the amount of wear within the prosthesis.

Trunnionosis is defined as the wear of the femoral head-stem interface and has been acknowledged as a source of total hip prosthesis failure (Pastides, Dodd et al. 2013). Previously, the determination of hip prosthesis wear has mainly focused on the bearing surfaces between the femoral head and acetabular cup (Teoh 2003, Fialho, Fernandes et al. 2007); however, trunnionosis was found to have a more profound effect as the wear characteristics on the bearing surfaces improved. Trunnionosis is estimated to account for up to 3% of all THA revision procedures (Porter, Urban et al. 2014, Drummond, Tran et al. 2015).

Adverse local tissue reactions have been found in patients with patients with MoP THRs (Svensson, Mathiesen et al. 1988, Cooper, Della Valle et al. 2012, Mao, Tay et al. 2012, Cook, Bolland et al. 2013, Scully and Teeny 2013, Shulman, Zywiell et al. 2015, Watanabe, Takahashi et al. 2015). Cooper, Della Valle et al. (2012) previously reviewed ten retrieved MoP THRs which had elevated serum cobalt and chromium levels within the patients and found visible damage at the femoral head-stem taper junction associated with tissue necrosis and lymphocytic infiltration. Kurtz, Kocagöz et al. (2013) and Dyrkacz, Brandt et al. (2013) investigated a total of 124 MoP modular hip prostheses for fretting wear damage at the femoral head-stem junction. They reported significant fretting wear and corrosion were found.

It was previously thought that metallosis would only affect patients with MoM THRs, however, these studies have indicated that damaging metallic debris can also be created

at the taper junction between a metallic femoral head and stem even in MoP or CoC prostheses.

2.5. Wear assessment

Wear rate measurements are routinely performed using standard or customized friction and wear testing equipment by measuring the material loss from surfaces based on contact forces, duration, and extent of the contact. The volume of material loss (V) per sliding distance unit (L) can be obtained from Equation (1):

$$V = \frac{W_v}{L} \quad (1)$$

where W_v is to the total volume of the material removed. The real area of contact of the friction couple (A_r) depends on the applied load (F_n) and hardness of the softer material (H) between the surfaces and can be calculated using Equation (2):

$$A_r = \frac{F_n}{H} \quad (2)$$

The wear ratio, or wear coefficient (k), can be defined as the ratio of the wear in units of volume removed per unit sliding distance to the real interfacial area of contact. This is expressed as a dimensionless coefficient and can be calculated by Equation (3):

$$k = \frac{V}{A_r} = \frac{\frac{W_v}{L}}{\frac{F_n}{H}} \quad (3)$$

Since the wear coefficient (k) is the ratio of two areas, the worn area (A_w), and the real contact area (A_r), the wear coefficient can thus be interpreted as the fraction of the real contact area (A_r) removed by wear. Considering a tribological system where the contact surfaces mate at N asperities, and n of those form wear debris, k can be further defined as Equation (4):

$$k = \frac{A_w}{A_r} = \frac{n}{N} \quad (4)$$

This interpretation indicates that while all asperity contacts contribute to friction, only a very small fraction of contacts result in wear. Furthermore, some asperities are only plastically deformed on the surfaces, and not removed from the component. As the quantity $\frac{F_n L}{H}$ has dimensions of volume, this represents the total volume of the plastically deformed zone underneath the surface of a worn area (V_p) following sliding by a distance L . Hence, k also represents the proportion of the plastically deformed volume that is removed by the wear process defined in Equation (5):

$$k = \frac{W_v}{V_p} \quad (5)$$

2.5.1. Wear Laws

There are two main types of wear laws used for wear assessment, “Archard’s Wear Law” or the “Dissipated Energy Wear Law”.

- **Archard’s Wear Law –**

The Archard’s wear law is the most frequently used wear law developed by Holm and Archard in 1953 (Archard 1953). This wear law considers adhesive wear and assumes the sliding spherical asperities to deform fully plastically in contact. The Archard’s wear equation states that the volume of worn material is proportional to the normal force, the sliding distance, and inversely proportional to the hardness of the material (Popov 2019). The dimensionless Archard wear coefficient (K), from Equation (3), which contains the hardness of the material ($K = \frac{k}{H}$) can usually be obtained with Equation (6).

$$K = \frac{W_v}{F_n S} \quad (6)$$

where s is the relative sliding distance or 'slip'. As the wear coefficient is correlated to material hardness, it has the units of Pa^{-1} . Equation (6) was initially developed for unidirectional sliding wearing processes but it has been widely adapted for other types of wear as well. Archard's wear law requires a gradual approach to obtaining the relative sliding distance. This can be represented as

$$W_v = K \sum F_n s_i \quad (7)$$

where s_i is the relative slip per stroke and $\sum F_n s_i$ is the sum of $F_n s$ products over the load cycles.

Numerous studies have shown that for the same material combination, the Archard wear coefficient (K), strongly depends on the wear mechanism, displacement amplitude, contact geometry, loading conditions, and other parameters. Johnson (1995) and Kapoor (1997) has stated that it is essential to consider the elastoplastic response of the structure when predicting wear rates of metallic structures under fretting. Under normal loading conditions, structures will maintain an elastic response, however when the loading occurs above the critical cyclic stress state, the material will undergo accumulated plastic dissipation. The shakedown boundary is a function of the Hertzian pressure and the friction coefficient. Other studies have also confirmed this theory (Van and Maitournam 1994, Johnson 1995, Fouvry, Kapsa et al. 2001, Fouvry, Liskiewicz et al. 2003) and demonstrated the limitation of the Archard model, which does not integrate the friction coefficient in its' formulation.

- **Dissipated Energy Wear Law –**

The energy wear law is dependent on the interfacial shear work (Fouvry, Kapsa et al. 2001, Teoh, Chan et al. 2002, Fouvry, Liskiewicz et al. 2003). This method relates the wear

volume to the frictional energy dissipated through the interface which gives the wear volume to be proportional to the sum of dissipated energy ($\sum E$) as given by Equation (8), where α is the energy wear coefficient.

$$W_v = \alpha \sum E \quad (8)$$

The dissipated energy (E) can be found by the product of tangential force (Q) and slip (s) given by Equation (9).

$$E = Qs \quad (9)$$

The Dissipated Energy wear law approach displays a higher stability than Archard's wear law which also facilitates different wear mechanisms such as abrasive, corrosive and fatigue wear. Similar to the Archard's wear coefficient (K), the Dissipated energy wear coefficient (α) is reliant on the material combination, sliding condition, and contact geometry.

2.5.2. Wear Coefficient

Traditionally, material wear has been characterized by weight loss or wear rate, however, studies have found that wear coefficient is more suitable to study wear characteristics (Yang and Loh 1995, Yang 1999, Yang 2003). Wear coefficients take into account the wear rate, applied load and the hardness of the materials. Wear coefficients are calculated in laboratory studies involving pin-on-disk (POD) wear testing rigs or hip simulators via gravimetric measurements.

POD wear testing rigs are an uncomplicated and inexpensive wear screening device which provides information exclusively on the intrinsic characteristics of the biomaterial under investigation. Atkinson, Dowson et al. (1985) determined wear coefficients based on the volumetric wear loss from 25 retrieved hip replacements between CoCr femoral heads

and UHMWPE bearing liners. The study found the average wear coefficient to be $2.90 \times 10^{-9} \text{ MPa}^{-1}$ with results ranging between $0.09 \times 10^{-9} - 7.20 \times 10^{-9} \text{ MPa}^{-1}$. Santavirta, Lappalainen et al. (1999) and Saikko and Kostamo (2013) determined the wear coefficients via pin-on-disk testing using a UHMWPE pins which slides over a CoCr plate either in a linear or randomised motion. The wear coefficients were found to be $3.50 \times 10^{-10} \text{ MPa}^{-1}$ for Santavirta, Lappalainen et al. (1999) and $3.92 \times 10^{-9} \text{ MPa}^{-1}$ for Saikko and Kostamo (2013). Kang, Galvin et al. (2008) investigated the wear factors of 0 MRad and 10 MRad UHMWPE with different kinematical combinations and found a range of wear coefficient between $1.03 \times 10^{-10} - 5.5 \times 10^{-10} \text{ MPa}^{-1}$.

Although POD wear testing rigs provide valuable information, further testing is necessary to evaluate the performance of actual hip prostheses in simulated physiological conditions. This is accomplished through hip simulators. Several studies have been performed on hip simulators to determine the wear coefficients from the biomaterials under simulated walking conditions. Maxian, Brown et al. (1997) and Matsoukas, Willing et al. (2009) determined the wear coefficient through a trial-and-error method using computational wear simulation of experimental tests and compared the computed volumetric wear with hip simulator experiments. The studies yielded a wear coefficient of $1.53 \times 10^{-9} \text{ MPa}^{-1}$ for UHMWPE and $5.32 \times 10^{-10} \text{ MPa}^{-1}$ for XLPE. Galvin, Ingham et al. (2006) investigated the wear of XLPE bearing liners in a hip simulator. The study used 28mm diameter femoral heads against XLPE bearing liners with volumetric wear measurements taken every million cycles. Using the volumetric wear, a wear coefficient of $2.00 \times 10^{-10} \text{ MPa}^{-1}$ was calculated for CoCr against XLPE. Other studies involving different materials combinations have also been performed. Di Puccio and Mattei (2015) proposed an approach to compute the wear coefficient on CoCr MoM THRs. The study first utilised a hip simulator to obtain the wear rates and found that although the femoral

head and cup had the same materials, the femoral head and cup exhibited different wear rates. Using a numerical model, the study calculated the wear coefficients for both the femoral head and cup separately and found the wear coefficient to be between $0.26 \times 10^{-11} - 7.30 \times 10^{-11} \text{ MPa}^{-1}$.

A study by Zhang, Harrison et al. (2013) used POD with linear reciprocating motion to determine the wear coefficients for two femoral head-stem material combinations (Co-28Cr-6Mo/DMLS Ti-6Al-4V and Co-28Cr-6Mo/forged Ti-6Al-4V). The study used the dissipated energy wear law approach to calculate the energy wear coefficients using the volumetric wear loss obtained from the POD studies. Volumetric wear loss was obtained through a scanning electron microscope (SEM) or a profilometer. For the Co-28Cr-6Mo/DMLS Ti-6Al-4V material combination, with a 10N load on the pin, the wear coefficient calculated was $5.35 \times 10^{-8} \text{ MPa}^{-1}$ and $3.91 \times 10^{-9} \text{ MPa}^{-1}$ using SEM and profilometry respectively. For the Co-28Cr-6Mo/forged Ti-6Al-4V material combination, with a 10N load on the pin, the wear coefficient calculated was $10.6 \times 10^{-8} \text{ MPa}^{-1}$ and $1.31 \times 10^{-8} \text{ MPa}^{-1}$ using SEM and profilometry respectively. The differences in values are due to the different measurement techniques used.

Calculations for fretting wear coefficients have also been investigated through fretting wear rigs. Fouvry, Liskiewicz et al. (2003) investigated fretting wear behaviour of Ti-6Al-4V through an electrodynamic fretting wear rig. The study covered a wide range of normal force loadings between 50N and 500N with displacement amplitudes from 2 to 200 μm . From the results of this study, the energy wear coefficient of $1.12 \times 10^{-8} \text{ MPa}^{-1}$ is determined.

Fridrici, Fouvry et al. (2001) also investigated Ti-6Al-4V fretting wear behaviour through a fretting wear rig. A number of tests were conducted with different normal loading

resulting in contact pressures of 525MPa and 830MPa respectively, with displacement amplitudes between 5 μ m and 50 μ m. The tests were conducted in dry conditions with a frequency of 5Hz up to a maximum of 1 million cycles. The wear is then measured through profilometry, and the energy wear coefficient was then determined. For a contact pressure of 830MPa, and a displacement amplitude of 50 μ m up to 250,000 cycles, the energy wear coefficient was determined to be $2.90 \times 10^{-8} \text{ MPa}^{-1}$.

Wear coefficients are fundamentally important to provide a valuable insight into wear modelling in different systems. The wear coefficients obtained from the studies show a wide range of values even for similar material combinations depending on the test machine, component design, test configurations and test conditions (Cawley, Metcalf et al. 2003). A summary of the wear coefficients obtained from the literature is shown in Table 2-2.

The ratio between the dimensional Archard and dissipated energy wear coefficients is found to be equal to the coefficient of friction (μ), assuming that the Coulomb relationship between friction and pressure holds (Leonard, Sadeghi et al. 2012), where $q = \mu p$, q is friction shear stress, p is normal force.

$$\mu = \frac{K}{\alpha} \quad (10)$$

Table 2-2: Values of wear coefficient for different material combinations of review wear models on bearing and taper surfaces

Material Combination	Wear Law	Method	Wear Measurement	Wear Coefficient MPa ⁻¹	Reference
Bearing Surfaces					
CoCr/UHMWPE	Archard	Retrievals	Volume Loss	2.90×10^{-9}	(Atkinson, Dowson et al. 1985)
CoCr/UHMWPE	Archard	Pin on Disk	Volume loss	1.06×10^{-9}	(Maxian, Brown et al. 1996, Maxian, Brown et al. 1996, Maxian, Brown et al. 1996)
CoCr/UHMWPE	Archard	Pin on Disk	Volume loss	3.50×10^{-10}	(Santavirta, Lappalainen et al. 1999)
CoCr/UHMWPE	Archard	Pin on Disk	Volume loss	$1.03 \times 10^{-10} - 5.50 \times 10^{-10}$	(Kang, Galvin et al. 2008)
CoCr/UHMWPE	Archard	Pin on Disk	Volume loss	3.92×10^{-9}	(Saikko and Kostamo 2013)
CoCr/UHMWPE	Archard	Hip Simulator	FEA	1.53×10^{-9}	(Maxian, Brown et al. 1997)
CoCr/XLPE	Archard	Hip Simulator	FEA	5.32×10^{-10}	(Matsoukas, Willing et al. 2009)
CoCr/XLPE	Archard	Hip Simulator	Volume loss	2.00×10^{-10}	(Galvin, Ingham et al. 2006)
CoCr/XLPE	Archard	Pin on Disk	Volume loss	$7.00 \times 10^{-10} - 8.70 \times 10^{-10}$	(Abdelgaied, Brockett et al. 2013)
CoCr/CoCr	Archard	Hip Simulator	Numerical	$0.26 \times 10^{-11} - 7.30 \times 10^{-11}$	(Di Puccio and Mattei 2015)
CoCrMo/CoCrMo	Archard	Hip Simulator	SEM	$0.95 \times 10^{-6} - 1.24 \times 10^{-6}$	(Cawley, Metcalf et al. 2003)
Taper Surfaces					
Co-28Cr-6Mo/DMLS Ti-6Al-4V	Energy	Pin on Disk	SEM	5.35×10^{-8} (10N load) 2.97×10^{-8} (6N load)	(Zhang, Harrison et al. 2013)
Co-28Cr-6Mo/forged Ti-6Al-4V	Energy	Pin on Disk	SEM	10.6×10^{-8} (10N load) 9.18×10^{-8} (6N load)	
Co-28Cr-6Mo/DMLS Ti-6Al-4V	Energy	Pin on Disk	Profilometry	3.91×10^{-9} (10N load) 2.76×10^{-9} (6N load)	
Co-28Cr-6Mo/forged Ti-6Al-4V	Energy	Pin on Disk	Profilometry	1.31×10^{-8} (10N load) 1.88×10^{-8} (6N load)	
Ti-6Al-4V/ Ti-6Al-4V	Energy	Electrodynamic fretting rig	SEM	1.12×10^{-8}	(Fouvry, Liskiewicz et al. 2003)
Ti-6Al-4V/ Ti-6Al-4V	Energy	Fretting wear rig	Profilometry	2.90×10^{-8}	(Fridrici, Fouvry et al. 2001)
Ti-6Al-4V/ High Strength Steel	Archard	From (McColl, Ding et al. 2004)	Fretting fatigue test	2.75×10^{-8}	(Madge, Leen et al. 2007)

2.5.3. Wear Fraction

During the wearing process, the amount of material removed from both components may be different due to differences in material properties such as hardness, wear resistance, and surface roughness. The proportion of material removed from each contacting surface is known as 'wear fraction'. A wear fraction of 0.5:0.5 would remove an equal amount of material on both contacting surfaces, while a wear fraction of 0.2:0.8 would remove 20% of material on one contacting surface and 80% of the other.

Employing a wear fraction is crucial in wear modelling and should not be neglected. Two such wear fractions have been applied in this study:

- **Between CoCr and Ti** – A study by Bone, Sidaginamale et al. (2015) found a median volumetric wear of 0.14mm^3 from 28 retrieved DePuy Corail Titanium stems trunnions. Langton, Sidaginamale et al. (2012) found a median volumetric wear in excess of 2mm^3 from 111 retrieved cobalt-chrome MoM femoral heads. The findings from their work indicate that the cobalt-chrome femoral head tapers wear by around a factor of 10 more than the titanium alloy stem trunnion surface. These findings are supported further by Bishop, Witt et al. (2013) and comprehensively explained by Moharrami, Langton et al. (2013) as occurring due to the preferential oxidation of titanium alloy over cobalt-chrome thus increasing the hardness of the titanium trunnion which subsequently wears the un-oxidised CoCr head taper surface.
- **Between CoCr and XLPE** – There are a huge number of studies performed on the wear rates on CoCr XLPE wear rates, however, most are focused on the wear at the polyethylene liner and do not measure CoCr femoral head wear. There is a large range of XLPE wear found in the current literature ($1.5 - 33.09\text{mm}^3/\text{yr}$). A

study by Anissian, Stark et al. (1999) investigated and compared the hip simulator wear between CoCr-XLPE THRs and found a wear rate of $0.021\text{mm}^3/\text{Mc}$. Using these findings, there is a range of wear fraction for the XLPE bearing liner which can be extrapolated: between 0.064% - 1.38% of total wear will be found on the CoCr femoral head. For this study, the wear fraction between CoCr and XLPE is specified at 99% wear on the XLPE bearing liner and 1% of wear on the CoCr femoral head.

2.5.4. Experimental Methods for measuring wear

In the process of developing newer designs and materials for total hip prosthesis, aggressive testing and screening should be utilized to help more accurately predict the success of hip prosthesis design. Currently, there are a few experimental methods to help evaluate the wear performance of newer designs:

- **Radiography:** Radiography imaging has been developed to measure polyethylene wear, including both two- and three-dimensional techniques. This has been vital to provide additional information on component orientation and enables assessment of periprosthetic osteolysis, which is an important consequence of polyethylene wear.
- **Retrievals:** Retrieved components of prostheses either from failed components or post-mortem are inspected visually for pitting, scratching and burnishing while a shadowgraph technique or CMM may be used to measure the extent of the wear (SYCHTERZ, MOON et al. 1996, JASTY, GOETZ et al. 1997, Choudhury, Ranuša et al. 2018).

- **Hip simulator testing:** A mechanical instrument designed to mimic walking through an application of dynamic motion and loading cycles. Using a hip simulator, a hip prosthesis is subjected to long-duration tests (up to 10 million cycles). It is able to simulate the movements acting in a hip joint in all three axes while being submerged in a synovial fluid with similar properties to the pseudo-synovial fluid acting *in vivo* after implantation. Hip simulators are useful in replicating wear rates, wear patterns and wear debris observed clinically, in controlled laboratory conditions using actual hip prostheses (Affatato, Leardini et al. 2006, Smith and Joyce 2017). An international standard has been established for wear testing and wear rates (ISO14242-1 2018). The standard established covers the testing parameters such as dynamic loading, the applied motion, frequency, and duration of testing. According to ISO 14242-1, the hip simulator test must be conducted until one of the three conditions occur: completion of 5 million cycles, break-up or delamination of the bearing surfaces, failure of the hip simulator to maintain the applied loading and rotational parameters.

Currently, as XLPE is a relatively new material for bearing use, many are still currently in service and the *in vivo* wear rates are determined through radiography or hip simulators. Devane, Horne et al. (2017), Haw, Battenberg et al. (2017), Atrey, Ward et al. (2017) and Khoshbin, Wu et al. (2020) have used radiography to analyse a total of 247 primary MoM THRs with XLPE bearing liners with CoCr femoral heads ranging between 28mm and 60mm. The wear rates determined from the studies have found a volumetric wear rate between 1.5 – 57.6mm³/yr. It is important to note that the patients' activity has not been accounted for in these studies which could impact the wear rates.

Essner, Sutton et al. (2005) investigated and compared the wear rates between MoM, CoC and CoP THRs. The study utilised two identical 12-station hip joint simulators with a physiological loading pattern between 150N and 2450N and at 1Hz frequency up to 5 million cycles. Wear assessment was conducted periodically with fresh lubricant applied after. The MoM THRs had a CoCrMo femoral head and acetabular cup, CoC THR had an alumina femoral head and acetabular cup, and the CoP THR had an alumina femoral head and a XLPE bearing liner. The study found the volumetric wear rates of the combined bearing couple to be 6.3 mm³/yr, <0.1mm³/yr, and 5.62 mm³/yr for the MoM, CoC, and CoP THRs. CoC bearing couples were found to have the least wear rate while the MoM bearing couples had the most.

Galvin, Ingham et al. (2006) investigated the wear of 28mm CoCr femoral head against 4 different polyethylene liners. A non-crosslinked bearing liner was used as control while the XLPE bearing liners were irradiated with 2.5MRad, 7.5MRad, and 10MRad. These bearing couples were articulated in a Leeds ProSim hip joint simulator at 1 Hz frequency up to 5 million cycles with wear assessment conducted every million cycles. Volume changes were determined using a profilometer. The study found the average volumetric wear rates of the non-crosslinked PE, 2.5MRad, 7.5MRad, and 10MRad XLPE bearing liners to be 45.6mm³/Mc, 46.9mm³/Mc, 15.04mm³/Mc, and 8.7mm³/Mc respectively. The study also noted the surface topography of the XLPE liners became smoother than the non-crosslinked PE. This would benefit the XLPE materials in aiding lubrication and could have contributed to the lower wear rates seen with these materials.

Fisher, Jennings et al. (2006) investigated the wear characteristics of five 36mm CoCr femoral head and XLPE bearing liners. The study utilised a hip simulator with a physiological walking cycle loading between 100N and 3000N at 1Hz frequency up to 7

million cycles. The volumetric wear loss of the XLPE bearing liner is determined geometrically using a three-dimensional co-ordinate measuring machine to map the liner surface. The study found the steady state wear rates to be between 9.2 – 9.5mm³/Mc.

Partridge, Tipper et al. (2018) evaluated a hip simulator method which assessed wear and damage between 36mm diameter CoCr femoral head and XLPE bearing liners. The study utilised a 10-station pneumatic hip simulator with a physiological walking cycle loading between 300N and 3000N up to 5 million cycles. Wear measurements were conducted at every million cycles through gravimetric and geometric measurements. The study found an average XLPE volumetric wear rate of 8.7mm³/Mc.

A summary of the experimental wear testing methods for bearing surfaces is compiled in Table 2-3. These studies have focused on the bearing surfaces of the THR except for a study by Bhalekar, Smith et al. (2020); other studies have not measured the wear of the femoral head during hip simulator studies, assuming the femoral head does not wear due to the difference in material properties between metal and polyethylene. It is vital to investigate wear of the metallic femoral head as well, as even a slight increase in metallic debris can lead to catastrophic issues for patients.

Langton, Sidaginamale et al. (2012) investigated the taper junction of 126 retrieved large-diameter MoM THRs from a single manufacturer. The wear assessment was carried out using coordinate measuring machines to calculate the volumetric wear rates of the surfaces of the CoCrMo/Ti6Al4V taper junctions. The study reported a wear rate of between 0.01 – 8.34mm³/year and found the primary factor leading to taper failure is the increased lever arm acting on the taper junction in large-diameter MoM THRs.

Bishop, Witt et al. (2013) investigated the taper junction of five retrieved MoM THR component sets. Wear measurements were measured using a coordinate measurement

machine and wear was quantified by comparison with an assumed initial geometry. The study found extensive wear of the femoral head taper surface with a volumetric wear rate between 0.59 – 4.87mm³/yr. The study also found that the wear on the bearing surface and femoral stem tapers were relatively low.

Kocagoz, Underwood et al. (2016) investigated the taper junction wear between ceramic and CoCr femoral heads. The study utilised a roundness machine equipped with a diamond stylus to measure the taper surface of 50 ceramic and 50 CoCr retrieved femoral head-stem pairs. The profiles of the taper surfaces were then analysed, and the volumetric material loss was estimated using a customized MATLAB script. The study found a femoral head taper volumetric wear rate range between 0.00 – 8.67mm³/yr and 0.00 – 0.04mm³/yr for the CoCr cohort and ceramic cohort respectively and the femoral stem volumetric wear rate range between 0.00 – 0.32mm³/yr and 0.00 – 0.37mm³/yr for the CoCr cohort and ceramic cohort. The majority of material loss from the ceramic cohort showed a reduction in the amount of metal released by an order of magnitude compared with the CoCr cohort.

Langton, Sidaginamale et al. (2017) investigated whether CoCr femoral stem tapers wear more than Ti alloy femoral stem tapers when used in large-diameter MoM THRs. The study performed explant analysis to determine the volumetric material loss at the taper surfaces of 28 Ti alloy femoral stems and 21 CoCr femoral stems. Material loss was mapped using a coordinate measuring machine, profilometry and scanning electron microscopy. The study found a range of wear rate between 0.01 – 2.16mm³/yr and 0.01 – 1.65mm³/yr for Ti alloy femoral stems and CoCr femoral stems respectively. It was found that the CoCr stem tapers were found to have significantly greater volumetric material loss than the Ti alloy stems.

Hothi, Kendoff et al. (2017) examined 94 retrieved MoP THRs for evidence of corrosion and volumetric material loss at the taper junction using a macroscopic inspection, microscopic analysis, and a roundness-measuring machine protocol. 87 of the THR prosthesis were reported to have failed due to aseptic loosening of the components and 7 from infection. No adverse tissue reactions were reported. The study found the femoral head taper volumetric material loss between a range of 0.00 – 0.24mm³/yr. The study concluded that trunnionosis for MoP THRs may be clinically insignificant as the volumetric wear rate found was notably less than that of previously reported MoM taper junctions.

Langton, Wells et al. (2018) investigated the volumetric material loss from tapers of MoP THRs and compared the taper wear rates against MoM THRs. The study examined a total of 95 MoP and 249 MoM THR prostheses using a coordinate measuring machine. The volumetric wear rates for the MoM and MoP groups were 0.01 – 8.34mm³/yr and 0.00 – 3.84mm³/yr respectively. The median volumetric loss from the MoM cohort was found to be over four times larger than that from the MoP cohort (1.01 mm³ vs 0.23 mm³).

Hothi, Eskelinen et al. (2018) compared the effect of bearing type (MoM vs MoP) on taper material loss in THRs for a single design. 30 retrieved MoM and 32 retrieved MoP THRs were measured for the severity of corrosion and volumetric material loss at each femoral head taper surface. The range of volumetric wear found for the MoM and MoP groups were 0.01 – 3.45mm³/yr and 0 – 1.07mm³/yr. MoP THR prostheses were found to have lost significantly less material from their taper junctions than MoM THR prostheses.

Bhalekar, Smith et al. (2020) investigated the material loss, if any, at both the articulating and taper-trunnion surface of five 32mm diameter CoCrMo femoral head against XLPE bearing liner up to 5 million cycles. The study utilised a 6-station hip joint simulator with a double peak loading between 400N and 2000N. Wear assessment was conducted every

500,000 cycles through gravimetric and geometric measurements using an analytical balance and a coordinate measuring machine respectively. The study found the wear rates of the XLPE bearing liner and CoCrMo femoral head to be $2.74\text{mm}^3/\text{Mc}$ and $0.057\text{mm}^3/\text{Mc}$ for the respectively. The wear rates of the CoCrMo femoral head includes both the wear at the articulating surface and at the taper surface as well. The study also found the wear rates of the femoral head taper and femoral stem trunnion to be $0.021 - 0.069\text{mm}^3/\text{Mc}$ and $0.041 - 0.047\text{mm}^3/\text{Mc}$. The study has confirmed the necessity of measuring the taper-trunnion junction wear in MoP THRs as it was found that the majority of wear at the CoCrMo femoral head was from the taper junction. To date, no other long-term hip simulator tests have investigated wear from the taper-trunnion junction of MoP THRs.

A summary of experimental wear testing methods for taper junctions is compiled in Table 2-4.

Table 2-3: Volumetric wear for bearing surfaces in current literature

Authors	Method	THR Type	Femoral head size (mm)	Volumetric Wear Rate (mm ³ /yr) (range)	
				Femoral head	Acetabular Cup
Devane, Horne et al. (2017)	Radiography	MoP (CoCrMo/XLPE)	48 – 60	Not measured	1.5 – 18.9
Haw, Battenberg et al. (2017)	Radiography	MoP (CoCrMo/XLPE)	36/40/44	Not measured	33.09 – 48.39
Atrey, Ward et al. (2017)	Radiography	MoP (CoCrMo/XLPE)	28	Not measured	29.29
Khoshbin, Wu et al. (2020)	Radiography	MoP (CoCrMo/XLPE)	51 – 57	Not measured	7.58 – 29.6
	Hip Simulator	CoC (Alumina/Alumina)	32	< 0.1 (combined head and cup)	
Essner, Sutton et al. (2005)	Hip Simulator	CoP (Alumina /XLPE)	32/36	5.62 (combined head and cup)	
	Hip Simulator	MoM (CoCrMo/CoCrMo)	40	6.30 (combined head and cup)	
Galvin, Ingham et al. (2006)	Hip Simulator	MoP (CoCrMo/XLPE)	28	Not measured	5.59 – 56.3
Fisher, Jennings et al. (2006)	Hip Simulator	MoP (CoCrMo/XLPE)	36	Not measured	9.5
Galvin, Jennings et al. (2010)	Hip Simulator	MoP (CoCrMo/XLPE)	36	Not measured	6.30 – 12
		CoP (Alumina /XLPE)	36	Not measured	3.40 – 12
Partridge, Tipper et al. (2018)	Hip Simulator	MoP (CoCrMo/XLPE)	36	Not measured	8.7
Bhalekar, Smith et al. (2020)	Hip Simulator	MoP (CoCrMo/XLPE)	32	0.037 – 0.077	2.00 – 3.48

Table 2-4: Volumetric wear for taper surfaces in current literature

Authors	Method	THR Type	Femoral head/stem material combination	Volumetric Wear Rate (mm ³ /yr)	
				Femoral head taper (range)	Femoral stem trunnion (range)
Langton, Sidaginamale et al. (2012)	Retrievals	MoM	CoCrMo/Ti6Al4V	0.01 – 8.34	Not measured
Bishop, Witt et al. (2013)	Retrievals	MoM	CoCrMo/Ti6Al4V	0.60 – 4.90	0.005 – 0.006
Kocagoz, Underwood et al. (2016)	Retrievals	MoP/CoP/CoC	CoCrMo/CoCrMo and	0.00 – 8.67	0.00 – 0.32
			CoCrMo/Ti6Al4V Ceramic/CoCrMo and Ceramic/Ti alloy	0.00 – 0.04	0.00 – 0.37
Langton, Sidaginamale et al. (2017)	Retrievals	MoM	CoCrMo/Ti6Al4V	0.01– 2.16	0.01 – 0.12
			CoCrMo/CoCrMo	0.01 – 1.65	0.03 – 0.53
Hothi, Kendoff et al. (2017)	Retrievals	MoP	CoCrMo/CoCrMo	0.00 – 0.24	Not measured
Langton, Wells et al. (2018)	Retrievals	MoM	CoCrMo/Ti6Al4V (MoM)	0.01 – 8.34	Not measured
		MoP	SS/SS (MoP)	0.00 – 3.84	
Hothi, Eskelinen et al. (2018)	Retrievals	MoM	CoCrMo/Ti6Al4V (MoM)	0.01 – 3.45	Not measured
		MoP	CoCrMo/Ti6Al4V (MoP)	0.00 – 1.07	
Gascoyne, Turgeon et al. (2018)	Retrievals	MoM/MoP	Not specified	0.00 – 3.46	Not measured
Bhalekar, Smith et al. (2020)	Hip Simulator	MoP	CoCrMo/Ti6Al4V	0.021 – 0.069	0.041 – 0.047

2.5.5. Computational method for predicting wear

Computational analysis is the process of simulating the behaviour of a part of an assembly under given conditions. It uses numerical models to understand and quantify the effect of real-world conditions. Computational analysis offers an alternative method which is faster, and cheaper than experimental testing. It can be used in addition to experimental testing to help decrease cost, and time consumed while improving the wear characteristics of mechanical designs. When validated experimentally or *in vivo*, it could be used to assess different gait cycles, functional performance of prosthetic devices and refine critical points in design.

There is evidence that work has been successful in the prediction of wear within THR. All methods presented in the literature have been significantly simplified due to the complexity of the prediction. A compilation of successful computational analysis is summarized in Table 2-5 and Table 2-6. These methods in literature have only considered either bearing surface wear or taper junction fretting wear separately.

Maxian, Brown et al. (1996) developed a whole-gait-cycle wear formulation that explicitly coupled polyethylene contact stresses and sliding distances to estimate polyethylene wear of three different femoral head sizes in THRs. Hip resultant loads from a validated gait analysis were used in the ABAQUS FE model to determine contact stress distributions on the PE bearing surface while sliding distances were obtained from obtained kinematics. The wear rates were then calculated through Fortran using $H = K_w p S$ where H is the wear depth, K_w is the wear coefficient, p is the contact stress and S is the sliding distance. The wear coefficient employed in this study was $1.067 \times 10^{-9} \text{ MPa}^{-1}$. The femoral head was assumed as rigid and did not have any wear losses. The numerical wear model

modelled up to 1 million cycles of walking and calculated a volumetric wear rate between 13 – 18mm³/Mc.

Teoh, Chan et al. (2002) developed a new computational model based on an elasto-plastic finite element model for the assessment of wear. In this study, an elasto-plastic material behaviour for the PE was proposed instead of purely elastic load stress characteristics. The yield stress of UHMPWE was set to be 8MPa, approximately 20% lower than the maximum yield stress of the material. The model dictates that any stresses in excess of 8 MPa will be redistributed to its neighbour and an increased area of high stresses is expected. Wear prediction utilised a form of Archard's wear law which incorporated the influences of contact stress, sliding distance and a surface wear coefficient. The wear coefficient employed in this study was $1.067 \times 10^{-9} \text{ MPa}^{-1}$, same as the study by Maxian, Brown et al. (1996). The new model proposed predicted significantly higher volumetric wear rates of 57mm³/yr, however, it is well within the average reported clinical values.

Bevill, Bevill et al. (2005) investigated the effects of femoral head size, liner thickness, and femoral head-liner clearance on linear and volumetric creep and wear in acetabular cups during a gait cycle. A parametric FE model of a femoral head contacting a polyethylene cup was modelled in ABAQUS v6.3 and creep and wear simulation was performed up to 1 million cycles. The femoral head was modelled as a rigid body; no wear will be applied onto the femoral head. The study found that liner creep occurred quickly and increased the predicted contact areas by up to 56%, subsequently reducing contact pressures by up to 41%. Greater creep penetration was found with smaller heads, thicker liners, and larger clearance. The volumetric wear rate of the PE liner was found to be between 12 – 19.5mm³/yr for femoral head sizes between 22mm and 36mm.

Kang, Galvin et al. (2006) developed a fully contact-coupled wear model based on the simple constrained column model for the contact mechanics analysis and to perform parametric studies on the clearance and the femoral head radius for both UHMWPE and XLPE bearing liners in THRs. The wear model was based on the classical Archard—Lancaster equation in common with all other studies reported in the literature. A wear coefficient of $1.066 \times 10^{-9} \text{ MPa}^{-1}$ was employed and the model was simulated for up to 20 million walking cycle. The volumetric wear rate was found to be $4.26 - 7.02 \text{ mm}^3/\text{yr}$ for the XLPE bearing liner.

Queiroz, Oliveira et al. (2013) investigated the effects of lateral tilt on the wear of PE liners in THRs. The study modelled the UHMWPE acetabular cup and CoCr femoral head in ANSYS 12.0 with a 0.1mm clearance between the bearing surfaces. An adaptation of the Archard equation was used to determine the abrasive wear of acetabular cups in UHMWPE as a function of their lateral tilts in relation to the coronal plane. Numerical simulations performed with acetabular cups at tilt angles of 30° , 45° , and 60° presented respectively linear wear of 0.19 mm, 0.17 mm, and 0.26 mm per year, and volumetric wear of 30.85 mm^3 , 30.97 mm^3 , and 47.41 mm^3 , for the same period. The result of the study suggests that acetabular cups assembled at 45° present lower linear wear rates, whereas a significant increase in the volumetric wear rate is obtained for sets positioned at tilts above 45° .

Pakhaliuk, Polyakov et al. (2015) aimed to improve the method of wear simulation of the THR bearing couple comprising of UHMWPE by taking into account the parametric dependence of wear factor on the contact pressure that has not been studied before. The study modelled the components within ANSYS v12.0 and subjected them to the loading and angular motions based on the ISO 14242-1 demands. Wear calculation was based on

the classical Archard-Lancaster equation with a variable wear coefficient. Two formulas for the variable wear coefficients were proposed. The volumetric wear calculated from the variable wear coefficients was then compared to volumetric wear rates with a fixed wear coefficient. For the fixed wear coefficient of $1.066 \times 10^{-9} \text{ MPa}^{-1}$, the volumetric wear rate was found to be $24 \text{ mm}^3/\text{Mc}$ while the variable wear coefficient calculated a wear rate of $23.6 \text{ mm}^3/\text{Mc}$ and $35.2 \text{ mm}^3/\text{Mc}$.

Lin, Wu et al. (2016) investigated wear behaviours of THRs with various abduction angles. A CoCr femoral head and 8mm UHMWPE bearing liner were modelled and subjected to 0.75 million gait cycles. A wear coefficient of $1.48 \times 10^{-9} \text{ MPa}^{-1}$ was employed to calculate the linear and volumetric wear of the bearing liner. The results reveal that the THR with larger abduction angles may produce deeper depth of wear but the volume of wear presents an opposite tendency.

Uddin and Zhang (2013) aimed to obtain an in-depth understanding of the wear of hard-on-hard bearing couples. A finite element hip model is established which considers a complete 3D physiological gait loading and kinematic motions of normal walking. The wear at the bearing surface in gait cycles was calculated based on the contact stress variation from the finite element analysis and the sliding distance obtained from three-dimensional hip gait motions. The geometry of the worn surface was updated considering the average routine activities of a patient. Due to the same materials used on both bearing surfaces, the wear fraction of 0.5:0.5 was employed. The volumetric wear of CoC and MoM (CoCr/CoCr) were found to be $0.173 \text{ mm}^3/\text{yr}$ and $0.143 \text{ mm}^3/\text{yr}$.

Peng, Arauz et al. (2019) investigated the variation of polyethylene wear among THR patients and identified key kinematic and component orientation factors associated with wear performance. The study used patient-specific data such as joint force, cup

orientation, and patient range of motions to quantify PE wear. The patient-specific data were extracted from patients performing treadmill walking at self-selected speed under surveillance of validated DFIS technique. The FE model was created in ABAQUS v6.12 including the acetabular cup shell, PE liner, and CoCr femoral head. The patient-specific gait kinematics (axial, sagittal and frontal rotations) and component orientations were used to define the dynamic model, together with the scaled spatiotemporal force profile applied on the femoral head centre. The wear rate was calculated using Archard's equation for 1 cycle only. The wear rates were then multiplied by a factor of 1×10^6 to approximate 1 year of activity. Strong variations in volumetric wear rates (3.9 – 8.3mm³/Mc) and locations across subjects were observed with increased axial range of motion leading to accelerated wear rates. Acetabular component orientations are also significant predictors to wear locations.

Wegrzyn, Antoniadis et al. (2022) compared PE wear between dual mobility cup and conventional acetabular component between both UHMWPE and XLPE bearing liners. A finite element model was developed in ABAQUS for each of the components, a dual mobility cup with a 22.2-mm-diameter femoral head against UHMWPE or XLPE (DM22PE or DM22XL), a conventional cup with a 22.2-mm-diameter femoral head against UHMWPE (SD22PE) and a conventional cup with a 32-mm-diameter femoral head against UHMWPE or XLPE (SD32PE or SD32XL). A patient-specific musculoskeletal model was used to model the kinematics up 1 million cycles. Archard's wear law was used to predict PE wear from contact pressure and sliding distance, with wear coefficients for UHMWPE and XLPE to be $1.066 \times 10^{-9} \text{ MPa}^{-1}$ and $2.13 \times 10^{-10} \text{ MPa}^{-1}$ respectively. It was found that DM22PE produced 4.6 times and 5.1 times more volumetric wear than SD32XL and DM22XL. However, even if significant, the differences in volumetric wear between

DM22XL and SD32XL as well as between DM22PE and SD22PE or SD32PE were small and could be therefore considered as clinically negligible.

In the following studies, the taper junction fretting wear has been modelled.

English, Ashkanfar et al. (2015) proposed a computational methodology utilising an energy wear law and a 3D finite element model to predict fretting wear at the taper junction. The study modelled a CoCrMo femoral head coupled with a Ti6Al4V femoral stem in ABAQUS v6.13 up to 5 million walking cycles. Instead of the traditional Archard's wear law, the study proposed using an energy wear law which bases the calculation of volumetric wear on the interfacial shear work being the predominant parameter determining wear. The energy wear approach unifies prediction of wear across a wider range of stroke than Archard and as such has a greater range of application. This study has a novel method which simulates the weakening of the initial taper 'fixation' due to wear from assembly impaction during surgery. A wear fraction was also employed to remove wear based on the differences in material properties, which here is 0.9:0.1 for CoCrMo: Ti6Al4V. The study found the volumetric wear rate range to be 0.329 – 0.603mm³/yr and 0.024 – 0.065mm³/yr for the CoCrMo femoral head and Ti6Al4V femoral stem trunnion.

Using the same methodology, English, Ashkanfar et al. (2016) investigated the effect of varying assembly forces on fretting wear at the taper junction over a 10 year period. Assembly forces between 160N and 6000N were used to investigate the amount of fretting wear seen. It is demonstrated that an increase in assembly force results in a reduction in fretting wear and it is recommended that surgeons should apply an impact force of at least 4000N to minimise wear rates.

Ashkanfar, Langton et al. (2017) also investigated the manufacturing tolerances at the taper junctions. The study investigated the effects of varying taper mismatches on the volumetric wear rates and wear damage at this junction and determined the optimum tolerances that could minimise wear rates. A 3D FE model of the femoral head and stem was modelled in ABAQUS v6.14 with a perfectly matched taper and varying taper mismatches. A wear algorithm was used to apply the wear onto the components. It was found that a large taper mismatch (e.g. 9.12') results in a high wear rate ($2.960\text{mm}^3/\text{Mc}$). It is recommended that the cone angles of femoral head and femoral trunnion should be manufactured to produce a taper mismatch of less than 6' at the taper junction.

Another study by Ashkanfar, Langton et al. (2017) investigated the effect of different trunnion designs on the wear rates at the taper junction. The study investigated whether a micro-grooved trunnion surface finish would improve the fixation and the effect this would have on the wear rates. A 3D FE model of the femoral head and femoral stem was modelled in ABAQUS v6.14. The study first compared initial fixation of the taper surface between a Ti micro-grooved trunnion and a smooth trunnion mated with a CoCr femoral head with a smooth taper. The fixation at the taper junction was found to be better for the smooth couplings. Secondly, the study investigated the wear evolution between the models and found that over a 7 million load cycle analysis in-silico, the linear wear depth and the total material loss was around 3.2 and 1.4 times higher for the femoral heads mated with micro-grooved trunnions. The study concluded that the smooth taper and trunnion surfaces will provide a better fixation at the taper junction and therefore reduce the volumetric wear.

Norman, Denen et al. (2019) investigated the effect of increasing head size on the trunnion stress using an FE analysis of a Ti femoral stem coupled with four CoCr femoral

head sizes (28mm, 32mm, 36mm and 44mm). The FE models were then subjected to four different loading cases, single legged stance, stumbling, average stairclimbing, and maximum force stairclimbing. The study found that trunnion stresses increase as head sizes increases, thus increasing the horizontal lever arm and trunnion load offset. The findings suggest that the use of larger femoral heads should be avoided as it may results in higher implant stresses under certain loading conditions.

Donaldson, Coburn et al. (2014) performed a stochastic investigation of key parameters on the mechanics of femoral head-neck contact, specifically, the relative sensitivity of mechanical fretting to a set of eight design variables. A CoCrMo femoral head and Ti femoral stem trunnion was modelled in ANSYS 14. Four-hundred parameter sets were simulated using realistic variations of design variables, material properties and loading parameters to predict contact pressures, micromotions, and fretting work over cycles of gait. Of the eight design variables investigated, results indicated that fretting work was correlated with only three parameters: taper angular mismatch, centre offset and body weight. Maximum contact pressure at the taper increased by 85MPa for every 0.1° of angular mismatch. Maximum micromotion increased by 5 μm per 10 mm additional head offset and 1 μm per 10 kg increased body weight. The study concluded that appropriate limiting of angular mismatch and centre offset could minimize fretting, and hence its contribution to corrosion, at modular connections.

A similar study performed by Dyrkacz, Brandt et al. (2015) also identified parameters which influence micromotion at the femoral head-neck taper junction. An FE analysis was performed with a 3D model of a Ti femoral stem trunnion mated onto CoCr femoral head sizes of 28mm, 36mm, and 44mm. The study found that micromotion increased as the head size, assembly force and taper size increased. Furthermore, the study found that

micromotion increases when a mixed alloy material combination (CoCr/Ti6Al4V) was used instead of an all-CoCr alloy prosthesis.

K N, Ogulcan et al. (2020) investigated the wear rate on the head-trunnion taper junction for both trapezoidal, and circular shaped stems. In this study, a circular and trapezoidal-shaped stem implant is designed with a femoral head size of 28mm within ANSYS R19. At the time of assembly of the femoral head into the stem, the stresses were found to be increasing with an increase in the top surface radius of the neck taper junctions.

However, when the walking conditions are considered for wear estimation of implants, the circular implants with the 12/14 mm taper exhibited the lesser linear wear rate of 0.003 mm/year. The trapezoidal implants with the 10/14 mm taper exhibited a lesser linear wear rate of 0.032 mm/year. Overall, the circular implants exhibited lower wear rate results over the trapezoidal-shaped stem implants.

Messellek, Ould Ouali et al. (2020) investigated the mechanical behaviour within a modular taper junction subjected to cyclic loading. In this study, the fretting wear simulation was performed within ABAQUS using a modified Archard's wear law with the implementation achieved using a user-defined subroutine UMESHMOTION provided within the ABAQUS. A femoral stem with a Type 1 taper and its matching adaptor is modelled within ABAQUS with Ti6Al4V as the material used. A 4000N load was applied to assemble the taper adaptor onto the taper. The study found that a transition from a partial slip regime to a large slip one, which is mainly controlled by the contact slip amplitude, reduced the fatigue life and a critical slip value was identified.

Table 2-5: Summary of computational analysis for bearing surfaces in THRs

Authors	Method	Material combination	Loading	Volumetric Wear Rate (mm ³ /yr)	
				Acetabular cup	Femoral head
Maxian, Brown et al. (1996)	ABAQUS v5.3+ FORTRAN	CoCr/UHMWPE	LC: 1 million WF: 1:0	13 – 18	No wear
Teoh, Chan et al. (2002)	ABAQUS v5.7	CoCr/UHMWPE	LC: 1 million WF: 1:0 WC: 1.066×10^{-9} MPa ⁻¹	57	No wear
Bevill, Bevill et al. (2005)	ABAQUS v6.3 + Python	CoCr/UHMWPE	LC: 1 million WF: 1:0 WC: 1.066×10^{-9} MPa ⁻¹	12 – 19.5	No wear
Kang, Galvin et al. (2006)	Numerical study	CoCr/XLPE	LC: 20 million WF: 1:0 WC: 1.00×10^{-9} MPa ⁻¹	4.26 – 7.02	No wear
Queiroz, Oliveira et al. (2013)	ANSYS v12.0 + MATLAB	CoCr/UHMWPE	LC: 1 million WC: 1.00×10^{-9} MPa ⁻¹ WF: 1:0	30.85 – 47.41	No wear
Uddin and Zhang (2013)	ANSYS	Al ₂ O ₃ / Al ₂ O ₃ CoCrMo/CoCrMo	LC: 2 million WC: 2.00×10^{-10} MPa ⁻¹ (Al ₂ O ₃ / Al ₂ O ₃) 5.00×10^{-10} MPa ⁻¹ (CoCr/CoCr running in) 1.50×10^{-10} MPa ⁻¹ (CoCr/CoCr steady state) WF: 0.5:0.5	0.173 0.143	Not specified
Pakhaliuk, Polyakov et al. (2015)	MATLAB	CoCr/UHMWPE	LC: 3 million WC: 1.48×10^{-9} MPa ⁻¹ WF: 1:0	24.0	No wear
Lin, Wu et al. (2016)	Not specified	CoCr/UHMWPE	LC: 7.5 million (5 years) WC: 1.48×10^{-9} MPa ⁻¹ WF: 1:0	58.16	No wear

Peng, Arauz et al. (2019)	ABAQUS v6.12 + Numerical	CoCr/XLPE	LC: Based on patient evaluated SF: 1,000,000 WC: unspecified WF: 1:0	3.9 – 8.3	No wear
Wegrzyn, Antoniadis et al. (2022)	ABAQUS	CoCr/XLPE	LC: 1 million WC: 2.13×10^{-10} MPa ⁻¹ WF: 1:0	3.8 – 5.7	No wear

Table 2-6: Summary of computational analysis for taper surfaces in THRs

Authors	Method	Method	Findings
English, Ashkanfar et al. (2015)	ABAQUS	Study proposes a computational methodology utilising an energy wear law and a 3D finite element model to predict fretting wear at the taper junction.	Used to determine taper wear patterns, wear damage and wear rates which have been shown to be consistent with those found from observation and measurement of retrieved prostheses. The numerical method could be used to consider the effect of design changes and clinical technique on subsequent fretting wear in modular prosthetic devices
English, Ashkanfar et al. (2016)	ABAQUS	This study investigates the effect of varying the magnitude of the assembly force on fretting wear at the taper over a 10-year period using a 3D finite element model and wear algorithm	An increase in assembly force results in a reduction in fretting wear and it is recommended that surgeons should apply an impact force of at least 4kN to minimise wear rates.
Ashkanfar, Langton et al. (2017)	ABAQUS	This study, 3D finite element (FE) models of a commercial THR from a perfectly matched interface to large taper mismatches and a wear algorithm were used to investigate the extent of wear that could occur at this junction and identify the optimum tolerances to reduce the wear	large taper mismatch (e.g., 9.12') results in a high wear rate (2.960 mm ³ per million load cycles). It is recommended that the cone angles of femoral head and femoral trunnion should be manufactured to produce a taper mismatch of less than 6' at the taper junction.
Ashkanfar, Langton et al. (2017)	ABAQUS	3D finite element (FE) models of THRs to, firstly, investigate the effect of initial fixation of a Cobalt-Chromium femoral head with a smooth taper surface mated with a Titanium (1) micro-grooved and (2) smooth, trunnion surface finishes.	Concluded that smooth taper and trunnion surfaces will provide better fixation at the taper junction and reduce the volumetric wear rates.

Norman, Denen et al. (2019)	ABAQUS	Finite element stress analysis of CoCr/Ti femoral head/stem subjected to sever physiological loading conditions	Trunnion stress increases with increasing head size, increased horizontal lever arm, and trunnion load offset.
Donaldson, Coburn et al. (2014)	ANSYS 14	Stochastic FE simulation of the taper junction was performed to identify the key parameters that influence the contact mechanics between the taper surfaces.	Fretting work was correlated with angular mismatch, centre offset and body weight. Uncorrelated parameters included trunnion diameter, trunnion length and impaction forces
Dyrkacz, Brandt et al. (2015)	ABAQUS v6.10	To identify parameters which influence the micromotion at the femoral head taper junction of modular THRs.	The micromotion increased as the head size, assembly force, and taper size increased. CoCr/Ti6Al4V material combination also increased micromotion instead of CoCr/CoCr.
K N, Ogulcan et al. (2020)	ANSYS R19	Investigated both trapezoidal, and circular shaped stems on the wear rate on femoral head-stem taper junction	Overall, the circular implants exhibited less wear rate results over the trapezoidal-shaped stem implants. Due to the less linear wear rate, the circular implant has a higher life over the trapezoidal-shaped implant.
Messellek, Ould Ouali et al. (2020)	ABAQUS	improve the comprehension of mechanical behaviour within a modular taper junction subjected to cyclic loading.	Presented a methodology based on the finite element approach to study both fretting wear and fatigue, considering their interaction in the modular taper. Archard's law was employed to compute wear depth and volume loss. UMESHMOTION subroutine within ABAQUS used for geometry changes.

2.6. Discussion and rationale

Total Hip Replacements have been successful in restoring mobility to patients when the hip has become diseased or damaged, however, a number of these prostheses are known to have failed prematurely with one of the main reasons being wear. Wear is known to be one of the most significant and complicated mechanical failures that can occur. Within hip prostheses, wear occurs between contacting surfaces, namely between the bearing surface and femoral head, and between the femoral head taper surface and femoral stem trunnion. Wear leads to the deformation of these mechanical components which can lead to the loosening of these devices and ultimately, to THR failure. Furthermore, wear also produces debris into the surrounding tissues causing a biological reaction to occur leading to periprosthetic tissue destruction. This debris may also act as an abrasive within the articulating surfaces and cause increased amounts of wear. As demonstrated in this chapter, there is evidence that more investigation is needed to determine the cause of failure within these implants.

The review presented in this chapter reveals possible gaps within the literature for prediction of wear in THRs and wear modelling. These gaps are:

- Long term effects of current and new designs of THRs remain unknown. Currently, for newer designs of THRs, there is no data on long term survivability as their long-term behaviour *in vivo* would need to be in service for a period of time before data can be established. Experimental simulations are able to provide an insight into long term behaviour, however, these simulations are limited based on the loading conditions, time needed and cost. Furthermore, only a limited number of tests can be carried out for a specific design and therefore it cannot be used for all the parameters that may affect the wear evolution at the contacting surfaces.

- Variable wear coefficients. Wear coefficients are known to change as time increases due to a number of variables such as surface characteristics, material geometry, and lubrication. Accurate wear coefficients occurring within a THR prosthesis are yet to be determined.
- Currently, a number of experimental and computational wear investigations have been proposed, however, there is a lack of a user friendly, all in one, computational wear approach reported in the literature.
- Lack of both bearing surface and taper junction wear investigation within the same analysis. Many of the investigations into the wear of THRs only focus on either the bearing surface or the taper junction.
- There is currently a lack of research into the survivability of prostheses under different types of activities. For instance, the assessment of the activities allowed post-THR is mostly based on the impact of the activity itself and is based on the opinions of surgeons.

The overall aim of this research in this field is to develop longer lasting prostheses which will be able to last the lifetime of patients without failures. Furthermore, patients implanted with total hip or knee prostheses are advised to only perform low impact activities such as swimming, walking, or golf which would not be satisfying for patients who wish to continue with an active lifestyle. This aim is achievable by further research and investigation to develop the design of these prostheses to increase the longevity with better performance in service to provide higher functionality.

Increasing the longevity of such implants has both economic and surgical benefits as a hip revision surgery is more costly than a primary hip replacement surgery and carries a higher risk of multiple surgical risks as it has higher levels of complexity. Reducing the

number of revisions will also help to minimise the input of resources such as equipment and finance from relevant health authorities.

To increase the longevity of these implants, being able to predict the extent of wear within these devices is vital to investigate the mechanisms behind their failures. The main aim of this research is to introduce a new methodology to predict wear at the contacting surfaces of a modular hip prosthesis using FE analyses. A comprehensive wear model is proposed in Chapter 3 to bridge the gaps between experimental and computational analysis to further streamline the design of these devices. The method is used in different studies between Chapters 4 and 7 to investigate the long-term performance of hip prosthesis implants in service considering different parameters affecting wear. The following objectives are met in order to achieve this goal.

- The method proposed in Chapter 3 could predict wear on two sets of contacting surfaces within the same analysis.
- The method is user-friendly so that it may be used in different parametric studies. Automation of the method is performed using a graphical user interface (GUI) within the ABAQUS FE work package.
- The wear algorithm is capable of considering different activities concurrently throughout the analysis.
- The method is capable of considering varying wear coefficients during the wear analysis, for when there is data on the changing wear coefficients throughout the lifespan of a THR prosthesis.

2.7. Conclusion

This chapter has presented a description of the human hip joint and the disorders which may arise followed by a detailed explanation on the need for total hip replacements. A total hip replacement procedure is detailed along with different designs and material combinations of a modular hip prosthesis. An overview of the reasons for THR failure is described with wear being one of the main factors. A comprehensive review of wear within THRs, including the different wear mechanisms and theoretical approaches was discussed. A comprehensive review on the current experimental and computational methods to predict and investigate wear proposed in the literature is presented.

Finally, a discussion on the gaps in current research, the overall aim of the present study and the considerations of the proposed methodology were presented. This study attempts to close these gaps by developing a wear model that is explained in Chapter 3, with illustration of four different studies following in Chapters 4,5,6 and 7.

Chapter 3

Computational method of wear prediction at contacting surfaces in total hip replacements

3.1. Introduction

In this chapter, a 3D model of a commercial total hip prosthesis is used to demonstrate the methodology and to highlight key features of a bespoke wear algorithm. The model, together with the wear algorithm, can be used to effectively study certain aspects of hip prosthesis design such as femoral head size, patient activity such as bicycling, and patient variables, such as body weight. The method presented in this chapter can subsequently be used to identify key factors leading to wear related failures at both bearing surfaces and taper junction so that appropriate prosthesis design, clinical and surgical recommendations can be made to improve the prosthesis lifespan. The method proposed

is also independent of model geometry and can be used for any FE models (not only prosthetic devices) to predict wear. The method and the FE models that are to be explained in this chapter will be, unless stated otherwise, the main analysis implementations for chapters that follow (Chapter 4,5, and 6).

3.2. Theoretical Wear Calculation

As discussed in section 2.5.1, the energy wear approach considers the interfacial shear work as the main parameter controlling wear modelling. Current literature has considered the energy wear approach to be superior to the Archard's wear law due to its ability to facilitate different wear mechanisms. Currently, this method is capable of considering both approaches based on the analysis needs. The theoretical approach and implementation for both the wear laws to the FE analysis are described within this section.

3.2.1. Dissipated Energy Wear Law

The energy wear law equation, Equation (11), bases the calculation of volumetric wear on the interfacial shear work being the predominant parameter of determining wear. It shows that the total volumetric wear (W_v), is equal to the product of the energy wear coefficient (α) and total local dissipated energy (E).

$$W_v = \alpha E \quad (11)$$

Equation (12) shows that the total local dissipated energy (E), can be found by the product of shear traction (Q) and the relative displacement (s) between the contacting surfaces.

$$E = Qs \quad (12)$$

Substituting Equation (12) into Equation (11) gives:

$$W_v = \alpha Qs \quad (13)$$

By dividing both sides of the equation by a contact area, the linear wear depth (W_d), can be calculated using Equation (14), where τ is the contact surface shear stress.

$$W_d = \alpha \tau s \quad (14)$$

To accurately model the effect of wear during a dynamic loading cycle, it is necessary to discretise the loading cycle into a number of time intervals (n). As such, the wear depth for a single loading cycle (W_c), can be calculated using Equation (15), where τ_i and s_i are the surface contact shear stress and relative displacement respectively, at each time interval, i .

$$W_c = \sum_{i=1}^n \alpha \tau_i s_i \quad (15)$$

As the wear analysis would need to be performed over millions of cycles, a scaling factor (β) needs to be introduced to make the execution of the analysis achievable in an acceptable time. The scaling factor is used to multiply the wear calculated after a single analysis (one walking step) to modify the surface geometry by a suitable amount to facilitate acceptable run times. The total wear depth that is generated over a specified total number of loading cycles, N , can be determined from Equation (16), where j represents a specific 'analysis stage' reflecting the evolution of wear.

$$W_c = \sum_{j=1}^{(N/\beta)} \beta \sum_{i=1}^n \alpha \tau_{i,j} s_{i,j} \quad (16)$$

The scaling factor used can vary across a large range. A large scaling factor would result in a faster computational run time but may affect the accuracy of the results. A small scaling

factor would increase the computational run time but should provide a greater accuracy of results. Hence, the scaling factor needs to be optimised to ensure the accuracy of the results within an acceptable time frame. The optimal scaling factor has been investigated and explained later in section 3.8.3.

3.2.2. Archard's Wear Law

The Archard's wear equation, Equation (17), is based on the calculation that volumetric wear is proportional to the work done by frictional forces. It shows that the total volumetric wear (W_v), is equal to the product of the dimensional Archard wear coefficient (K), contact force (F), and relative slip (s).

$$W_v = KFs \quad (17)$$

Linear wear depth can be calculated by dividing Equation (17) with the contacting area, giving Equation (18), where P is the normal contact pressure.

$$W_d = KPs \quad (18)$$

Similar to the energy wear law, the cyclic wear depth (W_c) can be derived by discretising the loading cycle into a number of time intervals (n), and by introducing a scaling factor (β), the analysis would be achievable in an acceptable time. As such, the wear depth for a single loading cycle (W_c), can be calculated using Equation (19), where P_i and s_i are the surface contact pressure and relative displacement respectively, at each time interval and j represents a specific 'analysis stage' reflecting the evolution of wear.

$$W_c = \sum_{j=1}^{(N/\beta)} \beta \sum_{i=1}^n K P_{i,j} S_{i,j} \quad (19)$$

The Archard's wear method is an option within the algorithm to be considered by the user during the wear analysis by a graphical user interface (GUI) in ABAQUS.

3.3. Wear implementation

The cyclic wear depth obtained from either Archard's or Dissipated Energy wear law in the form of Equation (16) and Equation (19) can be used in conjunction with the FE analysis to predict wear depth. The FE analysis can produce the relative displacement, contact shear stress and contact pressure, and when coupled with a suitable wear coefficient, is able to calculate the cyclic wear depth at the contact surfaces of the FE model.

Using the Dissipated Energy wear law in the form of Equation (19), the contact shear stress will need to be extracted. Within the output database file, the surface contact shear stress is calculated in the form of *CSHEAR1* and *CSHEAR2* where they are the relative contact shear stress in direction 1 and direction 2. The resultant contact shear stress ($\tau_{i,j}$) can be calculated by:

$$\tau_{i,j} = \sqrt{CSHEAR1_i^2 + CSHEAR2_i^2} \quad (20)$$

where i and j represents the time interval and analysis stage respectively.

Using the Archard wear law in the form of Equation (16), the contact pressures needed for the wear prediction will need to be extracted from the FE analysis. Within the output database file, the surface contact pressure can be directly extracted from the FE analysis in the form of *CPRESS*, $P_{i,j}$.

For both the Archard and Dissipated energy wear laws equations, the relative displacement will need to be obtained. The FE results file for nodal displacement is given in the form of *CSLIP1* and *CSLIP2* where they are the relative tangential motion in direction 1 and direction 2. The total nodal displacement for the time interval (s_i) can be calculated by:

$$s_i = \sqrt{CSLIP1_i^2 + CSLIP2_i^2} \quad (21)$$

As s_i is the total nodal displacement, the relative displacement will need to be calculated. To calculate the relative nodal displacement ($s_{i,j}$), the difference in s_i values will need to be calculated for the time interval of the analysis, where i is the current time interval.

$$s_{i,j} = |s_{i+1} - s_i| \quad (22)$$

To apply the wear depth onto the respective surfaces, groups or pairs of nodes will need to be created. This 'pairing' of nodes is achieved by determining which nodes on opposite mating surfaces are closest to each other at each time interval. The pairing is achieved by taking a node at the surface with the coarser mesh (Surface A) and determining which nodes are closest on the opposing surface (Surface B) (see Figure 3-1 and Figure 3-2)

At the articulating surfaces, there is a relatively large displacement and as such, node pairings between articulating surfaces will need to be paired to a cloud of nodes due to different mesh densities (see Figure 3-1): A node from 'Surface A' needs to be paired to a cloud of nodes on 'Surface B' due to different mesh densities on the surfaces. This will avoid any nodes on 'Surface B' being 'missed' which would cause wear to not be applied at the node and ultimately cause sharp areas on the surfaces of the components. At the taper junction, as there is only a relatively small amount of displacement due to fretting wear, a single node to node pairing is sufficient (see Figure 3-2).

This technique is novel as it addresses the different mesh densities on the interaction surfaces to evenly apply wear across their respective surfaces. In this study, both options for node pairings are available to the user within the wear implementation depending on the analysis requirements.

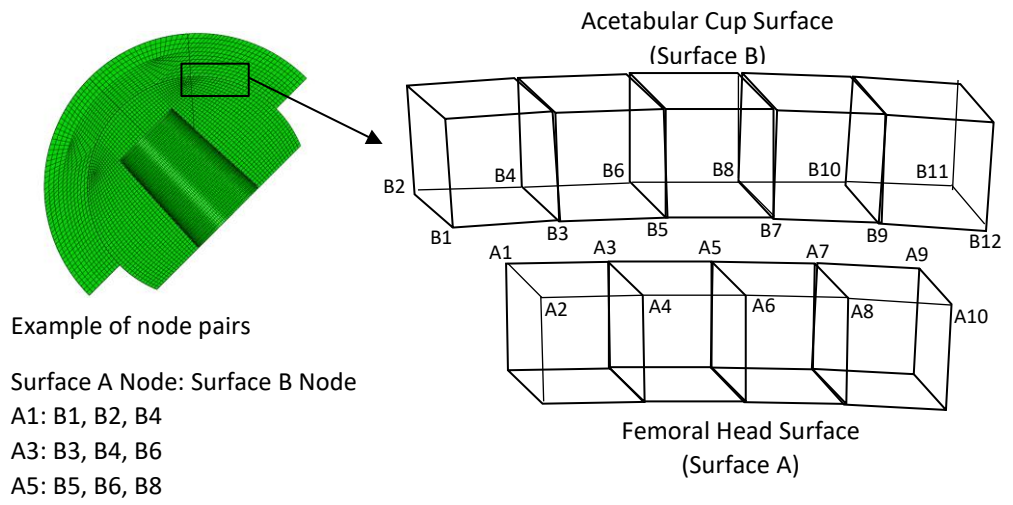


Figure 3-1: 1-to-3 node pairing implementation

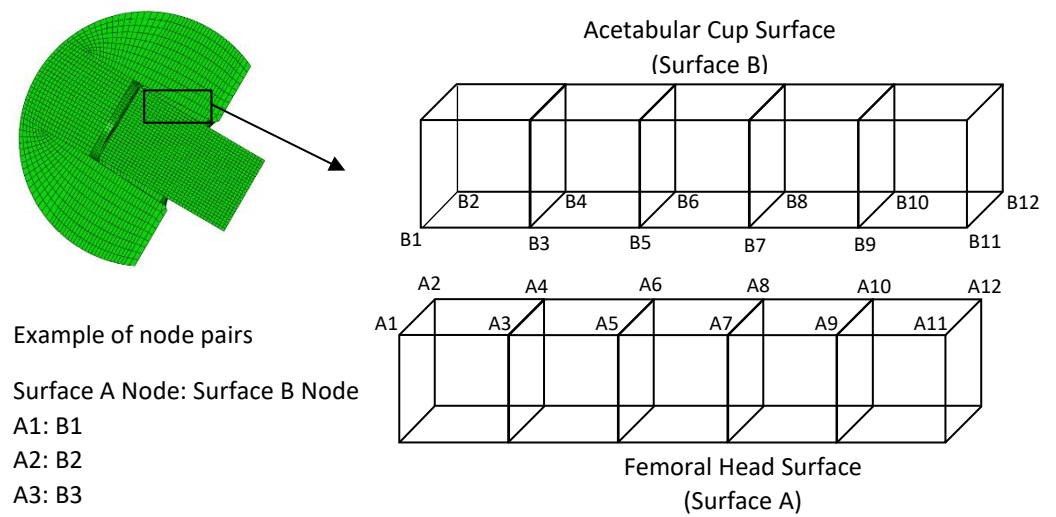


Figure 3-2: 1-to-1 node pairing implementation

3.4. Finite Element Implementation

3.4.1. Material Properties and Interaction Behaviour

For this study, a commercial THR is modelled consisting of a Titanium alloy (Ti) acetabular cup, highly cross-linked polyethylene (XLPE) bearing liner, Cobalt-chromium alloy (CoCrMo) femoral head and Titanium alloy femoral stem. The material properties of Ti, CoCrMo and XLPE assigned to the individual components are shown in Table 3-1. All components were modelled as deformable and linearly elastic in ABAQUS.

Table 3-1: Material Properties for THR

Material	Young's Modulus (GPa)	Density (kg/m ³)	Poisson's ratio	Reference
Ti-6Al-4V	114	4430	0.34	Bhalekar, Smith et al. (2020)
Co-28Cr-6Mo	210	7800	0.3	Gao, Hua et al. (2018)
XLPE	1	963	0.4	Anissian, Stark et al. (1999)

The contact interaction between both the bearing surfaces and taper junction was modelled as 'finite sliding' using the 'penalty' contact formulation in ABAQUS. The associated friction coefficient is dependent on several factors such as material combination, surface finish and surface cleanliness. Values for the friction coefficient at different total hip prosthesis bearing surfaces and modular taper have been documented by Fessler and Fricker (1989) and Wang, Ge et al. (2010). For this study, a constant isotropic coefficient of friction is defined on the FE models as shown in Table 3-2

Table 3-2: Friction coefficient based on contacting surfaces

Material Interaction	Friction coefficient
Ti-6Al-4V – Co-28Cr-6Mo	0.21 (Fessler and Fricker 1989)
Co-28Cr-6Mo – XLPE	0.11 (Wang, Ge et al. 2010)

3.4.2. Wear Fraction

The wear methodology in this study can facilitate the proportion of wear based on the different material combinations based on the contacting surfaces. As explained in section 2.5.3, a 'wear fraction' is specified to allow for proportional wearing of the materials. As such, the wear depth removed from the component is calculated as the product of the component's 'wear fraction' and the total wear cyclic wear depth. The wear fractions associated with the individual contacting surfaces are specified in Table 3-3.

Table 3-3: Wear fraction specified for individual contacting surfaces

Material Interaction	Wear Fraction
Ti-6Al-4V – Co-28Cr-6Mo	0.10 Ti : 0.90CoCr (English, Ashkanfar et al. 2015)
Co-28Cr-6Mo – XLPE	0.99 XLPE : 0.01 CoCr (Anissian, Stark et al. 1999)

3.4.3. Finite Element Models

3D FE models of a commercial MoP THR were modelled with a Ti acetabular cup, an XLPE bearing liner, a CoCrMo femoral head and Ti femoral stem. The models have been modelled and assembled as a perfect fit with no clearance at the bearing surface, and zero taper mismatch angle at the taper junction.

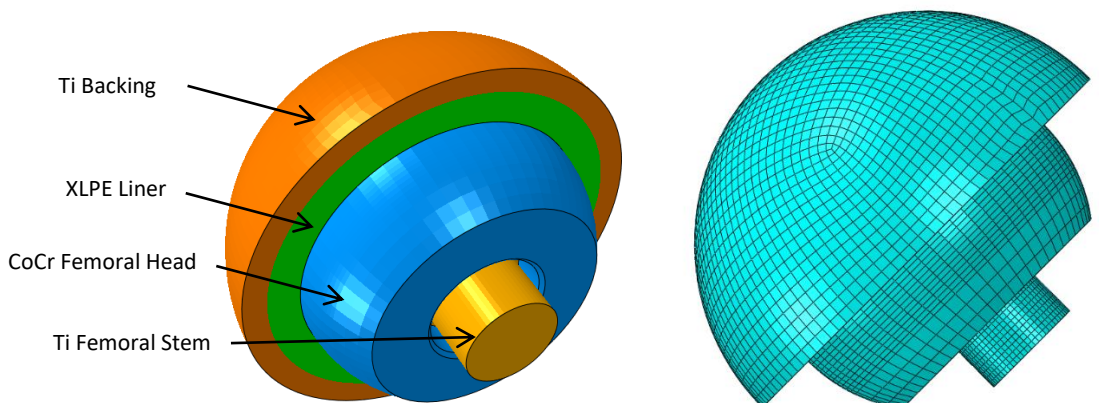


Figure 3-3: a) Assembled FE model b) Mesh assigned on 3D FE model

The acetabular cup, femoral head and femoral stem is assembled independently and then meshed in preparation for dynamic analysis in ABAQUS (2021 ABAQUS Inc, Providence, Rhode Island) using eight-node linear brick, reduced integration hourglass controlled elements (C3D8R).

3.4.4. Impaction Load

As previously explained in section 2.3.1, the femoral head and femoral stem are assembled during surgery using impaction. The loadings applied onto the model included an initial impact to simulate the assembly of the femoral head onto the femoral stem. A study by English, Ashkanfar et al. (2016) investigated the optimum impaction load needed to securely mate the femoral head onto the femoral stem and found that a minimum of 4kN of force was needed to ensure adequate mating between the two components. The measured impact duration for a polymer tipper impactor with a metal “test” head was measured as 0.7ms. The load-amplitude history obtained from the drop test are shown in Figure 3-4. To simulate the initial impaction for the component assembly in the FE model, the base of the femoral stem is fixed in all degrees-of-freedom and the impaction load is applied to the femoral head.

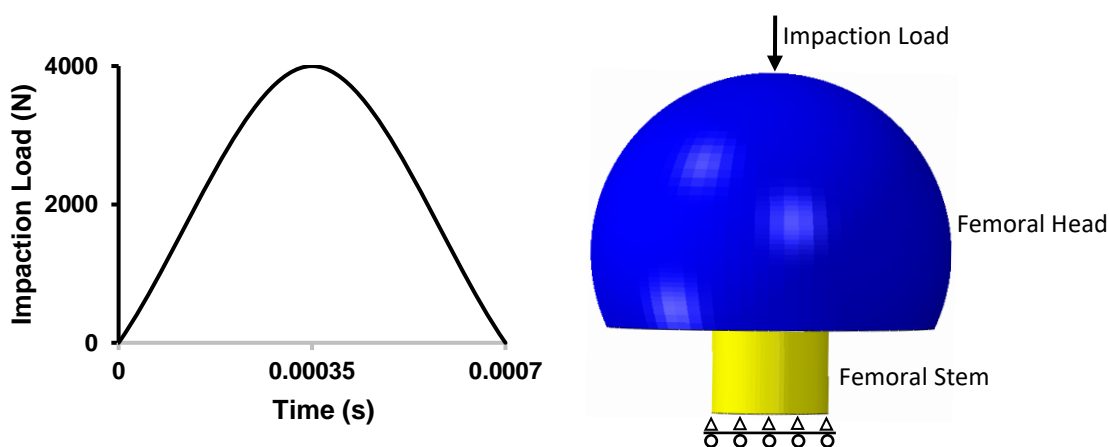


Figure 3-4: Impaction assembly load-time history

3.4.5. Loading and Boundary Conditions

To replicate a physiological walking cycle, the *in vivo* 3-dimensional hip joint loadings (Anterior-Posterior, Medial-Lateral, Superior-Inferior) (see Figure 3-5) and 3-dimensional hip rotations (Flexion-Extension, Internal-External, Adduction-Abduction) (see Figure 3-6) have been well documented in the literature (Bergmann, Graichen et al. 1993, Saikko, Ahlroos et al. 2001, Yoshida, Faust et al. 2006, Fialho, Fernandes et al. 2007, English, Ashkanfar et al. 2015).

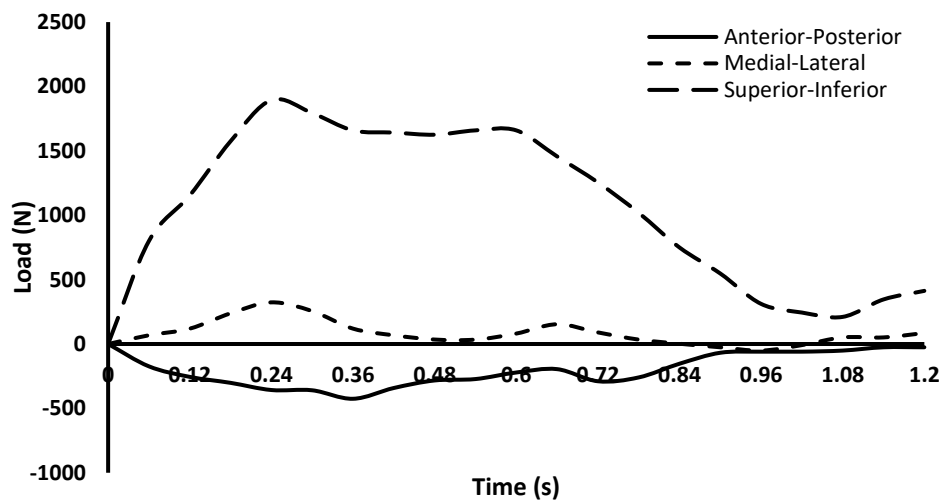


Figure 3-5: 3-dimensional hip joint loadings during a walking cycle

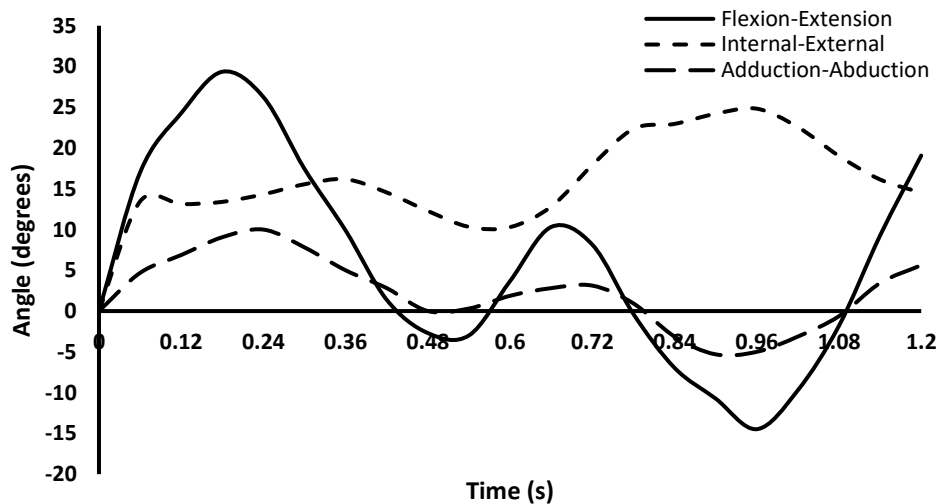


Figure 3-6: 3-dimensional hip joint rotations during a walking cycle

The loadings and boundary conditions ascribed to the 3D FE model during a walking cycle are shown in Figure 3-7. This includes both time variant rotations and loadings about the

three global coordinate directions. To model the walking cycle onto the 3D FE model of the hip prosthesis, the model replicates the conditions of a real hip prosthesis. The outer surface of the acetabular cup is modelled to be fixed which does not allow for movement. The loadings and rotations are applied to a point located at the centre of the femoral stem trunnion, where this point is coupled to the outer surface of the trunnion. The femoral head is allowed to move in all directions and rotations, with the femoral stem applying the loading and rotation. As such, the applied loadings and rotations on the femoral stem translate onto the femoral head.

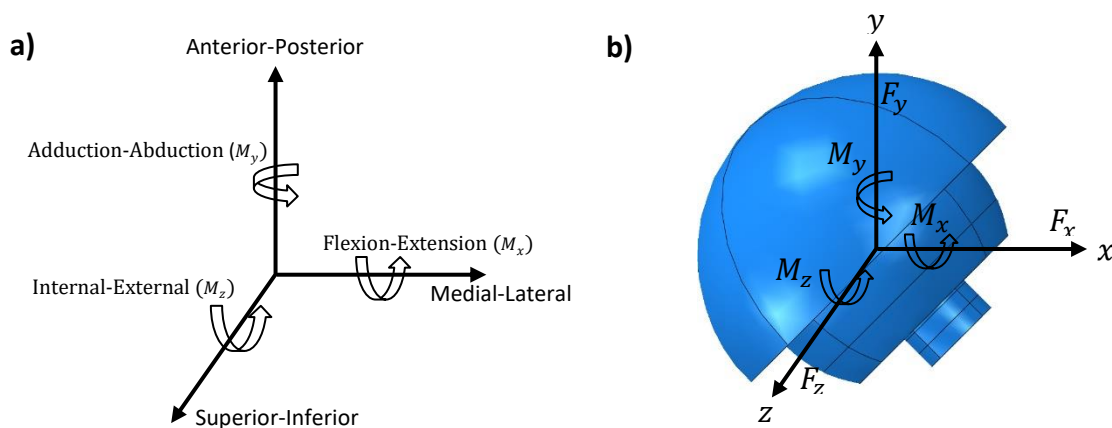


Figure 3-7: Loading and boundary conditions assigned onto the 3D FE model

Schmalzried, Szuszczewicz et al. (1998) previously performed a quantitative assessment of walking activity of 111 patients who have undergone various types of hip or knee replacements. Digital pedometers were used which indicated that on average, 910,310 steps were taken per year. The study had a varied group of patients in terms of age, activity and gender. For the purposes of this research, an average of 1 million walking steps per year has been assumed based on the work by Schmalzried, Szuszczewicz et al. (1998).

The walking cycle has been discretised into 10 equal time intervals during the 1.2 second walking cycle period. This number of time intervals has been investigated to be adequate to simulate the load-history for this study accurately.

In the chapters to follow, the studies will include an initial impact analysis to simulate the assembly of the femoral head onto the femoral stem before applying the time-variant loading and rotation cycles to simulate hip loadings during a walking cycle.

3.4.6. Applying wear onto the geometry

As the simulation progresses, the wear determined at each time interval is summed to provide a ‘cyclic’ wear depth which itself is scaled by β then proportioned by the wear fraction to provide the wear depth for the individual components.

The contact surface normal directions are then needed to apply the wear onto the individual components. Within the FE results file, the nodal contact tangent direction can be extracted in the form of *CTANDIR1* and *CTANDIR2* which are the local tangent directions of the node of the model. *CTANDIR1* and *CTANDIR2* is expressed in the form of a 3-dimensional vector. The resultant nodal vector (*CTANDIR*) of the node can be calculated through a cross product:

$$\vec{CTANDIR} = \vec{CTANDIR1} \times \vec{CTANDIR2} \quad (23)$$

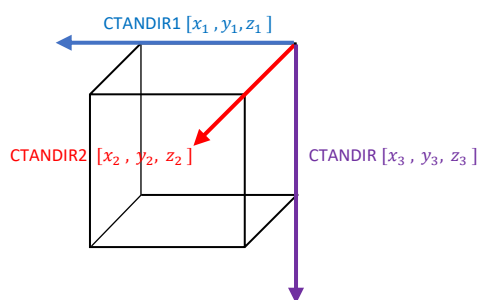


Figure 3-8: Visualisation of resultant nodal vector

Individual nodal wear of the components is then applied onto the components based on the paired nodes (by updating their coordinate positions) to create a new geometry for the analysis to resume. *CTANDIR* will need to be extracted for only the first time-interval as the wear will be applied on the first time-interval and calculated with every geometry update to account for changes during the wearing analysis.

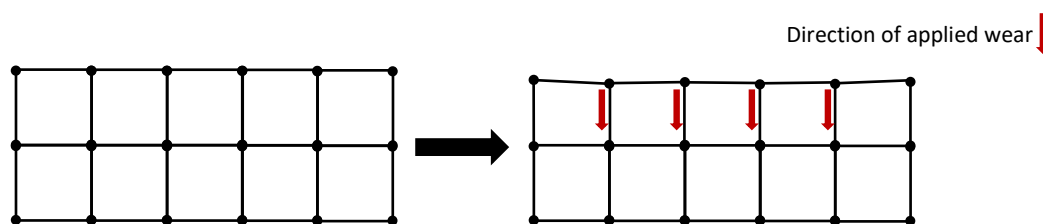


Figure 3-9: Applied wear depth direction

3.5. Computational Framework

The method to predict wear at the contacting surfaces of the hip prosthesis is explained in this section.

Initially, a model of the femoral head and femoral stem is assembled just into contact.

The model is then subjected to a dynamic impaction analysis as explained in section 3.4.4.

The average displacement of the individual parts is then extracted and imported into a new FE input file.

The femoral head and femoral stem is then assembled with an overlap based on the displacements from the impaction analysis. This creates an interference between the components at the contact interface, which accurately models the locking effect onto the taper junction. An implicit dynamic analysis is then defined with the walking loads and rotations applied onto the 3D model as explained in section 3.4.5.

Using the results from the FE analysis, the nodal contact stress and displacement at the contact surfaces is extracted and the wear depth can be calculated for a single walking

cycle as explained in section 3.2. This cyclic wear depth is then scaled up by a scaling factor, β , to provide a wear depth for the specific number of cycles and the wear is applied onto the part geometry as explained in 3.5.

The wear depth is then added into the results file to visualise the wear pattern. A new input file with the updated geometry is then created and the analysis repeats until the desired number of cycles is reached.

A flowchart illustrating the wear method presented in this chapter is shown in Figure 3-10. Within the flowchart, Interaction 1 comprises of the bearing liner and femoral head bearing surface, while interaction 2 comprises of the femoral head taper junction and femoral stem taper surface.

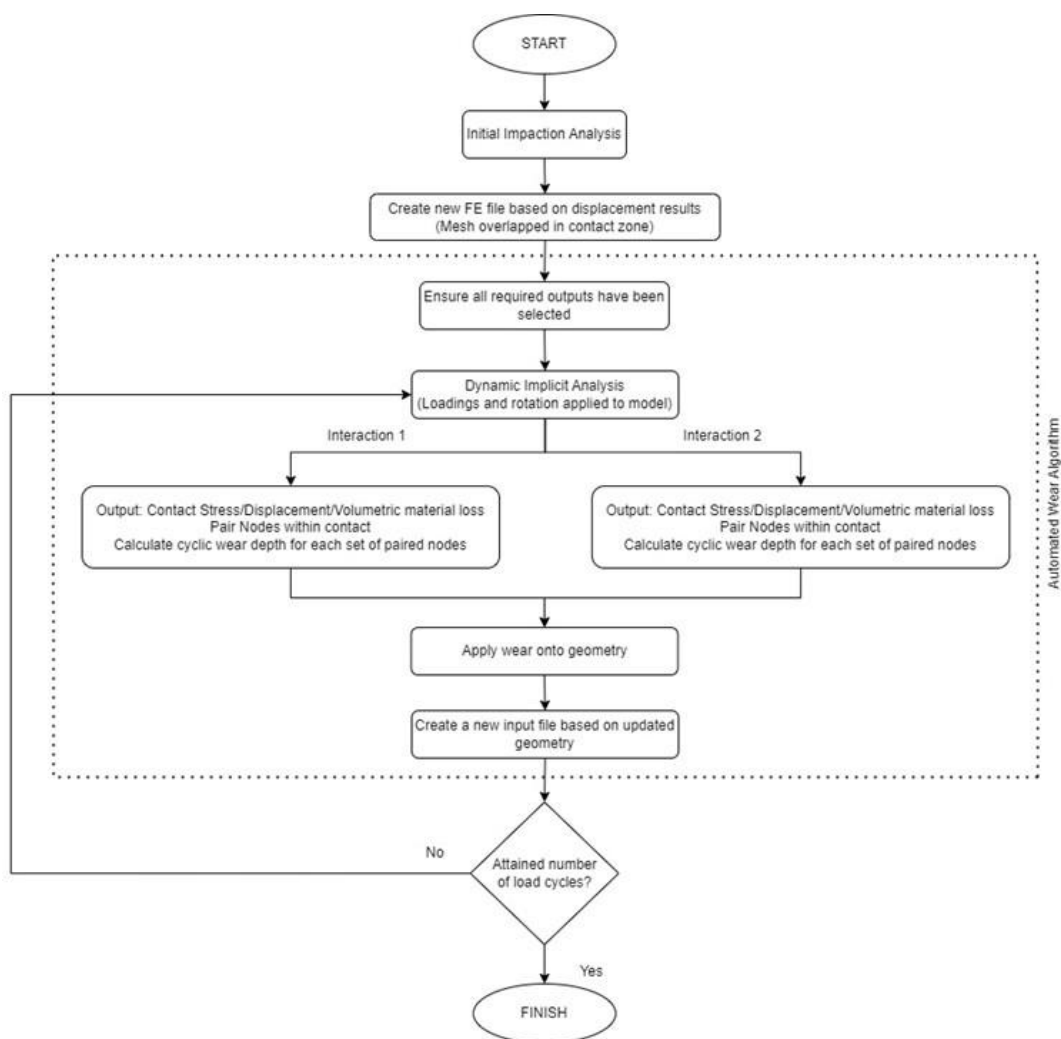


Figure 3-10: Flowchart illustrating method for wear prediction

3.6. Algorithms

Calculating wear for the paired nodes at the contacting surface and updating the geometry manually is time consuming and difficult. Consequently, the wearing process explained has been automated using a Python script linked within ABAQUS as a user plug-in. This has helped to develop a generalized wear algorithm that can be used for different studies and models.

The wear algorithm can be run straight from ABAQUS CAE (as a plug-in) after requesting initial input data from the user. Figure 3-11 shows the graphical user interface of the algorithm written in the ABAQUS Python environment to request input data from the user.

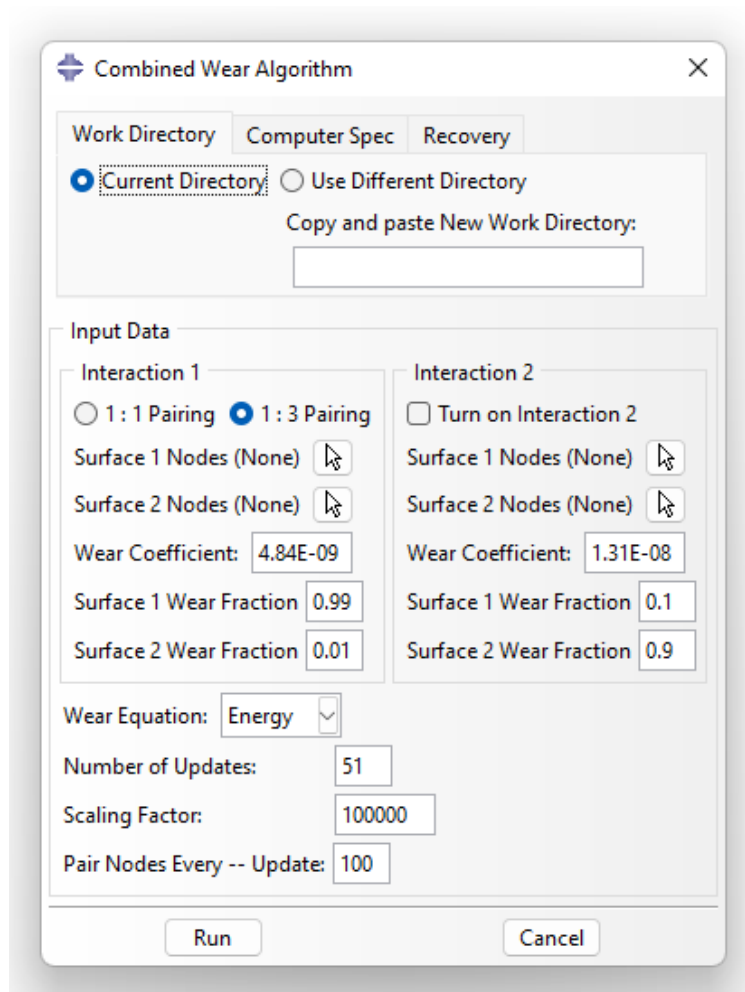


Figure 3-11: Graphical user interface (GUI) of the wear algorithm

After obtaining the input data from the user, the script initially checks through the initial FE input file to ensure that the required output variables have been selected and ensures that the input file has no errors. The initial FE input file is then submitted for analysis. At the end of the analysis, the data required for the wear calculation is extracted from the ABAQUS output database file (*.odb file), and the surface nodes are then paired to the closest nodes on the opposite surface. Using the paired nodes and the data extracted, the wear depth is then calculated and scaled up by the requested scaling factor. The normal directions of all contacting nodes are then calculated, and the wear depth is applied to the paired nodes by updating the coordinate positions to create the new geometry for the analysis. The normal directions for the nodes need to be calculated for each geometry update as they will change due to the wearing process.

The Python script contains a number of Python functions which are called through the “Kernel” in a main script function. In this section, these functions are described in detail.

3.6.1. Input requested from user

In order to run the wear algorithm within ABAQUS, the user will need to input initial data for wear modelling. This data can be provided in the graphical user interface (GUI) shown in Figure 3-11.

Function 1: *inputRequest*

Input: ABAQUS Dialog box builder

Output: Initial Data from user

1. Requested Data:
 2. WDIR: Work Directory
 3. CSPEC: Computer Specification for number of threads
 4. RECV: Recovery Option in the event of computer error
 5. On: Continue analysis from specified Job input file
 6. Off: Start Analysis from Job-1.inp
 - 7.
 8. INT1: Interaction 1 to be specified by user
 9. PT: Pairing Type
 10. 1:1 Pairing: Surface 1 nodes to be paired to closest Surface 2 node.
 11. 1:3 Pairing: Surface 1 nodes to be paired to closest 3 Surface 2 nodes.
 12. SS: Surface Sets
 13. INT1S1N: Nodes in contact for part 1
 14. INT1S2N: Nodes in contact for part 2
 15. INT1WC: Archard or Energy Wear Coefficient for Interaction 1
 16. WF1: Wear Fraction for Interaction 1
 17. INT1WF1: Wear Fraction for INT1 S1N
 18. INT1WF2: Wear Fraction for INT1 S2N
 - 19.
 20. INT2: Interaction 2 to be specified by user
 21. I2A: Activating Interaction 2
 22. SS: Surface Sets
 23. INT2S1N: Nodes in contact for part 2
 24. INT2S2N: Nodes in contact for part 3
 25. INT2WC: Archard or Energy Wear Coefficient for Interaction 2
 26. WF2: Wear Fraction for Interaction 2
 27. INT2WF1: Wear Fraction for INT2 S1N
 28. INT2WF2: Wear Fraction for INT2 S2N
 - 29.
 30. WM: Wear law to be used
 31. Archard: Archard Wear Equation
 32. Energy: Dissipated Energy Wear Equation
 - 33.
 34. UN: Number of update required
 35. SF: Scaling Factor for analysis
 36. PNU: Paired Nodes at every __ update
-

An ABAQUS input file, named 'Job-1.inp' (*.inp file), of the model will need to be generated in ABAQUS CAE prior to commencement. The default work directory has been set to the current ABAQUS work directory, the user may specify a different work directory if needed. The computer specification will need to be specified in the number of threads

required for analysis. A recovery option is embedded within the GUI which allows the user to restart from a specified job in the event of an error, or to change parameters within the study.

Parameters for the nodes in contact can be selected within the ABAQUS viewport in the mesh assembly module. The pairing type, nodes in contact, wear coefficient and wear fraction for the respective surfaces for both Interaction 1 and Interaction 2 (if activated) must also be assigned. The wear law to be used, number of geometry updates, scaling factor and number of times the nodes are to be paired will need to be specified for the program to run. All input data will be saved as variables, as shown in Function 1.

3.6.2. Main Algorithm

The inputs requests from the user in section 3.6.1. are then passed through the main algorithm which further refers and calls to functions within a “while” loop to execute the wear algorithm. This main algorithm is called by the “Kernel” in ABAQUS. Function 2 shows the main algorithm in the “while” loop, and the functions within the algorithm are further explained in later sections.

<i>Function 2: MainAlgorithm</i>	
1.	<i>Input: WDIR, CSPEC, RECV, INT1PT, INT1S1N, INT1S2N, INT1WC INT1WF1, INT1WF2, I2A, INT2S1N,</i>
2.	<i>INT2S2N, INT2WF1, INT2WF2, WM, UN, SF, PNU</i>
3.	<i>Output:</i>
4.	
5.	<i>Preprocessing</i>
6.	<i>GetInteractionNodes</i>
7.	<i>WearTotal</i>
8.	<i>While update < UN:</i>
9.	<i> Submit Job-[update] in ABAQUS</i>
10.	<i> Extract Values</i>
11.	<i> If update is 1 or specified pair nodes upate number:</i>
12.	<i> PairingNodes</i>
13.	<i> WearFunc</i>
14.	<i> WriteODB</i>
15.	<i> WriteINP</i>
16.	<i> Else:</i>
17.	<i> Abort all sequence and alert user to error.</i>

3.6.3. Pre-processing data

In order for the algorithm to proceed, the part names, translation matrix, rotation axis and rotation angle, are extracted from the initial input file for each individual part. The rotation values specified within the ABAQUS input file are in the form of axis-angle representation where the rotation in three dimensions is defined by its axis (a vector along this axis is unchanged by this rotation), and its angle (the amount of rotation about that axis by the Euler rotation theorem in radians).

An overall rotation matrix for the individual parts in the model is then derived by Equation (24) (Taylor and Kriegman 1994) where the rotation matrix (R) is rotated by angle (θ) around the unit vector axis $u = (u_x, u_y, u_z)$. The overall rotation matrix is then inversed so the initial positions of the model can be calculated at later stages of the analysis.

$$R = \begin{bmatrix} \cos \theta + u_x^2 (1 - \cos \theta) & u_x u_y (1 - \cos \theta) - u_z \sin \theta & u_x u_z (1 - \cos \theta) + u_y \sin \theta \\ u_y u_x (1 - \cos \theta) + u_z \sin \theta & \cos \theta + u_y^2 (1 - \cos \theta) & u_y u_z (1 - \cos \theta) - u_x \sin \theta \\ u_z u_x (1 - \cos \theta) - u_y \sin \theta & u_z u_y (1 - \cos \theta) + u_x \sin \theta & \cos \theta + u_z^2 (1 - \cos \theta) \end{bmatrix} \quad (24)$$

The function then also checks the initial input file for all required output database (ODB) field outputs for the program to run. If all required ODB field outputs are not selected, add the required ODB field outputs within the input file and run the initial analysis.

Function 3: Preprocessing

1. *Input: Job-1 input file*
 2. *Output: PN1, PN2, PN3, R1, R2, R3*
 - 3.
 4. *Search in the whole Job-1 input file*
 5. *Extract part names. PN1, PN2, (PN3, if applicable)*
 6. *Extract Translation matrix. T1, T2, (T3 if applicable)*
 7. *Extract Rotation axis and angle of individual parts. u1, u2, θ_1 , θ_2 , (u3 and θ_3 if applicable)*
 - 8.
 9. *Derive overall rotation matrix for individual parts. R1, R2, (R3 if applicable)*
 10. *Check input file for all required ODB outputs are included.*
 11. *If input file does not have required ODB outputs included:*
 12. *Add required ODB outputs and run Job-1*
-

3.6.4. Getting initial surface nodes in contact

From the interacting surface chosen by the user in section 3.7.1 (*INT1S1N*, *INT1S2N*, *INT2S1N*, *INT2S2N*), the nodal numbers are extracted into an array. The part names are then assigned onto each interaction surface, such as *INT1S1N*: “Bearing Liner” and *INT1S2N*: “Femoral head”. The rotation arrays extracted from section 3.7.2 are also assigned the part names.

Function 4: GetInteractionNodes

1. *Input: INT1S1N, INT1S2N, INT2S1N, INT2S2N*
 2. *Output:*
 - 3.
 4. *For all nodes picked from user input:*
 5. *Extract all nodal numbers into an array*
 - 6.
 7. *Assign PN1, PN2, PN3 to the respective interaction surfaces (INT1S1N, INT1S2N, INT2S1N, INT2S2N)*
 8. *Assign PN1, PN2, PN3 to the respective rotation arrays (R1, R2, R3)*
-

3.6.5. Extract data from ODB file

Results that are required by the wear algorithm are embedded within the ABAQUS results database file (*.odb). A number of variables required by the wear algorithm are extracted using Function 4. Firstly, the total number of frames present in the model and the step names are extracted. Data from the odb file is then extracted from all frames from the last step of the analysis.

The wear algorithm considers the chosen wear law in section 3.7.2, where if the Archard wear law was chosen, the contact pressure for all nodes at the interaction surfaces is extracted while the Dissipated energy wear law will extract *CSHEAR1* and *CSHEAR2* for all nodes at the interaction surfaces and calculate the resultant contact shear stress ($\tau_{i,j}$) using Equation (20) as explained in Section 3.3.

The relative nodal displacements are calculated from the extracted *CSLIP1* and *CSLIP2* and calculated using Equation (21) and Equation (22) as explained in Section 3.3. The 3-

dimensional resultant nodal vector (*CTANDIR*) is calculated through the extracted values of *CTANDIR1* and *CTANDIR2* as explained in section 3.4.6.

<i>Function 5: ExtractValues</i>	
1.	<i>Input: SSI, WM</i>
2.	<i>Output: CPRESS, $\tau_{i,j}$, $s_{i,j}$, $\overrightarrow{CTANDIR}$</i>
3.	
4.	<i>Open ODB file</i>
5.	<i>Extract Number of Frames (NF), Step Name (SN)</i>
6.	<i>For all frames in NF:</i>
7.	<i>If WM is Archard:</i>
8.	<i>Extract $K_{i,j}$ for INT1S1N, INT1S2N, INT2S1N, INT2S2N</i>
9.	<i>else If WM is Energy:</i>
10.	<i>Extract CSHEAR1 and CSHEAR2 for INT1S1N, INT1S2N, INT2S1N, INT2S2N</i>
11.	
12.	$\tau_{i,j} = \sqrt{CSHEAR1_i^2 + CSHEAR2_i^2}$
13.	
14.	<i>Extract CSLIP1 and CSLIP2 for INT1S1N, INT1S2N, INT2S1N, INT2S2N</i>
15.	
16.	$s_i = \sqrt{CSLIP1_i^2 + CSLIP2_i^2}$
17.	$s_{i,j} = s_{i+1} - s_i $
18.	
19.	<i>Extract CTANDIR1, CTANDIR2</i>
20.	$\overrightarrow{CTANDIR} = \overrightarrow{CTANDIR1} \times \overrightarrow{CTANDIR2}$
21.	

K_{i,j} : Contact pressure at time interval *i* at analysis stage *j*
τ_{i,j} : Contact shear stress at time interval *i* at analysis stage *j*
s_{i,j} : Relative nodal displacement at time interval *i* at analysis stage *j*
 $\overrightarrow{CTANDIR}$: 3-dimensional resultant nodal vector

3.6.6. Pairing nodes in contact

As explained in section 3.3, nodes in the contact area on one part will need to be paired to nodes on the other part (either paired to the closest node, or closest three nodes depending on the analysis requirements). This is facilitated by calculating the distances between the nodes in contact. The coordinates of all nodes in contact are firstly extracted, then the distance between the nodes on the other contact surface is calculated. Function 5 illustrates the process and returns an array which contains all paired nodes. After the nodes are paired, they are stored in the form of *[FN, INT1S1N, INT1S2N1, INT1S2N2, INT1S2N3, CWD]* where *INT1S1N* is the interaction 1 surface 1 node, *INT1S2N1, INT1S2N2, INT1S2N3* is the interaction 1 surface 2 node 1, 2, and 3 respectively, and *CWD* is the cyclic wear which will be calculated in section 3.6.7.

Function 6: PairingNodes

```
1.      Input: COORD
2.      Output: PN
3.
4.      Extract COORD for all INT1S1N, INT1S2N nodes
5.
6.      For all frames in the last step of ODB:
7.          If PT = "1:1 Pairing":
8.              For i in INT1S1N:
9.                  for j in INT1S2N:
10.                     x= INT1S1N[i]
11.                     y= INT1S2N[j]
12.                     distance= ||y-x||
13.                     if distance is smallest:
14.                         Pair node x with y
15.                         Store Paired node in the form of [FN, INT1S1N,
16.                            INT1S2N, 0, 0, CWD]
17.          else If PT = "1:3 Pairing":
18.              For i in INT1S1N:
19.                  for j in INT1S2N:
20.                     x= INT1S1N[i]
21.                     y= INT1S2N[j]
22.                     distance= ||y-x||
23.                     For the 3 smallest distance:
24.                         Pair node x with y
25.                         Store Paired node in the form of [FN, INT1S1N,
26.                            INT1S2N, INT1S2N, INT1S2N, CWD]
```

FN: Frame Number

INT1S1N: Interaction 1 Surface 1 node

INT1S2N: Interaction 1 Surface 2 node

CWD: Cyclic wear depth which will be calculated and stored in later stages.

Paired nodes are stored in form: [FN, INT1S1N, 1st closest INT1S2N, 2nd closest INT1S2N, 3rd closest INT1S2N, CWD]

3.6.7. Create a total wear

A total wear array is created to store all wear data from the extended analysis. This wear array will be updated throughout the analysis to update the maximum wear depth.

Function 7: WearTotal

```
1.      Input: -
2.      Output: WT
3.
4.      Create Arrays which will hold all Wear Data of extended analysis
```

3.6.8. Wear depth calculation

The wear depth at the paired nodes can be calculated based on either the Archard or the Dissipated Energy wear law as explained in section 3.2. Function 7 calculates the total wear depth for a set of paired nodes.

To be able to perform the wear depth calculation, a number of variables will first need to be calculated. From section 3.6.5, the node pair sets are in the form of: $[FN, INT1S1N, INT1S2N1, INT1S2N2, INT1S2N3, CWD]$.

The cyclic wear depth, CWD , is calculated using Equation (16) and Equation (19) based on the wear law chosen by the user. For the “1:3 Pairing” option, the average relative displacement, $s_{i,j_{AVG}}$, is taken from the 3 closest nodes from $INT1S2N1$, $INT1S2N2$, $INT1S2N3$ in the paired node set, as shown in Equation (25). For the “1:1 Pairing” option, the relative displacement is only taken from the 1st closest node, $INT1S2N1$.

$$s_{i,j_{AVG}} = \frac{s_{i,j_{S2N1}} + s_{i,j_{S2N2}} + s_{i,j_{S2N3}}}{3} \quad (25)$$

After extracting the relative displacement required for the wear equations, the cyclic wear depth for each time interval, CWD_i , is calculated using Equation (26) for the Archard wear law, and Equation (27) for the dissipated energy wear law.

$$CWD_i = INT1WC \times K_{i,j} \times s_{i,j_{AVG}} \quad (26)$$

$$CWD_i = INT1WC \times \tau_{i,j} \times s_{i,j_{AVG}} \quad (27)$$

CWD_i is then appended to the last element for the paired nodes sets, completing the population of the array. The total sum of all the CWD_i for $INT1S1N$ is then calculated using Equation (28).

$$Total\ cyclic\ wear\ between\ the\ paired\ nodes = \sum_{i=1}^n CWD_i \quad (28)$$

The wear depth for this stage of the analysis for surface 1, can then be calculated using the wear fraction, $INT1WF1$, total cyclic wear, and scaling factor, β shown in Equation (29).

$$INT1S1N WD = INT1WF1 \times \sum_{i=1}^n CWD_i \times \beta \quad (29)$$

For the nodes on surface 2, as they may be paired multiple times for each frame number, the average wear for the surface 2 node at each time interval is calculated, then the total wear sum of the cyclic wear for the analysis stage is obtained as shown in Equation (30). $\overline{INT1S2N1 CWD_i}$ represents the average wear for the surface 2 node at each time interval and $INT1WF2$ is the wear fraction for surface 2, and β is the scaling factor.

$$INT1S2N1 WD = INT1WF2 \times \sum_{i=1}^n \overline{INT1S2N1 CWD_i} \times \beta \quad (30)$$

Function 8: WearFunc

```

1.   Input: PT, WM,  $\tau_{i,j}$ ,  $S_{i,j}$ , INT1WC, INT1WF1, INT1WF2, INT1 Paired Nodes. INT2WC, INT2WF1,
2.   INT2WF2, INT2 Paired Nodes
3.   Output: INT1S1NWD, INT2SN1WD, INT2SN2WD, INT2SN3WD
4.
5.   Create individual surface wear arrays
6.
7.   PairedNodes format = [FN, INT1S1N, INT1S2N1, INT1S2N2, INT1S2N3, CWD]
8.
9.   For each line in INT1 Paired Nodes:
10.  if PT is "1:3 Pairing":
11.       $S_{i,jAVG} = \frac{S_{i,jS2N1} + S_{i,jS2N2} + S_{i,jS2N3}}{3}$ 
12.
13.  else if PT is "1:1 Pairing":
14.       $S_{i,jAVG} = S_{i,jS2N1}$ 
15.
16.  if WM is Archard:
17.       $CWD_i = INT1WC \times K_{i,j} \times S_{i,jAVG}$ 
18.      Append  $CWD_i$  onto the last element for PN array
19.
20.  else if WM is Energy:
21.       $CWD_i = INT1WC \times \tau_{i,j} \times S_{i,jAVG}$ 
22.      Append  $CWD_i$  onto the last element for PN array
23.
24.
25.  For each line in INT1 Paired Nodes:
26.      Calculate the sum of  $WD_i$  for INT1S1N from the last element of PN array
27.      Total cyclic wear between paired nodes =  $\sum_{i=1}^n CWD_i$ 
28.       $INT1S1N WD = INT1WF1 \times \sum_{i=1}^n CWD_i \times \beta$ 
29.
30.  For each line in INT1 Paired Nodes:
31.      For each frame number within Paired Nodes:
32.           $INT1S2N1 WD = INT1WF2 \times \sum_{i=1}^n \overline{INT1S2N1 CWD_i} \times \beta$ 
33.           $INT1S2N2 WD = INT1WF2 \times \sum_{i=1}^n \overline{INT1S2N2 CWD_i} \times \beta$ 
34.           $INT1S2N3 WD = INT1WF2 \times \sum_{i=1}^n \overline{INT1S2N3 CWD_i} \times \beta$ 
35.
36.  For each line in INT2 Paired Nodes:
37.  if PT is "1:3 Pairing":
38.       $S_{i,jAVG} = \frac{S_{i,jS2N1} + S_{i,jS2N2} + S_{i,jS2N3}}{3}$ 
39.
40.  else if PT is "1:1 Pairing":
41.       $S_{i,jAVG} = S_{i,jS2N1}$ 
42.

```

43. if WM is Archard:
44. $CWD_i = INT2WC \times K_{i,j} \times S_{i,j_{AVG}}$
45. Append CWD_i onto the last element for PN array
46.
47. else if WM is Energy:
48. $CWD_i = INT2WC \times \tau_{i,j} \times S_{i,j_{AVG}}$
49. Append CWD_i onto the last element for PN array
50.
51. For each line in INT2 Paired Nodes:
52. Calculate the sum of WD_i for INT2S1N from the last element of PN array
53. Total cyclic wear between paired nodes = $\sum_{i=1}^n CWD_i$
54. $INT2S1N\ WD = INT2WF1 \times \sum_{i=1}^n CWD_i \times \beta$
55.
56. For each line in INT2 Paired Nodes:
57. For each frame number within Paired Nodes:
58. $INT2S2N1\ WD = INT2WF2 \times \sum_{i=1}^n \overline{INT2S2N1\ CWD_i} \times \beta$
59. $INT2S2N2\ WD = INT2WF2 \times \sum_{i=1}^n \overline{INT2S2N2\ CWD_i} \times \beta$
60. $INT2S2N3\ WD = INT2WF2 \times \sum_{i=1}^n \overline{INT2S2N2\ CWD_i} \times \beta$
61.

PT : Pairing type

WM : Wear method

$\tau_{i,j}$: Contact shear stress at time interval, *i* , at analysis stage, *j*

$S_{i,j}$: Relative displacement at time interval, *i* , at analysis stage, *j*

INT1WC: Interaction 1 Wear Coefficient

INT1WF1: Interaction 1 Wear Fraction 1

INT1WF2: interaction 1 Wear Fraction 2

CWD : Cyclic wear depth

CWD_i : Cyclic wear depth at time interval, *i*

$S_{i,j_{S2N1}}$: CSLIP for S2N1

$S_{i,j_{S2N2}}$: CSLIP for S2N2

$S_{i,j_{S2N3}}$: CSLIP for S2N3

$S_{i,j_{AVG}}$: Average CSLIP value

$K_{i,j}$: Contact pressure at time interval, *i* , at analysis stage, *j*

n : Total number of time intervals

INT1S2N1: Interaction 1 Surface 2 Node 1

INT1S2N2: Interaction 1 Surface 2 Node 2

INT1S2N3: Interaction 1 Surface 2 Node 3

WD : Wear depth

3.6.9. Writing results into the ABAQUS output databases (*.odb format)

At the end of each analysis, the total wear depth is written into the ABAQUS odb file.

Function 8 illustrates the process of writing the results into the ABAQUS odb file. To write the results into the odb file, the part node number and the wear value will need to be defined for ABAQUS.

Function 9: writeOdb

1. Input: INT1S1W, INT1S2W, INT2S1W, INT2S2W
2. Output: ODB results
3.
4. Open current Job ODB file (not read only)

-
5. *For INT1S1W, INT1S2W, INT2S1W, INT2S2W:*
 6. *Find the relative nodes in ODB*
 7. *Write node number, and wear to part 1 in ODB*
 8. *Write node number, and wear to part 2 in ODB*
 9. *Write node number, and wear to part 3 in ODB (if applicable)*
 - 10.
 11. *Close the ODB file.*
-

3.6.10. Updating the geometry

To apply the wear onto the individual surfaces and update the geometry, as explained in section 3.5, Function 9 applies the wear depth onto the geometry. For each part, the original coordinates from the initial input file are extracted, and the wear in the 3-dimensional coordinates is applied onto the original coordinates which will then produce the updated geometry for the next stage of the analysis.

Function 10: writeInp

1. *Input: Current INP file*
 2. *Output: New INP file with geometry updated*
 - 3.
 4. *Open the current Job INP file (not read only)*
 5. *For each part:*
 6. *Find the corresponding node from INT1S1W, INT1S2W, INT2S1W, INT2S2W*
 7. *Add wear in XYZ coordinates from original INP file.*
 8. *Save INP file as Job-(x+1) INP file.*
 9. *Close both INP files*
-

3.6.11. Submitting the jobs

After updating the geometry, the input file with the updated geometry is submitted to the ABAQUS solver for analysis. Function 11 is a simple script to submit the new input file to the ABAQUS solver for analysis.

Function 11: Submit

1. *Input:*
 2. *Output:*
 - 3.
 4. *Submit Job based on Input Parameters from User*
-

3.6.12. Volumetric Wear

To calculate the volumetric wear loss from the gradual wearing process after completion of the analysis, a volumetric wear function script has been set up to calculate the volumetric wear loss. Function 12 illustrates the process of extracting the volumetric wear loss. As wear removes material, the initial job chosen will have the largest volume. The total volume of the individual parts is extracted through the sum of element volumes (EVOL) found within the ABAQUS odb file. The volumetric wear loss is then recorded in the form of a comma-separated file (*.csv) saved with the individual part names.

Function 12: VolumetricWear

1. *Input: First job number, last job number*
 2. *Output: Volumetric wear*
 - 3.
 4. *Open Job-1 ODB file*
 5. *Extract part names for each individual parts*
 6. *Extract volume of individual parts through the sum of element volume (EVOL)*
 7. *Create array to store volumetric wear loss in form of: [Job number, volumetric wear loss]*
 - 8.
 9. *While current job is: first job number < current job < last job number:*
 10. *Open current job ODB file*
 11. *Extract current job individual part volumes*
 12. *Volumetric wear loss = Job-1 part volume – current job part volume*
 13. *Add current job number and volumetric wear loss into array*
 - 14.
 15. *Save volumetric wear loss array into excel format with individual part names.*
-

3.7. Computational Cost

All analyses described in the chapters that follow were executed on a 64-bit windows 10 professional operating system with twin dual 12-core Intel Xeon central processing unit platforms at 3.20GHz configured with 128GB of random-access memory.

The FE analysis and wear algorithm running time for each 3D model is approximately 8 hours for each single model update.

3.8. Results Convergence

To ensure the accuracy of these studies, the mesh must be of suitable size and shape for the results to converge. Initially, a mesh study is performed to determine the minimum element size to achieve converged results. The mesh is then further refined to ensure a smooth wear profile across the surfaces. A scaling factor convergence has also been performed to ensure both accuracy and speed of the analysis.

3.8.1. Finite element mesh study

Initially, a uniform density mesh was generated and a mesh convergence study was performed. The criterion for mesh convergence was based on the contact pressure at the XLPE bearing liner and the taper junction. For the FE model used in this research, the results converged at approximately 100,000 elements with an element size of approximately 1.5mm at the bearing surface and approximately 8,000 elements with an element size of approximately 0.7mm at the taper junction (Figure 3-12).

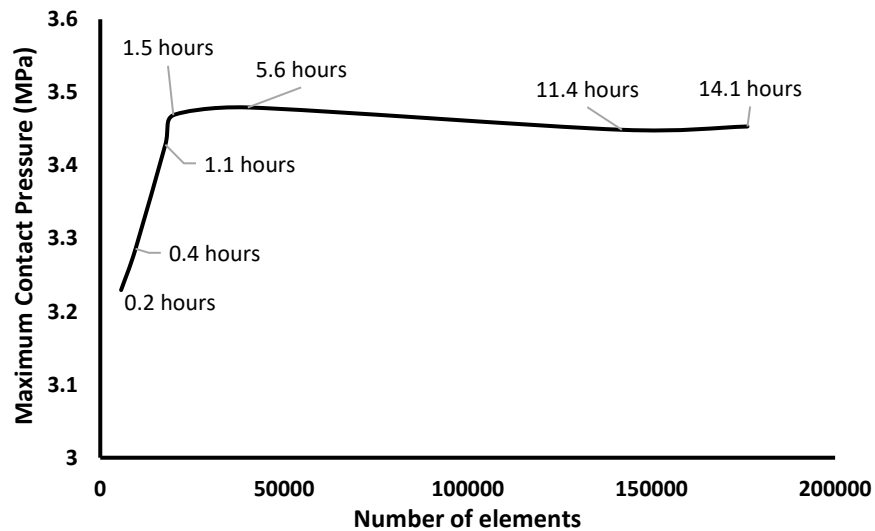


Figure 3-12: Mesh independence study

3.8.2. Mesh study for wear modelling

Alongside ensuring that the FE model has achieved convergence, a separate mesh study for wear modelling is vital to ensure that a suitably refined mesh is generated to ensure adequate wear results.

- **Bearing surface** – Figure 3-13 shows the wear profiles for the XLPE bearing liner for element sizes of 0.5mm, 1.0mm and 1.5mm. It was initially found that the initially converged mesh of 1mm was generating slightly uneven wear as the analysis progressed. This is attributed to the larger distance between the nodes causing sharp points along the contacting surface. It is therefore important to further refine the mesh in the contact zone so that the generated worn surface is as smooth as possible. An element size of 1.0mm on the bearing liner was found to be adequate which allowed a smooth wear pattern to develop on the model.

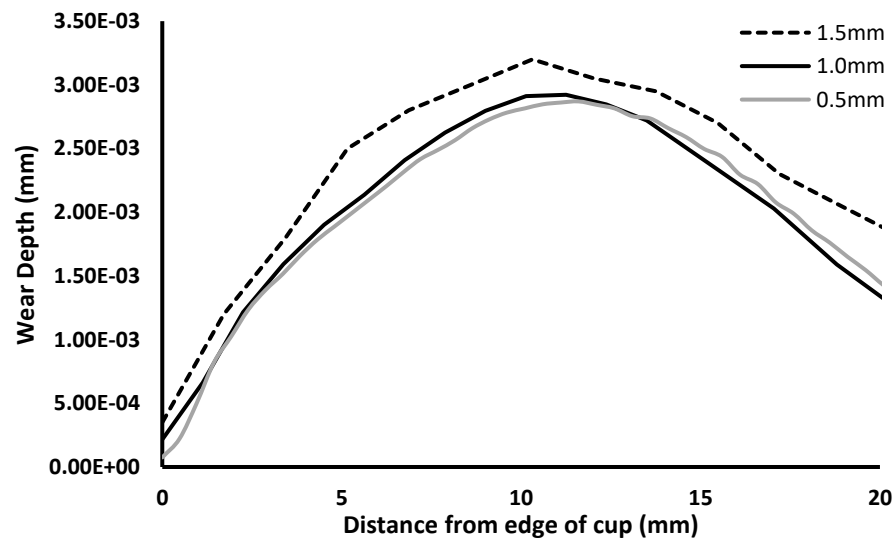


Figure 3-13: Wear modelling mesh convergence for bearing surface

- **Taper junction** – The same mesh study for wear modelling was performed for the taper surface for element sizes between 0.4mm and 2.0mm. Figure 3-14 shows the wear profile for the femoral stem trunnion surface for the different element

sizes. It can be seen that the 2.0mm element size would produce a relative rough wear profile which would generate an unevenly worn surface and can lead to future solution convergence problems and an inaccurate wear depth. The 0.6mm element size was found to adequately provide a smooth wear profile to develop on the model as the solution progressed.

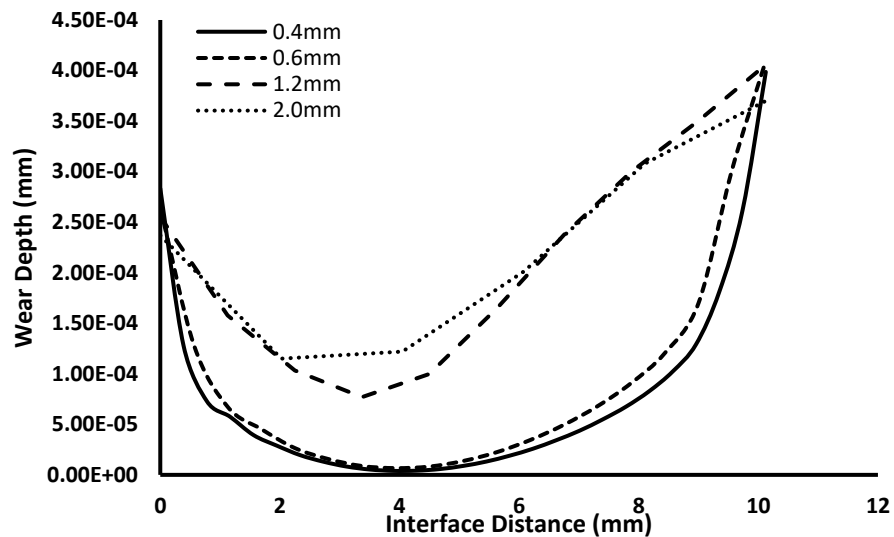


Figure 3-14: Wear modelling mesh convergence for taper junction

3.8.3. Scaling factor

The scaling factor (β) used in this study has a major impact on simulation times, wear evolution and accuracy. A large scaling factor will facilitate a relatively fast analysis, however, it may detrimentally affect the accuracy of the final calculated wear. On the other hand, a small scaling factor will increase solution times drastically, but will increase the accuracy of the results and wear profile. Figure 3-15 demonstrates the effect of the scaling factor on the average wear depth after 2 million load cycles when using scaling factors ranging from 10,000 to 2 million.

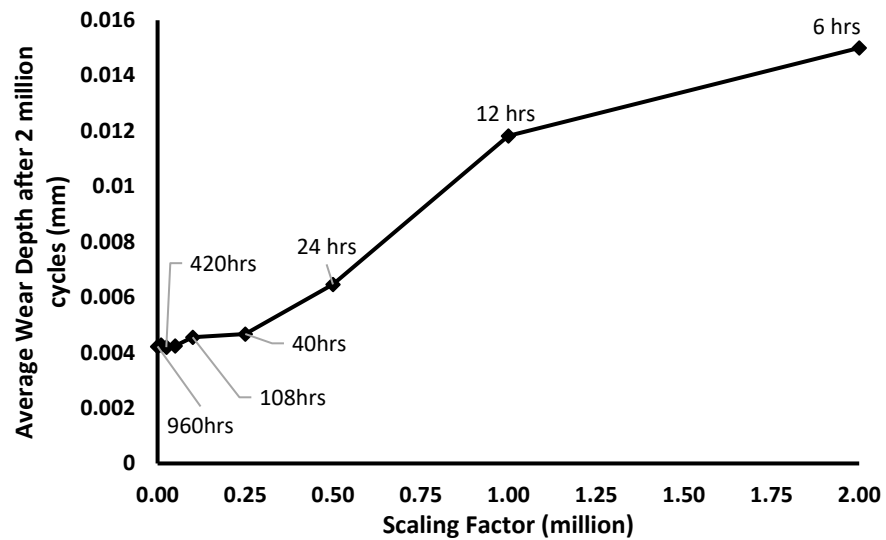


Figure 3-15: Effect of different scaling factors on simulation time and accuracy

Figure 3-16 shows the total cumulative wear and the wear that is applied at 2 million cycles using different scaling factors of 25,000, 50,000 and 100,000. Although the total cumulative wear at 2 million cycles remains similar, the wear that is being applied to the geometry is not smoothly distributed. As the analysis progresses, this will cause a sharp increase in wear depth at a certain contact area on the surfaces which would then lead to inconsistencies on the wear pattern. To mitigate this effect and to reduce the computational time, a node wear smoothing feature has been developed in the wear algorithm.

In this node smoothing feature, the wear applied to each node is checked with a cloud of surrounding nodes to ensure that the wear distribution is applied smoothly throughout the analysis. Figure 3-16 shows the difference between the wear applied onto the geometry with and without the node smoothing feature. As such, in this study, a scaling factor of $\beta = 10^5$ was found to be adequate to provide the accuracy required for the wear depth. The scaling factor in the algorithm can be adjusted throughout the analysis to optimise solution accuracy and run times. The following studies have used a scaling factor of $\beta = 10^5$ as it shows a smooth and relatively uniform wear profile created on the models.

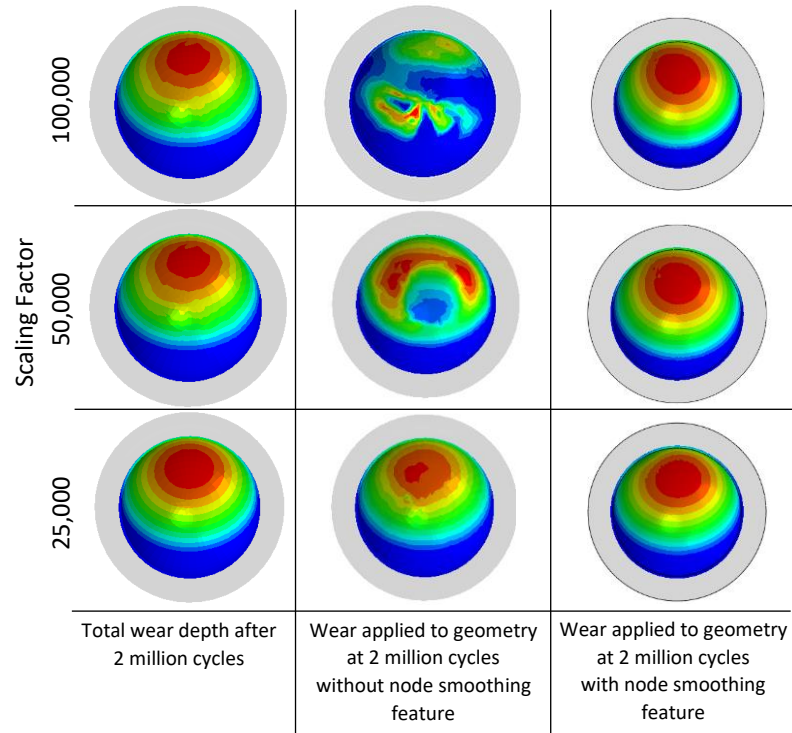


Figure 3-16: Effect of scaling factor on the wear occurring in the analysis

3.9. Summary and Conclusions

A computational model to predict the extent of wear within total hip replacement prostheses has been described within this chapter. This method has been automated using a Python script to extract the required outputs from the FE analysis and apply the wear onto the geometry to reflect the extent of wear that has occurred during the analysis. The wear damage pattern, linear and volumetric wear rate can also be extracted during the analysis to quantify the amount of wear.

This method has been applied to a 3D FE model of a THR prosthesis for a comprehensive illustration of the wear model. It has been successfully used to accurately predict wear at both the bearing surface and taper junction of the THR prosthesis during the expected operational lifespan. This method can be used in design or applied to clinical practice to help facilitate a reduction in wear by identifying key factors leading to the release of wear debris.

The method presented in this chapter can contribute to research in this area with the following advancement over the current methods proposed within the literature:

- The method here is unique as it models both bearing and taper junction wear within the same analysis.
- The method is able to consider two sets of activities within the same analysis.
- The method is able to modify the wear coefficient as the analysis progresses to simulate the changing surface characteristics. If the variation of wear coefficient during a wear analysis is known, the method will be able to incorporate the variation.
- The method developed is user friendly in the form of a graphical user interface (GUI) window within ABAQUS. A simple click and run process is only needed to run the wear analysis.
- Due to the time required to run the simulation, a recovery option is built into the GUI in the event of any failure. The user may continue the simulation and “pick up” where the simulation failed. The recovery tab is shown in the GUI interface and is attached in the appendix.

As with any proposed method and hypothesis, there are possible limitations which are as follows:

- The assessment of wear in this method is solely based on mechanical wear as the primary damage causing mechanism.
- The method is dependent on the wear coefficient employed within the analysis. The significance of the wear coefficient will need to be considered due to its effect on the wear depth calculated. This coefficient can only be obtained through controlled experiments.

Chapter 4

Technical Results and Validation of Methodology

4.1. Introduction

In the previous chapter, a new computational methodology has been proposed to predict wear between the articulating bearing surfaces and the taper junction surfaces. In this chapter, the proposed methodology will be used to demonstrate and discuss key features and functionality of this method. A 3D FE model of a femoral head and acetabular cup of a commercially available THR prosthesis has been used for this chapter to investigate predicted wear at the articulating bearing surface. This chapter will detail the wear patterns obtained from the initial methodology explained in Chapter 3 with the volumetric wear obtained from the wearing process. The results in this chapter are then used to validate the methodology and further investigate principal parameters which are critical for predicting wear accurately.

4.2. Wear Analysis Input

This chapter has utilised the 3D FE model shown in Figure 3-3 with only the bearing interaction selected. The material combination used in this study is highly crossed linked polyethylene (XLPE) for the bearing liner and cobalt-chrome (CoCr) for the femoral head. The wear analysis for this 3D model has been considered up to 5 million walking cycles. A summary of the input parameters is shown in Table 4-1.

Table 4-1: Input parameters for wear analysis in chapter 4

Input Data	
Model	3D FE Model (see Figure 3-3)
Interaction Combination	Bearing Liner and Femoral Head
Material Combination	Bearing Liner: XLPE Femoral Head: CoCr
Surface Picked	Surface 1: XLPE surface Surface 2: Femoral Head Bearing Surface
Node Pairing	1:3 Pairing
Walking load and Boundary Conditions	Loads with relative rotations (see Figure 3-5 and Figure 3-6)
Wear Law	Dissipated Energy
Wear Coefficient	$5.32 \times 10^{-10} \text{ MPa}^{-1}$
Wear Fraction	XLPE:CoCr = 0.99:0.01
Scaling Factor	100,000
Number of load cycles	5,000,000

The time taken for each analysis was approximately 17 hours for each 100,000 cycles on the system specification stated in section 3.8. Therefore, this analysis of 5 million cycles (5 years) has a total run-time of around 850 hours.

4.3. Results and discussion

Figure 4-1 shows the variation of contact shear stress (CSHEAR), distributed on the femoral head, and relative displacement (CSLIP) on the bearing liner for one walking cycle only. As explained in section 3.3, the nodes in contact are paired at each time interval of the analysis. For each set of paired nodes, the CSLIP (Figure 4-1a) and CSHEAR (Figure 4-1b) were extracted. These values are then used to calculate the wear depth using Eq. (7). The wear depth distribution after using a scaling factor of 100,000 is shown in Figure 4-1c. It is noticeable that at each time interval, the area of contact of the contact bearing surfaces are similar. The maximum CSHEAR is 0.352MPa which occurs at 0.60s while the maximum relative displacement of 10.9mm occurs at 0.24s over the walking cycle. As expected, due to the wear fraction, the highest wear depth occurs on the bearing liner with a wear depth of 4.25 μ m and the maximum wear depth on the femoral head is 0.0460 μ m which is around 99 times lower.

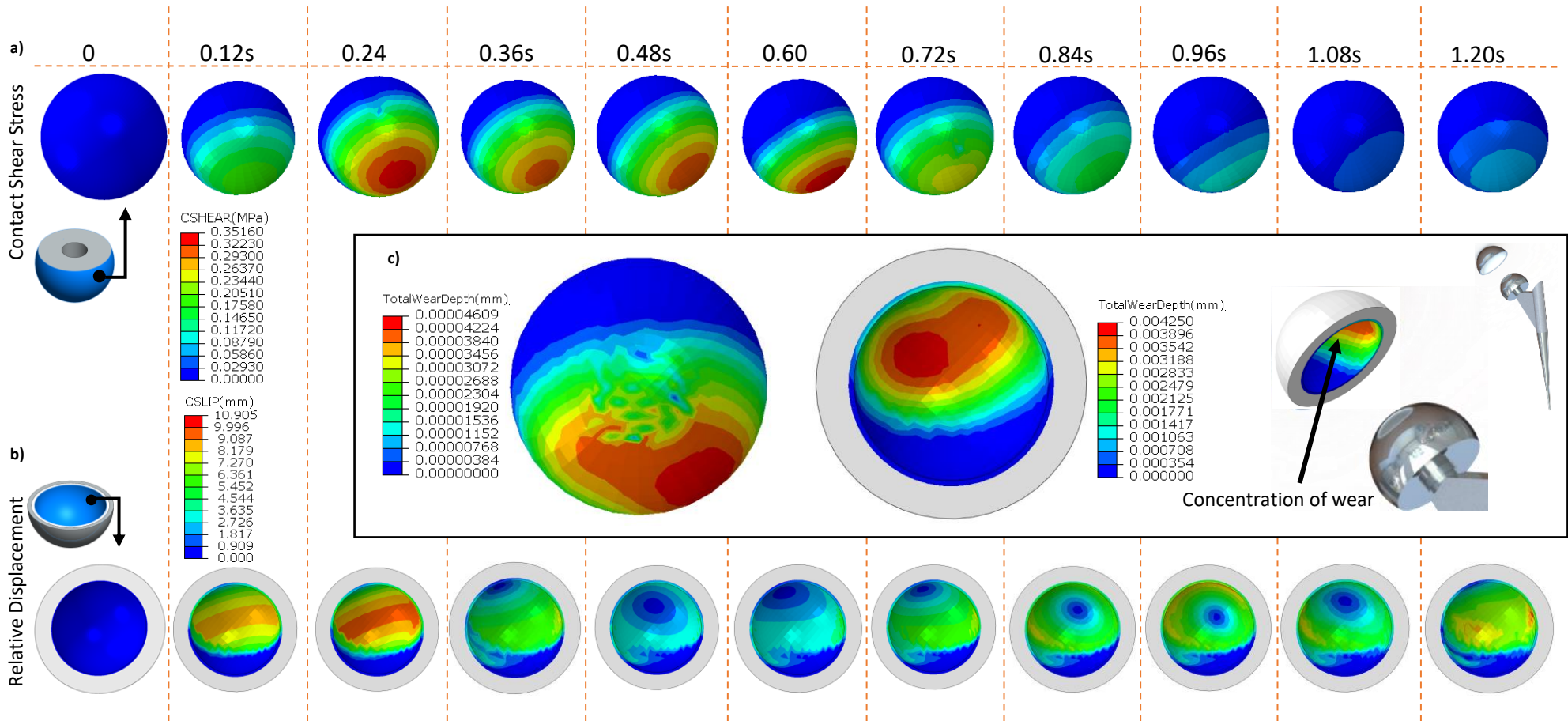


Figure 4-1: a) Variation of contact shear stresses, b) Variation of relative displacement during a walking cycle, c) Wear depth values at the end of 100,000 cycles

The same procedure as explained section 3, has been carried out to complete up to 5 million cycles and the evolution of wear is shown in Figure 4-2 at every million cycles. The maximum wear depth value reaches 192.5 μm and 2.20 μm after 5 million cycles for the bearing liner and femoral head respectively (Figure 4-2a, Figure 4-2b). It can be seen from Figure 4-2 that most of the wear occurs at a relatively small area compared to the rest of the surface.

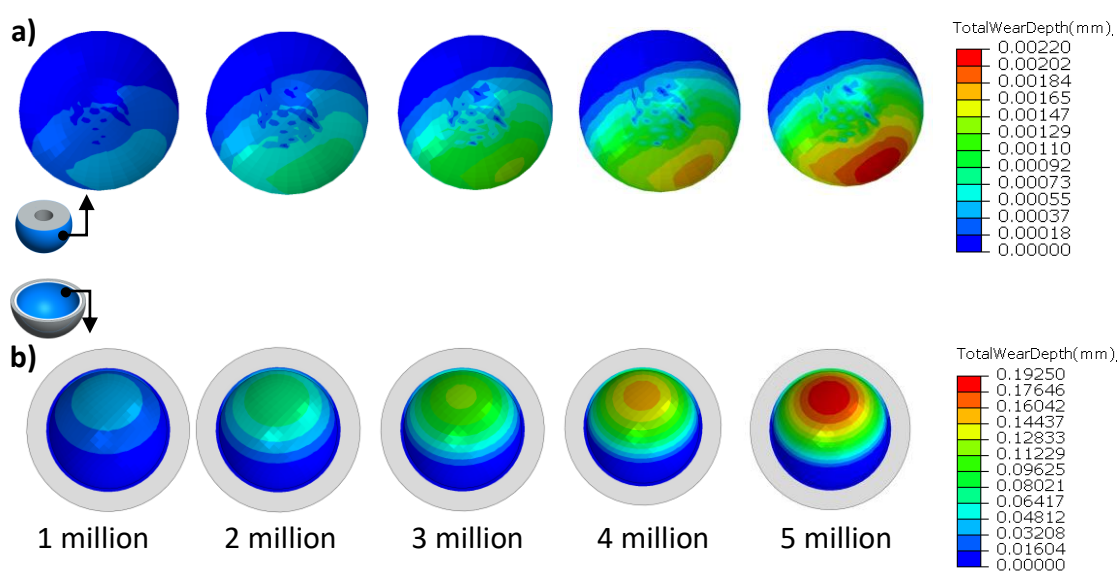


Figure 4-2: Variation in wear depth over 5 million walking cycles

Figure 4-3 show the cumulative volumetric wear and the volumetric wear rate up to 5 million cycles for both femoral head and XLPE bearing liner. The volumetric wear was determined at each 1 million cycles as the solution progressed based on the reduction of element volume for all the elements of the different parts.

As can be expected, the material loss from the surfaces increases over the 5 million load cycles as shown in Figure 4-3a. The cumulative volumetric loss at the end of 5 million cycles is 169.2 mm^3 and 1.75 mm^3 for the XLPE bearing liner and CoCr femoral head due to the material interaction properties. The total material loss from both bearing surfaces after 5 million load cycles is 170.96 mm^3 . The volumetric wear rate at each million-load cycle remains similar throughout the analysis between 33.6 mm^3/Mc and 34.1 mm^3/Mc

and $0.337\text{mm}^3/\text{Mc}$ to $0.362\text{mm}^3/\text{Mc}$ for the bearing liner and femoral head respectively (Figure 4-3b). This shows that the volumetric wear is increasing linearly throughout the analysis.

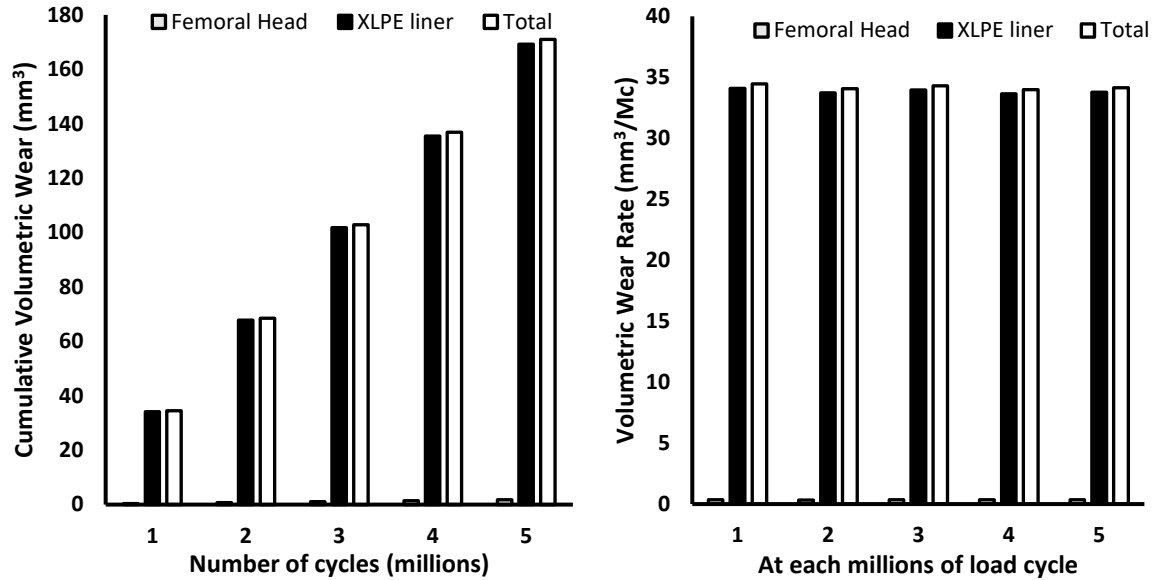


Figure 4-3: Variation in a) cumulative volumetric wear, b) volumetric wear rate with respect to n^{th} million cycles

Figure 4-4 shows the maximum linear wear and linear wear rate of the XLPE bearing liner. The maximum linear wear was determined from the largest wear depth at the XLPE liner at each 0.5 million cycles. The maximum linear wear is shown to have a linear increase at each 0.5 million cycles. The maximum linear wear is shown to have a linear increase with a maximum of 0.192mm at 5 million cycles. The linear wear rate was initially higher for the first million load cycles at $0.0418\text{mm}/\text{Mc}$ and then decreases to about $0.0375\text{mm}/\text{Mc}$ subsequently. The higher initial linear wear rate of $0.0418\text{mm}/\text{Mc}$ in the first million cycle (Figure 4-4b) may be due to an initial period of material deformation (bedding-in) and then steady-state wear which would continue after the first million cycles (Atrey, Ward et al. 2017).

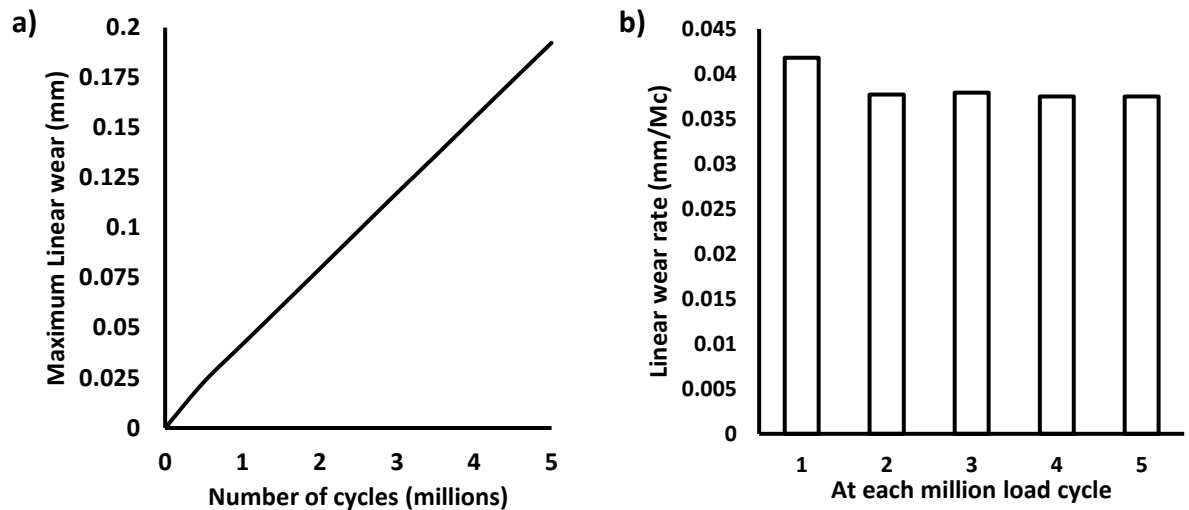


Figure 4-4: a) Maximum linear wear of XLPE liner at every million cycles, b) linear wear rate at each million load cycles

The contact pressures of the model during a gait cycle are found to be comparable to contact pressure variations in current literature. A comparison of the contact pressure evolution during a gait cycle at the first cycle and at the end of 5 million cycles is shown in Figure 4-5. The overall maximum contact pressure was found to be 3.21MPa throughout all 5 million cycles. These results are comparable to studies performed by Yoshida, Faust et al. (2006) and Saikko (2020). For a peak load of 2.5kN, Yoshida reported a maximum contact pressure of 3.2MPa while Saikko reported a maximum contact pressure of 3MPa.

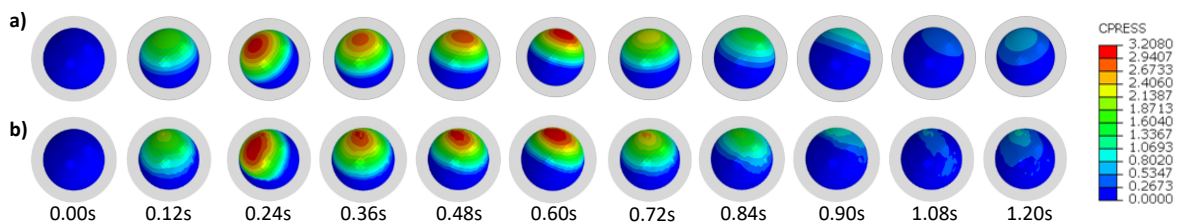


Figure 4-5: Variation of contact pressure (CPRESS) a) at the first gait cycle, b) at the end of 5 million cycle

The linear and volumetric wear rates shown in this study are comparable to several studies with XLPE in the literature (see Table 4-2). Atrey, Ward et al. (2017) and Haw, Battenberg et al. (2017) analysed a total of 32 and 48 primary total hip arthroplasties respectively with a 36mm CoCr femoral head size coupled with XLPE liners on serial radiographs. Atrey, Ward et al. (2017) showed a mean linear and volumetric wear rate of 0.07mm/yr and 29.29mm³/yr while Haw, Battenberg et al. (2017) showed a mean linear

and volumetric wear rate of 0.052mm/yr and 33.09mm³/yr. Khoshbin, Wu et al. (2020) analysed a total of 40 primary THR of XLPE liners with CoCr femoral heads using radiography. The results obtained showed a mean linear wear rate of 0.0387mm/yr and 31.51mm³/yr. The range of linear and volumetric wear rate for the XLPE liners coupled with a 36mm CoCr femoral head reported in the above studies (Atrey, Ward et al. 2017, Haw, Battenberg et al. 2017, Khoshbin, Wu et al. 2020) was between 0.039 - 0.07mm/yr and 29.29 - 33.09mm³/yr.

Table 4-2: Linear and volumetric wear rates of XLPE and UHMWPE in literature.

Material	Literature	Method of wear retrieval	Linear Wear rate (mm/yr)	Volumetric Wear rate (mm ³ /yr)
XLPE	Atrey, Ward et al. (2017)	Radiography	0.07	29.29
	Haw, Battenberg et al. (2017)	Radiography	0.052	33.09
	Khoshbin, Wu et al. (2020)	Retrieved THR	0.0387	31.51
	Range	-	0.039 – 0.07	29.3 – 33.1
	Current study	FEA	0.0375	33.8
UHMWPE	Ali, Al-Hajjar et al. (2016)	Hip Simulator	0.24	12.2
	Trommer, Maru et al. (2015)	Hip Simulator	0.8	56
	Callaghan, Pedersen et al. (2003)	Clinical database	0.08 – 0.12	32.71 – 89.27
	Fialho, Fernandes et al. (2007)	Computational Method	0.09	18
	Literature range	-	0.08 – 0.8	12.2 – 89.3

As XLPE liners are a relatively new material (around 15 years) compared to conventional ultra-high-molecular-weight polyethylene (UHMWPE) (around 50 years), many of the primary THRs conducted are still currently in service and the investigation on the wear rate is mainly based on radiography as shown in the above literature. Radiography is unable to show the wear pattern on the bearing surface which is paramount to understanding the evolution of wear. The wear algorithm presented in this study can show the wear pattern and highlight areas of concern.

To further understand and compare the wear evolution, the wear patterns of conventional UHMWPE were compared with the results shown in this study (see Figure 4-6). The wear patterns from this study were found to be comparable to studies from

current literature, although the linear and volumetric wear were much higher with the conventional UHMWPE.

Fialho, Fernandes et al. (2007) used a computational method to predict the extent of wear damage for a 28mm CoCr head size at 1 million load cycles. The study showed a linear and volumetric wear rate of 0.09mm/Mc and 18mm³/Mc. Callaghan, Pedersen et al. (2003) used a clinical database of more than 4,000 primary THRs with 22mm and 28mm femoral head sizes implanted by a surgeon to evaluate the wear mechanism between 5 and 22 years. The range of linear and volumetric wear presented was 0.08 - 0.12mm/yr and 32.71 - 89.27mm³/yr respectively. A study by Trommer, Maru et al. (2015) and Ali, Al-Hajjar et al. (2016), which both used a commercial hip simulator to evaluate the wear at 5 million load cycles, showed a linear and volumetric wear rate of 0.24mm/yr and 12.2mm³/yr for a 36mm CoCr femoral head and 0.8mm/yr and 56mm³/yr for a 28mm CoCr femoral head.

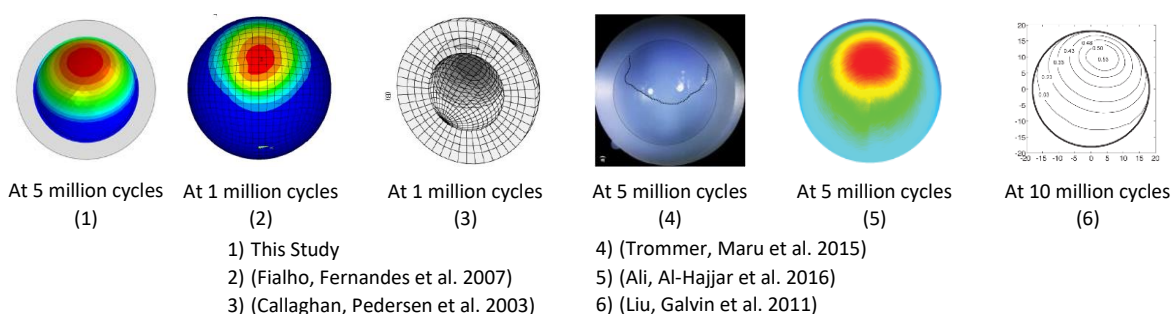


Figure 4-6: Comparison of wear pattern between this study and conventional UHMWPE

The range of linear and volumetric wear presented for conventional UHMWPE liners in the above studies (Callaghan, Pedersen et al. 2003, Fialho, Fernandes et al. 2007, Trommer, Maru et al. 2015, Ali, Al-Hajjar et al. 2016) was between 0.08 – 0.24mm/Mc and 12.2 – 89.27mm³/yr respectively. Although the wear patterns in our study are comparable to the wear pattern shown in conventional UHMWPE, the linear and volumetric wear rates of conventional UHMWPE are higher than the values shown in

XLPE as the overall amount of wear of XLPE may be up to 40% less (Ali, Al-Hajjar et al. 2016) than conventional UHMWPE (see Table 4-2).

The number of steps walked by a patient per year, undoubtedly influences the wear rate per year however by considering an average of 1 million walking steps per year (Schmalzried, Szuszczewicz et al. 1998), the linear and volumetric wear rate shown in our study (0.0375mm/yr and 33.8mm³/yr) are comparable to those found in the above literature (see Table 4-2). It is noticeable that if a patient walks more than the assumed 1 million cycles per year, it will only hasten the wear and not affect the wear rate per million cycles. There are many factors which can contribute to the wear damage, such as variable wear and friction coefficients, surface roughness, manufacturing tolerances, and the patient's activity level, weight, and implant design.

Although in this study we have used zero tolerances between the femoral head and bearing liner, defining tolerances for manufacturing is crucial. The tolerances may also translate into bearing surface clearances which will affect the outcome of wear and implant survivability. Surface roughness may also influence wear. There have been studies which incorporate surface roughness into the wear coefficient to simulate the actual wear (Pietrabissa, Raimondi et al. 1998, Raimondi, Santambrogio et al. 2001). The algorithm developed in this study can be used to perform parametric studies to propose the optimum tolerances for manufacturing and surface roughness.

A fixed friction coefficient and wear coefficient has been used in this study; however, they can be continuously changed over the implant's lifetime due to the changes in surface roughness, lubrication and wear debris. The algorithm developed in this study can investigate the effect of different friction and wear coefficients to improve the design and material characteristics of the implant.

4.4. Conclusion

A 3D FE model of a commercial THR prosthesis has been used to demonstrate the methodology explained in Chapter 3 for predicting bearing surface wear. The wear damage, rate and wear pattern are shown to be comparable with those found in current literature.

The methodology and FE model demonstrates that a dynamic implicit analysis can model the gait cycle effectively while the dissipated energy wear law and 3D FE model can predict wear patterns, linear and volumetric wear rates when compared to typically observed wear patterns from UHMWPE retrievals and XLPE *in vivo* wear rates. The results show promise in predicting the evolution of wear and can be used to investigate different parameters such as body weight, material properties, different implant size and design, manufacturing tolerances, and different surgical techniques.

The accurate and smooth evolution of wear across the bearing surface is influenced by the scaling factor and mesh size used. Using a courser mesh density and a large scaling factor would reduce the computational time but will affect the accuracy of the results. A smaller scaling factor would ensure that the wear is evenly distributed and will avoid cyclic wear 'hotspots' being overly exaggerated. A fine mesh and a small scaling factor can facilitate an accurate and smooth development of wear but with the cost of a much-increased computational time. To help reduce the computational time, a node smoothing feature was developed to be used so there is no sudden exaggeration in the node wear. As such, a balance of mesh density and the scaling factor is needed to ensure accurate results within a reasonable time. For example, the model presented in this study utilising a scaling factor of 100,000 coupled with the node smoothing feature, was found to provide a smooth wear evolution.

This chapter has only taken into account the bearing surface wear and not the taper surface wear and as such, the following chapters will include both bearing surface and taper junction wear within the same analysis.

Chapter 5

Impact of the human body weight on THR prosthesis wear

5.1. Introduction

As the current obesity epidemic grows, an increased number of obese patients undergoing Total Hip Arthroplasty (THA) can be expected in the coming years. It is understood that an increased body weight would increase the wear rates on the prostheses, however, the extent of increased wear and the impact on the longevity of the prosthesis is unclear. In this chapter, the computational methodology will be used to investigate the effect of body weight on the wear of the contacting surfaces of THRs using a 3D FE model. This chapter will investigate and compare the effect of varying body weight (between 60kg and 140kg) on the extent of wear at the contacting surfaces of a

THR prosthesis. The results obtained have been compared with wear damage of retrieved prostheses in current literature.

5.2. Wear Analysis Input

For this chapter, the 3D FE model shown in Figure 3-3 is used with the realistic gait cycle loading and rotation (see Figure 3-5 and Figure 3-6) applied over a 1.2 second duration. The 3D FE model has considered both bearing surface and taper junction interactions within the same analysis. The material chosen for the bearing liner was XLPE, the femoral head was CoCr, and the femoral stem was Ti. The bearing surfaces were chosen to have '1:3 node pairings' due to the relatively large displacement of the articulating surface, and the taper junction was chosen to have '1:1 node pairing' due to small relatively displacements (micromotion). An impaction force of 4,000N has been chosen to simulate the impaction during assembly of the femoral head onto the femoral stem in surgery. The wear analysis for this 3D model has been considered up to 5 million load cycles. A summary of the input parameters is shown in Table 5-1.

Table 5-1: Input parameters for wear analysis in chapter 5

Input Data		
Model	3D FE Model (see Figure 3-3)	
Loadings and Rotations	Loads with relative rotations (see Figure 3-5 and Figure 3-6)	
Wear Law	Dissipated Energy	
Scaling Factor	100,000	
Number of load cycles	5,000,000	
<hr/>		
Interaction 1	Interaction Combination	Bearing Liner and Femoral Head
	Material Combination	Bearing Liner: XLPE Femoral Head: CoCr
	Surface Picked	Surface 1: XLPE surface Surface 2: Femoral Head Bearing Surface
	Node Pairing	1:3 Pairing
	Wear Coefficient	$5.32 \times 10^{-10} \text{ MPa}^{-1}$
	Wear Fraction	XLPE:CoCr = 0.99:0.01
<hr/>		
Interaction 2	Interaction Combination	Femoral Head and Femoral Stem
	Material Combination	Femoral Head: CoCr Femoral Stem: Titanium
	Surface Picked	Surface 1: Femoral Stem Surface 2: Femoral Head Taper Surface
	Node Pairing	1:1 Pairing
	Wear Coefficient	$1.31 \times 10^{-8} \text{ MPa}^{-1}$
	Wear Fraction	CoCr:Ti = 0.9:0.1
Impact Force	4000N	

The time taken for each analysis was approximately 6 hours for each 100,000 cycles on the system specification stated in section 3.8. Therefore, this analysis of 5 million cycles (5 years) for 5 different body weights would have a total run-time of around 1,500 hours.

5.3. Results and Discussion

The linear and volumetric wear rates at the bearing surfaces and taper junction of THA shown in this section were presented at each million cycles as the solution progressed.

In order to investigate the effect of body weight on the wear evolution damage, the wear patterns are only shown on the XLPE bearing liner (Figure 5-1) and head taper surfaces (Figure 5-2). This is mainly because these surfaces carry 99% and 90% of the wear fraction calculated respectively.

It can be seen in Figure 5-1 for the XLPE bearing liner, by increasing the body weight the maximum linear wear increases also. For 60kg BW, the maximum linear wear was found to be 0.083mm at the end of 5 million load cycles, while for 140kg BW it had increased by 2.7 times to 0.221mm. However, the maximum linear wear at the femoral taper surface for all body weights is almost constant at approximately 0.004mm.

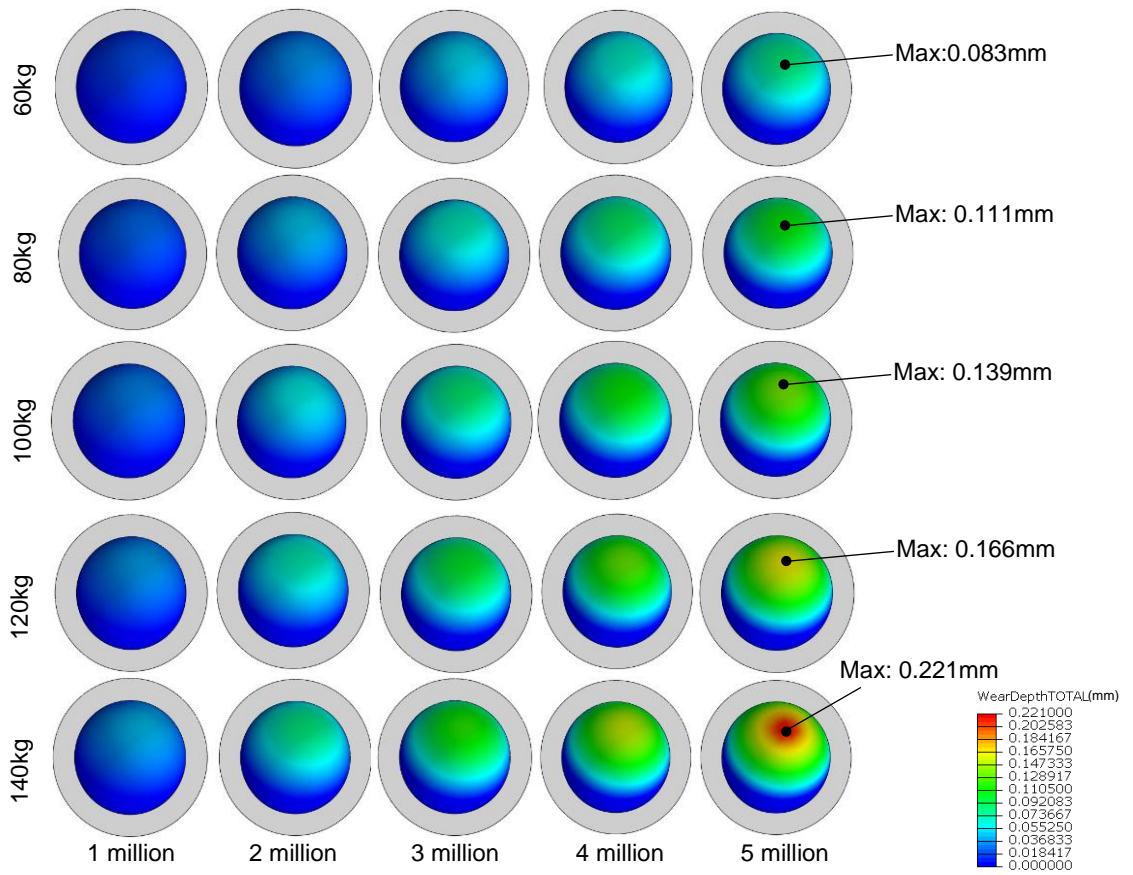


Figure 5-1: Evolution of wear pattern on the XLPE bearing liner during wear analysis for different patient's weights

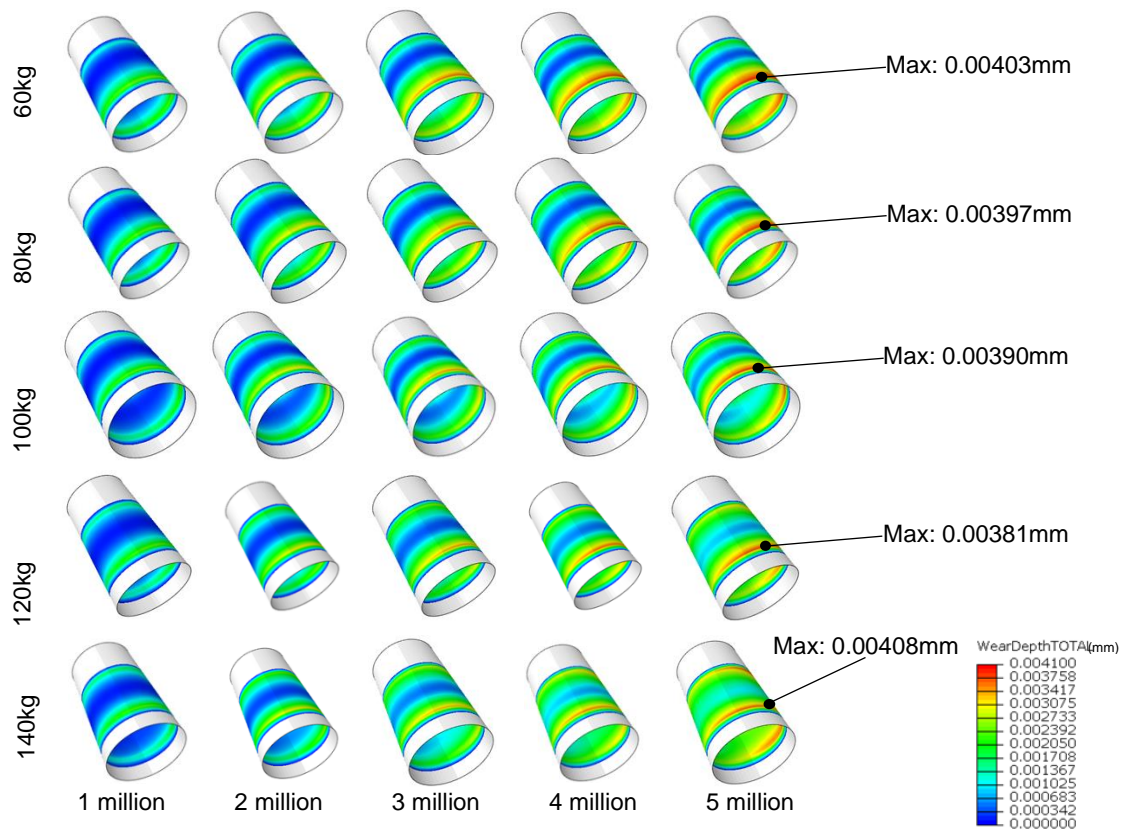


Figure 5-2: Evolution of wear pattern on the femoral head taper surface during wear analysis for different patient's weight

Figure 5-3a shows the volumetric wear and volumetric wear rates over 5 million cycles at the XLPE bearing liner. It can be seen in Figure 5-3a that the volumetric wear in all cases increases linearly. The total volume loss for 60kg BW is 75mm³ while for a 140kg BW, it increases to 175mm³. This linear behaviour is further highlighted in Figure 5-3b which shows a constant volumetric wear rate of 15mm³/Mc for 60kg BW and increases to 35mm³/Mc for 140kg BW.

As shown in Figure 5-1, although the wear damage for all BWs has a similar pattern, the linear wear for 140kg BW is 2.7 times higher than 60kg BW. It can be seen in Figure 5-3a, increasing the BW from 60kg to 140kg in 20kg intervals, the volumetric wear of the XLPE bearing liner increases linearly by 25mm³ at each interval over a 5 million load cycle.

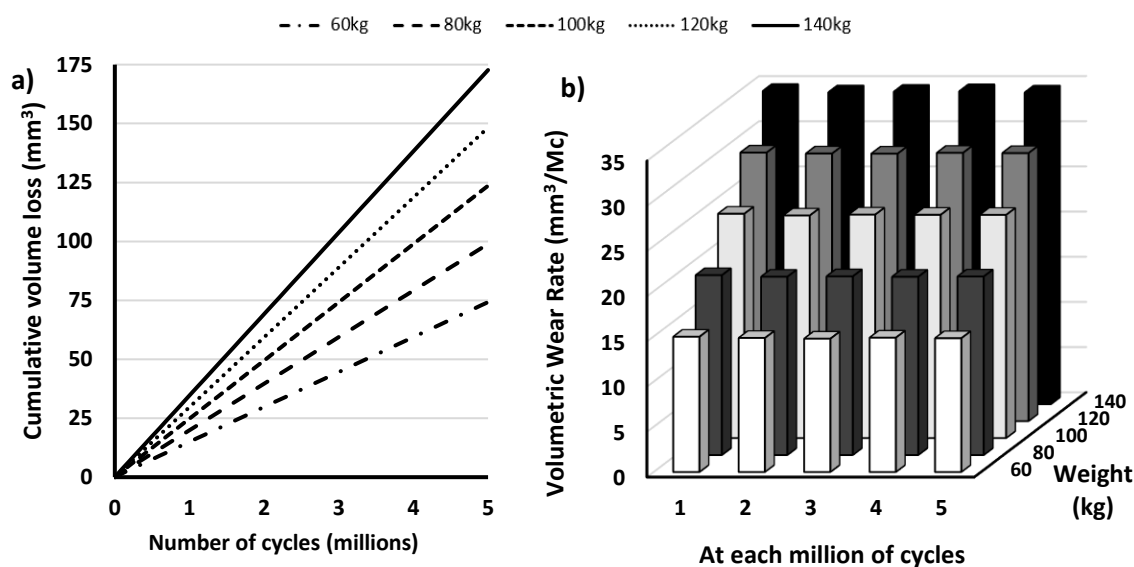


Figure 5-3:XLPE liner a) total volumetric wear b) volumetric wear rates over 5 million cycles

Figure 5-4 shows the volumetric wear and volumetric wear rates over 5 million cycles at the bearing surface of the femoral head. The total volume loss for 60kg BW is 0.7mm³ while for 140kg BW, it increases to 1.65mm³. The linear behaviour of the volume loss is further highlighted in Figure 5-4a which shows a constant volumetric wear rate of 0.14mm³/Mc for 60kg BW which increases to 0.33mm³/Mc for 140kg BW.

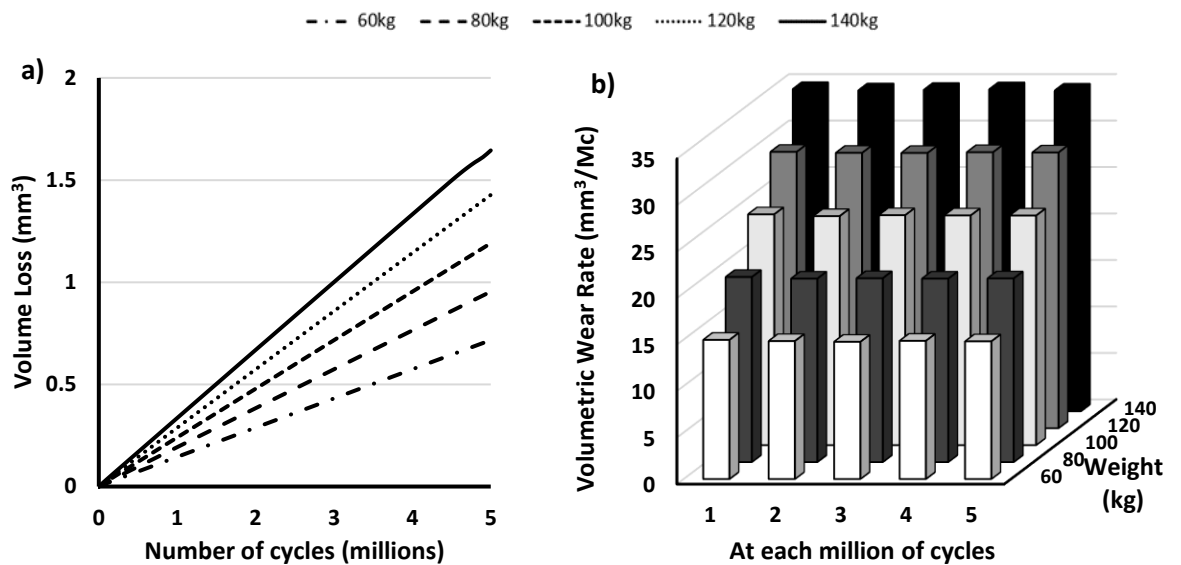


Figure 5-4: Femoral head bearing surface a) total volumetric wear, b) volumetric wear rates over 5 million cycles

Figure 5-5 shows the volumetric wear and volumetric wear rates over 5 million cycles at the femoral head taper surface. The total volume loss over 5 million load cycles is similar for body weights from 60kg to 100kg at 0.85mm³. While this total volume loss increases by 1.3 times to 1.12mm³ for a body weight of 140kg. It can further be seen in Figure 5-5b that the volumetric wear rate at the 1st million load cycle is approximately 0.34mm³/Mc for all cases regardless of the body weights while it decreases to 0.08mm³/Mc and 0.19mm³/Mc for 60kg and 140kg BW respectively over the 5 million load cycles.

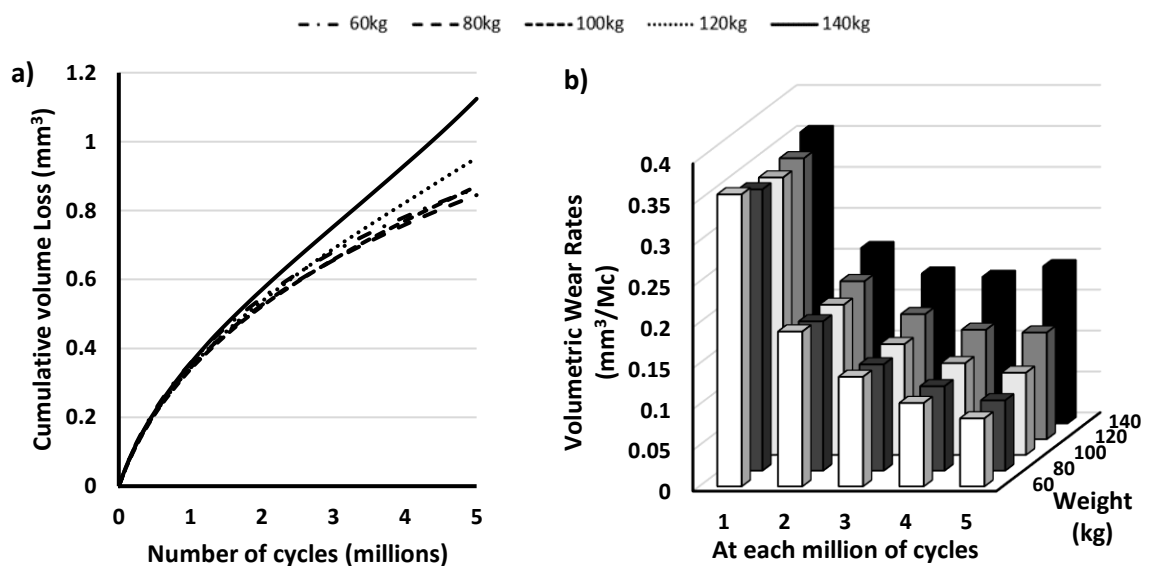


Figure 5-5: Femoral Head taper junction a) total volumetric wear, b) volumetric wear rates over 5 million cycles

Figure 5-6 shows the volumetric wear and volumetric wear rates over 5 million cycles for the femoral stem taper surface. The total volume loss evolution over 5 million load cycles follows a similar trend for body weights from 60kg to 100kg at an approximate maximum value of 0.08mm^3 while it increases to approximately 0.11mm^3 and 0.13mm^3 for 120kg and 140kg BW respectively.

It can be further seen in Figure 5-6b that there is an initial higher volumetric wear rate of $0.046\text{mm}^3/\text{Mc}$ on average which decreases to $0.015\text{mm}^3/\text{Mc}$ at the end of the 2nd million cycle for a body weight of 60kg and further decreases to approximately $0.005\text{mm}^3/\text{Mc}$ between the 3rd and 5th million cycle. The decrease in volumetric wear rates between 1 and 2 million cycles can be attributed to the removal of the initial taper locking effect which is explained further in depth by English, Ashkanfar et al. (2015). The same exponentially decreasing trend is seen as the body weight increases to 100kg, where the initial volumetric wear rate was $0.041\text{mm}^3/\text{Mc}$ and decreases to $0.021\text{mm}^3/\text{Mc}$ at the end the 2nd million cycle and further decreases to approximately $0.0088\text{mm}^3/\text{Mc}$ between the 3rd and 5th million cycle. As the BW increases past 100kg, the volumetric wear loss for 140kg BW retains its initial high volumetric wear rate, however, the volumetric wear rate remains similar at $0.022\text{mm}^3/\text{Mc}$ between the 2nd million cycle and 5th million cycle.

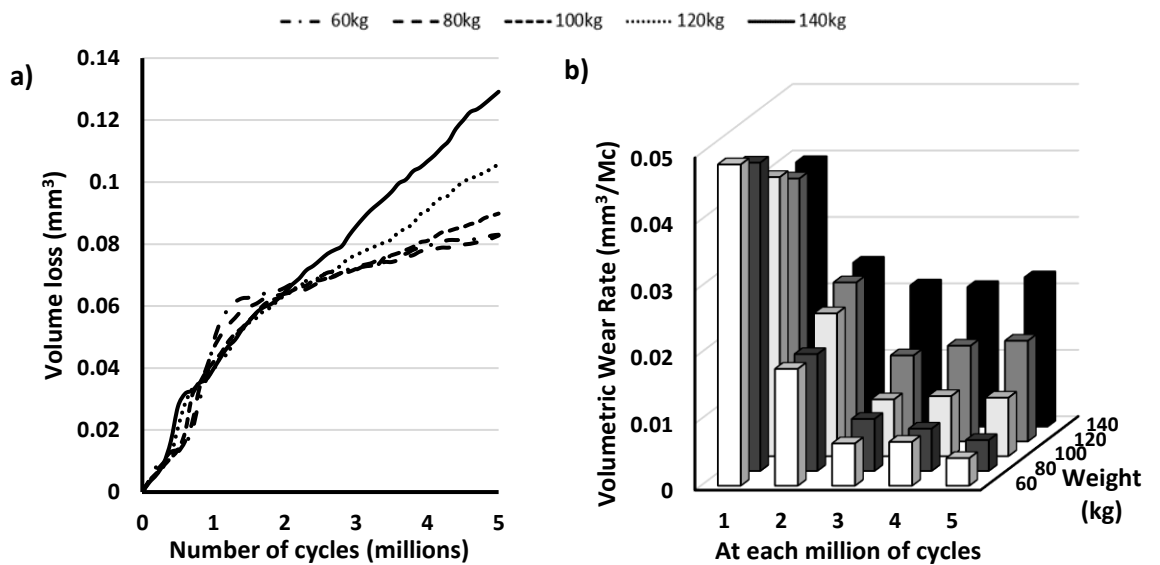


Figure 5-6: Femoral stem a) total volumetric wear b) volumetric wear rates over 5 million cycles

Although the femoral head bearing surface accounts for 1% and the femoral head taper surface accounts for 90% of the total wear between their respective surfaces, it can be seen in Figure 5-7, for a 60kg BW, the taper surface accounts for 56% of the total volumetric wear on the femoral ball and decreases to 40% for a 140kg BW. This highlights the relatively high amount of wear at the bearing surface despite having a low wear fraction.

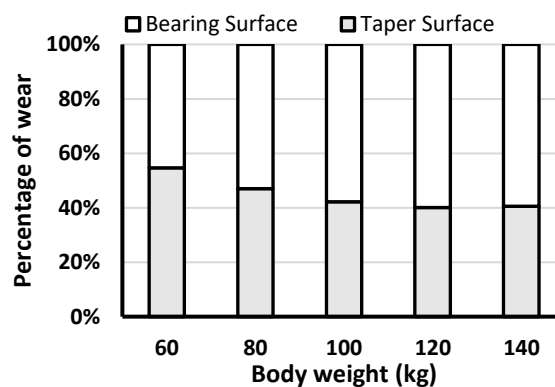


Figure 5-7: Percentage of wear between the bearing surface and taper surface at the femoral ball at 5 million cycles

Metallosis is the adverse reaction to metallic ions in the body which can lead to a variety of complications such as, infection, dislocation, or even the death of the tissue surrounding the prostheses (Pritchett 2012). Figure 5-8 shows the total metallic volumetric loss of the components in this study from the femoral head bearing and taper

surface, and the femoral stem taper. Approximately 95% of metallic wear loss is from the femoral head for all different BW's. At lower BW's, the main metallic wear loss is from the femoral head taper surface at approximately 52%. However, as BW increases, this metallic wear decreases to just 38% and the majority of wear shifts to the femoral head bearing surface.

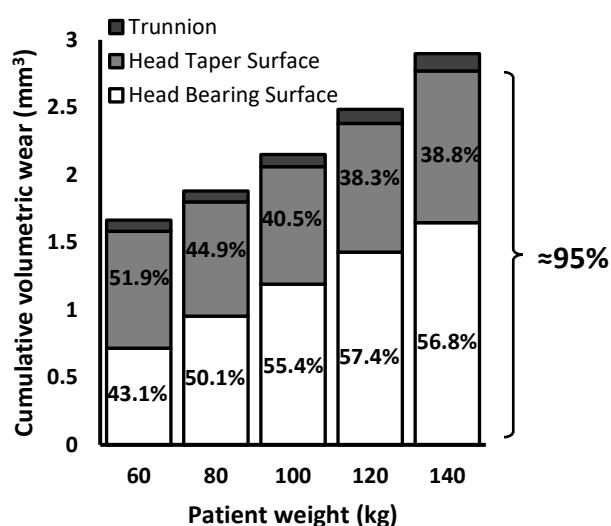


Figure 5-8: Total metallic volumetric wear at 5 million cycles

There are a variety of manufacturing and surgical factors, such as a taper mismatch or different assembly loads, which may affect the longevity of the prostheses in terms of wear. Although in this study zero taper mismatch was assumed, previous investigations showed an acceptable 6" taper mismatch did not significantly increase the wear rates (Ashkanfar, Langton et al. 2017). Another factor which could affect the wear rates is the effect of assembly loads during impaction of the modular head onto the femoral stem trunnion. It was found that a minimum assembly load of 4kN was needed to minimise wear rates. A lower assembly load below 4kN would severely increase the total volumetric wear loss at the taper junction (English, Ashkanfar et al. 2016).

5.4. Discussion

The results highlight that the body weight is directly proportional to the amount of volumetric wear on the bearing contacting surfaces. The XLPE volumetric wear rates reported in this study are closely comparable to results in the literature (Atrey, Ward et al. 2017, Devane, Horne et al. 2017, Haw, Battenberg et al. 2017, Khoshbin, Wu et al. 2020) (see Table). As XLPE liners are a relatively new material (around 15 years) compared to conventional polyethylene (around 50 years), many of the primary hip arthroplasties performed are still in service. Hence, the main method for analysing wear is through radiography. Khoshbin, Wu et al. (2020) analysed a total of 40 primary THA of XLPE liners with CoCr femoral heads and found the volumetric wear rate was between 7.8 – 31.51mm³/yr. Devane, Horne et al. (2017) analysed a total of 57 primary THA of XLPE liners with CoCr femoral heads and found the volumetric wear rate was between 1.5 – 18.9mm³/yr. Haw, Battenberg et al. (2017) analysed a total of 48 primary THA of XLPE liners with CoCr femoral heads and found the volumetric wear rate was between 19.2 – 46.9 mm³/yr. Atrey, Ward et al. (2017) analysed a total of 102 primary THA of XLPE liners with CoCr femoral heads and found the volumetric wear rate was between 5.82 – 52.76mm³/yr.

Table 5-2: Volumetric wear rates of XLPE liner in contact with CoCr femoral via radiography

Literature	Volumetric Wear (mm ³ /yr)
Khoshbin, Wu et al. (2020)	7.80 – 31.51
Devane, Horne et al. (2017)	1.50 – 18.90
Haw, Battenberg et al. (2017)	19.20 – 46.90
Atrey, Ward et al. (2017)	5.82 – 52.76
Range	1.5 – 57.6
Current Study	15 – 35

The volumetric wear rates reported in this study are closely comparable to results in the literature (Langton, Sidaginamale et al. 2012, Ashkanfar, Langton et al. 2017) (see Table

5-3). A co-ordinate measuring machine (CMM) has been previously used to measure the volumetric wear at 54 retrieved femoral head tapers. It showed the mean volumetric wear rate was 0.475mm³/yr with a range between 0.021 – 1.860 mm³/yr. Additionally, a study by Langton, Sidaginamale et al. (2012) also used a CMM to measure the volumetric wear rate at the taper surface of 48 retrieved hip prostheses and found the mean volumetric wear rate to be 0.127mm³/yr with a range between 0.01 – 3.15mm³/yr. Considering different BWs in this study, the mean volumetric wear up to 5 million cycles in this study was between 0.174 – 0.225mm³/Mc for 60 – 140kg BWs which is within the range in literature of 0.01 – 3.15mm³/yr.

Table 5-3: Volumetric wear rates of femoral head taper surface in literature

Literature	Mean Volumetric Wear (mm ³ /yr) (range)
Ashkanfar, Langton et al. (2017)	0.475 (0.021 – 1.860)
Langton, Sidaginamale et al. (2012)	0.127 (0.01 – 3.15)
Range	0.01 – 3.15
Current Study	0.174 – 0.225

As there are many variables which could influence the wear rates, such as patient’s activity level, weight, surgical techniques, and prostheses design variations, there is a large range of volumetric wear rates as shown in the above studies. To further improve the design and ultimately increase the longevity of THAs, it is crucial to understand the evolution of wear throughout the lifespan of these devices. In this study, our previous wear algorithms have been further developed to investigate the effect of different patient weights on the evolution of wear at the contacting surfaces of the implants. The result of this study showed that reducing the initial BW from 140kg to 100kg before THA would decrease the metallic wear by 26% and polyethylene wear by 30%. This can significantly improve the longevity of the prosthesis. As such losing weight down to 100kg before THA

can be highly recommended, however, further research is required to investigate the effect of losing weight on the longevity of these devices while in service.

5.5. Conclusion

In this chapter, a 3D FE model of a commercial THR prosthesis has been used to investigate the effect of body weight on the evolution of wear at the contacting surfaces of the prosthesis. Five different body weights between 60kg and 140kg in 20kg increments were used to simulate up to 5 million walking cycles.

The methodology has demonstrated that the wear damage, rate and wear patterns were comparable with current literature. The results of this chapter showed that that reducing the initial BW from 140kg to 100kg before THA would decrease the metallic wear by 26% and polyethylene wear by 30%. This can significantly improve the longevity of the prosthesis. As such losing weight down to 100kg before THA can be highly recommended, however, further research is required to investigate the effect of losing weight on the longevity of these devices while in service.

Chapter 6

Impact of different femoral head sizes on THR wear

6.1. Introduction

Modular THR prostheses come in many different designs and sizes as explained in Chapter 2. The differences in design may influence the amount of wear observed on the contacting surfaces of a THR prosthesis. In this chapter, the effect of different femoral head sizes on the wear of THR prostheses is investigated.

In this chapter, femoral head sizes of 22mm, 28mm, 32mm and 36mm were chosen, based on the NJR report (NJR 2022), to simulate walking up to 10 million cycles using the methodology described in Chapter 3. The wear depth, rate, and wear patterns obtained were then compared with results seen in current literature of both retrieved and *in vivo* prostheses. This study can be used for design recommendations to improve the lifespan of these THR prostheses.

6.2. Wear Analysis Input

For this chapter, four different 3D FE models were modelled to study the effects of different head sizes on the THR prosthesis contacting surfaces. The femoral head size increased from 22mm to 36mm while the taper dimensions did not change. The acetabular cup size was increased to accommodate the different femoral head sizes. The XLPE bearing liner remained at a 6mm thickness throughout.

The 3D FE models were then subjected to the realistic gait loading and rotation (see Figure 3-5 and Figure 3-6) which is applied over a 1.2 second duration. The analysis then continued until 10 million cycles of walking was completed.

Table 6-1: Input parameters for wear analysis in chapter 8

Input Data		
Model	3D FE Model (see Figure 3-3)	
Loadings and Rotations	Loads with relative rotations (see Figure 3-5 and Figure 3-6)	
Wear Law	Dissipated Energy	
Scaling Factor	100,000	
Number of load cycles	10,000,000	
Interaction 1	Interaction Combination	Bearing Liner and Femoral Head
	Material Combination	Bearing Liner: XLPE Femoral Head: CoCr
	Surface Picked	Surface 1: XLPE surface Surface 2: Femoral Head Bearing Surface
	Node Pairing	1:3 Pairing
	Wear Coefficient	$5.32 \times 10^{-10} \text{ MPa}^{-1}$
	Wear Fraction	XLPE:CoCr = 0.99:0.01
Interaction 2	Interaction Combination	Femoral Head and Femoral Stem
	Material Combination	Femoral Head: CoCr Femoral Stem: Titanium
	Surface Picked	Surface 1: Femoral Stem Surface 2: Femoral Head Taper Surface
	Node Pairing	1:1 Pairing
	Wear Coefficient	$1.06 \times 10^{-7} \text{ MPa}^{-1}$
	Wear Fraction	CoCr:Ti = 0.9:0.1
	Impaction Force	4000N

6.3. Results

The wear evolution and volumetric wear rates at the bearing surfaces and the taper junction of the hip prosthesis are shown in this section at each 2 million cycles as the solution progressed. The study has modelled walking up to 10 million cycles (1 million steps per year). The wear pattern evolution of the XLPE bearing liner and CoCr femoral head taper surface is shown in Figure 6-1 and Figure 6-2 respectively.

As can be seen in Figure 6-1, the XLPE bearing liner maximum wear depth decreases as the femoral head diameter increase. The XLPE bearing liner of the 22mm femoral head is shown to have a maximum linear wear of 0.37mm while the 36mm femoral head only showed a maximum linear wear of 0.22mm. The overall observed wear pattern remains similar throughout the analysis.

Figure 6-2 shows the wear pattern evolution over 10 years at the femoral head taper surface. As the femoral head size increased, the maximum wear depths were observed to be similar, approximately between 0.027 and 0.032mm. The 36mm femoral head taper surface was observed to have more wear towards the centre of the taper when compared to the 22mm femoral head taper surface.

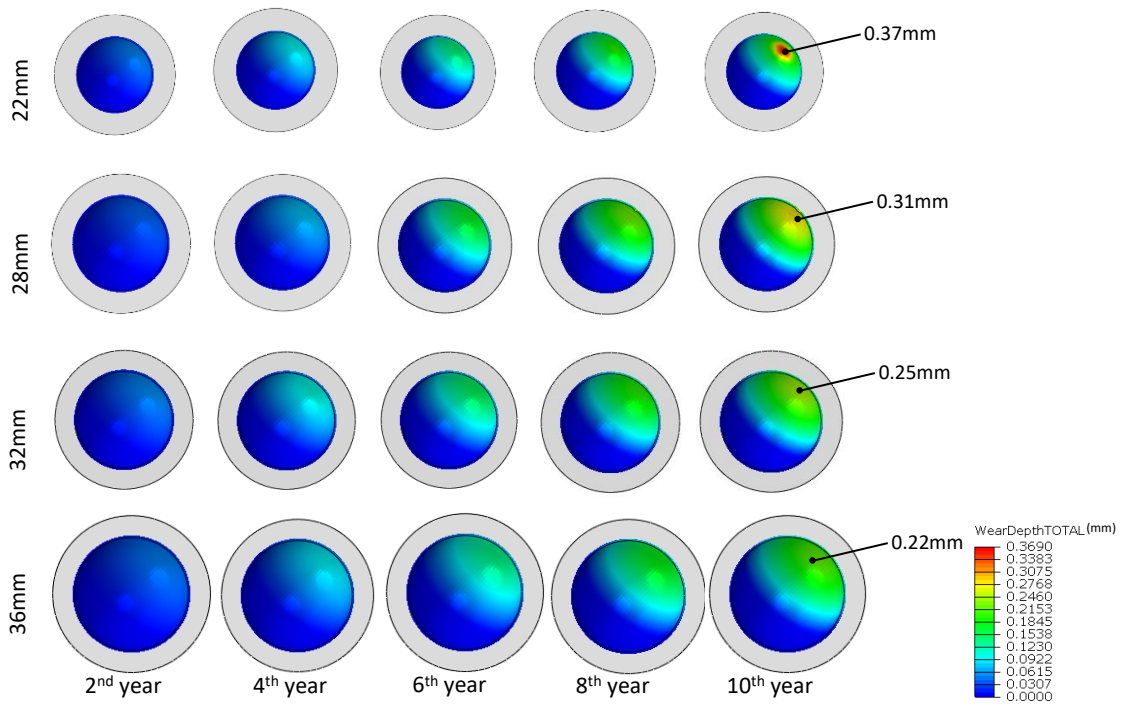


Figure 6-1: Evolution of wear pattern over 10 years at XLPE bearing liner for different head sizes

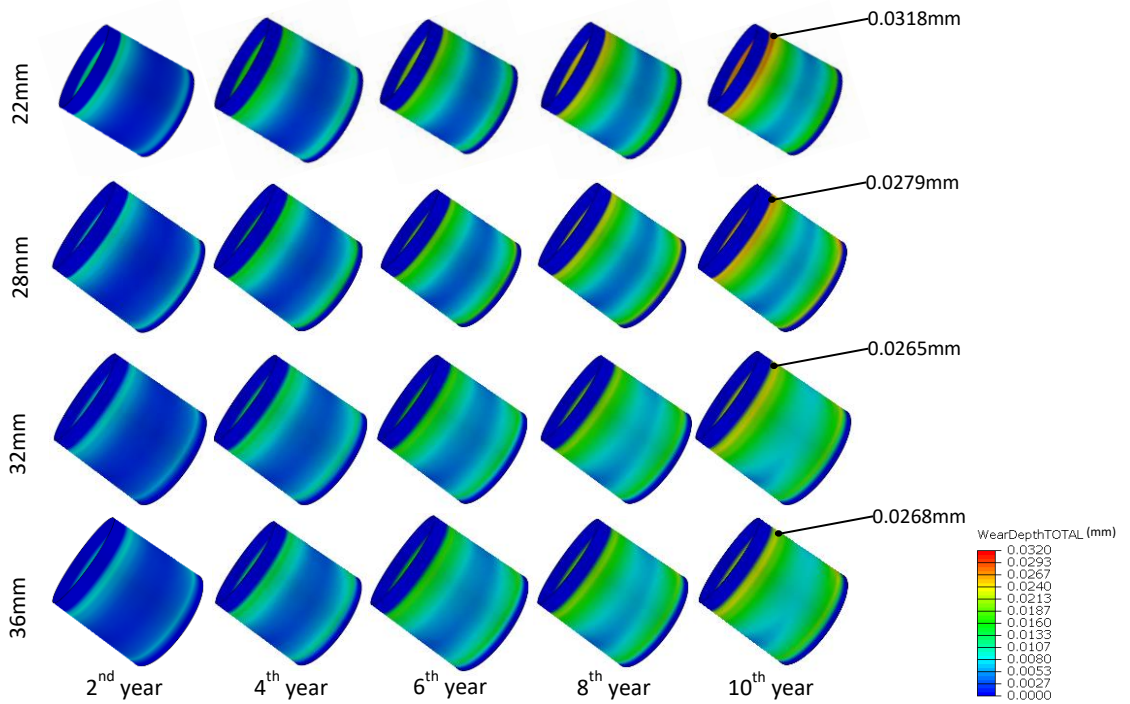


Figure 6-2: Evolution of wear pattern over 10 years at femoral head taper surface

Figure 6-3 shows the cumulative volumetric wear and volumetric wear rates of the XLPE bearing liner, femoral head, and femoral stem.

In Figure 6-3a, it is shown that the cumulative volumetric wear for the XLPE bearing liner increases as the femoral head diameter increases. It can be seen that the maximum XLPE volumetric wear for a 22mm femoral head increases to 98.6mm³ while a 36mm femoral head increases to 159.5mm³ at the end of 10 years. The XLPE volumetric wear rate was found to be constant for each of the femoral head sizes. For a 22mm femoral head, the volumetric wear rate was 10.4mm³/yr while the 36mm femoral head showed a volumetric wear rate of 15.9mm³/yr.

Figure 6-3b shows the cumulative volumetric wear and volumetric wear rate for the femoral head bearing surface. It can be seen that the maximum volumetric wear for a 22mm femoral head increases to 1.01mm³ while a 36mm femoral head increases to 1.64mm³ at the end of 10 years. The cumulative volumetric wear follows the same general trend as the XLPE bearing liner, and the wear corresponds to the wear fraction applied to the model. For the 22mm femoral head, the volumetric wear rate was 0.11mm³/yr and the 36mm femoral head showed a volumetric wear rate of 0.16mm³/yr throughout the study.

Figure 6-3c shows the cumulative volumetric wear and volumetric wear rate for the femoral head taper surface. For a 22mm femoral head, the maximum volumetric wear increases to 4.18mm³ while the 36mm femoral head increases to 4.95mm³. It can be seen that there is a similar trend for different femoral head sizes, where it increases at a lower volumetric wear rate and around 7 million cycles, it increases to a higher stable wear rate. For the 22mm femoral head, the initial volumetric wear rate of the taper surface was 0.34mm³/yr which increases to a stable wear rate of 0.92mm³/yr after 7 years. For the

36mm femoral head, the initial volumetric wear rate for the taper surface was $0.35\text{mm}^3/\text{yr}$ and increases to the stable wear rate of $1.08\text{mm}^3/\text{yr}$ after approximately 7 years. The increase in volumetric wear rate can be attributed to the initial taper locking reducing as explained previously (English, Ashkanfar et al. 2015)

Figure 6-3d shows the cumulative volumetric wear and volumetric wear rate for the femoral stem. For a 22mm femoral head, the femoral stem showed a cumulative volumetric wear of 0.36mm^3 while for the 36mm femoral head, the femoral stem shows a cumulative volumetric wear of 0.44mm^3 . The different femoral heads showed similar trends to the femoral stem wear with the wear increasing to a stable wear rate after 7 years. For the 22mm femoral head, the initial volumetric wear rate for the femoral stem was $0.028\text{mm}^3/\text{yr}$ and increases to $0.080\text{mm}^3/\text{yr}$ after 7 years. For a 36mm femoral head, the femoral stem showed an initial volumetric wear rate of $0.035\text{mm}^3/\text{yr}$ which increases to $0.097\text{mm}^3/\text{yr}$ after 7 years.

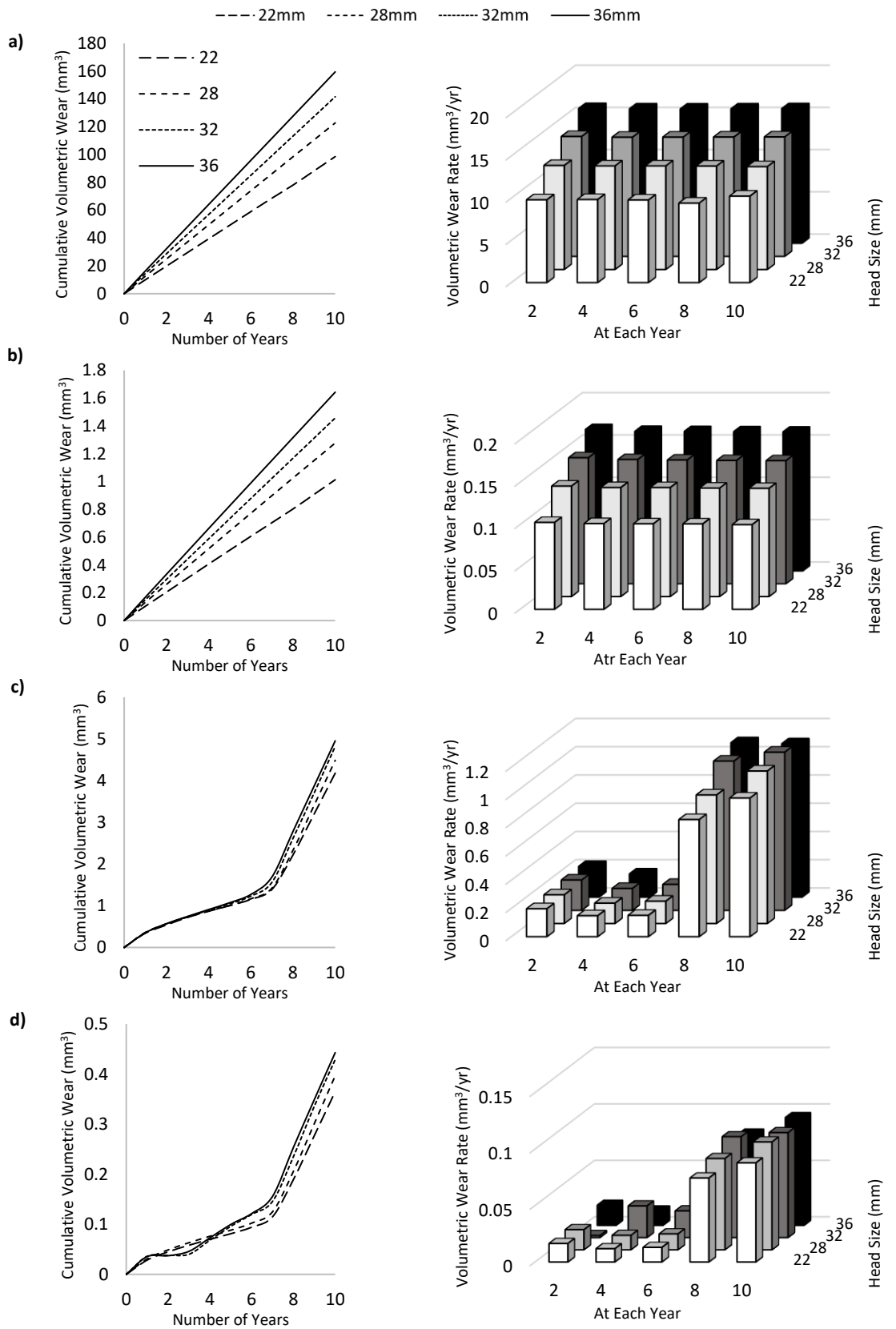


Figure 6-3: Cumulative Volumetric Wear and Volumetric Wear Rate of a) XLPE bearing liner, b) Femoral head bearing surface, c) Femoral head taper surface, d) Femoral stem trunnion

Figure 6-4 shows the evolution of maximum liner wear and linear wear rate at the XLPE bearing liner for the various femoral head sizes. As the femoral head size increases, the maximum linear wear decreases; a 22mm femoral head has a maximum linear wear of 0.37mm while the 36mm femoral head has a maximum linear wear of 0.22mm. There is a steady linear wear rate as the simulation progresses for the different femoral head sizes. For the 22mm femoral head, the maximum linear wear rate was approximately 0.04mm/yr while the 36mm was approximately 0.02mm/yr. Although there is varying XLPE maximum linear wear, the average linear wear was found to be approximately 0.1mm for all femoral head sizes at the end of 10 years.

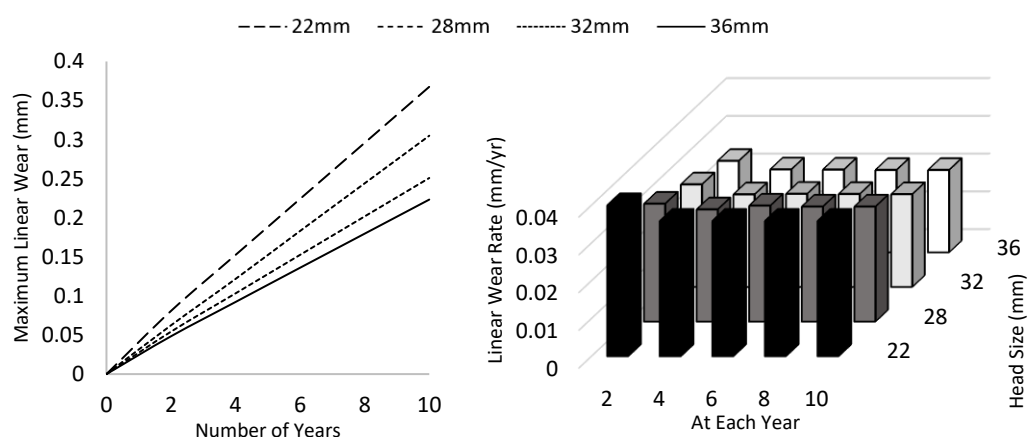


Figure 6-4: Evolution of maximum linear wear and linear wear rate at the XLPE bearing liner

6.4. Discussion

Table 6-2 compares the volumetric wear rates obtained in this study with those available in the current literature. Khoshbin, Wu et al. (2020), Devane, Horne et al. (2017), Haw, Battenberg et al. (2017) and Atrey, Ward et al. (2017) investigated XLPE volumetric wear rates for a total of 247 primary THA prosthesis through radiograph analysis. The studies have observed a range of wear between 1.5 – 33.09mm³/yr. The large range of XLPE volumetric wear is attributed to the many factors which affect wear rates such as patient-specific factors, different prosthesis designs and surgical factors. The XLPE wear rates in this study ranged between 9.4 – 15.9mm³/yr which are within the range seen in the current literature.

Although there is a range of XLPE volumetric wear rate for different femoral head sizes, the average linear wear was found to be similar throughout at approximately 0.1mm. A study by Lachiewicz, Soileau et al. (2016) investigating the effect of femoral head sizes on the XLPE bearing liner wear at between 10 and 14 years, through radiography, have also found that femoral head sizes did not have an impact on the linear wear; however, larger femoral heads were associated with higher volumetric wear.

For the femoral head taper surface, the volumetric wear rates of 0.15 – 1.09mm³/yr from this study are comparable to current literature which shows a range between 0.05 – 1.04mm³/yr. From current literature, Ashkanfar, Langton et al. (2017), Langton, Sidaginamale et al. (2012), Langton, Wells et al. (2018), and Gascoyne, Turgeon et al. (2018) measured the amount of wear using a coordinate-measuring-machine (CMM) from a total of 308 retrieved prostheses. Bhalekar, Smith et al. (2020) investigated the femoral head taper volumetric wear through a 6-station hip simulator. Although the results from this study are within the range seen in current literature, there are other factors which

can influence the amount of wear seen at the taper junction such as taper mismatch (Ashkanfar, Langton et al. 2017), surgical positioning (English, Ashkanfar et al. 2016) or the patients' activity (Toh, Ashkanfar et al. 2022).

Table 6-2: Volumetric wear rates of XLPE liner in current study vs literature

Part	Volumetric wear rate (mm ³ /yr)		
	Current Study	Literature	Reference
XLPE liner	9.4 – 15.9	1.5 – 33.09	(Atrey, Ward et al. 2017, Devane, Horne et al. 2017, Haw, Battenberg et al. 2017, Khoshbin, Wu et al. 2020)
Femoral Head Taper Surface	0.15 – 1.09	0.05 – 1.04	(Langton, Sidaginamale et al. 2012, English, Ashkanfar et al. 2016, Ashkanfar, Langton et al. 2017, Gascoyne, Turgeon et al. 2018, Langton, Wells et al. 2018)

The volumetric wear at the taper junction was observed to increase as the femoral head size increased. The increase in femoral head size from 22mm to 36mm showed an increase in cumulative volumetric wear by 21%. This is comparable to a previous study conducted by Langton, Sidaginamale et al. (2012) which showed that there was increased taper wear for larger femoral head sizes.

A study conducted by Valente, Lanting et al. (2019) investigated a total of 79 retrieved femoral head taper junctions between 28mm and 32mm femoral head diameters with the same taper design. The study also accounted for similar age, gender, BMI, and implantation time. The study concluded that there was no statistical difference in the mean linear wear at the femoral head taper surface against femoral head size. Another study by Langton, Wells et al. (2018) investigated the material loss at the femoral head taper from a retrieval database of Exeter V40 and Universal MoP THAs through use of a coordinate-measuring machine (CMM). The results showed a 4-fold increase in median volumetric wear rate between femoral head sizes of 28mm and 32mm. Upon inspection of the tapers, it was found that the V40 system was designed with a larger taper than trunnion angle, resulting

in a preferential engagement at the trunnion tip. The reverse is true with the Universal system, which engages at the base of the trunnion. A study by Ashkanfar, Langton et al. (2017) showed that a taper mismatch of 9.12' increased the wear by up to 4 times. The study has also found that a slight reduction in the taper mismatch would significantly reduce the magnitude of the wear rates. The findings from these studies and this study can suggest that taper and trunnion design and their tolerances are more likely to play an important role in taper wear rather than femoral head size. This is mainly due to the horizontal lever arm distance which does not change significantly by increasing the femoral head size (Langton, Sidaginamale et al. 2012, Langton, Sidaginamale et al. 2017, Langton, Wells et al. 2018, Norman, Denen et al. 2019).

Wear is an important factor to consider due to the potential release of wear particles into the body (Varnum 2017, Gascoyne, Turgeon et al. 2018). The ideal hip prosthesis would have low wear, low revision risk, and have no adverse reactions with the body. The stability and range of motion of the hip prosthesis can be changed by the femoral head diameter; a smaller femoral head would reduce the range of motion. Burroughs, Hallstrom et al. (2005) evaluated the effect of different femoral heads between 28mm and 44mm diameter on the range of motion of the joint. The study found a significant increase in both flexion before dislocation and displacement between the femoral head and acetabulum for femoral heads greater than 32mm diameter. Matsushita, Nakashima et al. (2009) found that the range of motion improved as the femoral head size increased primarily due to the increased distance required for impingement of the femoral head to occur.

Data from both the Australian Orthopaedic Association National Joint Replacement Registry and Danish Hip Arthroplasty Register analysed the risk factors for dislocations of

different femoral head diameters between 28mm and 36mm (Hermansen, Viberg et al. 2021, Hoskins, Rainbird et al. 2022). Both studies found the 36mm femoral head to have lower dislocation rates than the 28mm and 32mm femoral heads. Further data from the Finnish Arthroplasty Register, found that femoral heads greater than 32mm were associated with a lower risk of dislocation when compared to 28mm femoral heads (Kostensalo, Junnila et al. 2013). These studies highlighted the use of large femoral heads due to the high stability and lower dislocation rates, however the Swedish Hip Arthroplasty Registry have reported no statistically significant difference between 28mm, 32mm and 36mm femoral heads using 28 mm as a reference (Hailer, Weiss et al. 2012). A study by de Steiger (2017) from the Australian Orthopaedic Association National Joint Replacement Registry, investigated late dislocations after primary THR performed with 28mm, 32mm and 36mm of MoP, CoP and CoC bearings. The authors concluded that the 36mm MoP THR had a higher risk of revision due to late dislocation when compared to 36mm CoP and CoC. Moreover, they suggested that this difference was due to the effect of the 36mm metal head on taper corrosion rather than the effect of the 36mm head on XLPE wear. The results suggest caution when 36mm MoXLPE hips are used as their long-term survival could be compromised by late dislocation despite the initial short-to-medium-term stabilizing benefits of 36mm femoral heads.

Hall, Unsworth et al. (1996) previously suggested a cumulative volumetric wear of 500mm³, on average, was necessary for a polyethylene wear related failure of a THR. Based on this assumption, it can be concluded that the 22mm femoral head and the 36mm femoral head in this study would have a lifespan of 53 years and 31 years respectively based on polyethylene wear failures. Other failures such as infection, metallosis, or adverse reaction to particulate debris may drastically reduce the lifespan.

The results from this study are largely dependent on the wear coefficient and amount of activity by the patient. Currently, the simulation only accounts for up to 1 million walking cycles per year and no other activities to be performed by a patient. If a patient is to walk more than 1 million cycles a year, the wear would clearly increase. Increasing the amount of activity and including other activities such as cycling would also further increase the amount of wear observed in the hip prosthesis (Toh, Ashkanfar et al. 2022). It is also noted that a fixed wear coefficient was employed throughout the analysis which does not account for surface roughness changes, but it can show the effect of the head size on the wear evolution parametrically.

6.5. Conclusion

In this study, the 3D FE model coupled with an advanced wear algorithm has been used to investigate the effect of different femoral head diameters on the wear rates on the contacting surfaces of the THR. At the bearing contacting surface, the results show that as the femoral head size increased from 22mm to 36mm, the volumetric wear increased from 98.6mm³ to 159.5mm³ and increased from 1.01mm³ to 1.64mm³ for the XLPE bearing liner and femoral head bearing surface respectively at the end of 10 years. At the taper junction, the results show that as the femoral head size increased from 22mm to 36mm, the volumetric wear increased from 4.18mm³ to 4.95mm³ and 0.36mm³ to 0.44mm³ for the femoral head taper surface and femoral stem trunnion respectively at the end of 10 years. Wear is an important factor to consider due to the potential release of wear particles into the body. If wear was the only factor in prosthesis design, the 22mm femoral head would be best suited, however, there are other factors to consider, such as dislocation risk arising from using a smaller femoral head. This study has provided an insight into the amount of increased wear by increasing the femoral head diameter.

Chapter 7

Impact of bicycling on the wear of THR prostheses

7.1. Introduction

As the number of young and active individuals undergoing Total Hip Arthroplasty (THA) is increasing yearly, there is a need for hip prostheses to have increased longevity. Current investigations into the longevity of these prostheses only include walking as the patient's activity as there is limited data on the amount and intensity of other activity performed by the patient. To further understand the evolution of wear and increase the longevity of these implants, the impact of different activities on the hip prosthesis needs to be investigated. This chapter will investigate the effect of an additional activity, bicycling, alongside walking, on the wear damage evolution on the contact surfaces of a THR prosthesis using the methodology described in Chapter 3.

The following section will utilise the computational methodology presented in Chapter 3 with additional methodology introduced to allow for the automatic transition between walking and bicycling on the 3D FE model. A detailed explanation of the updated methodology will follow in this chapter.

7.2. Methodology

In this chapter, the computational wear algorithm has been further developed to include the effect of bicycling on the wear of the hip prosthesis. A finite element (FE) model of the hip prosthesis was created to simulate the loadings and rotations of both walking and bicycling for up to 5 years of activity. In the simulations it has been assumed that a person post THA, walks 15.5 km per week, equivalent to 1 million cycles a year (Schmalzried, Szuszczewicz et al. 1998), and rides a bicycle 80 km a week, equivalent to 400,000 hip rotations per year (Dickinson, Kingham et al. 2003).

To replicate a walking and bicycling cycle, the femoral head has been assembled towards the orientation for the respective activities as shown in Figure 7-1a and Figure 7-1c. The respective loadings and rotations for both walking and bicycling are shown in Figure 7-1b and Figure 7-1d.

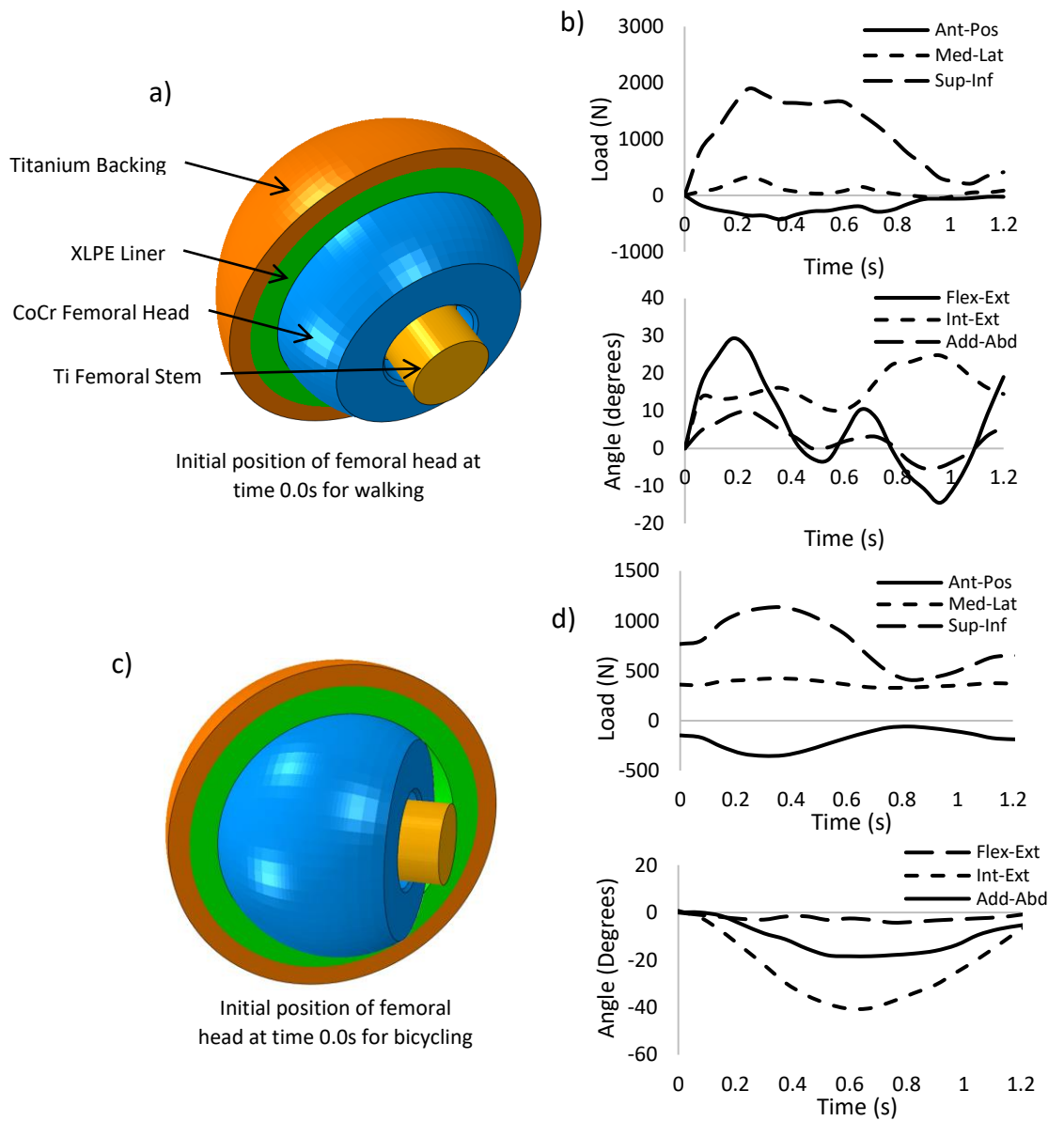


Figure 7-1: a) FE model of hip prosthesis assembled for walking, b) Loadings and rotations for walking cycle, c) FE model of hip prosthesis assembled for bicycling cycle, d) Loadings and rotations for bicycling cycle

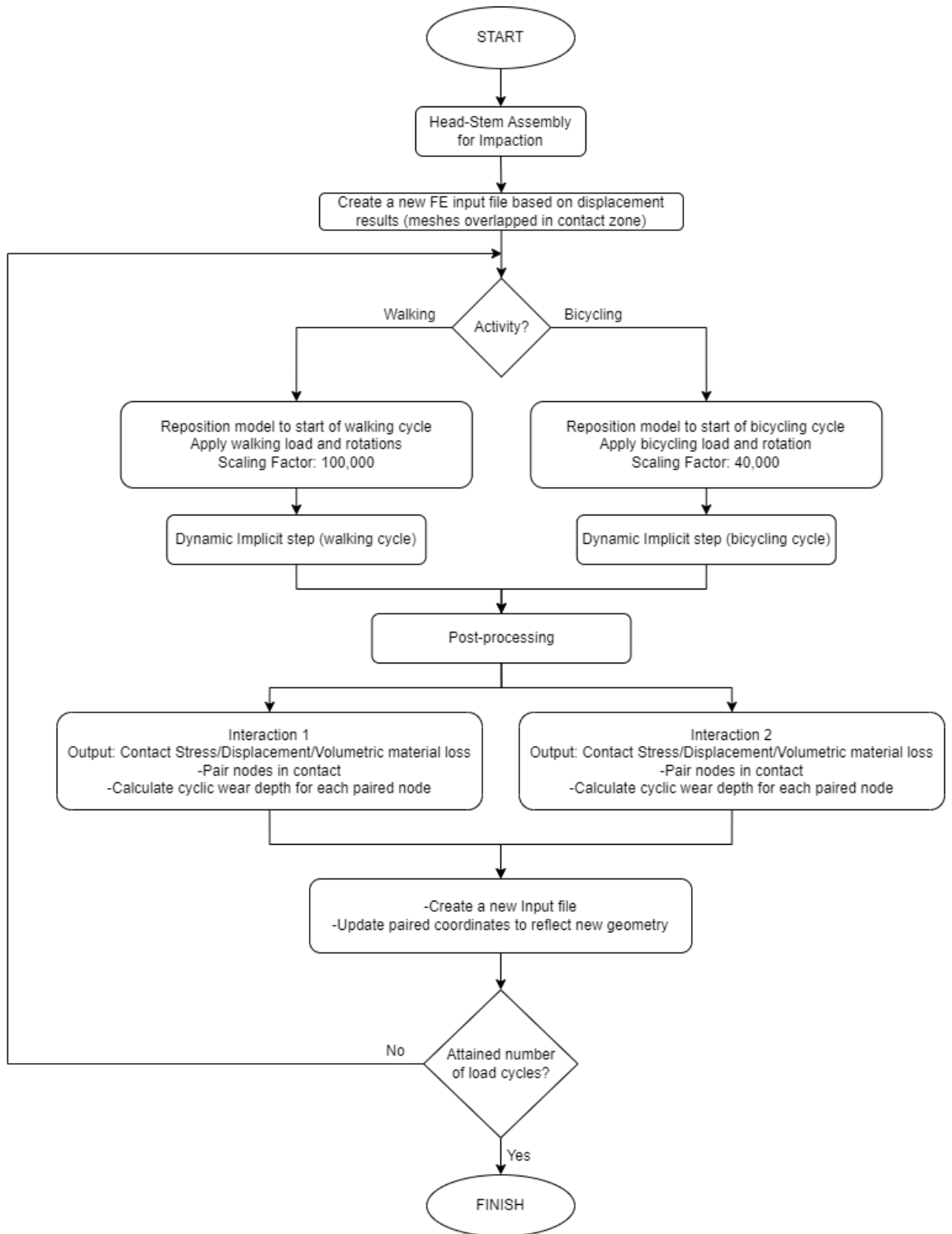


Figure 7-2: Flowchart detailing the modified wear algorithm

7.3. Wear Analysis Input

For this chapter, the 3D FE model shown in Figure 3-3 is used to model both walking and bicycling activities. The starting positions of the FE model for walking and bicycling is shown in Figure 7-1a and Figure 7-1c respectively. The realistic gait and bicycling cycles time-varied loadings and rotations applied over 1.2s for both walking and bicycling is shown in Figure 7-1b and Figure 7-1d. The FE model in this chapter has also accounted for both bearing surface and taper junction interactions within the same analysis.

A summary of the input parameters for the wear analysis is shown in Table 7-1.

Table 7-1: Input parameters for wear analysis in chapter 7

Input Data		
Model	3D FE Model (see Figure 3-3)	
Loadings and Rotations	Loads with relative rotations (see Figure 7-1b and Figure 7-1d)	
Wear Law	Dissipated Energy	
Scaling Factor	Walking: 100,000 Cycling: 40,000	
Number of load cycles	5,000,000 Walking + 2,000,000 Cycling	
Interaction 1	Interactions	Bearing Liner and Femoral Head
	Materials	Bearing Liner: XLPE Femoral Head: CoCr
	Surfaces	Surface 1: XLPE surface Surface 2: Femoral Head Bearing Surface
	Node Pairing	1:3 Pairing
	Wear Coefficient	$5.32 \times 10^{-10} \text{ MPa}^{-1}$
	Wear Fraction	XLPE:CoCr = 0.99:0.01
Interaction 2	Interactions	Femoral Head and Femoral Stem
	Materials	Femoral Head: CoCr Femoral Stem: Titanium
	Surfaces	Surface 1: Femoral Stem Surface 2: Femoral Head Taper Surface
	Node Pairing	1:1 Pairing
	Wear Coefficient	$1.31 \times 10^{-8} \text{ MPa}^{-1}$
	Wear Fraction	CoCr:Ti = 0.9:0.1
	Impaction Force	4000N

7.4. Results and Discussion

Initially, a study was performed for bicycling only to better understand the wear pattern observed on the XLPE bearing liner due to the difference in range of motion. Figure 7-3 compares the wear pattern observed from walking only and bicycling only up to 5 years of activity. The difference in wear area highlights that, different activities may have considerable impact on the evolution of wear rate and the lifespan of the prosthesis.

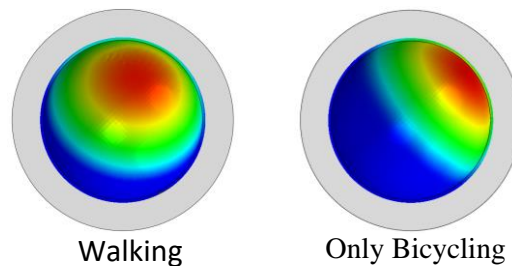


Figure 7-3: Comparison of wear patterns between walking and bicycling up to 5 years of XLPE liner

Figure 7-4 shows the wear pattern of the contacting surfaces of the hip prostheses up to 5 years of walking and bicycling. At the bearing surfaces, the XLPE liner had a maximum linear wear of 0.28mm while the femoral head had a maximum linear wear of 0.0018mm at the end of 5 years. At the taper junction, the femoral head taper surface had a maximum linear wear of 0.0065mm while the femoral stem had a maximum linear wear of 0.0007mm. The results are consistent with the wear fraction applied onto the model: 99% wear on the XLPE liner and 1% wear on the femoral head bearing surface, 90% wear on the femoral head taper surface and 10% wear on the femoral stem.

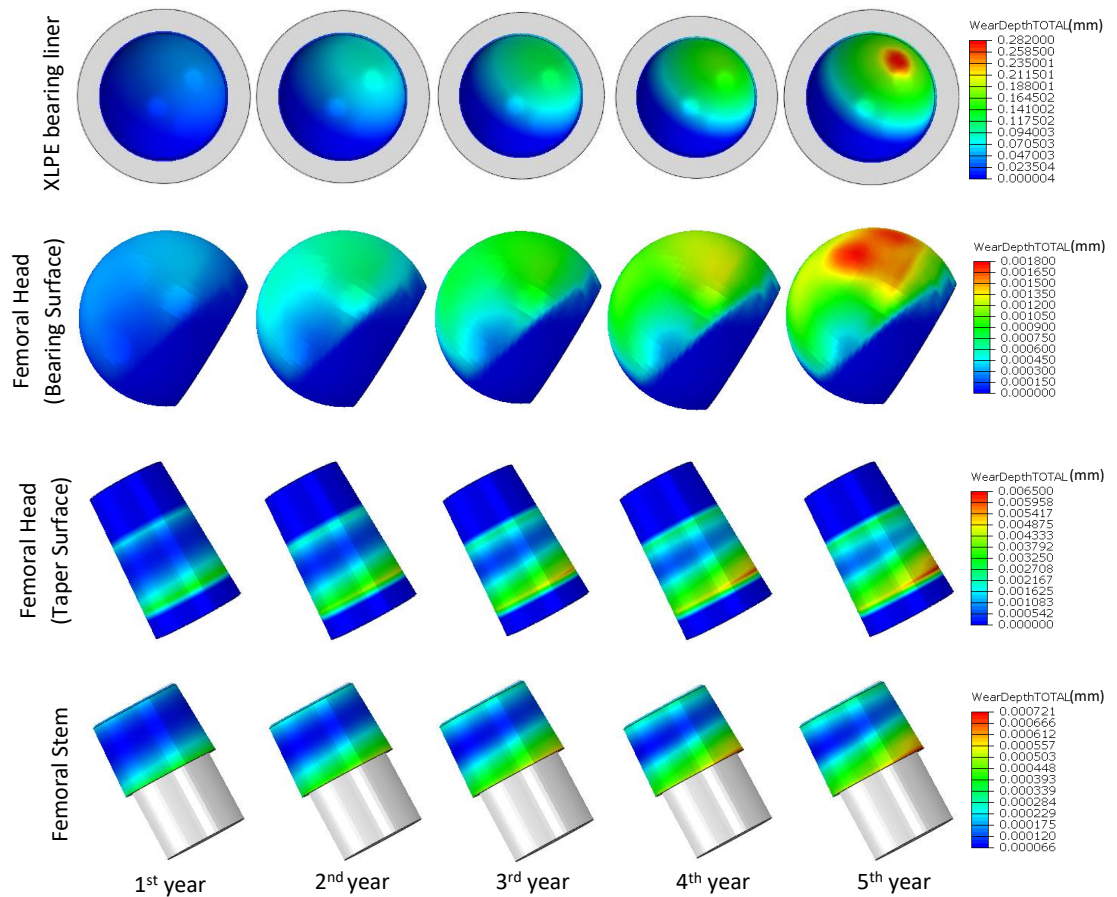


Figure 7-4: Evolution of wear patterns of the XLPE bearing liner, femoral head bearing surface, femoral head taper surface, femoral stem surface for walking and bicycling up to 5 years

Figure 7-5a shows the total volumetric wear and volumetric wear rates over 5 years of walking and bicycling at the XLPE bearing liner, femoral head, and femoral stem. Figure 7-5a shows that the XLPE bearing liner has a total volume loss of 166mm^3 at the end of 5 years, and the volumetric wear rate is maintained at approximately $33\text{mm}^3/\text{yr}$ throughout the analysis.

Figure 7-5b shows the total metallic volumetric wear and volumetric wear rate of the femoral head which includes both the wear from the taper junction and the bearing surface. It also shows the proportion of wear distributed between the taper junction and bearing surface. As the analysis progresses, the total volumetric wear increases to approximately 2.06mm^3 , and the volumetric wear rate has an initially high wear rate of $0.63\text{mm}^3/\text{yr}$ and decreases to a stable volumetric wear rate of $0.3\text{mm}^3/\text{yr}$ approximately after 3 years of

activity. It can be also seen that the taper junction initially contributes to the higher amounts of wear but decreases as the analysis progresses.

Figure 7-5c shows the total volumetric loss and volumetric wear rate at the femoral stem taper. The total volumetric loss increases to approximately 0.088mm^3 at the end of 5 years of activity. The volumetric wear rate for the femoral stem has an initially high wear rate, approximately $0.053\text{mm}^3/\text{yr}$ at the end of the first year which quickly decreases to approximately $0.006\text{mm}^3/\text{yr}$.

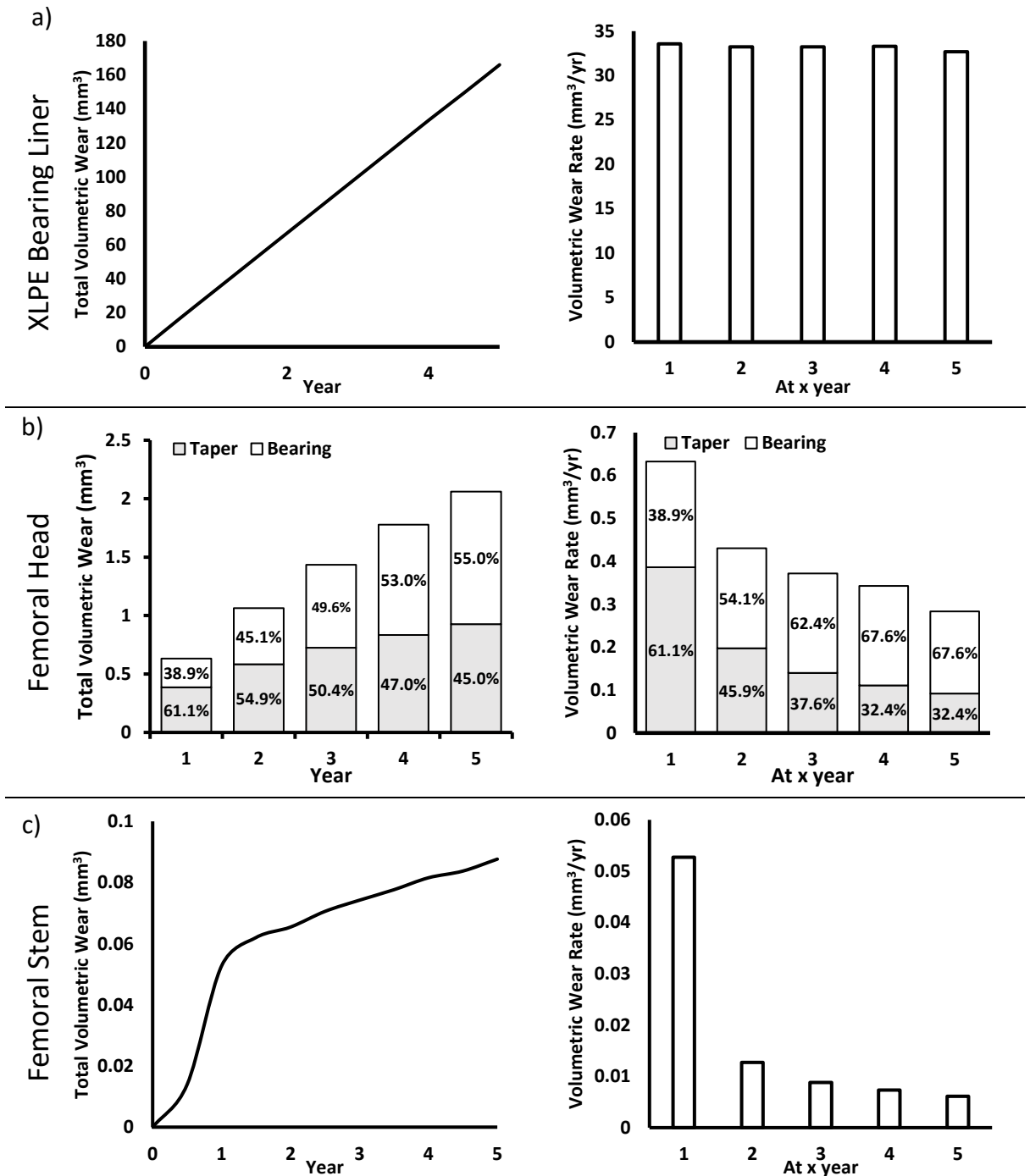


Figure 7-5: Total volumetric wear and volumetric wear rates for a) XLPE bearing liner, b) Femoral head, c) Femoral stem

The volumetric wear rates observed in this study are comparable to previous studies in the literature as shown in Table 7-2. As XLPE is a relatively new material (15 years) used in THRs compared to conventional polyethylene (>50 years), many of the prostheses using XLPE bearing liners are still currently in service. Hence, radiography has been used to estimate the volumetric wear loss of the XLPE bearing liner. The use of XLPE has risen quickly as it has better wear characteristics than conventional polyethylene allowing for lower amounts

of wear. Khoshbin, Wu et al. (2020), Devane, Horne et al. (2017), Haw, Battenberg et al. (2017) and Atrey, Ward et al. (2017) have used radiography to analyse a total of 247 primary THA with XLPE bearing liners with CoCr femoral heads and found that the volumetric wear rate ranged between 1.5 – 57.6mm³/yr. The results in this study of 33mm³/yr XLPE volumetric wear rate was within the range obtained from the literature.

A co-ordinate measuring machine (CMM) has been previously used to measure the volumetric wear of 54 retrieved femoral stems which reported a mean volumetric wear rate of 0.55mm³/yr with a range between 0.02 – 2.241mm³/yr (Ashkanfar, Langton et al. 2017). Additionally, a study by Langton, Sidaginamale et al. (2012) also used a CMM to measure the volumetric wear rate at the taper surface of 48 retrieved hip prostheses and found the mean volumetric wear rate to be 0.127mm³/yr with a range between 0.01 – 3.15mm³/yr. The results in this study of between 0.1 – 0.39mm³/yr are within agreement with those in the literature of 0.01 – 3.15mm³/yr.

It is important to note that the results obtained from previous literature do not account for the patients' activity as the amount of activity performed by an individual is unknown. Furthermore, a variety of distinct factors can influence prostheses wear such as patient activity, weight, prostheses design, or surgical positioning of components.

Table 7-2: Volumetric wear rates of XLPE liner in current study vs literature

Part	Volumetric wear rate (mm ³ /yr)		
	Current Study	Literature	Reference
XLPE liner	33	1.5 – 57.6	(Atrey, Ward et al. 2017, Devane, Horne et al. 2017, Haw, Battenberg et al. 2017, Khoshbin, Wu et al. 2020)
Femoral Stem	0.1 – 0.39	0.01 – 3.15	(Langton, Sidaginamale et al. 2012, Ashkanfar, Langton et al. 2017)

Table 7-3 highlights the increased amount of volumetric wear rate induced by additional bicycling of 80km per week for 5 years (over walking alone). It can be seen that the mean volumetric wear increases by 67% for XLPE and 11% for metallic wear. Previously, a study by Hall, Unsworth et al. (1996) examined over 100 explanted Charnley UHMWPE sockets and found that the median volume of wear at revision to be 508mm³. If UHMWPE and XLPE debris is assumed to have the same effect on the human body, a life span of 25.7 years can be calculated with walking only, compared to 15.4 years with walking and bicycling. Given that the average age of the recipient of an artificial hip joint in the UK is 69 (NJR 2021), the benefits of exercise such as bicycling over a 15 year period will likely outweigh the drawback of additional polyethylene wear (Oja, Titze et al. 2011). It is also important to note that the amount of bicycling simulated in this study was the higher end of activity by the patient. Furthermore, Haw, Battenberg et al. (2017) identified hips with risk of osteolysis to have wear above 80mm³/yr. The walking and bicycling wear rate of 33mm³/year is less than half of the osteolysis wear rate offered by Haw, Battenberg et al. (2017).

Table 7-3: Volumetric wear rate between walking and bicycling up to 5 years

Part	Mean Volumetric Wear Rate (mm ³ /yr)			% Increase
	Walking	Walking and Bicycling		
XLPE bearing liner	19.8	33.0		67%
Metallic Wear	0.365	0.406		11%

Walking and bicycling are currently two of the most performed activities by patients. The hip joint forces during a normal walking cycle were found to be between 2.9 – 4.7 times body weight (Kuster 2002) while it was found that during bicycling, the hip joint forces are between 0.5 – 1.4 times body weight (Ericson and Nisell 1986, Damm, Dymke et al. 2017). To lower the amount of loading the prosthesis experiences during bicycling, THA patients

may consider utilising an electric bicycle to reduce the impact on the hip prosthesis especially during uphill bicycling. This will further reduce the wear rates and help patients be active post-surgery, which will in turn improve the long-term outcomes and lifespan of the hip prosthesis.

In this study, the upper limit of 80km per week for bicycling activity was used to simulate a patient's activity and as such, the findings of this study show the wear of a hip prosthesis higher than what could be seen in patients. This study also has not considered for other activities performed by patients which could be paramount to the wear pattern shown.

7.5. Conclusion

As a number of THA patients are increasingly active, it is important to investigate the impact of different sports on the wear of the hip prosthesis. In this study, an FE model coupled with an advanced wear algorithm has been used to investigate the impact of bicycling up to 80km a week on the wear of the contacting surfaces of a hip prosthesis over a period of 5 years. The results have shown that the XLPE bearing liner undergoes steady volumetric wear rate of $33\text{mm}^3/\text{yr}$, the femoral head undergoes a decreasing volumetric wear rate from $0.54\text{mm}^3/\text{yr}$ to $0.26\text{mm}^3/\text{yr}$ at the end of 5 years, while the femoral stem showed an initial volumetric wear of $0.073\text{mm}^3/\text{yr}$ which reduces to a steady volumetric wear rate of $0.009\text{mm}^3/\text{yr}$. It was found that by adding bicycling up to 80km per week, the volumetric wear rate increases up to 67% on the XLPE bearing liner, 11% on the femoral head and 12.5% on the femoral stem when compared to just walking up to 5 years. If XLPE and UHMWPE wear debris is assumed to have the same effect on the body, the THA lifespan can be calculated as 25.7 years for walking only compared to 15.4 years with walking and bicycling. The findings of this study have considered the upper limit of a patient's activity and as such, may show higher wear than what could be seen in patients. There are also other health

benefits such as improved cardiovascular health, weight loss, and general fitness improvement.

Chapter 8

Conclusion and future work

8.1. Conclusion

A theoretical approach into predicting wear aided with computational capability and experimental variables can be used to increase the longevity of total hip prostheses in service. Furthermore, this can be used to predict long term behaviour of these devices without requiring experimental testing.

Experimental wear testing for a hip prosthesis is time consuming, expensive, and complicated. Computational wear modelling has been found to be an alternative method to predict wear for its relatively low cost, faster speeds, with complete and detailed solutions available. These combined, will allow for a fast assessment of designs and performance in service to determine functionality of the prosthesis device and validate existing or new designs. It could also provide guidelines for clinical practice to recommend patients for activity post total hip replacement.

The aim of this research was to develop a computational methodology to predict wear at both the bearing surfaces (between the XLPE bearing liner and femoral head) and taper surfaces (between the femoral head and femoral stem).

Based on the wear model presented in this research, the main contributions of this research can be summarised as follows:

- The methodology can simulate both the bearing surface wear and taper junction wear within the same analysis with individual wear parameters.
- The results obtained using the 3D FE model of the hip prosthesis have been compared against observation of retrieved prostheses and wear measurements found in literature. From these comparisons, the computational results show considerable promise, but are clearly dependent on the wear coefficient used for the study.
- The wear method presented has been generalized which can be used for different designs of hip prostheses and for other applications such as other prosthetic devices.
- The method has been used to investigate different patient body weights.
- The method can consider different material combinations and specific wear fractions for different hip prosthesis designs to predict wear at the contacting surfaces.
- The method can vary the wear coefficient throughout the analysis. The variation of wear coefficient can be obtained from controlled wear tests.
- The method can vary the activity performed by the model concurrently. This can be used to investigate the impact of multiple activities on the longevity of the hip prosthesis to improve the patient's quality of life.

- The method can use either the Archard's or Dissipated energy wear law.

The wear methodology and algorithm in this research can be used for further investigations in the future, which could indeed help designers, physicians, and surgeons to minimise the effects of hip prosthesis wear, surface damage and increase the longevity of the designs in operation.

8.2. Future work

Wear is a complicated process to predict computationally. The research presented within this research is a step towards predicting wear between contacting surfaces while under load. As discussed in Chapter 2, a review of literature has highlighted areas which need further investigations. This present research has completed a computational approach to predicting wear in total hip prosthesis which still warrants further research. Future research can be listed as below:

- It is apparent that the wear predicted throughout this study is critically dependent on the wear coefficient used. Currently, the values for wear coefficient vary largely due to the materials and surface characteristics. Furthermore, the wear coefficient changes throughout the wearing process and as such, an investigation into the variation of wear coefficients throughout a wear analysis could be studied which could be applied into the computational method presented here.
- The effects of corrosion and material creep has not been considered in this study. Further research into corrosion and material creep can be beneficial to incorporate other methods of damage into the computational method presented here.

- Friction plays a crucial role in the wearing process due to the changes in the magnitude of relative slip. The effect of a varied friction coefficient on the wear of the hip prosthesis could be investigated.
- The computational method here is currently generalized, and as such, investigations into using this computational method for other orthopaedic applications such as knee or shoulder prosthesis to predict wear and ultimately increase their longevities through design, material, or surgical methods.

References

- A., R., K. D. and B. T. N. (2014). "The current state of bearing surfaces in total hip replacement." The Bone & Joint Journal **96-B**(2): 147-156.
- Abdelgaied, A., C. L. Brockett, F. Liu, L. M. Jennings, J. Fisher and Z. Jin (2013). "Quantification of the effect of cross-shear and applied nominal contact pressure on the wear of moderately cross-linked polyethylene." Proceedings of the Institution of Mechanical Engineers, Part H: Journal of Engineering in Medicine **227**(1): 18-26.
- Affatato, S., W. Leardini and M. Zavalloni (2006). Hip Joint Simulators: State of the Art. Bioceramics and Alternative Bearings in Joint Arthroplasty, Darmstadt, Steinkopff.
- Ali, M., M. Al-Hajjar and L. M. Jennings (2016). 31 - Tribology of UHMWPE in the Hip. UHMWPE Biomaterials Handbook (Third Edition). S. M. Kurtz. Oxford, William Andrew Publishing: 579-598.
- Ali, M., M. Al-Hajjar, S. Partridge, S. Williams, J. Fisher and L. M. Jennings (2016). "Influence of hip joint simulator design and mechanics on the wear and creep of metal-on-polyethylene bearings." Proceedings of the Institution of Mechanical Engineers, Part H: Journal of Engineering in Medicine **230**(5): 389-397.
- Amlie, E., Ø. Høvik and O. Reikerås (2010). "Dislocation after total hip arthroplasty with 28 and 32-mm femoral head." J Orthop Traumatol **11**(2): 111-115.
- Anissian, L., A. Stark, K. Sorensen, A. Gustafson, B. Downs, V. Good and I. Clarke (1999). HIP-SIMULATOR WEAR COMPARISONS OF COCR/COCR VERSUS COCR/PE THR AT 10 MILLION CYCLES. Proceedings of the Annual Meeting of the Orthopaedic Research Society, Anaheim, California.
- Archard, J. F. (1953). "Contact and Rubbing of Flat Surfaces." Journal of Applied Physics **24**(8): 981-988.
- Arden, N. and M. C. Nevitt (2006). "Osteoarthritis: Epidemiology." Best Practice & Research Clinical Rheumatology **20**(1): 3-25.
- Ashkanfar, A., D. J. Langton and T. J. Joyce (2017). "Does a micro-grooved trunnion stem surface finish improve fixation and reduce fretting wear at the taper junction of total hip replacements? A finite element evaluation." Journal of Biomechanics **63**: 47-54.
- Ashkanfar, A., D. J. Langton and T. J. Joyce (2017). "A large taper mismatch is one of the key factors behind high wear rates and failure at the taper junction of total hip replacements: A finite element wear analysis." Journal of the mechanical behavior of biomedical materials **69**: 257-266.
- Atkinson, J. R., D. Dowson, J. H. Isaac and B. M. Wroblewski (1985). "Laboratory wear tests and clinical observations of the penetration of femoral heads into acetabular cups in total replacement hip joints: III: The measurement of internal volume changes in explanted Charnley sockets after 2–16 years in vivo and the determination of wear factors." Wear **104**(3): 225-244.
- Atrey, Ward, Khoshbin, Hussain, Bogoch, Schemitsch and Waddell (2017). "Ten-year follow-up study of three alternative bearing surfaces used in total hip arthroplasty in young patients." The Bone & Joint Journal **99-B**(12): 1590-1595.
- Bergmann, G., F. Graichen and A. Rohlmann (1993). "Hip joint loading during walking and running, measured in two patients." Journal of Biomechanics **26**(8): 969-990.
- Bevill, S. L., G. R. Bevill, J. R. Penmetsa, A. J. Petrella and P. J. Rullkoetter (2005). "Finite element simulation of early creep and wear in total hip arthroplasty." Journal of Biomechanics **38**(12): 2365-2374.
- Bhalekar, R. M., S. L. Smith and T. J. Joyce (2020). "Hip simulator testing of the taper-trunnion junction and bearing surfaces of contemporary metal-on-cross-linked-polyethylene hip prostheses." Journal of Biomedical Materials Research Part B: Applied Biomaterials **108**(1): 156-166.
- Bishop, N., F. Witt, R. Pourzal, A. Fischer, M. Rüttschi, M. Michel and M. Morlock (2013). "Wear patterns of taper connections in retrieved large diameter metal-on-metal bearings." J Orthop Res **31**(7): 1116-1122.
- Bitar, D. and J. Parvizi (2015). "Biological response to prosthetic debris." World J Orthop **6**(2): 172-189.

Bone, M. C., R. P. Sidaginamale, J. K. Lord, S. C. Scholes, T. J. Joyce, A. V. Nargol and D. J. Langton (2015). "Determining material loss from the femoral stem trunnion in hip arthroplasty using a coordinate measuring machine." Proc Inst Mech Eng H **229**(1): 69-76.

Bosker, B. H., H. B. Ettema, M. van Rossum, M. F. Boomsma, B. J. Kollen, M. Maas and C. C. Verheyen (2015). "Pseudotumor formation and serum ions after large head metal-on-metal stemmed total hip replacement. Risk factors, time course and revisions in 706 hips." Arch Orthop Trauma Surg **135**(3): 417-425.

Boutin, P., P. Christel, J. M. Dorlot, A. Meunier, A. De Roquancourt, D. Blanquaert, S. Herman, L. Sedel and J. Witvoet (1988). "The use of dense alumina–alumina ceramic combination in total hip replacement." Journal of biomedical materials research **22**(12): 1203-1232.

Buckwalter, J. A., C. Saltzman and T. Brown (2004). "The Impact of Osteoarthritis: Implications for Research." Clinical Orthopaedics and Related Research® **427**: S6-S15.

Bullock, J., S. A. A. Rizvi, A. M. Saleh, S. S. Ahmed, D. P. Do, R. A. Ansari and J. Ahmed (2018). "Rheumatoid Arthritis: A Brief Overview of the Treatment." Medical Principles and Practice **27**(6): 501-507.

Burroughs, B. R., B. Hallstrom, G. J. Golladay, D. Hoeffel and W. H. Harris (2005). "Range of Motion and Stability in Total Hip Arthroplasty With 28-, 32-, 38-, and 44-mm Femoral Head Sizes: An In Vitro Study." The Journal of Arthroplasty **20**(1): 11-19.

Byrne, D., K. Mulhall and J. Baker (2010). "Anatomy & Biomechanics of the Hip." The Open Sports Medicine Journal **4**.

Callaghan, J. J., D. R. Pedersen, R. C. Johnston and T. D. Brown (2003). "Clinical biomechanics of wear in total hip arthroplasty." The Iowa orthopaedic journal **23**: 1.

Castro, F. and R. Barrack (2000). Core decompression and conservative treatment for avascular necrosis of the femoral head: a meta-analysis. Database of Abstracts of Reviews of Effects (DARE): Quality-assessed Reviews [Internet], Centre for Reviews and Dissemination (UK).

Cawley, J., J. E. P. Metcalf, A. H. Jones, T. J. Band and D. S. Skupien (2003). "A tribological study of cobalt chromium molybdenum alloys used in metal-on-metal resurfacing hip arthroplasty." Wear **255**(7): 999-1006.

CHAPPARD, D., L. RONY, F. DUCELLIER, V. STEIGER and L. HUBERT (2021). "Wear debris released by hip prosthesis analysed by microcomputed tomography." Journal of Microscopy **282**(1): 13-20.

Charbonnier, C., S. Chagué, J. Schmid, F. C. Kolo, M. Bernardoni and P. Christofilopoulos (2015). "Analysis of Hip Range of Motion in Everyday Life: A Pilot Study." HIP International **25**(1): 82-90.

Charnley, J. (1961). "ARTHROPLASTY OF THE HIP: A New Operation." The Lancet **277**(7187): 1129-1132.

Chaudhary, M., S. Boruah, O. K. Muratoglu and K. M. Varadarajan (2020). "Evaluation of pull-off strength and seating displacement of sleeved ceramic revision heads in modular hip arthroplasty." Journal of Orthopaedic Research **38**(7): 1523-1528.

Choudhury, D., M. Ranuša, R. A. Fleming, M. Vrbka, I. Křupka, M. G. Teeter, J. Goss and M. Zou (2018). "Mechanical wear and oxidative degradation analysis of retrieved ultra high molecular weight polyethylene acetabular cups." Journal of the Mechanical Behavior of Biomedical Materials **79**: 314-323.

Cipriano, C. A., P. S. Issack, B. Beksaç, A. G. Della Valle, T. P. Sculco and E. A. Salvati (2008). "Metallosis after metal-on-polyethylene total hip arthroplasty." Am J Orthop (Belle Mead NJ) **37**(2): E18-25.

Cohen, D. (2011). "Out of joint: The story of the ASR." BMJ : British Medical Journal **342**: d2905.

Cook, R. B., B. J. R. F. Bolland, J. A. Wharton, S. Tilley, J. M. Latham and R. J. K. Wood (2013). "Pseudotumour Formation Due to Tribocorrosion at the Taper Interface of Large Diameter Metal on Polymer Modular Total Hip Replacements." The Journal of Arthroplasty **28**(8): 1430-1436.

Cooper, H. J., C. J. Della Valle, R. A. Berger, M. Tetreault, W. G. Paprosky, S. M. Sporer and J. J. Jacobs (2012). "Corrosion at the head-neck taper as a cause for adverse local tissue reactions after total hip arthroplasty." The Journal of bone and joint surgery. American volume **94**(18): 1655.

Crawford, R. W. and D. W. Murray (1997). "Total hip replacement: indications for surgery and risk factors for failure." Annals of the Rheumatic Diseases **56**(8): 455.

Damm, P., J. Dymke, A. Bender, G. Duda and G. Bergmann (2017). "In vivo hip joint loads and pedal forces during ergometer cycling." Journal of Biomechanics **60**: 197-202.

Danoff, J. R., J. Longaray, R. Rajaravivarma, A. Gopalakrishnan, A. F. Chen and W. J. Hozack (2018). "Impaction Force Influences Taper-Trunnion Stability in Total Hip Arthroplasty." The Journal of Arthroplasty **33**(7, Supplement): S270-S274.

Davis, K. E., M. A. Ritter, M. E. Berend and J. B. Meding (2007). "The Importance of Range of Motion after Total Hip Arthroplasty." Clinical Orthopaedics and Related Research® **465**: 180-184.

Day, M. S., D. Nam, S. Goodman, E. P. Su and M. Figgie (2012). "Psoriatic arthritis." JAAOS-Journal of the American Academy of Orthopaedic Surgeons **20**(1): 28-37.

de Steiger, R. (2017). "Late dislocations after total hip arthroplasty: is the bearing a factor?".

Devane, P. A., J. G. Horne, A. Ashmore, J. Mutimer, W. Kim and J. Stanley (2017). "Highly Cross-Linked Polyethylene Reduces Wear and Revision Rates in Total Hip Arthroplasty: A 10-Year Double-Blinded Randomized Controlled Trial." JBJS **99**(20): 1703-1714.

Di Puccio, F. and L. Mattei (2015). "A novel approach to the estimation and application of the wear coefficient of metal-on-metal hip implants." Tribology International **83**: 69-76.

Dickinson, J. E., S. Kingham, S. Copsy and D. J. P. Hougie (2003). "Employer travel plans, cycling and gender: will travel plan measures improve the outlook for cycling to work in the UK?" Transportation Research Part D: Transport and Environment **8**(1): 53-67.

Donaldson, F. E., J. C. Coburn and K. L. Siegel (2014). "Total hip arthroplasty head-neck contact mechanics: A stochastic investigation of key parameters." Journal of Biomechanics **47**(7): 1634-1641.

Doorn, P., P. Campbell, J. Worrall, P. Benya, H. McKellop and H. Amstutz (1998). "Metal wear particle characterization from metal on metal total hip replacements: Transmission electron microscopy study of periprosthetic tissues and isolated particles." Journal of biomedical materials research **42**: 103-111.

Dorr, L. D., Z. Wan, D. B. Longjohn, B. Dubois and R. Murken (2000). "Total Hip Arthroplasty with Use of the Metasul Metal-on-Metal Articulation : Four to Seven-Year Results*." JBJS **82**(6): 789.

Drake, R., A. W. Vogl and A. W. Mitchell (2009). Gray's anatomy for students, Elsevier Health Sciences.

Drummond, J., P. Tran and C. Fary (2015). "Metal-on-metal hip arthroplasty: a review of adverse reactions and patient management." Journal of functional biomaterials **6**(3): 486-499.

Dyrkacz, R. M. R., J.-M. Brandt, O. A. Ojo, T. R. Turgeon and U. P. Wyss (2013). "The Influence of Head Size on Corrosion and Fretting Behaviour at the Head-Neck Interface of Artificial Hip Joints." The Journal of Arthroplasty **28**(6): 1036-1040.

Dyrkacz, R. M. R., J. M. Brandt, J. B. Morrison, S. T. O' Brien, O. A. Ojo, T. R. Turgeon and U. P. Wyss (2015). "Finite element analysis of the head-neck taper interface of modular hip prostheses." Tribology International **91**: 206-213.

Edgar, C. and T. Einhorn (2014). "Treatment of Avascular Necrosis of the Femoral Head With Drilling and Injection of Concentrated Autologous Bone Marrow." Techniques in Orthopaedics **29**: 218-224.

Electricwala, A. J., R. Narkbunnam, J. I. Huddleston III, W. J. Maloney, S. B. Goodman and D. F. Amanatullah (2016). "Obesity is associated with early total hip revision for aseptic loosening." The Journal of arthroplasty **31**(9): 217-220.

Engh, C. A., S. J. MacDonald, S. Sritulanondha, A. Korczak, D. Naudie and C. Engh (2014). "Metal ion levels after metal-on-metal total hip arthroplasty: a five-year, prospective randomized trial." J Bone Joint Surg Am **96**(6): 448-455.

English, R., A. Ashkanfar and G. Rothwell (2015). "A computational approach to fretting wear prediction at the head-stem taper junction of total hip replacements." Wear **338-339**: 210-220.

English, R., A. Ashkanfar and G. Rothwell (2016). "The effect of different assembly loads on taper junction fretting wear in total hip replacements." Tribology International **95**: 199-210.

Ericson, M. O. and R. Nisell (1986). "Tibiofemoral joint forces during ergometer cycling." The American Journal of Sports Medicine **14**(4): 285-290.

Essner, A., K. Sutton and A. Wang (2005). "Hip simulator wear comparison of metal-on-metal, ceramic-on-ceramic and crosslinked UHMWPE bearings." Wear **259**(7): 992-995.

Ferguson, R. J., A. J. R. Palmer, A. Taylor, M. L. Porter, H. Malchau and S. Glyn-Jones (2018). "Hip replacement." The Lancet **392**(10158): 1662-1671.

Ferguson, S., J. Bryant, R. Ganz and K. Ito (2000). "The acetabular labrum seal: a poroelastic finite element model." Clinical Biomechanics **15**(6): 463-468.

Ferguson, S., J. Bryant, R. Ganz and K. Ito (2000). "The influence of the acetabular labrum on hip joint cartilage consolidation: a poroelastic finite element model." Journal of biomechanics **33**(8): 953-960.

Ferguson, S., J. T. Bryant, R. Ganz and K. Ito (2003). "An in vitro investigation of the acetabular labral seal in hip joint mechanics." Journal of biomechanics **36**(2): 171-178.

Fessler, H. and D. C. Fricker (1989). "Friction in femoral prosthesis and photoelastic model cone taper joints." Proceedings of the Institution of Mechanical Engineers, Part H: Journal of Engineering in Medicine **203**(1): 1-14.

Fialho, J. C., P. R. Fernandes, L. Eça and J. Folgado (2007). "Computational hip joint simulator for wear and heat generation." Journal of Biomechanics **40**(11): 2358-2366.

Fisher, J., L. M. Jennings and A. L. Galvin (2006). Wear of Highly Crosslinked Polyethylene against Cobalt Chrome and Ceramic femoral heads. Bioceramics and Alternative Bearings in Joint Arthroplasty, Darmstadt, Steinkopff.

Fouvry, S., P. Kapsa and L. Vincent (2001). "An elastic–plastic shakedown analysis of fretting wear." Wear **247**(1): 41-54.

Fouvry, S., T. Liskiewicz, P. Kapsa, S. Hannel and E. Sauger (2003). "An energy description of wear mechanisms and its applications to oscillating sliding contacts." Wear **255**(1): 287-298.

Fridrici, V., S. Fouvry and P. Kapsa (2001). "Effect of shot peening on the fretting wear of Ti–6Al–4V." Wear **250**(1): 642-649.

Galvin, A. L., E. Ingham, M. H. Stone and J. Fisher (2006). Penetration, creep and wear of highly crosslinked UHMWPE in a hip joint simulator. Orthopaedic Proceedings, The British Editorial Society of Bone & Joint Surgery.

Galvin, A. L., L. M. Jennings, J. L. Tipper, E. Ingham and J. Fisher (2010). "Wear and creep of highly crosslinked polyethylene against cobalt chrome and ceramic femoral heads." Proc Inst Mech Eng H **224**(10): 1175-1183.

Gao, L., Z. Hua and R. Hewson (2018). "Can a “pre-worn” bearing surface geometry reduce the wear of metal-on-metal hip replacements? – A numerical wear simulation study." Wear **406-407**: 13-21.

Garcia-Cimbrelo, E., J.-M. Martinez-Sayanes, A. Minuesa and L. Munuera (1996). "Mittelmeier ceramic—ceramic prosthesis after 10 years." The Journal of arthroplasty **11**(7): 773-781.

Gascoyne, T. C., T. R. Turgeon and C. D. Burnell (2018). "Retrieval Analysis of Large-Head Modular Metal-on-Metal Hip Replacements of a Single Design." The Journal of Arthroplasty **33**(6): 1945-1952.

Ginaldi, L., M. C. Di Benedetto and M. De Martinis (2005). "Osteoporosis, inflammation and ageing." Immun Ageing **2**: 14.

Goldring, M. B. and M. Otero (2011). "Inflammation in osteoarthritis." Curr Opin Rheumatol **23**(5): 471-478.

Grammatico-Guillon, L., C. Perreau, K. Miliani, F. L’Heriteau, P. Rosset, L. Bernard, D. Lepelletier, E. Rusch and P. Astagneau (2017). "Association of Partial Hip Replacement With Higher Risk of Infection and Mortality in France." Infection Control & Hospital Epidemiology **38**(1): 123-125.

Gray, H. (1878). Anatomy of the human body, Lea & Febiger.

Greene, J. W., A. L. Malkani, F. R. Kolisek, N. M. Jessup and D. L. Baker (2009). "Ceramic-on-Ceramic Total Hip Arthroplasty." The Journal of Arthroplasty **24**(6, Supplement): 15-18.

Griss, P. and G. Heimke (1981). "Five years experience with ceramic-metal-composite hip endoprostheses." Archives of orthopaedic and traumatic surgery **98**(3): 157-164.

Grosso, M. J., E. S. Jang, J. Longaray, S. Buell, E. Alfonso and R. P. Shah (2018). "Influence of Assembly Force and Distraction on the Femoral Head-Taper Junction." The Journal of Arthroplasty **33**(7, Supplement): S275-S279.

H., M., S. M. H., W. B. M., L. J. G., I. E. and F. J. (1998). "Quantification of third-body damage and its effect on UHMWPE wear with different types of femoral head." The Journal of Bone and Joint Surgery. British volume **80-B**(5): 894-899.

Hailer, N. P., R. J. Weiss, A. Stark and J. Kärrholm (2012). "The risk of revision due to dislocation after total hip arthroplasty depends on surgical approach, femoral head size, sex, and primary diagnosis: an analysis of 78,098 operations in the Swedish Hip Arthroplasty Register." Acta orthopaedica **83**(5): 442-448.

Hall, R. M., A. Unsworth, P. Siney and B. M. Wroblewski (1996). "Wear in Retrieved Charnley Acetabular Sockets." Proceedings of the Institution of Mechanical Engineers, Part H: Journal of Engineering in Medicine **210**(3): 197-207.

Hallab, N. J., C. Messina, A. Skipor and J. J. Jacobs (2004). "Differences in the fretting corrosion of metal-metal and ceramic-metal modular junctions of total hip replacements." Journal of Orthopaedic Research **22**(2): 250-259.

Hallaçeli, H., V. Uruç, H. H. Uysal, R. Ozden, C. Hallaçeli, F. Soyuer, T. Ince Parpucu, E. Yengil and U. Cavlak (2014). "Normal hip, knee and ankle range of motion in the Turkish population." Acta Orthop Traumatol Turc **48**(1): 37-42.

Hannouche, D., M. Hamadouche, R. Nizard, P. Bizot, A. Meunier and L. Sedel (2005). "Ceramics in total hip replacement." Clinical Orthopaedics and Related Research® **430**: 62-71.

Harms, L. and M. Kansen (2018). "Cycling facts." Netherlands Institute for Transport Policy Analysis (KiM).

Haschke, H., T. Konow, G. Huber and M. M. Morlock (2019). "Influence of flexural rigidity on micromotion at the head-stem taper interface of modular hip prostheses." Medical Engineering & Physics **68**: 1-10.

Haw, J. G., A. K. Battenberg, D.-C. T. Huang and T. P. Schmalzried (2017). "Wear Rates of Larger-Diameter Cross-Linked Polyethylene at 5 to 13 Years: Does Liner Thickness or Component Position Matter?" The Journal of Arthroplasty **32**(4): 1381-1386.

Heiney, J. P., S. Battula, G. A. Vrabec, A. Parikh, R. Blice, A. J. Schoenfeld and G. O. Njus (2009). "Impact magnitudes applied by surgeons and their importance when applying the femoral head onto the Morse taper for total hip arthroplasty." Archives of orthopaedic and trauma surgery **129**(6): 793-796.

Hermansen, L. L., B. Viberg, L. Hansen and S. Overgaard (2021). "'True' Cumulative Incidence of and Risk Factors for Hip Dislocation within 2 Years After Primary Total Hip Arthroplasty Due to Osteoarthritis: A Nationwide Population-Based Study from the Danish Hip Arthroplasty Register." JBSJ **103**(4): 295-302.

Hopper, R. H., Jr., A. M. Young, K. F. Orishimo and C. A. Engh, Jr. (2003). "Effect of terminal sterilization with gas plasma or gamma radiation on wear of polyethylene liners." J Bone Joint Surg Am **85**(3): 464-468.

Hoskins, W., S. Rainbird, C. Holder, J. Stoney, S. E. Graves and R. Bingham (2022). "A Comparison of Revision Rates and Dislocation After Primary Total Hip Arthroplasty with 28, 32, and 36-mm Femoral Heads and Different Cup Sizes: An Analysis of 188,591 Primary Total Hip Arthroplasties." JBSJ **104**(16): 1462-1474.

Hothi, H. S., A. P. Eskelinen, J. Henckel, Y.-M. Kwon, G. W. Blunn, J. A. Skinner and A. J. Hart (2018). "Effect of Bearing Type on Taper Material Loss in Hips From 1 Manufacturer." The Journal of Arthroplasty **33**(5): 1588-1593.

Hothi, H. S., D. Kendoff, C. Lausmann, J. Henckel, T. Gehrke, J. Skinner and A. Hart (2017). "Clinically insignificant trunnionosis in large-diameter metal-on-polyethylene total hip arthroplasty." Bone Joint Res **6**(1): 52-56.

Howie, D. W., S. D. Rogers, M. A. McGee, M. J. Percy and D. R. Haynes (1993). "The Response to Particulate Debris." Orthopedic Clinics of North America **24**(4): 571-581.

Hu, C. Y. and T.-R. Yoon (2018). "Recent updates for biomaterials used in total hip arthroplasty." Biomaterials Research **22**(1): 33.

Hunter, A. M., A. Hsu, A. Shah and S. M. Naranje (2019). "A case example and literature review of catastrophic wear before catastrophic failure: identification of trunnionosis and metallosis in

metal-on-polyethylene hip arthroplasty prior to frank failure or fracture." European Journal of Orthopaedic Surgery & Traumatology **29**(3): 711-715.

ISO14242-1 (2018). *Implants for surgery — Wear of total hip-joint prostheses Part 1*. Geneva, Switzerland; International Organization for Standardization (ISO).

JASTY, M., D. D. GOETZ, C. R. BRAGDON, K. R. LEE, A. E. HANSON, J. R. ELDER and W. H. HARRIS (1997). "Wear of Polyethylene Acetabular Components in Total Hip Arthroplasty. An Analysis of One Hundred and Twenty-eight Components Retrieved at Autopsy or Revision Operations*." JBJS **79**(3): 349-358.

Jenabzadeh, A.-R., S. J. Pearce and W. L. Walter (2012). "Total Hip Replacement: Ceramic-on-Ceramic." Seminars in Arthroplasty **23**(4): 232-240.

Jiang, Y., T. Jia, P. Wooley and S. Yang (2013). "Current research in the pathogenesis of aseptic implant loosening associated with particulate wear debris." Acta Orthop Belg **79**: 1-9.

Johnson, K. L. (1995). "Contact mechanics and the wear of metals." Wear **190**(2): 162-170.

KN, C., G. Ogulcan, S. Bhat N, M. Zuber and S. Shenoy B (2020). "Wear estimation of trapezoidal and circular shaped hip implants along with varying taper trunnion radiuses using finite element method." Computer Methods and Programs in Biomedicine **196**: 105597.

Kang, L., A. L. Galvin, T. D. Brown, Z. Jin and J. Fisher (2008). "Quantification of the effect of cross-shear on the wear of conventional and highly cross-linked UHMWPE." Journal of Biomechanics **41**(2): 340-346.

Kang, L., A. L. Galvin, Z. M. Jin and J. Fisher (2006). "A simple fully integrated contact-coupled wear prediction for ultra-high molecular weight polyethylene hip implants." Proceedings of the Institution of Mechanical Engineers, Part H: Journal of Engineering in Medicine **220**(1): 33-46.

Kapoor, A. (1997). "Wear by plastic ratchetting." Wear **212**(1): 119-130.

Karachalios, T., G. Komnos and A. Koutalos (2018). "Total hip arthroplasty: Survival and modes of failure." EFORT open reviews **3**(5): 232-239.

Kato, K. (2000). "Wear in relation to friction — a review." Wear **241**(2): 151-157.

Khoshbin, A., J. Wu, S. Ward, L. T. Melo, E. H. Schemitsch, J. P. Waddell and A. Atrey (2020). "Wear Rates of XLPE Nearly 50% Lower Than Previously Thought After Adjusting for Initial Creep: An RCT Comparing 4 Bearing Combinations." JBJS Open Access **5**(2): e0066.

Kim, Y., H.-C. Oh, J. W. Park, I.-S. Kim, J.-Y. Kim, K.-C. Kim, D.-S. Chae, W.-L. Jo and J.-H. Song (2017). "Diagnosis and Treatment of Inflammatory Joint Disease." hp **29**(4): 211-222.

Knight, S. R., R. Aujla and S. P. Biswas (2011). "Total Hip Arthroplasty - over 100 years of operative history." Orthop Rev (Pavia) **3**(2): e16.

Kocagoz, S. B., R. J. Underwood, D. W. MacDonald, J. L. Gilbert and S. M. Kurtz (2016). "Ceramic Heads Decrease Metal Release Caused by Head-taper Fretting and Corrosion." Clin Orthop Relat Res **474**(4): 985-994.

Koo, K. H., R. Kim, G. H. Ko, H. R. Song, S. T. Jeong and S. H. Cho (1995). "Preventing collapse in early osteonecrosis of the femoral head. A randomised clinical trial of core decompression." J Bone Joint Surg Br **77**(6): 870-874.

Korovessis, P., G. Petsinis, M. Repanti and T. Repantis (2006). "Metallosis after contemporary metal-on-metal total hip arthroplasty. Five to nine-year follow-up." J Bone Joint Surg Am **88**(6): 1183-1191.

Kostensalo, I., M. Junnila, P. Virolainen, V. Remes, M. Matilainen, T. Vahlberg, P. Pulkkinen, A. Eskelinen and K. T. Mäkelä (2013). "Effect of femoral head size on risk of revision for dislocation after total hip arthroplasty: a population-based analysis of 42,379 primary procedures from the Finnish Arthroplasty Register." Acta orthopaedica **84**(4): 342-347.

Krakowski, P., A. Gerkowicz, A. Pietrzak, D. Krasowska, A. Jurkiewicz, M. Gorzelak and R. A. Schwartz (2019). "Psoriatic arthritis—new perspectives." Archives of Medical Science **15**(3): 580-589.

Krull, A., M. M. Morlock and N. E. Bishop (2018). "Maximizing the fixation strength of modular components by impaction without tissue damage." Bone & Joint Research **7**(2): 196-204.

Kurtz, S. M., S. B. Kocagöz, J. A. Hanzlik, R. J. Underwood, J. L. Gilbert, D. W. MacDonald, G.-C. Lee, M. A. Mont, M. J. Kraay and G. R. Klein (2013). "Do ceramic femoral heads reduce taper fretting

corrosion in hip arthroplasty? A retrieval study." Clinical Orthopaedics and Related Research® **471**(10): 3270-3282.

Kurtz, S. M. and J. D. Patel (2016). 6 - The Clinical Performance of Highly Cross-linked UHMWPE in Hip Replacements. UHMWPE Biomaterials Handbook (Third Edition). S. M. Kurtz. Oxford, William Andrew Publishing: 57-71.

Kuster, M. S. (2002). "Exercise Recommendations After Total Joint Replacement." Sports Medicine **32**(7): 433-445.

Kwon, Y. M., S. Glyn-Jones, D. J. Simpson, A. Kamali, P. McLardy-Smith, H. S. Gill and D. W. Murray (2010). "Analysis of wear of retrieved metal-on-metal hip resurfacing implants revised due to pseudotumours." J Bone Joint Surg Br **92**(3): 356-361.

Lachiewicz, P. F., E. S. Soileau and J. M. Martell (2016). "Wear and Osteolysis of Highly Crosslinked Polyethylene at 10 to 14 Years: The Effect of Femoral Head Size." Clinical Orthopaedics and Related Research® **474**(2): 365-371.

Lamb, J. N., C. Holton, P. O'Connor and P. V. Giannoudis (2019). "Avascular necrosis of the hip." BMJ **365**: l2178.

Langton, Sidaginamale, Lord, Nargol and Joyce (2012). "Taper junction failure in large-diameter metal-on-metal bearings." Bone & Joint Research **1**(4): 56-63.

Langton, D., T. Joyce, S. Jameson, J. Lord, M. Van Orsouw, J. Holland, A. Nargol and K. De Smet (2011). "Adverse reaction to metal debris following hip resurfacing: the influence of component type, orientation and volumetric wear." The Journal of bone and joint surgery. British volume **93**(2): 164-171.

Langton, D. J., S. S. Jameson, T. J. Joyce, N. J. Hallab, S. Natsu and A. V. Nargol (2010). "Early failure of metal-on-metal bearings in hip resurfacing and large-diameter total hip replacement: A consequence of excess wear." J Bone Joint Surg Br **92**(1): 38-46.

Langton, D. J., R. Sidaginamale, J. K. Lord, A. V. F. Nargol and T. J. Joyce (2012). "Taper junction failure in large-diameter metal-on-metal bearings." Bone & joint research **1**(4): 56-63.

Langton, D. J., R. P. Sidaginamale, T. J. Joyce, R. D. Meek, J. G. Bowsher, D. Deehan, A. V. F. Nargol and J. P. Holland (2017). "A comparison study of stem taper material loss at similar and mixed metal head-neck taper junctions." Bone Joint J **99-b**(10): 1304-1312.

Langton, D. J., S. R. Wells, T. J. Joyce, J. G. Bowsher, D. Deehan, S. Green, A. V. F. Nargol and J. P. Holland (2018). "Material loss at the femoral head taper." The Bone & Joint Journal **100-B**(10): 1310-1319.

Lavernia, C. J., L. Baerga, R. L. Barrack, E. Tozakoglou, S. D. Cook, L. Lata and M. D. Rossi (2009). "The effects of blood and fat on Morse taper disassembly forces." Am J Orthop (Belle Mead NJ) **38**(4): 187-190.

Learmonth, I. D., C. Young and C. Rorabeck (2007). "The operation of the century: total hip replacement." The Lancet **370**(9597): 1508-1519.

Leonard, B., F. Sadeghi, S. Shinde and M. Mittelbach (2012). "A Numerical and Experimental Investigation of Fretting Wear and a New Procedure for Fretting Wear Maps." Tribology Transactions - TRIBOL TRANS **55**: 313-324.

Lewis, G. (1997). "Polyethylene wear in total hip and knee arthroplasties." Journal of Biomedical Materials Research **38**(1): 55-75.

Lieberman, J., C. M. Rimnac, K. L. Garvin, R. W. Klein and E. A. Salvati (1994). "An analysis of the head-neck taper interface in retrieved hip prostheses." Clinical Orthopaedics and Related Research(300): 162-167.

Lin, J. T. and J. M. Lane (2004). "Osteoporosis: A Review." Clinical Orthopaedics and Related Research (1976-2007) **425**: 126-134.

Lin, Y.-T., J. S.-S. Wu and J.-H. Chen (2016). "The study of wear behaviors on abducted hip joint prostheses by an alternate finite element approach." Computer Methods and Programs in Biomedicine **131**: 143-155.

Livermore, J., D. Ilstrup and B. Morrey (1990). "Effect of femoral head size on wear of the polyethylene acetabular component." J Bone Joint Surg Am **72**(4): 518-528.

Madge, J. J., S. B. Leen, I. R. McColl and P. H. Shipway (2007). "Contact-evolution based prediction of fretting fatigue life: Effect of slip amplitude." Wear **262**(9): 1159-1170.

Mao, X., G. H. Tay, D. B. Godbolt and R. W. Crawford (2012). "Pseudotumor in a well-fixed metal-on-polyethylene uncemented hip arthroplasty." The Journal of arthroplasty **27**(3): 493. e413-493. e417.

Massin, P. and S. Achour (2017). "Wear products of total hip arthroplasty: The case of polyethylene." Morphologie **101**(332): 1-8.

Matsoukas, G., R. Willing and I. Y. Kim (2009). "Total Hip Wear Assessment: A Comparison Between Computational and In Vitro Wear Assessment Techniques Using ISO 14242 Loading and Kinematics." Journal of Biomechanical Engineering **131**(4).

Matsushita, A., Y. Nakashima, S. Jingushi, T. Yamamoto, A. Kuraoka and Y. Iwamoto (2009). "Effects of the Femoral Offset and the Head Size on the Safe Range of Motion in Total Hip Arthroplasty." The Journal of Arthroplasty **24**(4): 646-651.

Maxian, T. A., T. D. Brown, D. R. Pedersen and J. J. Callaghan (1996). "Adaptiive finite element modeling of long-term polyethylene wear in total hip arthroplasty." Journal of Orthopaedic Research **14**(4): 668-675.

Maxian, T. A., T. D. Brown, D. R. Pedersen and J. J. Callaghan (1996). "The Frank Stinchfield Award. 3-Dimensional sliding/contact computational simulation of total hip wear." Clinical orthopaedics and related research(333): 41-50.

Maxian, T. A., T. D. Brown, D. R. Pedersen and J. J. Callaghan (1996). "A sliding-distance-coupled finite element formulation for polyethylene wear in total hip arthroplasty." Journal of biomechanics **29**(5): 687-692.

Maxian, T. A., T. D. Brown, D. R. Pedersen, H. A. McKellop, B. Lu and J. J. Callaghan (1997). "Finite element analysis of acetabular wear. Validation, and backing and fixation effects." Clinical orthopaedics and related research(344): 111-117.

McCull, I. R., J. Ding and S. B. Leen (2004). "Finite element simulation and experimental validation of fretting wear." Wear **256**(11): 1114-1127.

McKellop, H., F. W. Shen, B. Lu, P. Campbell and R. Salovey (2000). "Effect of sterilization method and other modifications on the wear resistance of acetabular cups made of ultra-high molecular weight polyethylene. A hip-simulator study." J Bone Joint Surg Am **82**(12): 1708-1725.

McMinn, D. J. W., J. Daniel, H. Ziaee and C. Pradhan (2011). "Indications and results of hip resurfacing." International Orthopaedics **35**(2): 231-237.

Messellek, A. C., M. Ould Ouali and A. Amrouche (2020). "Adaptive finite element simulation of fretting wear and fatigue in a taper junction of modular hip prosthesis." Journal of the Mechanical Behavior of Biomedical Materials **111**: 103993.

Mirra, J. M., R. A. Marder and H. C. Amstutz (1982). "The pathology of failed total joint arthroplasty." Clin Orthop Relat Res(170): 175-183.

Mittelmeier, H. and J. Heisel (1992). "Sixteen-years' experience with ceramic hip prostheses." Clinical Orthopaedics and Related Research (1976-2007) **282**: 64-72.

Moharrami, N., D. J. Langton, O. Sayginer and S. J. Bull (2013). "Why does titanium alloy wear cobalt chrome alloy despite lower bulk hardness: A nanoindentation study?" Thin Solid Films **549**: 79-86.

Mont, M. A., P. S. Ragland, G. Etienne, T. M. Seyler and T. P. Schmalzried (2006). "Hip Resurfacing Arthroplasty." JAAOS - Journal of the American Academy of Orthopaedic Surgeons **14**(8): 454-463.

Mulholland, S. J. and U. P. Wyss (2001). "Activities of daily living in non-Western cultures: range of motion requirements for hip and knee joint implants." International Journal of Rehabilitation Research **24**(3): 191-198.

Napier, R. J. and A. J. Shimmin (2016). "Ceramic-on-ceramic bearings in total hip arthroplasty: "The future is now". " Seminars in Arthroplasty **27**(4): 235-238.

NHS, U. (2022). "Overview - Arthritis." from <https://www.nhs.uk/conditions/arthritis/>.

NJR (2021). National Joint Registry: National Joint Registry for England, Wales and Northern Ireland; 18th Annual Report, 2021.

NJR (2022). National Joint Registry: National Joint Registry for England, Wales and Northern Ireland; 19th Annual Report, 2022.

Norman, T. L., J. E. Denen, A. J. Land, D. M. Kienitz and T. A. Fehring (2019). "Taper-Trunnion Interface Stress Varies Significantly With Head Size and Activity." The Journal of Arthroplasty **34**(1): 157-162.

Oja, P., S. Titze, A. Bauman, B. de Geus, P. Krenn, B. Reger-Nash and T. Kohlberger (2011). "Health benefits of cycling: a systematic review." Scandinavian Journal of Medicine & Science in Sports **21**(4): 496-509.

Oliveira, C. A., I. S. Candelária, P. B. Oliveira, A. Figueiredo and F. Caseiro-Alves (2015). "Metallosis: A diagnosis not only in patients with metal-on-metal prostheses." European Journal of Radiology Open **2**: 3-6.

Ouellette, E. S., S. A. Mali, J. Kim, J. Grostefon and J. L. Gilbert (2019). "Design, Material, and Seating Load Effects on In Vitro Fretting Corrosion Performance of Modular Head-Neck Tapers." The Journal of Arthroplasty **34**(5): 991-1002.

Pakhaliuk, V., A. Polyakov, M. Kalinin and V. Kramar (2015). "Improving the Finite Element Simulation of Wear of Total Hip Prosthesis' Spherical Joint with the Polymeric Component." Procedia Engineering **100**: 539-548.

Paleochorlidis, I. S., L. S. Badras, E. F. Skretas, V. A. Georgaklis, T. S. Karachalios and K. N. Malizos (2009). "Clinical outcome study and radiological findings of Zweymuller metal on metal total hip arthroplasty. a follow-up of 6 to 15 years." Hip International **19**(4): 301-308.

Panagiotidou, A., T. Cobb, J. Meswania, J. Skinner, A. Hart, F. Haddad and G. Blunn (2018). "Effect of impact assembly on the interface deformation and fretting corrosion of modular hip tapers: An in vitro study." Journal of Orthopaedic Research **36**(1): 405-416.

Partridge, S., J. L. Tipper, M. Al-Hajjar, G. H. Isaac, J. Fisher and S. Williams (2018). "Evaluation of a new methodology to simulate damage and wear of polyethylene hip replacements subjected to edge loading in hip simulator testing." J Biomed Mater Res B Appl Biomater **106**(4): 1456-1462.

Pastides, P. S., M. Dodd, K. M. Sarraf and C. A. Willis-Owen (2013). "Trunnionosis: a pain in the neck." World Journal of Orthopedics **4**(4): 161-166.

Peng, Y., P. Arauz, S. An and Y.-M. Kwon (2019). "Computational modeling of polyethylene wear in total hip arthroplasty using patient-specific kinematics-coupled finite element analysis." Tribology International **129**: 162-166.

Pennock, A. T., A. H. Schmidt and C. A. Bourgeault (2002). "Morse-type tapers: Factors that may influence taper strength during total hip arthroplasty." The Journal of Arthroplasty **17**(6): 773-778.

Pierre, D., V. Swaminathan, L. Scholl, K. TenHuisen and J. L. Gilbert (2019). "Effects of seating load magnitude and load orientation on seating mechanics in 5°40' mixed-alloy modular taper junctions." Journal of Biomechanics **82**: 251-258.

Pietrabissa, R., M. Raimondi and E. Di Martino (1998). "Wear of polyethylene cups in total hip arthroplasty: a parametric mathematical model." Medical Engineering & Physics **20**(3): 199-210.

Popov, V. (2019). "Generalized Archard law of wear based on Rabinowicz criterion of wear particle formation." Facta Universitatis, Series: Mechanical Engineering **17**: 39-45.

Porter, D. A., R. M. Urban, J. J. Jacobs, J. L. Gilbert, J. A. Rodriguez and H. J. Cooper (2014). "Modern trunnions are more flexible: a mechanical analysis of THA taper designs." Clinical Orthopaedics and Related Research **472**(12): 3963-3970.

Pritchett, J. W. (2012). "Adverse reaction to metal debris: metallosis of the resurfaced hip." Current Orthopaedic Practice **23**(1): 50-58.

Queiroz, R. D., A. L. L. Oliveira, F. C. Trigo and J. A. Lopes (2013). "A finite element method approach to compare the wear of acetabular cups in polyethylene according to their lateral tilt in relation to the coronal plane." Wear **298-299**: 8-13.

Rachner, T. D., S. Khosla and L. C. Hofbauer (2011). "Osteoporosis: now and the future." The Lancet **377**(9773): 1276-1287.

Raghunathan, V. K., M. Devey, S. Hawkins, L. Hails, S. A. Davis, S. Mann, I. T. Chang, E. Ingham, A. Malhas, D. J. Vaux, J. D. Lane and C. P. Case (2013). "Influence of particle size and reactive oxygen species on cobalt chrome nanoparticle-mediated genotoxicity." Biomaterials **34**(14): 3559-3570.

Raimondi, M. T., C. Santambrogio, R. Pietrabissa, F. Raffelini and L. Molfetta (2001). "Improved mathematical model of the wear of the cup articular surface in hip joint prostheses and

comparison with retrieved components." Proceedings of the Institution of Mechanical Engineers, Part H: Journal of Engineering in Medicine **215**(4): 377-390.

Ramoutar, D. N., E. A. Crosnier, F. Shivji, A. W. Miles and H. S. Gill (2017). "Assessment of Head Displacement and Disassembly Force With Increasing Assembly Load at the Head/Trunnion Junction of a Total Hip Arthroplasty Prosthesis." The Journal of Arthroplasty **32**(5): 1675-1678.

Rehmer, A., N. E. Bishop and M. M. Morlock (2012). "Influence of assembly procedure and material combination on the strength of the taper connection at the head–neck junction of modular hip endoprotheses." Clinical Biomechanics **27**(1): 77-83.

Revell, P. A., B. Weightman, M. A. Freeman and B. V. Roberts (1978). "The production and biology of polyethylene wear debris." Arch Orthop Trauma Surg (1978) **91**(3): 167-181.

Rieker, C. B., R. Schön, R. Konrad, G. Liebenritt, P. Gnepf, M. Shen, P. Roberts and P. Grigoris (2005). "Influence of the clearance on in-vitro tribology of large diameter metal-on-metal articulations pertaining to resurfacing hip implants." Orthopedic Clinics **36**(2): 135-142.

Rony, L., R. Lancigu and L. Hubert (2018). "Intraosseous metal implants in orthopedics: A review." Morphologie **102**(339): 231-242.

Saikko, V. (2020). "Effect of inward-outward rotation on hip wear simulation." Journal of Biomechanics **101**: 109638.

Saikko, V., T. Ahlroos, O. Calonijs and J. Keränen (2001). "Wear simulation of total hip prostheses with polyethylene against CoCr, alumina and diamond-like carbon." Biomaterials **22**(12): 1507-1514.

Saikko, V. and J. Kostamo (2013). "Performance analysis of the RandomPOD wear test system." Wear **297**(1): 731-735.

Salem, K. H., N. Lindner, M. Tingart and A. D. Elmoghazy (2019). "Severe metallosis-related osteolysis as a cause of failure after total knee replacement." Journal of Clinical Orthopaedics and Trauma.

Santavirta, S. S., R. Lappalainen, P. Pekko, A. Anttila and Y. T. Konttinen (1999). "The Counterface, Surface Smoothness, Tolerances, and Coatings in Total Joint Prostheses." Clinical Orthopaedics and Related Research® **369**: 92-102.

Schmalzried, T. P., M. Jasty and W. H. Harris (1992). "Periprosthetic bone loss in total hip arthroplasty. Polyethylene wear debris and the concept of the effective joint space." J Bone Joint Surg Am **74**(6): 849-863.

Schmalzried, T. P., E. S. Szuszczewicz, M. R. Northfield, K. H. Akizuki, R. E. Frankel, G. Belcher and H. C. Amstutz (1998). "Quantitative assessment of walking activity after total hip or knee replacement." Journal of Bone and Joint Surgery - Series A **80**(1): 54-59.

Schmidig, G., A. Patel, I. Liepins, M. Thakore and D. C. Markel (2010). "The effects of acetabular shell deformation and liner thickness on frictional torque in ultrahigh-molecular-weight polyethylene acetabular bearings." J Arthroplasty **25**(4): 644-653.

Scholl, L., D. Pierre, R. Rajaravivarma, R. Lee, A. Faizan, V. Swaminathan, K. TenHuisen, J. L. Gilbert and J. Nevelos (2018). "Effect of the support systems' compliance on total hip modular taper seating stability." Proceedings of the Institution of Mechanical Engineers, Part H: Journal of Engineering in Medicine **232**(9): 862-870.

Scully, W. F. and S. M. Teeny (2013). "Pseudotumor associated with metal-on-polyethylene total hip arthroplasty." Orthopedics **36**(5): e666-e670.

Shebubakar, L., E. Hutagalung, S. Sapardan and B. Sutrisna (2009). "Effects of older age and multiple comorbidities on functional outcome after partial hip replacement surgery for hip fractures." Acta Med Indones **41**(4): 195-199.

Shulman, R. M., M. G. Zywiell, R. Gandhi, J. R. Davey and D. C. Salonen (2015). "Trunnionosis: the latest culprit in adverse reactions to metal debris following hip arthroplasty." Skeletal radiology **44**(3): 433-440.

Siguiet, T., M. Siguiet, T. Judet, G. Charnley and B. Brumpt (2001). "Partial Resurfacing Arthroplasty of the Femoral Head in Avascular Necrosis: Methods, Indications, and Results." Clinical Orthopaedics and Related Research (1976-2007) **386**: 85-92.

Sinusas, K. (2012). "Osteoarthritis: diagnosis and treatment." Am Fam Physician **85**(1): 49-56.

Smith, M. H. and J. R. Berman (2022). "What Is Rheumatoid Arthritis?" JAMA **327**(12): 1194-1194.

Smith, S. L. and T. J. Joyce (2017). 10 - A hop, skip, and a jump: Towards better wear testing of hip implants. Mechanical Testing of Orthopaedic Implants. E. Friis, Woodhead Publishing: 183-206.

Steinberg, M. E., P. G. Larcom, B. Strafford, W. B. Hosick, A. Corces, R. E. Bands and K. E. Hartman (2001). "Core Decompression With Bone Grafting for Osteonecrosis of the Femoral Head." Clinical Orthopaedics and Related Research® **386**: 71-78.

Sundfeldt, M., L. V Carlsson, C. B Johansson, P. Thomsen and C. Gretzer (2006). "Aseptic loosening, not only a question of wear: A review of different theories." Acta Orthopaedica **77**(2): 177-197.

Svensson, O., E. B. Mathiesen, F. Reinholt and G. Blomgren (1988). "Formation of a fulminant soft-tissue pseudotumor after uncemented hip arthroplasty. A case report." JBJs **70**(8): 1238-1242.

SYCHTERZ, C. J., K. H. MOON, Y. HASHIMOTO, K. M. TREFENKO, C. A. J. ENGH and T. W. BAUER (1996). "Wear of Polyethylene Cups in Total Hip Arthroplasty. A Study of Specimens Retrieved Post Mortem*." JBJs **78**(8): 1193-1200.

Szostakowski, B., J. Jagiello and J. A. Skinner (2017). "ArtiFacts: Ivory Hemiarthroplasty: The Forgotten Concept Lives On." Clinical Orthopaedics and Related Research® **475**(12): 2850-2854.

Tateiwa, T., I. C. Clarke, P. A. Williams, J. Garino, M. Manaka, T. Shishido, K. Yamamoto and A. Imakiire (2008). "Ceramic total hip arthroplasty in the United States: safety and risk issues revisited." Am J Orthop **37**(2): E26-E31.

Taylor, C. J. and D. J. Kriegman (1994). Minimization on the Lie Group SO(3) and Related Manifolds.

Teoh, S. H. (2003). 9.01 - Failure in Biomaterials. Comprehensive Structural Integrity. I. Milne, R. O. Ritchie and B. Karihaloo. Oxford, Pergamon: 1-33.

Teoh, S. H., W. H. Chan and R. Thampuran (2002). "An elasto-plastic finite element model for polyethylene wear in total hip arthroplasty." Journal of Biomechanics **35**(3): 323-330.

Toh, S. M. S., A. Ashkanfar, R. English, G. Rothwell, D. J. Langton and T. Joyce (2022). "How Does Bicycling Affect the Longevity of Total Hip Arthroplasty? A Finite Element Wear Analysis." SSRN Electronic Journal.

Trommer, R. M., M. M. Maru, W. L. Oliveira Filho, V. P. S. Nykanen, C. P. Gouvea, B. S. Archanjo, E. H. Martins Ferreira, R. F. Silva and C. A. Achete (2015). "Multi-Scale Evaluation of Wear in UHMWPE-Metal Hip Implants Tested in a hip Joint Simulator." Biotribology **4**: 1-11.

Uddin, M. S. and L. C. Zhang (2013). "Predicting the wear of hard-on-hard hip joint prostheses." Wear **301**(1): 192-200.

Valente, G., B. Lanting, S. MacDonald, M. G. Teeter, D. Van Citters and J. Howard (2019). "Femoral head material loss at the head-neck junction in total hip arthroplasty: the effect of head size, stem material and stem offset." HIP International **29**(6): 647-651.

Van, K. D. and M. Maitournam (1994). "Elasto-plastic calculations of the mechanical state in reciprocating moving contacts: Application to fretting fatigue." Fretting Fatigue, Mechanical Engineering Publications, London: 161-168.

Varady, P. A., U. Glitsch and P. Augat (2015). "Loads in the hip joint during physically demanding occupational tasks: A motion analysis study." Journal of Biomechanics **48**(12): 3227-3233.

Varnum, C. (2017). "Outcomes of different bearings in total hip arthroplasty - implant survival, revision causes, and patient-reported outcome." Dan Med J **64**(3).

Walter, W. L., G. C. O'Toole, W. K. Walter, A. Ellis and B. A. Zicat (2007). "Squeaking in Ceramic-on-Ceramic Hips: The Importance of Acetabular Component Orientation." The Journal of Arthroplasty **22**(4): 496-503.

Wang, B. L., W. Sun, Z. C. Shi, N. F. Zhang, D. B. Yue, W. S. Guo, S. Q. Xu, J. N. Lou and Z. R. Li (2010). "Treatment of nontraumatic osteonecrosis of the femoral head with the implantation of core decompression and concentrated autologous bone marrow containing mononuclear cells." Arch Orthop Trauma Surg **130**(7): 859-865.

Wang, S. B., S. R. Ge, H. T. Liu and X. L. Huang (2010). Wear behaviour and wear debris characterization of UHMWPE on alumina ceramic, stainless steel, CoCrMo and Ti6Al4V hip prostheses in a hip joint simulator. Journal of Biomimetics, Biomaterials and Tissue Engineering, Trans Tech Publ.

Watanabe, H., K. Takahashi, K. Takenouchi, A. Sato, H. Kawaji, H. Nakamura and S. Takai (2015). "Pseudotumor and deep venous thrombosis due to crevice corrosion of the head–neck junction in metal-on-polyethylene total hip arthroplasty." *Journal of Orthopaedic Science* **20**(6): 1142-1147.

Wegrzyn, J., A. Antoniadis, E. Sarshari, M. Boubat and A. Terrier (2022). "Polyethylene wear of dual mobility cups: a comparative analysis based on patient-specific finite element modeling." *International Orthopaedics* **46**(4): 779-787.

Wieland, H. A., M. Michaelis, B. J. Kirschbaum and K. A. Rudolphi (2005). "Osteoarthritis — an untreatable disease?" *Nature Reviews Drug Discovery* **4**(4): 331-344.

Williams, D., M. Royle and M. Norton (2009). "Metal-on-metal hip resurfacing: the effect of cup position and component size on range of motion to impingement." *J Arthroplasty* **24**(1): 144-151.

Witzleb, W.-C., J. Ziegler, F. Krummenauer, V. Neumeister and K.-P. Guenther (2006). "Exposure to chromium, cobalt and molybdenum from metal-on-metal total hip replacement and hip resurfacing arthroplasty." *Acta orthopaedica* **77**(5): 697-705.

Yang, L. J. (1999). "Pin-on-disc wear testing of tungsten carbide with a new moving pin technique." *Wear* **225-229**: 557-562.

Yang, L. J. (2003). "Wear coefficient equation for aluminium-based matrix composites against steel disc." *Wear* **255**(1): 579-592.

Yang, L. J. and N. L. Loh (1995). "The wear properties of plasma transferred arc cladded stellite specimens." *Surface and Coatings Technology* **71**(2): 196-200.

Yoshida, H., A. Faust, J. Wilckens, M. Kitagawa, J. Fetto and E. Y. S. Chao (2006). "Three-dimensional dynamic hip contact area and pressure distribution during activities of daily living." *Journal of Biomechanics* **39**(11): 1996-2004.

Zahiri, C. A., T. P. Schmalzried, E. Ebramzadeh, E. S. Szuszczewicz, D. Salib, C. Kim and H. C. Amstutz (1999). "Lessons learned from loosening of the McKee-Farrar metal-on-metal total hip replacement." *J Arthroplasty* **14**(3): 326-332.

Zhang, T., N. M. Harrison, P. F. McDonnell, P. E. McHugh and S. B. Leen (2013). "A finite element methodology for wear–fatigue analysis for modular hip implants." *Tribology International* **65**: 113-127.

Appendices

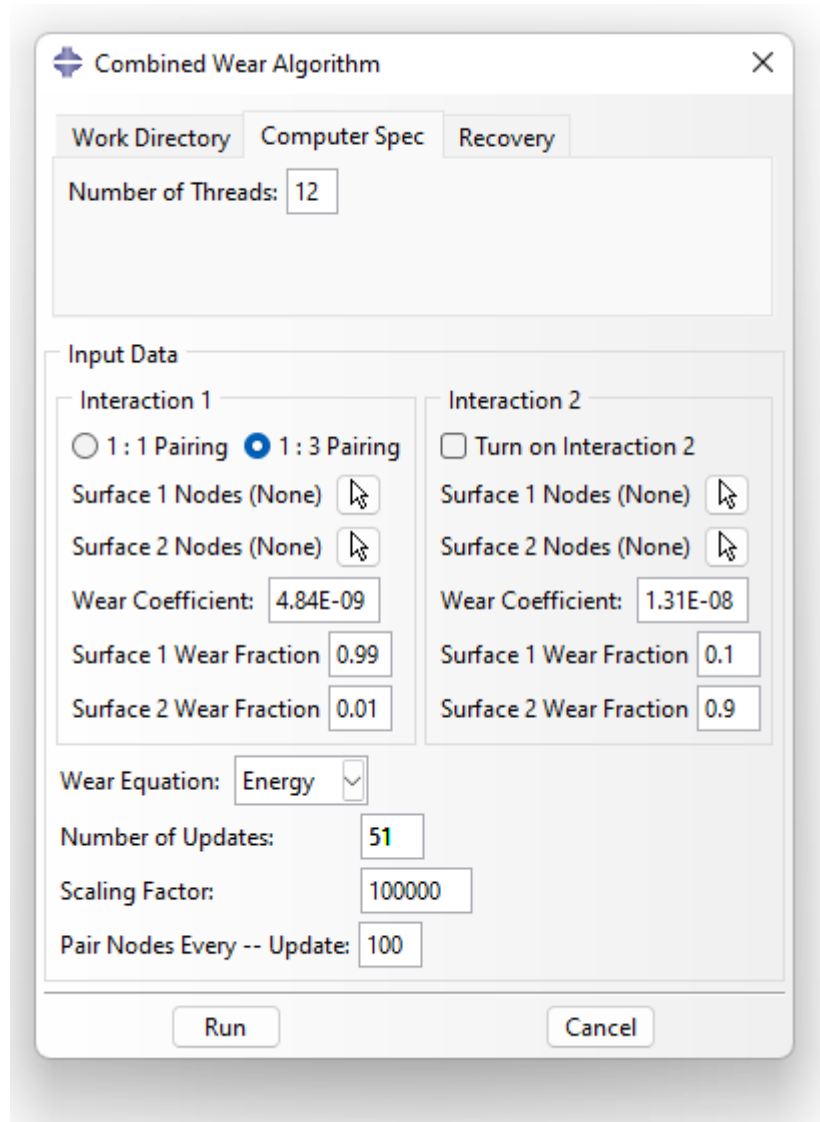
List of Appendix

Appendix I : Graphical user interface of the wear algorithm

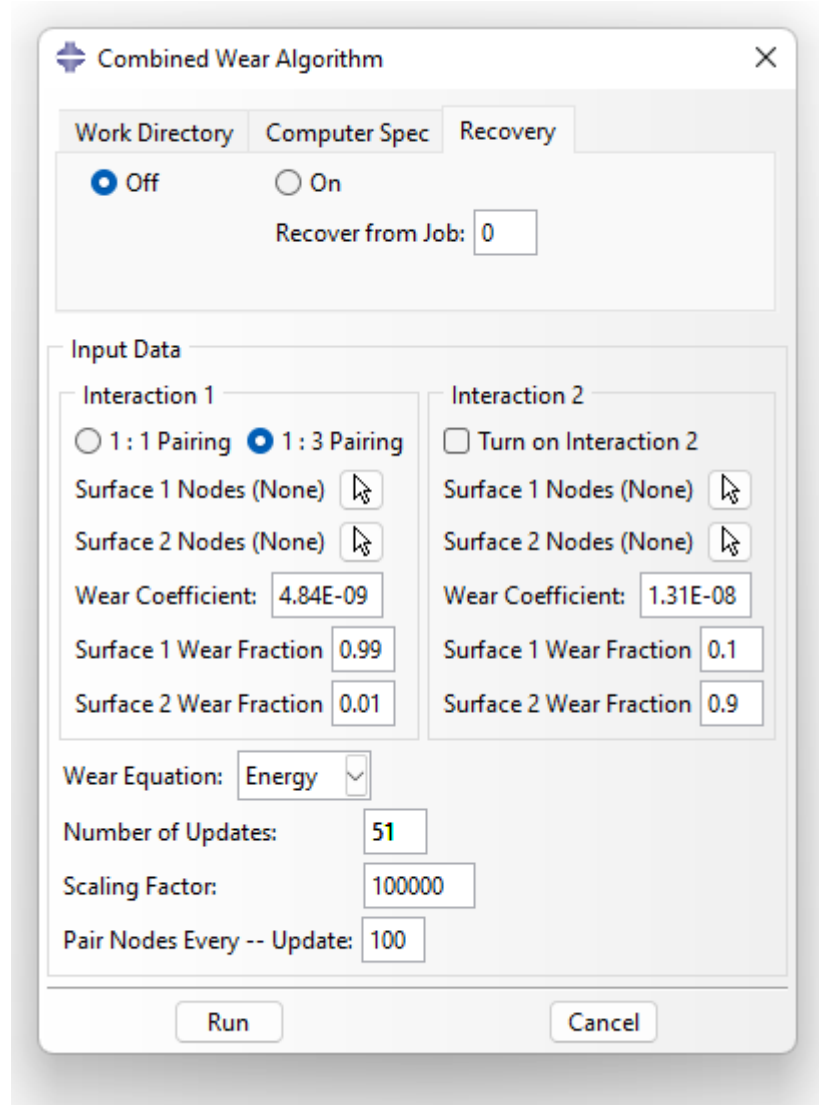
Appendix II : Publications

Appendix III : Poster Presentation

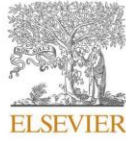
Appendix I: Graphical user interface of the wear algorithm



Graphical user interface of the wear algorithm (1st tab)



Graphical user interface of the wear algorithm (2nd tab)



Contents lists available at ScienceDirect

Journal of the Mechanical Behavior of Biomedical Materials

journal homepage: <http://www.elsevier.com/locate/jmbbm>

Computational method for bearing surface wear prediction in total hip replacements

Shawn Ming Song Toh^{*}, Ariyan Ashkanfar, Russell English, Glynn Rothwell

School of Engineering, Liverpool John Moores University, Byrom Street, Liverpool, L3 3AF, UK

ARTICLE INFO

Keywords:

Wear modelling
Total hip replacement
Hip joint prosthesis
Finite element modelling
Polyethylene wear

ABSTRACT

Total hip replacement (THR) is a revolutionary treatment when a hip joint becomes severely damaged. Wear is known as one of the main reasons for THR failure. Current experimental techniques to investigate the wear at the bearing surfaces of THRs are time-consuming, complicated and expensive. In this study, an in-house fretting wear algorithm has been further developed to investigate the wear damage that occurs on bearing surfaces of THRs and its consequence on the longevity of the implants. A 3D finite element model has been created with a 36 mm diameter Cobalt-Chromium femoral head and a 4 mm thick cross-linked polyethylene bearing liner. A gait loading cycle was used to simulate walking for up to 5 million cycles (Mc). The wear algorithm extracts relative displacements and contact shear stresses from the finite element package to predict the linear and volumetric wear rates. This method is shown to have modelled the evolution of wear effectively and found it to be similar to those from experimental analyses. The linear and volumetric wear per million cycles predicted in this study were 0.0375mm/Mc and 33.6mm³/Mc which are comparable to those measured in-vivo THRs. The wear patterns obtained from this study are also comparable to the wear patterns shown on available conventional polyethylene liners. This method can be used to further aid in the design and clinical technique to reduce wear rate in THRs.

1. Introduction

A hip joint is one of the most important joints in our body. It bears our body weight in static and dynamic postures and plays an important role in retaining body balance; however, it may lose its functionality due to diseases such as osteoarthritis which causes pain and also in extreme cases, loss of mobility (Holcomb et al., 2012; Kumar et al., 2017). When the joint has been severely damaged and physiotherapy, steroid injections or other treatments have not helped to improve mobility, the damaged joint may be removed and replaced with a prosthesis. According to the NJR's report in 2019, 82.6% of patients who received a total hip replacement (THR) had been suffering from osteoarthritis (NJR 2019). THR has become a revolutionary treatment (Nambiarbib, Nambiar et al., 2017; Nambiar et al., 2017) over the last decades (Towheed and Hochberg 1996; Learmonth et al., 2007; Ashman et al., 2016). A THR usually consists of four parts, an acetabular cup, a bearing liner, a femoral head and a femoral stem (Fig. 1). (Ali et al., 2016a; Varnum 2017).

Data from the National Joint Registry (NJR) shows there were approximately 92,000 THR procedures performed in the United

Kingdom using arthroplasty in 2018 with over a million THR's performed since 2003 (NJR 2019). Further statistics from the NJR in 2019, also shows that there is an average of 11.5% increase every year in the number of patients under 55 years old undergoing THR which suggests that more young active patients will undergo THR in the coming years. The longevity of these implants will need to be increased, as the current average lifespan of a THR implant is at 15 years (Evans et al., 2019). Furthermore, nearly 8% of cases had failed prematurely, less than 15 years in service, and needed a revision surgery (NJR 2019). Wear is one of the main reasons for premature failure in THRs (Karachaliosbib, Karachalios et al., 2018; Karachalios et al., 2018 et al., 2018) and can cause a multitude of failure such as aseptic loosening, dislocation, infection or metallosis (Karachaliosbib, Karachalios et al., 2018; Karachalios et al., 2018 et al., 2018; Neil G. Burke 2018; Sipek et al., 2018). Aseptic loosening accounts for approximately 45% of hip revisions (Bulybib, Buly et al., 1992; Buly et al., 1992 et al., 1992; Neil G. Burke 2018; Sipek et al., 2018; NJR 2019).

Current experimental techniques to investigate the wear damage in THRs, such as radiography, tribo-testing, and hip joint simulators, are

^{*} Corresponding author.

E-mail addresses: shawntoh15@gmail.com, s.m.toh@2016.ljmu.ac.uk (S.M.S. Toh).

<https://doi.org/10.1016/j.jmbbm.2021.104507>

Received 15 January 2021; Received in revised form 22 March 2021; Accepted 1 April 2021

Available online 8 April 2021

1751-6161/© 2021 Elsevier Ltd. All rights reserved.

Appendix II: Publication

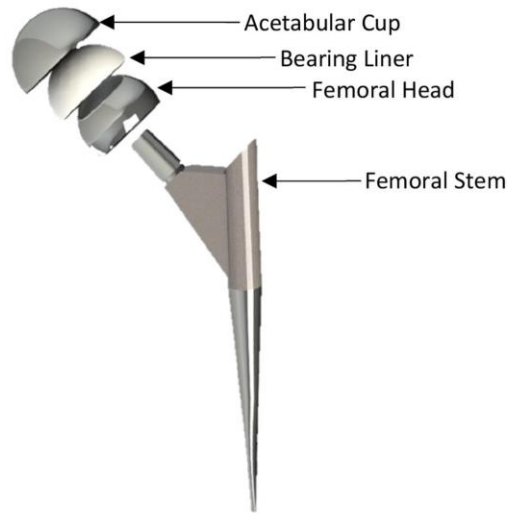


Fig. 1. The four main parts of a total hip replacement (THR).

time-consuming, complicated and expensive (Hallan et al., 2006; Hua et al., 2019; Ramesh et al., 2019). Computational analysis has several benefits when compared to experimental testing such as lower cost, lower run time, and having detailed solutions which can be an alternative to experimental techniques. With these added benefits, current computational analysis has led to the understanding of different design and material variations, (Shen et al., 2011; Ashkanfar et al., 2017; Gao et al., 2018; Ruggiero et al., 2018), manufacturing tolerances (Kluess et al., 2007; Affatato et al., 2018b; Ashkanfar et al., 2017b), and surgical techniques (English et al., 2016).

Recently, studies by Ruggiero et al. (2020) have used an in-silico approach to link experimental investigations to computational investigation to predict wear in the implant over millions of cycles. The main purpose of their study was to propose a wear prediction approach which would reproduce the classical in-vitro wear testing of total hip replacements accounting for unsteady synovial lubrication effects between the femoral head and the acetabular liner (Ruggiero and Sicilia 2020; Ruggiero et al., 2020). Understanding the wear pattern, damage and the wear rates are crucial to identify the different key factors in prosthesis design, materials, tolerances and surgical methods which would minimise the wear rates and increase overall longevity.

Previously, an in-house fretting wear algorithm (English et al., 2015) was developed using a 3D finite element model and a Python script within the Abaqus environment. The algorithm has led to the further

understanding of different design and material variations (Ashkanfar et al., 2017a), manufacturing tolerances (Ashkanfar et al., 2017b) and surgical techniques (English et al., 2016). The fretting wear algorithm was only able to predict wear due to micromotion at the taper junction of the THRs. In this study, a new wear algorithm has been developed to predict wear at the bearing surfaces for the larger movement of the femoral head.

2. Methodology

2.1. Finite element model

A model of the acetabular cup and femoral head with a liner insert was created in the finite element package (ABAQUS, 2019) (Fig. 2). In this model, the acetabular cup has a 4 mm thick liner with a 3 mm thick metal backing (Fig. 2b) (Shen et al., 2011). The materials used in this analysis are Cobalt–Chromium (CoCr) for both the femoral head and acetabular cup and cross-linked polyethylene (XLPE) for the liner. XLPE has been widely used since the 2000s for its low wear by improving wear resistance and oxidative degradation while maintaining its mechanical properties (Affatato et al., 2018; Hu and Yoon 2018; Carli et al., 2020). The material properties are listed in Table 1 (Innocenti et al., 2014; Innocenti et al., 2014). The cup and head were meshed in preparation for analysis using the eight-node bilinear hexahedral reduced integration elements (C3D8R).

To replicate a walking cycle, the rotations and loadings occurring on a typical hip joint were applied onto the model (Fig. 3a). The acetabular cup was fixed on its outer surface whereas the femoral head was free to rotate based on the rotation and loading cycles specified. The walking loads and rotations (following their amplitude (Fig. 4)) are both applied to the centre of the femoral head (Fig. 3b and c). These conditions simulate the acetabular cup as being cemented into the hip while the femoral head transfers the walking and rotation loads onto the inner surface of the acetabular cup. A friction coefficient of 0.11 (Wang et al., 2010) has been applied between the contacting surfaces using the penalty method in Abaqus.

2.2. Computational wear analysis

There are two main types of wear law, ‘Archard’s’ and the ‘Dissipated Energy’ wear law (Zmitrowicz 2006; Abdo 2015). The Dissipated Energy wear law is used throughout this study as it predicts wear across a wider range of motion with a greater range of application than Archard’s wear law (Fouvry et al., 2003; Fouvry et al., 2003).

Table 1
Material properties for THR.

Material	Young’s Modulus (GPa)	Density (kg/m ³)	Poisson’s ration
CoCr	210	7800	0.3
XLPE	1	963	0.4

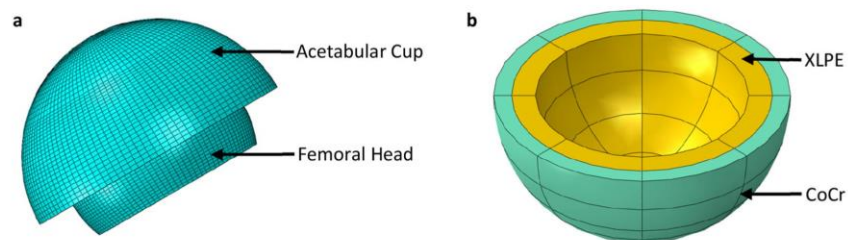


Fig. 2. FE Model (a) Mesh of the FE model, (b) Partitions showing material assignments.

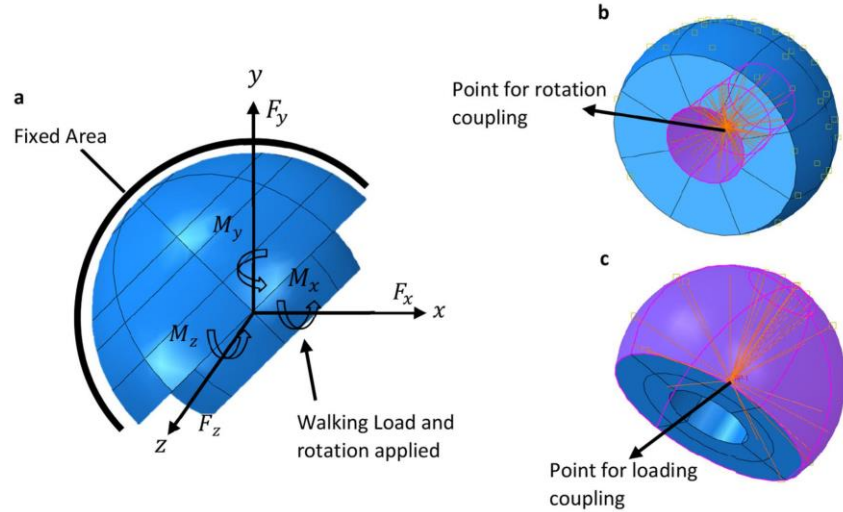


Fig. 3. FE model: (a) showing boundary conditions on FE model, (b) area of rotation boundary applied, (c) area of loading boundary applied.

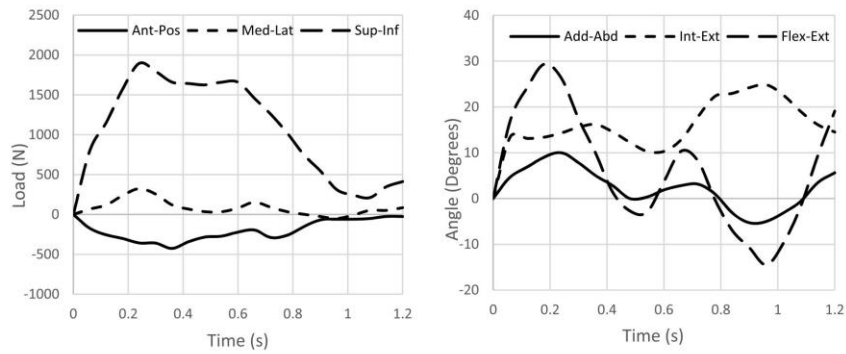


Fig. 4. (a) Time variant loading cycle, (b) Time variant rotation walking gait cycle.

Abdo 2015). As elaborated previously by English et al. (2015), the wear depth (W_d) can be calculated using Eq. (1), where α is the energy wear coefficient, τ is the contact shear stress and s is the relative displacement between bearing surfaces.

$$W_d = \alpha \tau s \tag{1}$$

As the wear analysis would need to be performed for over millions of cycles, a scaling factor (β) needs to be introduced to make the execution of the analysis achievable in acceptable time. The scaling factor is used to multiply the wear calculated after a single analysis (one walking step) so as to create a wear value that can be used to modify the surface geometry by a suitable amount to facilitate acceptable run times. The scaling factor used can vary across a large range (25,000 to 2 million). A large scaling factor would result in a faster computational run time but may affect the accuracy of the results. A small scaling factor would increase the computational run time but should provide a greater accuracy of results. Hence, the scaling factor needs to be optimised to ensure the accuracy of the results within an acceptable time frame. The wear for a single cycle of loading of a node can be calculated using Eq. (2), where τ_i

and s_i are the surface contact shear stress and relative displacement respectively, at each time interval.

$$W_C = \beta \sum_i^n \alpha \tau_i s_i \tag{2}$$

The calculation of wear at the contact surfaces requires creating sets of "node pairs". The pairing is achieved by taking a node at the surface with the coarser mesh (Surface A) and determining which nodes are closest on the opposing surface (Surface B). In the previously developed fretting wear algorithm (English et al., 2015), as fretting wear does not involve any large displacements, a single node-to-node pairing method was sufficient to ensure that all the nodes would have wear depth applied. For the larger relative displacement, in this study, a node from 'Surface A' needs to be paired to a cloud of nodes on 'Surface B' due to different mesh densities on the surfaces. This will avoid any nodes on 'Surface B' to be left unpaired which may cause wear to not be applied at the node and subsequently cause sharp points in the geometry of the model. This has been optimised for each node from 'Surface A' to be paired to three to nine nodes on 'Surface B' (Fig. 5). This depends on the

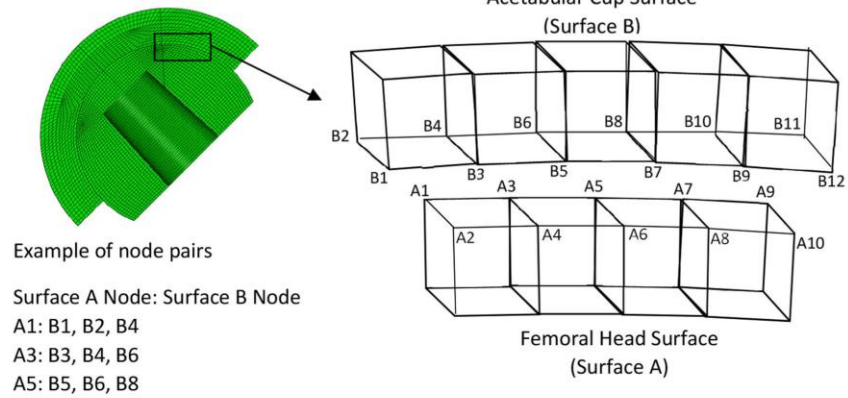


Fig. 5. Node pairs diagram.

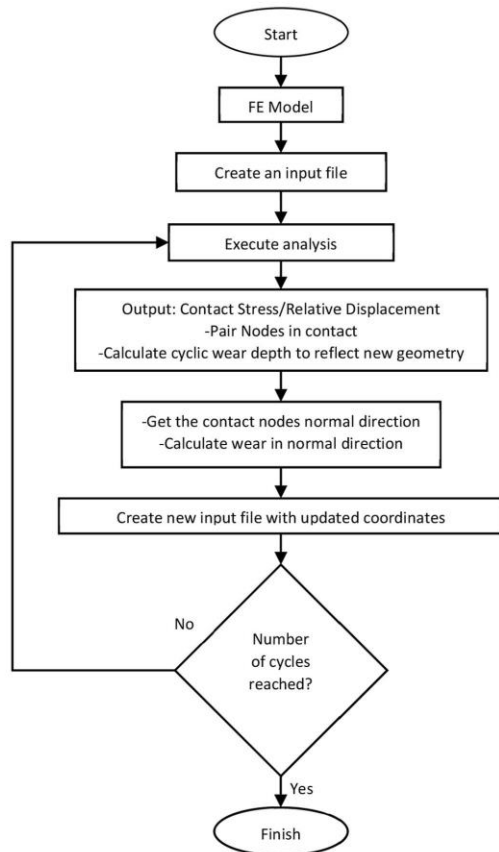


Fig. 6. Flowchart outlining python script.

difference in the mesh density on the coupling surfaces. The pairing procedure needs to be undertaken at each time interval of the walking cycle. The contact stress and relative displacement are extracted for all

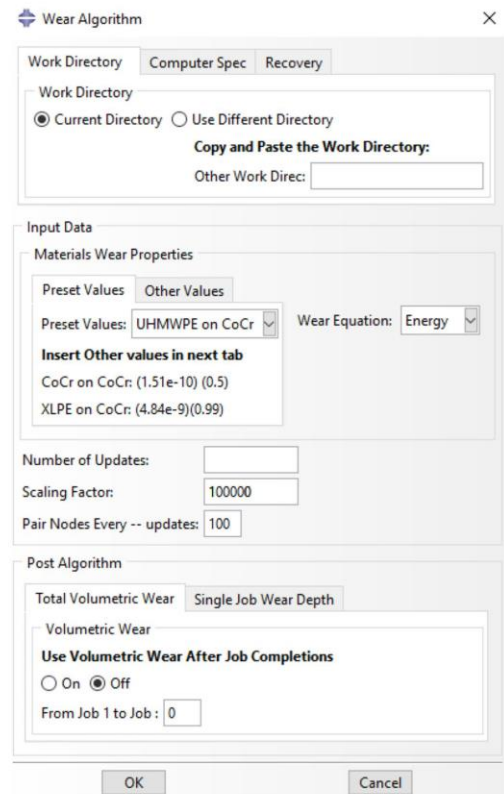


Fig. 7. Graphical user interface of the wear algorithm.

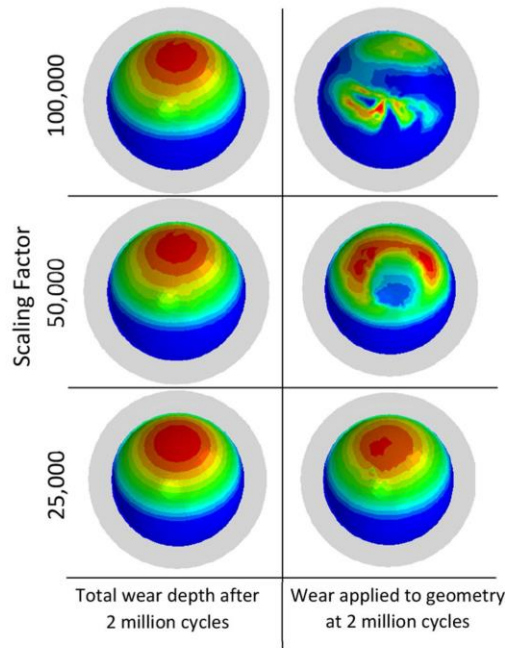


Fig. 12. Effect of scaling factor on the wear occurring in the analysis.

elements of the different parts. As can be expected, the material loss from the surfaces increases over the 5 million load cycles as shown in Fig. 10a. The cumulative volumetric loss at the end of 5 million cycles is 169.2 mm³ and 1.75 mm³ for the XLPE bearing liner and CoCr femoral head due to the material interaction properties. The total material loss from both bearing surfaces after 5 million load cycles is 170.96 mm³. The volumetric wear rate at each million load cycle remains similar throughout the analysis between 33.6mm³/Mc to 34.1mm³/Mc and 0.337mm³/Mc to 0.362mm³/Mc for the bearing liner and femoral head respectively (Fig. 10b). This shows that the volumetric wear is increasing linearly throughout the analysis.

The maximum linear wear was determined from the largest wear depth at the XLPE liner at each 0.5 million cycles (Fig. 11). The maximum linear wear is shown to have a linear increase with a maximum of 0.192 mm at 5 million cycles. The linear wear rate was initially higher for the first million load cycles at 0.0418mm/Mc and then decreases to about 0.0375 mm/Mc subsequently. The higher initial linear wear rate of 0.0418mm/Mc in the first million cycle (Fig. 11b) may be due to an initial period of material deformation (bedding-in) and then steady-state wear which would continue after the first million cycle

Table 2
Linear and volumetric wear rates of XLPE and UHMWPE in literature.

Material	Literature	Method of wear retrieval	Linear Wear rate (mm/yr)	Volumetric Wear rate (mm ³ /yr)
XLPE	Atrey et al. (2017)	Radiography	0.07	29.29
	Haw et al. (2017)	Radiography	0.052	33.09
	Khoshbin et al. (2020)	Retrieved THR	0.0387	31.51
	Range	–	0.039–0.07	29.3–33.1
UHMWPE	Current study	FEA	0.0375	33.8
	Ali et al. (2016b)	Hip Simulator	0.24	12.2
	Trommer et al. (2015)	Hip Simulator	0.8	56
	Callaghan et al. (2003)	Clinical database	0.08–0.12	32.71–89.27
	Fialho et al. (2007)	Computational Method	0.09	18
Literature range	–	0.08–0.8	12.2–89.3	

(Atrey et al., 2017).

4. Discussion

The scaling factor used in the analysis has a major impact on the solution time, wear evolution, and solution accuracy. Fig. 12 shows the total cumulative wear and the wear that is applied at 2 million cycles using different scaling factors of 25,000, 50,000 and 100,000. Although the total cumulative wear at 2 million cycles remains similar, the wear that is being applied to the geometry is not smoothly distributed (Fig. 12). As the analysis progresses, this will cause a sharp increase in wear depth at a certain contact area on the surfaces which would then lead to inconsistencies on the wear pattern. To mitigate this effect and to reduce the computational time, a node wear smoothing feature has been developed in the wear algorithm. In this node smoothing feature, the wear applied to each node is checked with a cloud of surrounding nodes to ensure that the wear distribution is applied smoothly throughout the analysis.

The maximum contact pressure variation over the first gait cycle is shown to be 3.21 MPa (Fig. 13a). At the end of 5 million cycles, the variation in contact pressure remains similar to the variation at the first gait cycle. These results are comparable to studies performed by Yoshida et al. (2006) and Saikko (2020). For a peak load of 2.5 kN, Yoshida reported a maximum contact pressure of 3.2 MPa while Saikko reported a maximum contact pressure of 3 MPa.

The linear and volumetric wear rates shown in this study are comparable to several studies with XLPE in the literature (see Table 2). Atrey et al. (2017) and Haw et al. (2017) analysed a total of 32 and 48 primary total hip arthroplasties respectively with a 36 mm CoCr femoral head size coupled with XLPE liners on serial radiographs. Atrey et al. (2017) showed a mean linear and volumetric wear rate of 0.07 mm/yr and 29.29 mm³/yr while Haw, Battenberg et al. (2017) showed a mean

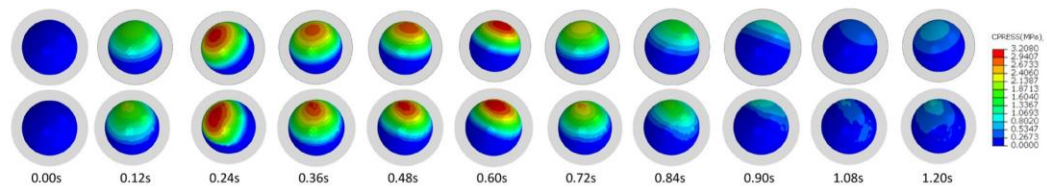


Fig. 13. Variation of contact pressure (CPRESS) a) at the first gait cycle, b) at the end of 5 million cycles.

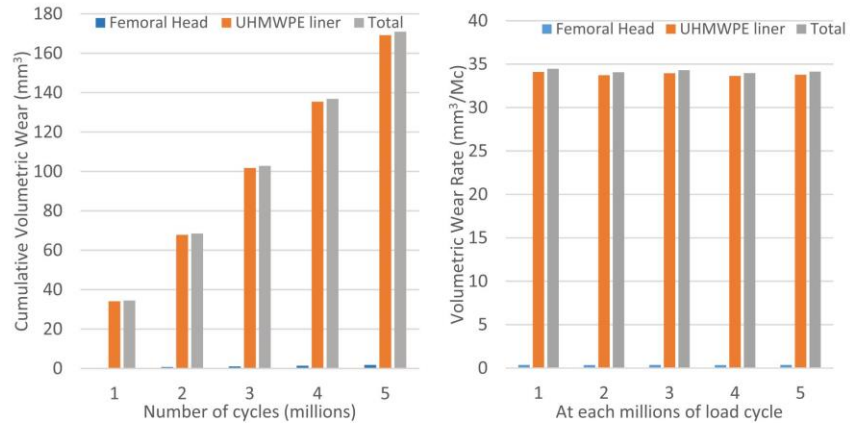


Fig. 10. Variation in a) cumulative volumetric wear, b) volumetric wear rate with respect to nth million cycles.

Energy' wear law, the algorithm can utilise both 'Archard' and 'Dissipated Energy' wear laws for calculations.

The graphical user interface of the current wear algorithm is shown in Fig. 7. All the necessary variable inputs are taken from the user such as the wear coefficient (α), wear fraction, wear equation to be used, the total number of updates and scaling factor. In addition to calculating the wear depth, the volumetric wear can also be determined with the algorithm by extracting the reduction of element volume for all elements throughout the entire part and calculated at each defined time interval.

All analyses were executed on a 64-bit Windows 10 professional operating system with a four-core processor Intel central processing unit platform at 3.8 GHz which had a total run time of 850 h.

3. Results

3.1. Variation of contact shear and relative displacement during a gait cycle

Fig. 8 shows the contact shear stress (CSHEAR), distributed on the femoral head, and relative displacement (CSLIP) on the bearing liner. It is noticeable that at each time interval, the CSHEAR and CSLIP at each point of the contact bearing surfaces are similar. The maximum CSHEAR is 0.352 MPa which occurs at 0.60s while the maximum relative

displacement of 10.9 mm occurs at 0.24s over the walking cycle.

As explained earlier, the nodes in contact are paired at each time interval of the analysis. For each set of paired nodes, the CSLIP (Fig. 8a) and CSHEAR (Fig. 8b) were extracted. These values are then used to calculate the wear depth using Eq. (2). The wear depth distribution after using a scaling factor of 100,000 is shown in Fig. 8c. As expected, due to the wear fraction, the highest wear depth occurs on the bearing liner with a wear depth of 4.25 μm and the maximum wear depth on the femoral head is 0.0460 μm which is around 99 times lower.

3.2. Predicted wear damage over 5 million cycles

The same procedure as explained in 3.1 has been carried out to complete up to 5 million cycles and the evolution of wear is shown in Fig. 9 at every million cycles. The maximum wear depth value reaches 192.5 μm and 2.20 μm after 5 million cycles for the bearing liner and femoral head respectively (Fig. 9a and b). It can be seen from Fig. 9 that most of the wear occurs at a relatively small area.

3.3. Volumetric wear and linear wear of XLPE liner

The volumetric wear was determined at each 1 million cycles as the solution progressed based on the reduction of element volume for all the

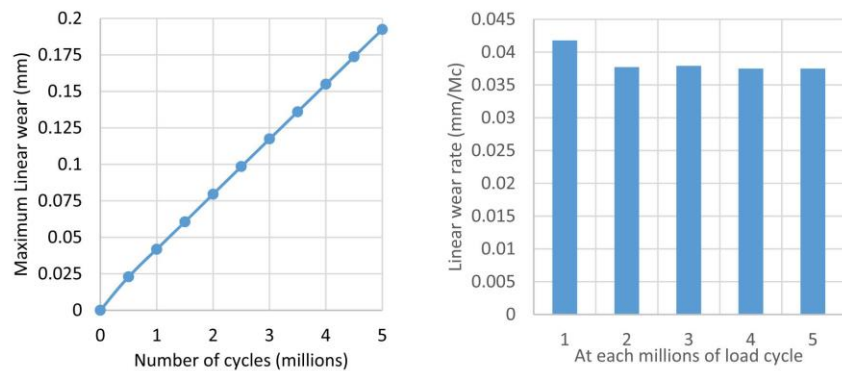


Fig. 11. a) Maximum linear wear of XLPE liner at every million cycles, b) linear wear rate at each million of load cycles.

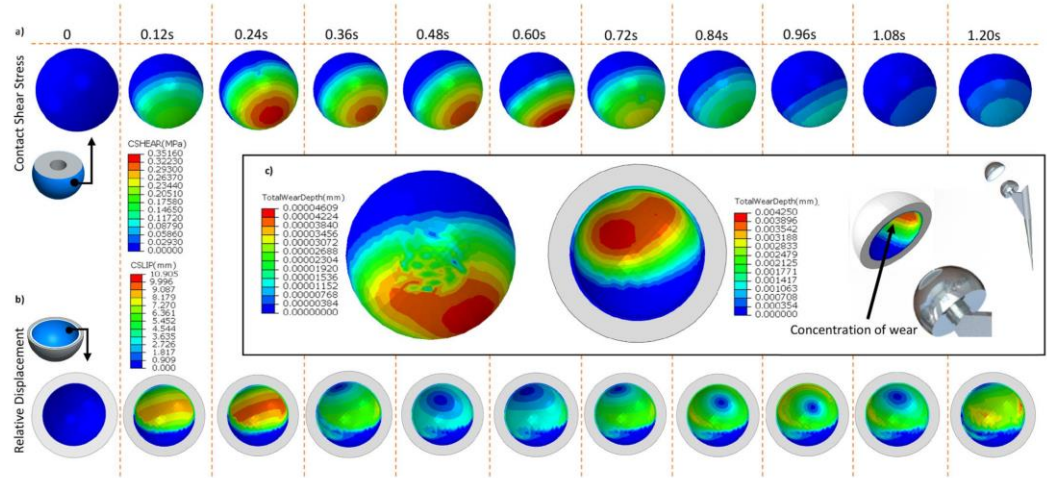


Fig. 8. a) Variation of shear stresses, b) relative displacement during a walking cycle and the wear from the first 10,000 cycles, c) Wear depth values at the end of 100,000 cycles.

paired nodes at each time interval as illustrated in Fig. 6

Using Eq. (2), the wear depth for each set of paired nodes is calculated using an energy wear coefficient of $5.32(10^{-10})\text{mm}^3/\text{Nmm}$ (Matsoukas et al., 2009). A fraction of the wear depth calculated for each paired node is used to update the nodal coordinates. This fraction depends on the contact surface interaction properties of the materials in contact. The algorithm applies a fraction of the wear depth calculated on each contacting surface to each paired node. The wear fraction introduced is 0.99:0.01 for the interaction of XLPE with CoCr respectively (Anissian et al., 1999). Although the wear present in the CoCr is relatively small compared to XLPE, small amounts of metal present in the body can lead to a metallosis. The wear fraction is used to highlight the amount of metal particles that would be released into the body.

To be able to translate wear depth into normal coordinates to update the geometry, the normal direction vectors of the nodes are obtained

from the initial position of the model. The geometry is then updated based on the defined coordinates and a new input file is generated. The analysis is then continued until the number of cycles has been reached.

The scaling factor (β) used in the analysis has a great impact on computational time and wear accuracy. A larger scaling factor would result in a quicker analysis but may greatly impact the accuracy of the results. A smaller scaling factor would increase the computational effort. An optimum scaling factor of $\beta = 10^5$ was used in this study as previously investigated by (English et al., 2015).

The method to calculate the wear depth for hundreds of thousands of paired nodes needs to be automated. As such a Python script has been written within the Python Development Environment (PDE) in Abaqus to automate the procedure. An outline of the python script is shown in Fig. 6. The python script is then converted into an Abaqus plug-in. Although the methodology here presented is using the 'Dissipated

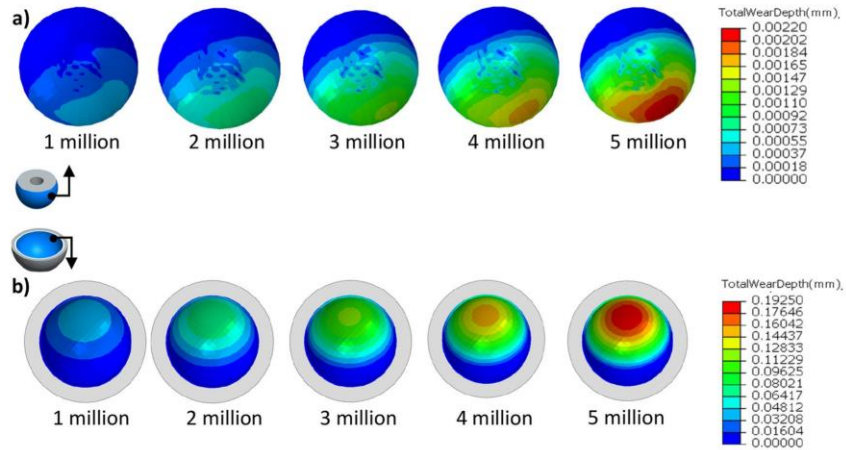


Fig. 9. Variation in wear depth over 5 million walking cycles.

linear and volumetric wear rate of 0.052 mm/yr and 33.09 mm³/yr. Khoshbin, Wu et al. (2020) analysed a total of 40 primary THR of XLPE liners with CoCr femoral heads using radiography. The results obtained showed a mean linear wear rate of 0.0387 mm/yr and 31.51 mm³/yr.

The range of linear and volumetric wear rate for the XLPE liners coupled with a 36 mm CoCr femoral head reported in the above studies (Atrey et al., 2017; Haw et al., 2017; Khoshbin et al., 2020) was between 0.039 and 0.07 mm/yr and 29.29–33.09 mm³/yr. The number of steps walked by a patient per year, undoubtedly influences the wear rate per year however by considering an average of 1 million walking steps per year (Schmalzried et al., 1998), the linear and volumetric wear rate shown in our study (0.0375 mm/yr and 33.8 mm³/yr) are comparable to those found in the above literature (see Table 2). It is noticeable that if a patient walks more than the assumed 1 million cycles per year, it will only hasten the wear and not affect the wear rate per million cycles. There are many factors which can contribute to the wear damage, such as variable wear and friction coefficients, surface roughness, manufacturing tolerances, and the patient's activity level, weight, and implant design.

As XLPE liners are a relatively new material (around 15 years) compared to conventional ultra-high-molecular-weight polyethylene (UHMWPE) (around 50 years), many of the primary THR conducted are still currently in service and the investigation on the wear rate is mainly based on radiography as shown in the above literature. Radiography is unable to show the wear pattern on the bearing surface which is paramount to understanding the evolution of wear. The wear algorithm presented in this study can show the wear pattern and highlight areas of concern.

To further understand and compare the wear evolution, the wear patterns of conventional UHMWPE were compared with the results shown in this study (see Table 2). A study by Ali et al. (2016b) and Trommer et al. (2015) which both used a commercial hip simulator to evaluate the wear at 5 million load cycles showed a linear and volumetric wear rate of 0.24 mm/yr and 12.2 mm³/yr for a 36 mm CoCr femoral head and 0.8 mm/yr and 56 mm³/yr for a 28 mm CoCr femoral head. Callaghan, Pedersen et al. (2003) used a clinical database of more than 4000 primary THRs with 22 mm and 28 mm femoral head sizes implanted by a surgeon to evaluate the wear mechanism between 5 and 22 years. The range of linear and volumetric wear presented was 0.08–0.12 mm/yr and 32.71–89.27 mm³/yr respectively. Fialho, Fernandes et al. (2007) used a computational method to predict the extent of wear damage for a 28 mm CoCr head size at 1 million load cycles. The study showed a linear and volumetric wear rate of 0.09mm/Mc and 18mm³/Mc.

The range of linear and volumetric wear presented for conventional UHMWPE liners in the above studies (Callaghan et al., 2003; Fialho et al., 2007; Trommer et al., 2015; Ali et al., 2016b) was between 0.08 and 0.24mm/Mc and 12.2–89.27 mm³/yr respectively. Although the wear patterns in our study are comparable to the wear pattern shown in conventional UHMWPE, the linear and volumetric wear rates of conventional UHMWPE are higher than the values shown in XLPE as the overall amount of wear of XLPE may be up to 40% less (Ali et al., 2016b) than conventional UHMWPE (see Table 2).

Although in this study we have used zero tolerances between the femoral head and bearing liner, defining tolerances for manufacturing is crucial. The tolerances may also translate into bearing surface clearances which will affect the outcome of wear and implant survivability. Surface roughness may also influence wear. There have been studies which incorporate surface roughness into the wear coefficient to simulate the actual wear (Pietrabissa et al., 1998; Raimondi et al., 2001). The algorithm developed in this study can be used to perform parametric studies to propose the optimum tolerances for manufacturing and surface roughness.

A fixed friction coefficient and wear coefficient has been used in this study; however, they can be continuously changed over the implant's lifetime due to the changes in surface roughness, lubrication and wear

debris. The algorithm developed in this study can investigate the effect of different friction and wear coefficients to improve the design and material characteristics of the implant.

5. Conclusion

The combination of using a wear algorithm written in the PDE and a 3D FE model presented in this study can be used to predict the extent of bearing surface wear damage for millions of load cycles. The algorithm developed can be applied to clinical practice such as determining appropriate bearing size, bearing liner thickness, implantation angle, and to improve the design of the prosthesis to increase its longevity.

The methodology demonstrates that a dynamic implicit analysis can model the gait cycle effectively. The total dissipated energy wear law and the FE model described can predict wear patterns, linear and volumetric wear rates when compared to typically observed wear patterns from UHMWPE retrievals and XLPE in-vivo wear rates. These results have been validated with literature and show promise in predicting the evolution of wear and can be used to investigate different parameters such as body weight, material properties, different implant size and design, manufacturing tolerances and different surgical techniques.

The accurate and smooth evolution of wear across the bearing surface are influenced by the scaling factor and mesh size used. Using a coarser mesh density and a large scaling factor would reduce the computational time but will affect the accuracy of the results. A smaller scaling factor (Fig. 12) would ensure that the wear is evenly distributed and will avoid cyclic wear 'hotspots' being overly exaggerated. A fine mesh and a small scaling factor can facilitate an accurate and smooth development of wear but with the cost of a much-increased computational time. To help reduce the computational time, a node smoothing feature was developed to be used so there is no sudden exaggeration in the node wear. As such, a balance of mesh density and the scaling factor is needed to ensure accurate results within a reasonable time. For example, the model presented in this study has utilised a scaling factor of 100,000 coupled with the node smoothing feature was found to provide a smooth wear evolution.

The wear methodology can be utilised generically in the analysis of other prosthetic devices such as knee and shoulder implants. Also, the method can be generalised to involve parts in contact subject to cyclic loadings.

CRedit authorship contribution statement

Shawn Ming Song Toh: Methodology, Software, Formal analysis, Investigation, Writing – original draft, Writing – review & editing. **Ariyan Ashkanfar:** Methodology, Software, Investigation, Writing – original draft, Writing – review & editing. **Russell English:** Methodology, Writing – review & editing, Supervision. **Glynn Rothwell:** Methodology, Writing – review & editing, Supervision.

Declaration of competing interest

The authors declare that they have no known competing financial interests or personal relationships that could have appeared to influence the work reported in this paper.

Acknowledgement

This work is funded by the School of Engineering, Liverpool John Moores University, Liverpool, UK.

References

- Abdo, J., 2015. Materials sliding wear model based on energy dissipation. *Mech. Adv. Mater. Struct.* 22 (4), 298–304.

- Affatato, S., Merola, M., Ruggiero, A., 2018a. Development of a novel in silico model to investigate the influence of radial clearance on the acetabular cup contact pressure in hip implants. *Materials* 11 (8), 1282.
- Affatato, S., Ruggiero, A., Jaber, S.A., Merola, M., Bracco, P., 2018b. Wear behaviours and oxidation effects on different UHMWPE acetabular cups using a hip joint simulator. *Materials* 11 (3), 433.
- Ali, M., Al-Hajjar, M., Jennings, L.M., 2016a. 31 - Tribology of UHMWPE in the Hip. *UHMWPE Biomaterials Handbook*. In: Kurtz, S.M. (Ed.), third ed. William Andrew Publishing, Oxford, pp. 579–598.
- Ali, M., Al-Hajjar, M., Partridge, S., Williams, S., Fisher, J., Jennings, L.M., 2016b. Influence of hip joint simulator design and mechanics on the wear and creep of metal-on-polyethylene bearings. *Proc. IME H J. Eng. Med.* 230 (5), 389–397.
- Anissian, L., Stark, A., Sorensen, K., Gustafson, A., Downs, B., Good, V., Clarke, I., 1999. HIP-SIMULATOR WEAR COMPARISONS OF COCR/COCR VERSUS COCR/PE THR AT 10 MILLION CYCLES. Proceedings of the Annual Meeting of the Orthopaedic Research Society, Anaheim, California.
- Ashkanfar, A., Langton, D.J., Joyce, T.J., 2017a. Does a micro-grooved trunnion stem surface finish improve fixation and reduce fretting wear at the taper junction of total hip replacements? A finite element evaluation. *J. Biomech.* 63, 47–54.
- Ashkanfar, A., Langton, D.J., Joyce, T.J., 2017b. A large taper mismatch is one of the key factors behind high wear rates and failure at the taper junction of total hip replacements: a finite element wear analysis. *Journal of the mechanical behavior of biomedical materials* 69, 257–266.
- Ashman, B., Cruikshank, D., Moran, M., 2016. Total hip replacement: relieving pain and restoring function. *Br. Columbia Med. J.* 58 (9), 505–513.
- Atrey, A., Ward, S.E., Khoshbin, A., Hussain, N., Bogoch, E., Schemitsch, E.H., Waddell, J.P., 2017. Ten-year follow-up study of three alternative bearing surfaces used in total hip arthroplasty in young patients. *The Bone & Joint Journal* 99-B (12), 1590–1595.
- Buly, R.L., Htoo, M.H., Salvati, E., Brien, W., Bansal, M., 1992. Titanium wear debris in failed cemented total hip arthroplasty: an analysis of 71 cases. *J. Arthroplasty* 7 (3), 315–323.
- Callaghan, J.J., Pedersen, D.R., Johnston, R.C., Brown, T.D., 2003. Clinical biomechanics of wear in total hip arthroplasty. *Iowa Orthop. J.* 23, 1.
- Carli, A.V., Patel, A.R., Cross, M.B., Mayman, D.J., Carroll, K.M., Pellicci, P.M., Jerabek, S.A., 2020. Long-term performance of oxidized zirconium on conventional and highly cross-linked polyethylene in total hip arthroplasty. *SICOT J* 6.
- English, R., Ashkanfar, A., Rothwell, G., 2015. A computational approach to fretting wear prediction at the head-stem taper junction of total hip replacements. *Wear* 338–339, 210–220.
- English, R., Ashkanfar, A., Rothwell, G., 2016. The effect of different assembly loads on taper junction fretting wear in total hip replacements. *Tribol. Int.* 95, 199–210.
- Evans, J.T., Evans, J.P., Walker, R.W., Blom, A.W., Whitehouse, M.R., Sayers, A., 2019. How long does a hip replacement last? A systematic review and meta-analysis of case series and national registry reports with more than 15 years of follow-up. *Lancet* 393 (10172), 647–654.
- Fialho, J.C., Fernandes, P.R., Eça, L., Folgado, J., 2007. Computational hip joint simulator for wear and heat generation. *J. Biomech.* 40 (11), 2358–2366.
- Fouvy, S., Liskiewicz, T., Kapsa, P., Hannel, S., Sauger, E., 2003. An energy description of wear mechanisms and its applications to oscillating sliding contacts. *Wear* 255 (1), 287–298.
- Gao, L., Hua, Z., Hewson, R., 2018. Can a “pre-worn” bearing surface geometry reduce the wear of metal-on-metal hip replacements? – a numerical wear simulation study. *Wear* 406–407, 13–21.
- Hallan, G., Lie, S.A., Havelin, L.I., 2006. High wear rates and extensive osteolysis in 3 types of uncemented total hip arthroplasty: a review of the PCA, the Harris Galante and the Profile/Tri-Lock Plus arthroplasties with a minimum of 12 years median follow-up in 96 hips. *Acta Orthop.* 77 (4), 575–584.
- Haw, J.G., Battenberg, A.K., Huang, D.-C.T., Schmalzried, T.P., 2017. Wear rates of larger-diameter cross-linked polyethylene at 5 to 13 Years: does liner thickness or component position matter? *J. Arthroplasty* 32 (4), 1381–1386.
- Holcomb, W.R., Miller, M.G., Rubley, M.D., 2012. Importance of comprehensive hip strengthening. *Strength Condit. J.* 34 (1), 16–19.
- Hu, C.Y., Yoon, T.-R., 2018. Recent updates for biomaterials used in total hip arthroplasty. *Biomater. Res.* 22, 33, 33.
- Hua, Z., Dou, P., Jia, H., Tang, F., Wang, X., Xiong, X., Gao, L., Huang, X., Jin, Z., 2019. Wear test apparatus for friction and wear evaluation hip prostheses. *Front. Mech. Eng.* 5 (12).
- Innocenti, B., Labey, L., Kamali, A., Pascale, W., Pianigiani, S., 2014. Development and validation of a wear model to predict polyethylene wear in a total knee arthroplasty: a finite element analysis. *Lubricants* 2 (4), 193–205.
- Karachalios, T., Konnos, G., Koutalos, A., 2018. Total hip arthroplasty: survival and modes of failure. *EFORT open reviews* 3 (5), 232–239.
- Khoshbin, A., Wu, J., Ward, S., Melo, L.T., Schemitsch, E.H., Waddell, J.P., Atrey, A., 2020. Wear rates of XLPE nearly 50% lower than previously thought after adjusting for initial creep: an RCT comparing 4 bearing combinations. *JBUS Open Access* 5 (2), e0066.
- Khuss, D., Martin, H., Mittelmeier, W., Schmitz, K.-P., Bader, R., 2007. Influence of femoral head size on impingement, dislocation and stress distribution in total hip replacement. *Med. Eng. Phys.* 29 (4), 465–471.
- Kumar, A., Bloch, B.V., Esler, C., 2017. Trends in total hip arthroplasty in young patients - results from a regional register. *Hip Int.* 27 (5), 443–448.
- Learmonth, I.D., Young, C., Rorabeck, C., 2007. The operation of the century: total hip replacement. *Lancet* 370 (9597), 1508–1519.
- Matsoukas, G., Willing, R., Kim, I.Y., 2009. Total hip wear assessment: a comparison between computational and in vitro wear assessment techniques using ISO 14242 loading and kinematics. *J. Biomech. Eng.* 131 (4).
- Nambiar, S.M., Jagani, N.S., Sharoff, L., D'souza, J.J., 2017. Total hip replacement the ideal joint for failed osteosynthesis of hip fractures. *International Journal of Orthopaedics* 3 (3), 667–672.
- Neil, G., Burke, J.P.G., Cassar-Gheiti, Adrian J., Walsh, Fionnuala M., Cashman, James P., 2018. Total hip replacement—the cause of failure in patients under 50 years old? *Ir. J. Med. Sci.* 188, 879, 2019.
- NJR, 2019. National Joint Registry: National Joint Registry for England, Wales and Northern Ireland. 16th Annual Report, 2019.
- Pietrabissa, R., Raimondi, M., Di Martino, E., 1998. Wear of polyethylene cups in total hip arthroplasty: a parametric mathematical model. *Med. Eng. Phys.* 20 (3), 199–210.
- Raimondi, M.T., Santambrogio, C., Pietrabissa, R., Raffellini, F., Molfetta, L., 2001. Improved mathematical model of the wear of the cup articular surface in hip joint prostheses and comparison with retrieved components. *Proc. IME H J. Eng. Med.* 215 (4), 377–390.
- Ramesh, V., van Kuilenburg, J., Wits, W.W., 2019. Experimental analysis and wear prediction model for unfilled polymer–polymer sliding contacts. *Tribol. Trans.* 62 (2), 176–188.
- Ruggiero, A., Merola, M., Affatato, S., 2018. Finite element simulations of hard on soft hip joint prosthesis accounting for dynamic loads calculated from a musculoskeletal model during walking. *Materials* 11 (4), 574.
- Ruggiero, A., Scilla, A., 2020. Lubrication modeling and wear calculation in artificial hip joint during the gait. *Tribol. Int.* 142, 105993.
- Ruggiero, A., Scilla, A., Affatato, S., 2020. In silico total hip replacement wear testing in the framework of ISO 14242-3 accounting for mixed elasto-hydrodynamic lubrication effects. *Wear* 460–461, 203420.
- Saikko, V., 2020. Effect of inward-outward rotation on hip wear simulation. *J. Biomech.* 101, 109638.
- Schmalzried, T.P., Szuszczewicz, E.S., Northfield, M.R., Akizuki, K.H., Frankel, R.E., Belcher, G., Amstutz, H.C., 1998. Quantitative assessment of walking activity after total hip or knee replacement. *Journal of Bone and Joint Surgery - Series A* 80 (1), 54–59.
- Shen, F.-W., Lu, Z., McKellop, H.A., 2011. Wear versus thickness and other features of 5-Mrad crosslinked UHMWPE acetabular liners. *Clin. Orthop. Relat. Res.* 469 (2), 395–404.
- Sipek, K., Lyvers, M., Mathew, M., 2018. Failure causes in total hip replacements: a review. *Austin J Orthopade & Rheumatol* 5, 1064.
- Towheed, T.E., Hochberg, M.C., 1996. Health-related quality of life after total hip replacement. *Semin. Arthritis Rheum.* 26 (1), 483–491.
- Trommer, R.M., Maru, M.M., Oliveira Filho, W.L., Nykanen, V.P.S., Gouvea, C.P., Archanjo, B.S., Martins Ferreira, E.H., Silva, R.F., Achete, C.A., 2015. Multi-scale evaluation of wear in UHMWPE-metal hip implants tested in a hip joint simulator. *Biotribology* 4, 1–11.
- Varnum, C., 2017. Outcomes of different bearings in total hip arthroplasty - implant survival, revision causes, and patient-reported outcome. *Dan Med J* 64 (3).
- Wang, S.B., Ge, S.R., Liu, H.T., Huang, X.L., 2010. Wear behaviour and wear debris characterization of UHMWPE on alumina ceramic, stainless steel, CoCrMo and Ti6Al4V hip prostheses in a hip joint simulator. *Journal of Biomimetics, Biomaterials and Tissue Engineering, Trans Tech Publ.*
- Yoshida, H., Faust, A., Wilckens, J., Kitagawa, M., Fetto, J., Chao, E.Y.S., 2006. Three-dimensional dynamic hip contact area and pressure distribution during activities of daily living. *J. Biomech.* 39 (11), 1996–2004.
- Znitrowicz, A., 2006. Wear patterns and laws of wear - a review. *J. Theor. Appl. Mech.* 44, 219–253.



Contents lists available at ScienceDirect

Computer Methods and Programs in Biomedicine Update

journal homepage: www.sciencedirect.com/journal/computer-methods-and-programs-in-biomedicine-update

The relation between body weight and wear in total hip prosthesis: A finite element study

Shawn Ming Song Toh^{1,*}, Ariyan Ashkanfar¹, Russell English¹, Glynn Rothwell¹¹ School of Engineering, Liverpool John Moores University, Byrom Street, Liverpool, L3 3AF, UK

ARTICLE INFO

Keywords:

Wear modelling
Total hip arthroplasty
Hip joint prosthesis
Finite element modelling
Fretting wear
Polyethylene wear

ABSTRACT

As the current obesity epidemic grows, an increased number of obese patients undergoing Total Hip Arthroplasty (THA) can be expected in the coming years. The National Health Service of the UK (NHS) recommends that an obese patient should undergo weight loss before THA. It is understood that an increased body weight would increase the wear rates on the prostheses, however, the extent of increased wear and the impact on the longevity of the prosthesis is unclear. The NHS found that 45% of THA failures in 2019 were caused by wear which led to a multitude of failures such as infection, aseptic loosening and dislocation such that a revision surgery is then needed. In this study, a finite element model was created to model a walking cycle and a newly developed wear algorithm was used to perform a series of computational wear analyses to investigate the effect of different patient weights on the evolution of wear in THAs up to 5 million cycles. The wear rates shown in this study are closely comparable to previous literature. The XLPE volumetric wear rates were found to be between 15 and 35 mm³/yr (range: 1.5–57.6 mm³/yr) and femoral head taper surface volumetric wear rates were between 0.174 and 0.225 mm³/yr (range: 0.01–3.15 mm³/yr). The results also showed that an increased weight of 140 kg can increase the metallic wear by 26% and polyethylene wear by 30% when compared to 100 kg body weight. As increased wear can lead to a multitude of failure such as aseptic loosening, dislocation and metallosis, from this study, it is recommended that obese patients undergo recommended weight loss and maintain this lesser weight to reduce wear and prolong the life of the THA.

1. Introduction

In recent years, there have been a rise in obesity in adults and is now being described as reaching epidemic proportions [1]. Generally, obesity is measured based on the body mass index (BMI) which divides the body weight in kilograms by the square of the body height in meters. According to the National Health Service, UK (NHS), the classification for an overweight person is someone with a BMI over 25, an obese person has a BMI over 30, and a morbidly obese person has a BMI over 40. Between 1993 and 2019, the Health Survey for England (HSE) showed an increase of 11% of adults who are either overweight or obese [2]. It can also be seen that, during the COVID-19 pandemic, approximately 27% of the 7,753 participants in a study have had an increase in their body weight [3].

It is projected that just under 5 million people across the UK will be classed as morbidly obese by the year 2035 which is a 165% increase from 1.9 million in 2015 [4]. With increasing numbers of people being obese, it is also expected that the number of obese patient's receiving

total hip arthroplasty (THA) will also increase in the coming years. It was found that the mean age of a THA recipient was 10 years younger for morbidly obese patients when compared to those with a normal BMI [5]. Morbidly obese patients would normally be advised to undergo weight loss before a THA is performed, however, it may depend on the circumstances [6]. Several studies in the literature have examined the impact of obesity on the longevity of THAs, which all found that there was no significant difference in the rates of complication or revision surgery between obese and non-obese patients [7–11]. Although, it has also been shown that obese patients would have a lower satisfaction and range of movement when compared to non-obese patients, arthroplasty would still be advised [11,12].

Traina, Bordini [13] investigated the revision rates of THAs with the BMI and body weight as the main categories. The BMI category was subdivided into normal, overweight, obese, and morbidly obese while the body weight category was subdivided into less than 80 kg and above 80 kg. The statistics showed that BMI had no effect on the revision rates, however, the revision rates were higher for patients above 80 kg. This

* Corresponding author.

E-mail address: s.m.toh@2016.ljmu.ac.uk (S.M.S. Toh).<https://doi.org/10.1016/j.cmpbup.2022.100060>

Available online 23 May 2022

2666-9900/© 2022 The Authors. Published by Elsevier B.V. This is an open access article under the CC BY-NC-ND license (<http://creativecommons.org/licenses/by-nc-nd/4.0/>).

showed that weight rather than BMI influences the survival of hip prostheses. Other studies have also suggested that BMI should not be an indicator of hip arthroplasty risk, but rather their weight as the loading applied to an implant depends on the weight of the patients [7,9-11, 13-19].

A THA prosthesis normally consists of 4 components, acetabular cup, acetabular bearing liner, femoral head, and femoral stem with 2 contacting surfaces. Wear is known to be the main cause of premature failures in THAs and can cause a multitude of failures such as aseptic loosening, dislocation, infection or metallosis. The sites of wear can be found at the contacting surfaces between the femoral head and bearing liner, and the contacting surfaces at the taper junction between the femoral head and stem. There are many factors which can influence the longevity on the implant. Current literature on the impact of body weight on the wear rates of a THA is unknown. In this study, the effect of body weight in THAs is investigated to provide a clearer understanding on evolution of wear damage and wear patterns up to 5 million cycles at both the bearing surfaces and taper junction. This equates to approximately 5 years as it is estimated that 1 million cycles are walked by a patient in one year [20].

2. Methodology

2.1. Finite element model

A finite element model of the acetabular cup with an liner insert, femoral head and femoral stem was created in a finite element package (ABAQUS 2019) (Fig. 1a). In this study, a THA prosthesis with a 36 mm femoral head was considered for this study. The acetabular cup was modelled to include a 4 mm thick liner and a 3 mm thick metal backing [21]. The materials used in this analysis are Cobalt-Chromium (CoCr) for the femoral head, highly cross-linked polyethylene (XLPE) for the bearing liner and Titanium (Ti) for the femoral stem and acetabular cup

metal backing. The material and interaction properties are shown in Table 1. A body weight of 60 kg is then applied to the model and the analysis was completed to 5 million walking cycles. An average of 1 million walking cycles per year has been assumed in this study [20] to compare the results of the study to results from literature. The body weight applied on the model was then changed to 80 kg and further increased in increments of 20 kg up to 140 kg.

The computational model has also modelled the initial impaction to simulate the assembly of the head onto the stem. In a previous study [23], a 4kN initial assembly force was found to be optimal and as such, used for all the models subsequently (see Fig. 1a). To replicate a walking cycle, the walking loadings and rotations following their amplitude for a gait cycle is shown in Fig. 1b and Fig. 1c respectively [24]. The models were then meshed using eight-node bilinear hexahedral reduced integration elements (C3D8R). The model is then submitted as a dynamic implicit analysis and the analysis time is discretised into 10 equal time intervals over 1.2 s period. A mesh convergence analysis has been performed with an approximate element size of 0.8 mm for both acetabular liner and femoral head, and 0.4 mm for the femoral stem.

2.2. Wear law

The “Dissipated Energy” wear law predicts wear across a wide range of motion and has been used in this study [31,32]. This law considers the interfacial shear work and relative motion as predominant parameters to calculate the volumetric wear. Its implementation and methodology into the finite element analysis model has been explained previously by Toh, Ashkanfar [33] and English, Ashkanfar [27]. Briefly, according to the “Dissipated Energy” wear law, the total wear depth (W_d) for β walking cycles can be determined using Eq. (1), where β is the scaling factor used, α is the energy wear coefficient, τ_i and s_i are the surface contact shear stress, and relative displacement respectively, over the total time interval, n , and specified time interval i . As the simulation

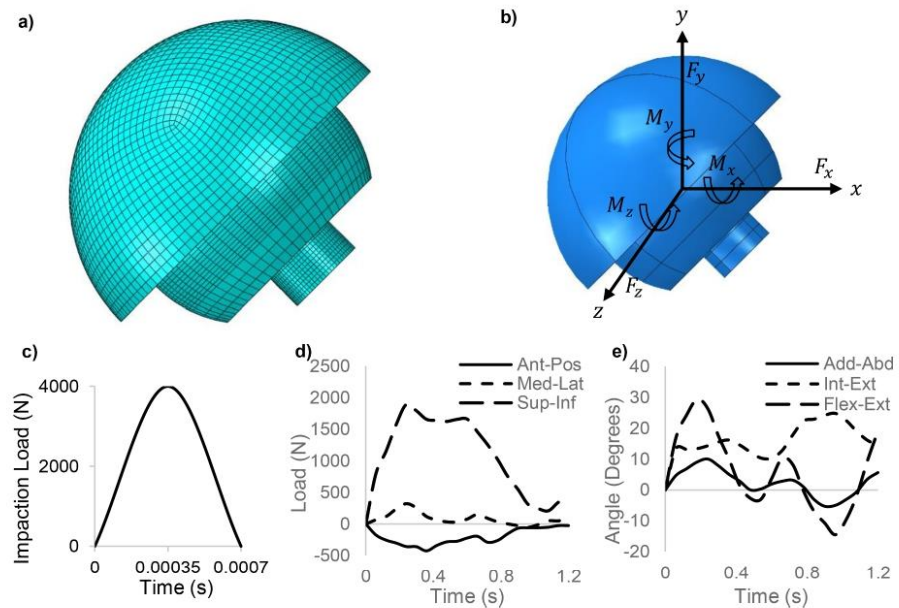


Figure 1. a) FE model with mesh, b) Point of loadings and rotations applied associated with a gait cycle c) Impaction load, d) Loadings of a gait cycle, e) Rotations of a gait cycle

Table 1
Material Properties for THA with interaction properties, Friction Coefficient (FC), Wear coefficient (WC) and Wear Fractions (WF)

Material	Young's Modulus (GPa)	Density (kg/m ³)	Poisson's Ratio	Interaction properties			
Ti	114	4430	0.34	Ti - CoCr	FC: 0.21 [25]	-	FC: 0.11 [28]
CoCr	210	7800	0.3	-	WC: 1.31×10^{-8} MPa ⁻¹ [26]	XLPE - CoCr	WC: 4.84×10^{-8} MPa ⁻¹ [29]
XLPE	1	963	0.4	-	WF: 0.9 CoCr: 0.1 Ti [27]	-	WF: 0.99 XLPE: 0.01 CoCr [30]

would be performed for up to 5 million cycles, a scaling factor is introduced to execute the analysis which can vary across a large range. A previous study on the effect of β on the calculation of wear demonstrated that $\beta = 10^5$ modelled the evolution of wear accurately and smoothly within an acceptable amount of time [27].

$$W_d = \beta \sum_{i=1}^n \alpha \tau_i s_i \tag{1}$$

As the wear depth is the total wear on both the interacting surfaces, a wear fraction is introduced as different fractions of wear would be removed from the individual parts. The wear fraction is dependent on the material interaction properties. The wear fractions and wear coefficients used in this study are shown in Table 1.

In previous studies, an in-house Python algorithm was developed to simulate micromotion wear (fretting wear) [27]. Utilising the framework of the fretting wear algorithm, a new algorithm was developed to simulate wear at the bearing surfaces of the prostheses [33]. This algorithm was validated against over 50 clinical retrievals. The algorithm was used to investigate different factors which contribute to fretting wear such as manufacturing tolerances resulting from taper mismatch [34], surgical techniques during assembly of the prostheses [23], and different surface roughness [35]. In this study, we have further developed the wear algorithm to combine both fretting and the bearing

surface wear within the same analysis. Further add-ons have also been developed for this wear algorithm in order to calculate the total volumetric material loss and volumetric wear rate for each individual part to investigate and compare the material loss individually at each surface pairs.

3. Results

The linear and volumetric wear rates at the bearing surfaces and taper junction of THA shown in this section were presented at each million cycles as the solution progressed. In order to investigate the effect of body weight on the wear evolution damage, the wear patterns are only shown on the XLPE bearing liner (Fig. 2) and head taper surfaces (Fig. 3). This is mainly because these surfaces carry 99% and 90% of the wear fraction calculated respectively.

It can be seen in Fig. 2 for the XLPE bearing liner, by increasing the body weight the maximum linear wear increases also. For 60 kg BW, the maximum linear wear was found to be 0.083 mm at the end of 5 million load cycles, while for 140 kg BW it had increased by 2.7 times to 0.221 mm. However, the maximum linear wear at the femoral taper surface for all body weights is almost constant at approximately 0.004 mm as seen in Fig. 3.

Fig. 4 shows the volumetric wear and volumetric wear rates over 5

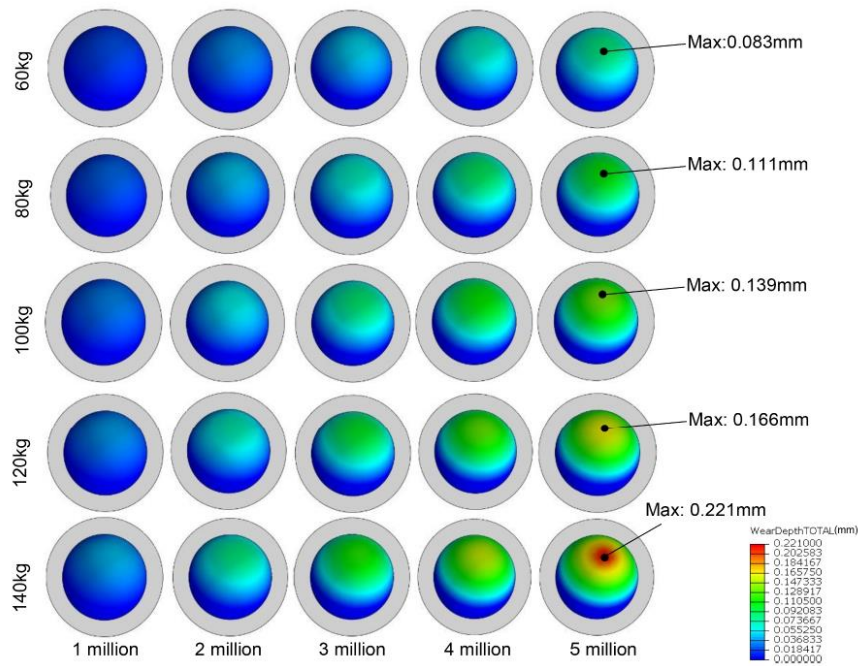


Figure 2. Evolution of wear pattern on the XLPE bearing liner during wear analysis for different patient's weights

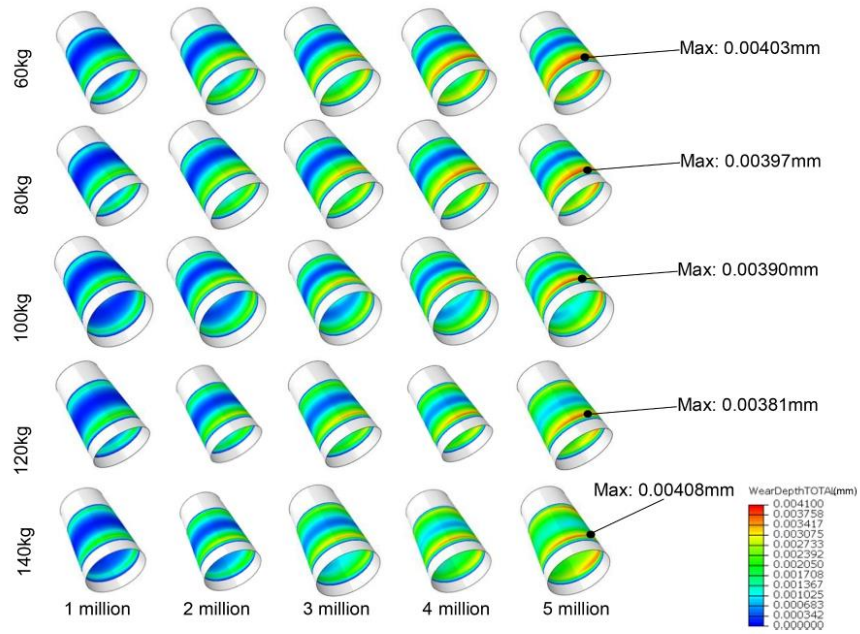


Figure 3. Evolution of wear pattern on the femoral head taper surface during wear analysis for different patient's weight

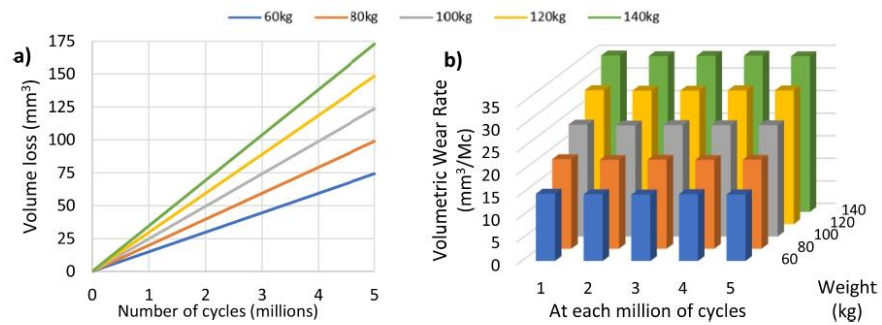


Figure 4. :XLPE liner a) total volumetric wear b) volumetric wear rates over 5 million cycles

million cycles at the XLPE bearing liner. It can be seen in Fig. 4a that the volumetric wear in all cases increases linearly. The total volume loss for 60 kg BW is 75 mm³ while for a 140 kg BW, it increases to 175 mm³. This linear behaviour is further highlighted in Fig. 4b which shows a constant volumetric wear rate of 15 mm³/Mc for 60 kg BW and increases to 35 mm³/Mc for 140 kg BW.

As shown in Fig. 2, although the wear damage for all BWs has a similar pattern, the linear wear for 140 kg BW is 2.7 times higher than 60 kg BW. It can be seen in Fig. 4a, increasing the BW from 60 kg to 140 kg in 20 kg intervals, the volumetric wear of the XLPE bearing liner increases linearly by 25 mm³ at each interval over a 5 million load cycle.

Fig. 5 shows the volumetric wear and volumetric wear rates over 5 million cycles at the bearing surface of the femoral head. The total volume loss for 60 kg BW is 0.7 mm³ while for 140 kg BW, it increases to 1.65 mm³. The linear behaviour of the volume loss is further highlighted

in Fig. 5b which shows a constant volumetric wear rate of 0.14 mm³/Mc for 60 kg BW which increases to 0.33 mm³/Mc for 140 kg BW.

Fig. 6 shows the volumetric wear and volumetric wear rates over 5 million cycles at the femoral head taper surface. The total volume loss over 5 million load cycles is similar for body weights from 60 kg to 100 kg at 0.85 mm³. While this total volume loss increases by 1.3 times to 1.12 mm³ for a body weight of 140 kg. It can further be seen in Fig. 6b that the volumetric wear rate at the 1st million load cycle is equal to 0.34 mm³/Mc for all cases regardless of the body weights. While it decreases to 0.08 mm³/Mc and 0.19 mm³/Mc for 60 kg and 140 kg BW respectively over the 5 million load cycles.

Fig. 7 shows the volumetric wear and volumetric wear rates over 5 million cycles for the femoral stem taper surface. The total volume loss evolution over 5 million load cycles follows a similar trend for body weights from 60 kg to 100 kg at an approximate maximum value of 0.08

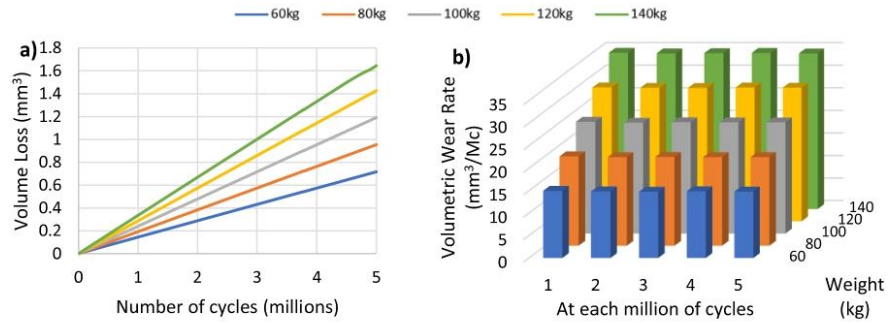


Figure 5. Femoral head bearing surface a) total volumetric wear, b) volumetric wear rates over 5 million cycles

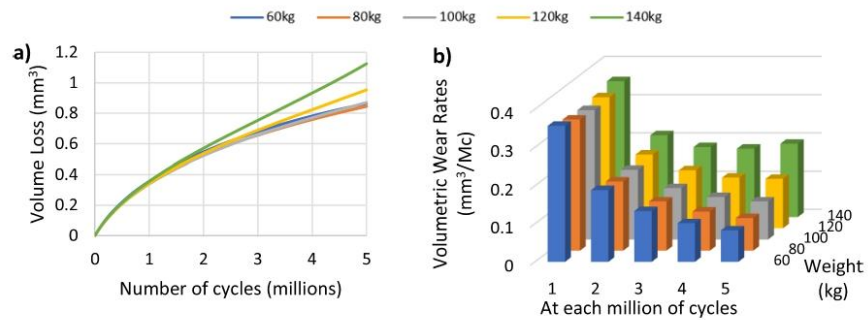


Figure 6. Femoral head taper junction a) total volumetric wear, b) volumetric wear rates over 5 million cycles

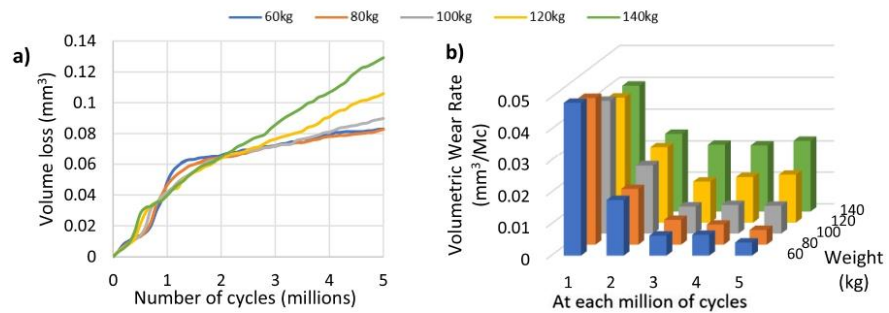


Figure 7. Femoral stem a) total volumetric wear b) volumetric wear rates over 5 million cycles

mm^3 while it increases to approximately 0.11 mm^3 and 0.13 mm^3 for 120 kg and 140 kg BW respectively.

It can be further seen in Fig. 7b that there is an initial higher volumetric wear rate of $0.046 \text{ mm}^3/\text{Mc}$ on average which decreases to $0.015 \text{ mm}^3/\text{Mc}$ at the end of the 2nd million cycle for a body weight of 60 kg and further decreases to approximately $0.005 \text{ mm}^3/\text{Mc}$ between the 3rd and 5th million cycle. The decrease in volumetric wear rates between 1 and 2 million cycle can be attributed to the removal of the initial taper locking effect which is explained further in depth by English, Ashkanfar [27]. The same exponentially decreasing trend is seen as the body weight increases to 100 kg, where the initial volumetric wear rate was $0.041 \text{ mm}^3/\text{Mc}$ and decreases to $0.021 \text{ mm}^3/\text{Mc}$ at the end the 2nd

million cycle and further decreases to approximately $0.0088 \text{ mm}^3/\text{Mc}$ between the 3rd and 5th million cycle. As the BW increases past 100 kg, the volumetric wear loss for 140 kg BW retains its initial high volumetric wear rate, however, the volumetric wear rate remains similar at $0.022 \text{ mm}^3/\text{Mc}$ between the 2nd million cycle and 5th million cycle.

4. Discussion

The FE wear model and results presented in this study has clearly shown that heavier body weight increases the wear damage at contacting surfaces. Due to the Data Protection Act it is not possible to access any details about patient's weight and prostheses from the studies

performed on retrievals [34,36-40], however, the results obtained in this study are within range of published literature on retrievals as shown in Tables 2 and 3 and highlights the amount of increased wear based on different body weights.

The results highlight that the body weight is directly proportional to the amount of volumetric wear on the bearing contacting surfaces. The XLPE volumetric wear rates reported in this study are closely comparable to results in the literature [36-39] (see Table 2). As XLPE liners are a relatively new material (around 15 years) compared to conventional polyethylene (around 50 years), many of the primary hip arthroplasty performed are still in service. Hence, the main method for analysing wear is through radiography. Khoshbin, Wu [36] analysed a total of 40 primary THA of XLPE liners with CoCr femoral heads and found the volumetric wear rate was between 7.8 and 31.51 mm³/yr. Devane, Home [37] analysed a total of 57 primary THA of XLPE liners with CoCr femoral heads and found the volumetric wear rate was between 1.5 and 18.9 mm³/yr. Haw, Battenberg [38] analysed a total of 48 primary THA of XLPE liners with CoCr femoral heads and found the volumetric wear rate was between 19.2 and 46.9 mm³/yr. Atrey, [39] analysed a total of 102 primary THA of XLPE liners with CoCr femoral heads and found the volumetric wear rate was between 5.82 and 52.76 mm³/yr.

The volumetric wear rates reported in this study are closely comparable to results in the literature [34,40] (see Table 3). A co-ordinate measuring machine (CMM) has been previously used to measure the volumetric wear at 54 retrieved femoral head tapers. It showed the mean volumetric wear rate was 0.475 mm³/yr with a range between 0.021 and 1.860 mm³/yr. Additionally, a study by Langton et al. [40] also used a CMM to measure the volumetric wear rate at the taper surface of 48 retrieved hip prostheses and found the mean volumetric wear rate to be 0.127 mm³/yr with a range between 0.01 and 3.15 mm³/yr. Considering different BWs in this study, the mean volumetric wear up to 5 million cycles in this study was between 0.174 and 0.225 mm³/Mc for 60-140 kg BWs which is within the range in literature of 0.01-3.15 mm³/yr.

As there are many variables which could influence the wear rates, such as patient's activity level, weight, surgical techniques, and prostheses design variations, there is a large range of volumetric wear rates as shown in the above studies.

Although the femoral head bearing surface accounts for 1% and the femoral head taper surface accounts for 90% of the total wear between their respective surfaces, it can be seen in Fig. 8, for a 60 kg BW, the taper surface accounts for 56% of the total volumetric wear on the femoral ball and decreases to 40% for a 140 kg BW. This highlights the relative high amount of wear at the bearing surface despite having a lower wear fraction.

Metallosis is the adverse reaction to metallic ions in the body which can lead to a variety of complications such as, infection, dislocation, or even the death of the tissue surrounding the prostheses [41]. Fig. 9 shows the total metallic volumetric loss of the components in this study from the femoral head bearing and taper surface, and the femoral stem taper. It can be seen that approximately 95% of metallic wear loss is from the femoral head for all different BWs. At lower BW's, the main metallic wear loss is from the femoral head taper surface at approximately 52%. However, as BW increases, this metallic wear decreases to just 38% and the majority of wear shifts to the femoral head bearing surface.

Table 2
Volumetric wear rates of XLPE liner in contact with CoCr femoral via radiography

Literature	Volumetric Wear (mm ³ /yr)
Khoshbin, Wu [36]	7.8-31.51
Devane, Home [37]	1.5-18.9
Haw, Battenberg [38]	19.2-46.9
Atrey, E. [39]	5.82-52.76
Range	1.5-57.6
Current Study	15-35

Table 3
Volumetric wear rates of femoral head taper surface in literature

Literature	Mean Volumetric Wear (mm ³ /yr) (range)
Ashkanfar, Langton [34]	0.475 (0.021-1.860)
J., R. [40]	0.127 (0.01-3.15)
Range	0.01-3.15
Current Study	0.174-0.225

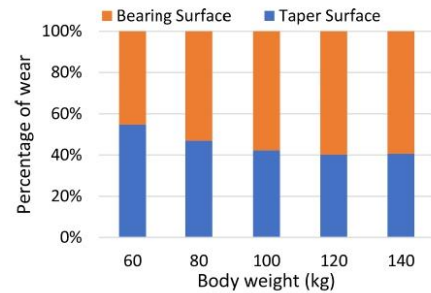


Figure 8. Percentage of wear between the bearing surface and taper surface at the femoral ball at 5 million cycles

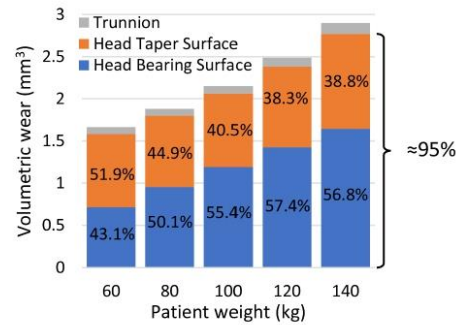


Figure 9. Total metallic volumetric wear at 5 million cycles

There are a variety of manufacturing and surgical factors, such as a taper mismatch or different assembly loads, which may affect the longevity of the prostheses in terms of wear. Although in this study zero taper mismatch was assumed, previous investigations showed an acceptable 6° taper mismatch did not significantly increase the wear rates [34]. Another factor which could affect the wear rates is the effect of assembly loads during impaction of the modular head onto the femoral stem trunnion. It was found that a minimum assembly load of 4kN was needed to minimise wear rates. A lower assembly load below 4kN would severely increase the total volumetric wear loss at the taper junction [23].

5. Conclusion

To further improve the design and ultimately increase the longevity of THAs, it is crucial to understand the evolution of wear throughout the lifespan of these devices. In this study, our previous wear algorithms have been further developed to investigate the effect of different patient weights on the evolution of wear at the contacting surfaces of the implants. The result of this study showed that reducing the initial BW from

140 kg to 100 kg before THA would decrease the metallic wear by 26% and polyethylene wear by 30%. This can significantly improve the longevity of the prosthesis. As such losing weight down to 100 kg before THA can be highly recommended, however, further research is required to investigate the effect of losing weight on the longevity of these devices while in service.

Declaration of Competing Interest

The authors declare that they have no known competing financial interests or personal relationships that could have appeared to influence the work reported in this paper.

Acknowledgment

This work is funded by the School of Engineering, Liverpool John Moores University, Liverpool, UK

References

- [1] A. Ayton, A. Ibrahim, Obesity is a public health emergency, *BMJ: British Medical Journal* (Online) (2019) 366.
- [2] NHS, *Health Survey for England 2019: Overweight and obesity in adults and children, 2020*.
- [3] E.W. Flanagan, et al., The Impact of COVID-19 Stay-At-Home Orders on Health Behaviors in Adults, *Obesity* 29 (2) (2021) 438–445.
- [4] L. Keaver, et al., Morbid obesity in the UK: a modelling projection study to 2035, *Scandinavian Journal of Public Health* 48 (4) (2020) 422–427.
- [5] M. Changulani, et al., The relationship between obesity and the age at which hip and knee replacement is undertaken, *The Journal of Bone and Joint Surgery, British volume* 90-B (3) (2008) 360–363.
- [6] NHS, *Hip and knee replacement surgery in obese patients, 2019*.
- [7] J. Andrew, et al., Obesity in total hip replacement, *The Journal of bone and joint surgery, British volume* 90 (4) (2008) 424–429.
- [8] M. Jackson, et al., *The effect of obesity on the mid-term survival and clinical outcome of cementless total hip replacement*. *The Journal of bone and joint surgery, British volume* 91 (10) (2009) 1296–1300.
- [9] T. Ibrahim, et al., No influence of body mass index on early outcome following total hip arthroplasty, *International Orthopaedics* 29 (6) (2005) 359–361.
- [10] P.K. Michalka, et al., The influence of obesity on early outcomes in primary hip arthroplasty, *The Journal of arthroplasty* 27 (3) (2012) 391–396.
- [11] E. Yeung, et al., The effect of obesity on the outcome of hip and knee arthroplasty, *International orthopaedics* 35 (6) (2011) 929–934.
- [12] Y. Chee, et al., Total hip replacement in morbidly obese patients with osteoarthritis: results of a prospectively matched study, *The Journal of bone and joint surgery, British volume* 92 (8) (2010) 1066–1071.
- [13] F. Traina, et al., Patient weight more than body mass index influences total hip arthroplasty long term survival, *HIP International* 21 (6) (2011) 694–699.
- [14] S. Kessler, W. Käfer, Overweight and obesity: two predictors for worse early outcome in total hip replacement? *Obesity* 15 (11) (2007) 2840–2845.
- [15] R. McCalden, et al., Does morbid obesity affect the outcome of total hip replacement? An analysis of 3290 THRs, *The Journal of bone and joint surgery, British volume* 93 (3) (2011) 321–325.
- [16] B. Espehaug, et al., Patient-related risk factors for early revision of total hip replacements: a population register-based case-control study of 674 revised hips, *Acta Orthopaedica Scandinavica* 68 (3) (1997) 207–215.
- [17] J. McLaughlin, K. Lee, *The outcome of total hip replacement in obese and non-obese patients at 10-to 18-years*. *The Journal of bone and joint surgery, British volume* 88 (10) (2006) 1286–1292.
- [18] M. Moran, et al., Does body mass index affect the early outcome of primary total hip arthroplasty? *The Journal of arthroplasty* 20 (7) (2005) 866–869.
- [19] D. Haverkamp, et al., Obesity in total hip arthroplasty—does it really matter? A meta-analysis, *Acta orthopaedica* 82 (4) (2011) 417–422.
- [20] T.P. Schmalzried, et al., Quantitative assessment of walking activity after total hip or knee replacement, *Journal of Bone and Joint Surgery - Series A* 80 (1) (1998) 54–59.
- [21] F.-W. Shen, Z. Lu, H.A. McKellop, Wear versus thickness and other features of 5-Mrad crosslinked UHMWPE acetabular liners, *Clinical Orthopaedics and Related Research* 469 (2) (2011) 395–404.
- [22] R. English, A. Ashkanfar, and G. Rothwell, *The effect of different assembly loads on taper junction fretting wear in total hip replacements*. *Tribology International* 95 (2016) 199–210.
- [23] G. Bergmann, F. Graichen, and A. Rohlmann, *Hip joint loading during walking and running, measured in two patients*, *Journal of Biomechanics* 26 (8) (1993) 969–990.
- [24] H. Fessler, D.C. Fricker, Friction in femoral prosthesis and photoelastic model cone taper joints, *Proceedings of the Institution of Mechanical Engineers, Part H: Journal of Engineering in Medicine* 203 (1) (1989) 1–14.
- [25] Zhang, T., et al., *A finite element methodology for wear-fatigue analysis for modular hip implants*. *Tribology International*, 2013. 65: p. 113–127.
- [26] R. English, A. Ashkanfar, and G. Rothwell, *A computational approach to fretting wear prediction at the head-stem taper junction of total hip replacements*, *Wear* 338–339 (2015) 210–220.
- [27] S.B. Wang, et al., Wear behaviour and wear debris characterization of UHMWPE on alumina ceramic, stainless steel, CoCrMo and Ti6Al4V prostheses in a hip joint simulator, in *Journal of Biomimetics, Biomaterials and Tissue Engineering* (2010). Trans Tech Publ.
- [28] G. Matsoukas, R. Willing, I.Y. Kim, Total hip wear assessment: a comparison between computational and in vitro wear assessment techniques using ISO 14242 loading and kinematics, *Journal of Biomechanical Engineering* 131 (4) (2009).
- [29] L. Anissian, et al., HIP-SIMULATOR WEAR COMPARISONS OF COCR/COCR VERSUS COCR/PE THR AT 10 MILLION CYCLES, in: *Proceedings of the Annual Meeting of the Orthopaedic Research Society*, Anaheim, California, 1999.
- [30] S. Fouvry, et al., An energy description of wear mechanisms and its applications to oscillating sliding contacts, *Wear* 255 (1) (2003) 287–298.
- [31] J. Abdo, Materials sliding wear model based on energy dissipation, *Mechanics of Advanced Materials and Structures* 22 (4) (2015) 298–304.
- [32] S.M.S. Toh, et al., Computational method for bearing surface wear prediction in total hip replacements, *Journal of the Mechanical Behavior of Biomedical Materials* 119 (2021), 104507.
- [33] A. Ashkanfar, D.J. Langton, T.J. Joyce, A large taper mismatch is one of the key factors behind high wear rates and failure at the taper junction of total hip replacements: a finite element wear analysis, *Journal of the mechanical behavior of biomedical materials* 69 (2017) 257–266.
- [34] A. Ashkanfar, D.J. Langton, T.J. Joyce, Does a micro-grooved trunnion stem surface finish improve fixation and reduce fretting wear at the taper junction of total hip replacements? A finite element evaluation, *Journal of Biomechanics* 63 (2017) 47–54.
- [35] A. Khoshbin, et al., Wear rates of XLPE nearly 50% lower than previously thought after adjusting for initial creep: an RCT comparing 4 bearing combinations, *JBJS Open Access* 5 (2) (2020) e0066.
- [36] P.A. Devane, et al., Highly cross-linked polyethylene reduces wear and revision rates in total hip arthroplasty: a 10-year double-blinded randomized controlled trial, *JBJS* 99 (20) (2017) 1703–1714.
- [37] J.G. Haw, et al., Wear rates of larger-diameter cross-linked polyethylene at 5 to 13 years: does liner thickness or component position matter? *The Journal of Arthroplasty* 32 (4) (2017) 1381–1386.
- [38] A. Atrey, et al., *Ten-year follow-up study of three alternative bearing surfaces used in total hip arthroplasty in young patients*, *The Bone & Joint Journal* 99-B (12) (2017) 1590–1595.
- [39] D.J. Langton, et al., *Taper junction failure in large-diameter metal-on-metal bearings*, *Bone & Joint Research* 1 (4) (2012) 56–63.
- [40] J.W. Pritchett, Adverse reaction to metal debris: metallosis of the resurfaced hip, *Current Orthopaedic Practice* 23 (1) (2012) 50–58.

Development of a wear algorithm using finite element analysis to investigate design variations on the wear rates in total hip replacement

Shawn Toh, Ariyan Ashkanfar, Russell English, Glynn Rothwell

Department of Mechanical and Maritime Engineering

Liverpool John Moores University, Byrom Street, L3 3AF, UK

E-mail: s.m.toh@2016.ljmu.ac.uk, A.Ashkanfar@ljmu.ac.uk, R.English@ljmu.ac.uk, G.Rothwell@ljmu.ac.uk

Abstract. *The number of people receiving Total Hip Replacement (THR) are increasing every year at around 3.5% while the average age of the recipients is decreasing. The current average life of a THR is between 15 to 20 years which is not adequate for young active patients. Wear is known to be one of the main factors affecting the longevity of these implants which can lead to infection or loosening of the prosthesis. Computational analysis can improve the design and increase the longevity of the implants by investigating different parameters including design variations and surgical techniques. A previously developed in-house fretting wear algorithm has been shown to model effectively the evolution of wear at the taper junction of THRs which exhibit short relative displacements as validated against retrievals. The overall aim of this study is to develop a general wear algorithm to simulate the wear rate at the taper junction and the bearing surfaces (which are subject to much larger relative displacements). As such, in this study, the in-house fretting wear algorithm which uses a Python program in the Abaqus environment has been generalized to facilitate the analysis for wear and material loss at the taper junction of THR. It has been shown that the generalized fretting wear algorithm can predict the evolution of wear at the taper junction of any design of THRs and can be used to investigate design variations on wear rates.*

Keywords: *Total hip replacement (THR), Finite Element Analysis (FEA), Wear analysis, Taper junction, Python programming, Wear modelling.*

1. Introduction

The hip joint is one of the most important joints in our body. It bears our body's weight and is one of the most flexible joints. However, it can be damaged to the extent that it loses mobility and experiences pain even when resting (Holcomb, Miller, and Rubley 2012). A total hip replacement (THR) is one of the alternatives when other treatments such as physiotherapy or steroid injections have not helped in relieving the pain or improved mobility. A THR typically consists of a femoral head, femoral stem and a metal acetabular cup (Figure 1). There currently are four bearing surface material types of hip prosthesis available in the UK which are metal-on-polyethylene, metal-on-metal, ceramic-on-polyethylene, and ceramic-on-metal (16th Annual Report 2019, NJR for England, Wales and Northern Ireland, 2019). The type of hip prosthesis chosen, is based on the patients age, sex, pain level and level of activity (Crawford and Murray 1997).



Figure 1: Components of THR

Recent data from the National Joint Registry (NJR) shows that there were approximately 92,000 THR procedures performed in the UK using arthroplasty in 2018 with over a million THRs performed since 2003 (NJR, 2019). Overall, 2.9% of the primary THR needed an associated first revision with the aseptic loosening, infection and dislocation cited as the most common indications for revisions. Approximately 75% of all current THRs last between 15 to 20 years with around 8% of cases requiring a revision before the expected 15 years. Although 75% of THRs last between 15 to 20 years, 58% of THRs have lasted up to 25 years (Evans et al. 2019). According to the NJR, there is an average of 11.5% increase in the number of patients under 55 years old undergoing THR which suggests that more young active patients will undergo THR in the coming years. As such, the longevity of these implants needs to be increased.

Wear is known as one of the most influencing factors for THR longevity (Sipek, Lyvers, and Mathew 2018; Ashkanfar, Langton, and Joyce 2017). Wear debris can cause side effects such as bone loss which leads to aseptic loosening (Buly et al. 1992), dislocation and metallosis which is inflammation caused by immunological responses (Man et al. 2017; Salem et al. 2019). As wear rate is the amount of material removed as time progresses, one of the requirements to increase the operating life of the components is to minimise the wear rates. Current experimental techniques to investigate the wear rates in THRs such as radiography, tribotesting, and hip joint simulator are time-consuming, complicated and expensive (Hallan, Lie, and Havelin 2006; Ramesh, van Kuilenburg, and Wits 2019; Hua et al. 2019). Computational analysis can be used to further aid in improving and investigating different parameters such as design and material variations (Brock et al. 2015), manufacturing tolerances (Ashkanfar, Langton, and Joyce 2017) and surgical techniques (Teoh 2003; English, Ashkanfar, and Rothwell 2015) to improve the longevity of the implants.

The in-house fretting wear algorithm (English, Ashkanfar, and Rothwell 2015) has been further developed in the Python Development Environment (PDE) of ABAQUS, which is capable of predicting the evolution of fretting wear at the taper junction of THRs, shown in Figure 1. The method has been validated against the measurement of wear rate at retrieved THRs (Ashkanfar, Langton, and Joyce 2017). The overall aim is to develop a general wear algorithm to simulate the evolution of fretting wear at the taper junction of THRs. A generalised wear algorithm could help to increase the operating life of the implants by investigating the different parameters such as different femoral head sizes in design variations (Langton et al. 2010; Affatato et al. 2007), manufacturing tolerances (Ashkanfar, Langton, and Joyce 2017), surface topography (English, Ashkanfar, and Rothwell 2015) and trunnion length at the tapers (Brock et al. 2015).

2. Methodology

2.1. Computational Analysis

A model of the femoral head and femoral stem taper was created in ABAQUS as shown in Figure 2. The head and stem tapers were meshed in preparation for analysis using the eight-node bilinear hexahedral reduced integration elements (C3D8R). The materials used in this analysis are cobalt-chrome for the femoral head and titanium for the femoral stem (NJR 2019). The material properties of the materials are listed in Table 1.

Table 1: Material properties for THR

Material	Young's Modulus (GPa)	Density (kg/m^3)	Poisson's ratio
Cobalt-chrome	210	7800	0.3
Titanium	119	4400	0.29

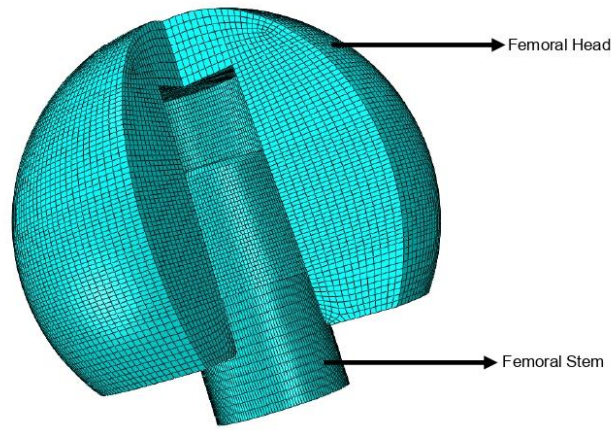


Figure 2: Mesh of FE model

A mesh convergence study was conducted and it was found that there was an effect of element sizes, and wear evolution. The mesh of the contact zone was refined so that the variations in values extracted across an individual element were kept to a minimum. An element size of 0.2mm in the contact zone was used to achieve a smooth wear pattern which has been investigated by English, Ashkanfar, and Rothwell (2015). For the nodes in the contact area, each node between the femoral head and taper is paired to determine the wear depth. There are two main wear laws, the Archard Wear law and the Dissipated Energy Wear law (Zmitrowicz 2006; Abdo 2015). This study utilises the Dissipated energy wear law as it predicts wear across a wider range of motion than the Archard wear law and has a greater range of application (Abdo 2015; Fouvry et al. 2003).

In order to simulate the effect of impact onto the stem and the subsequent walking cycles. The head and stem were assembled so that they just come into contact. This is to keep the effect of the initial impact during the assembly of the THR. A dynamic implicit step is then defined, and the rotations and loading associated with a hip walking cycle are added. On completion, the extent of fretting wear at the taper junction can be determined as wear depth at each of the paired nodes of the model. The coordinates of the paired nodes are updated to reflect the wear that has occurred at each stage of the analysis. The analysis is then continued until the number of cycles is reached.

The wear fraction is the proportion of wear that is removed from each of the contacting parts. A wear fraction 0.9:0.1 is introduced here for the femoral head and femoral stem respectively (English, Ashkanfar, and Rothwell 2015). Cobalt-chrome head tapers wears by around a factor of 10 more than the titanium alloy stem (Langton et al. 2012). The reason for this occurring is due to the preferential oxidation of the titanium alloy stem over the cobalt-chrome surface which increases the hardness of the titanium surface and subsequently wears the unoxidized cobalt-chrome surface (Moharrami et al. 2013).

In order to automate the procedure in determining the wear at each paired node set at the contact interface, a Python script linked within ABAQUS as a user plug-in was developed. The script automates the process by submitting the FE input file to the ABAQUS solver which then pairs the nodes at the contact zone prior to hip loading. On completion of each analysis, the script extracts the data from output databases such as shear stress and relative displacements for all the paired nodes. The algorithm has been further developed to calculate the volumetric material loss. Wear is then applied to the paired nodes by updating the coordinate positions from the displacements in the opposite direction of the nodal normal in order to create a new geometry for execution in the next FE analysis. At the end of each analysis, the nodal wear depth, volumetric wear and volumetric element loss is written to the output database of ABAQUS for each contacting node to plot the wear depth pattern. An outline of the procedure is shown in Figure 3

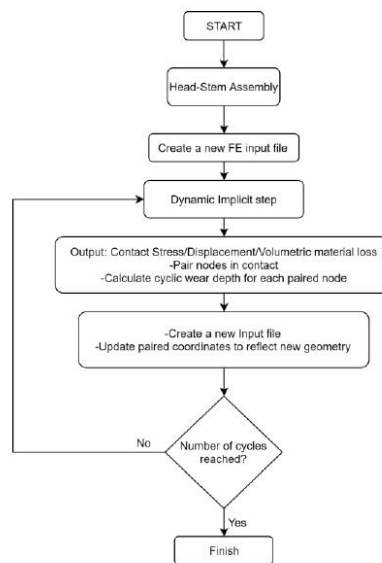


Figure 3: Flowchart outlining procedure

2.2. Experimental Methodology

To validate the FE wear results, a method to measure the surface roughness and surface profile is needed. To measure for the surface profiles, a contour and surface finish measurement equipment shown in Figure 4 (Talysurf i-Series 1; Taylor Hobson, Leicester, England) is used. A retrieved femoral head taper, shown in Figure 1, was measured for its surface profile. The stylus was traversed across the surface and the pickup converted its vertical movements into an electrical signal and used to operate a recorder. The surface profile is then used to determine the average surface roughness and estimate the volumetric material loss from the surface.



Figure 4: Talysurf by Taylor Hobson

For this study, a retrieved femoral head taper was used for measurements. Surface profile measurements were performed at the trough of the taper junction using a diamond conisphere inductive recess styli. The measuring accuracy for the Talysurf is 68nm. The femoral head taper was first cleaned using compressed air to ensure all unwanted particles were removed. The femoral head was then fixed and the Talysurf was calibrated to ensure the stylus matched the profile of the taper angle. Two sets of measurements were taken, one in as a linear surface profile and another in 3D on a section of the taper (Figure 5) using 3D contact measurement methods. Three sets of data were recorded and an average of the data plots were used to further analyse the results. The 2D surface profile was then processed using the Ultra software by Taylor Hobson and the 3D surface texture was processed using Talymap Universal software.



Figure 5: Top view of taper

3. Results and Discussion

A computational and experimental methodology has been presented to outline the steps to generalise the in-house algorithm. The predicted volumetric material wear against hip loading cycles is shown in Figure 6. Due to the wear fraction, 90% of the total volumetric material loss is at the femoral head while only 10% is at the femoral stem. The curve suggests that as time increases, the wear rate of the implant decreases.

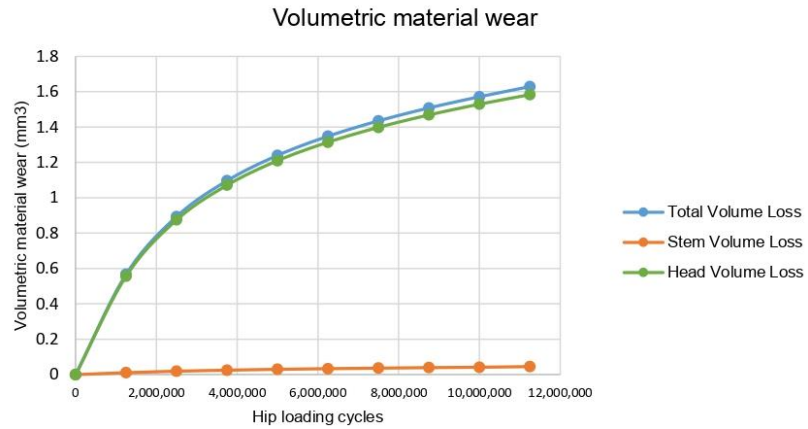


Figure 6: Volumetric material wear vs hip loading cycles

A wear contour map was produced to show the evolution of wear depth as time progresses and is shown in Figure 7. The data and wear pattern is similar to the wear pattern measured using a coordinate measuring machine (CMM) shown by Ashkanfar, Langton, and Joyce (2017) which has been compared with 54 retrieved samples. The wear depth pattern shows that the wear starts to develop from the bottom of the taper and slowly move towards the middle as the time progresses.

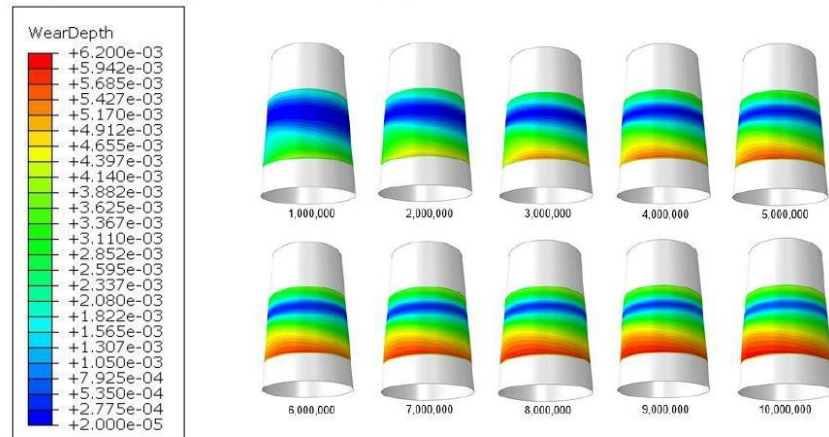


Figure 7: Wear contour map on taper surface as hip loading cycles increases

The 2D surface profile taken from the taper is shown in Figure 8b. The results show one major drop in surface profile. This can be seen from Figure 8a where there is a distinct groove in the taper. According to the data, the groove is approximately 20µm deep. This groove may be due to damage while retrieving the implant. The graph is also shown to be slightly skewed downwards. This may be due to the limitations of the Talysurf as it is only able to adjust its tilt angle by 0.1°. After removing the form and correcting the tilt angle using Ultra, the average roughness graph is plotted and shown in Figure 8c. The average roughness of the taper is shown to be 0.3859µm.

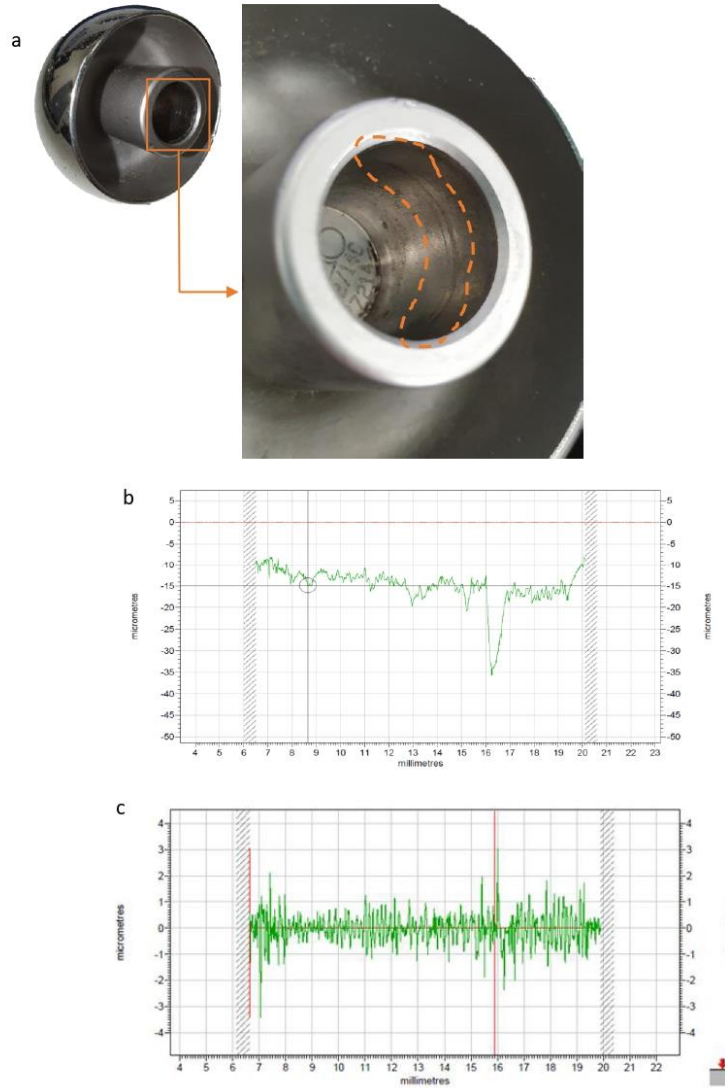


Figure 8: Surface profile of taper

The 3D surface profile taken from the taper is shown in Figure 9. Figure 9a show the 2D profile of the taper section. The deep groove is shown in Figure 9a and the depth of the groove is shown to be around 20 μm . The groove is shown to be at 20 μm evenly throughout the taper. Figure 9b shows a zoomed in 3D profile of the groove. Figure 9c shows a simulated surface texture of the taper according to the data collected from the Talysurf.

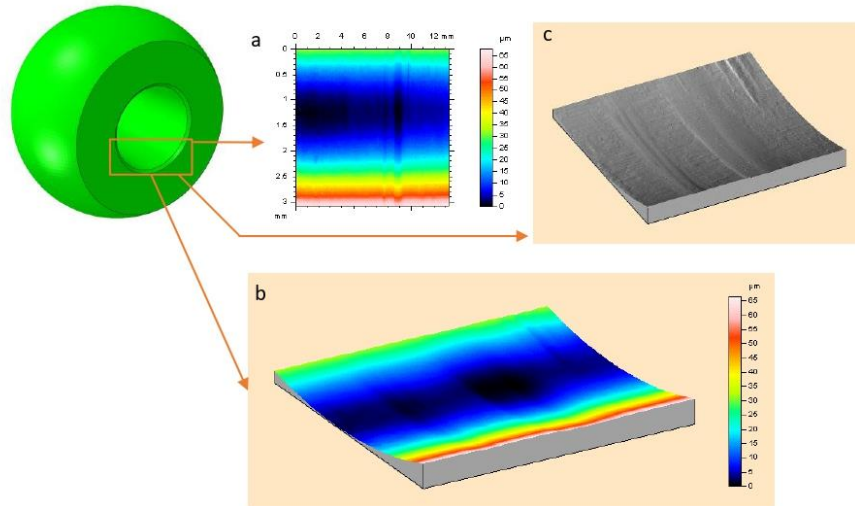


Figure 9: 3D contact measurement of femoral head taper

4. Conclusion

The current computational analysis on fretting wear at the taper junction has been compared with results from a CMM. To further validate the FE results, a compressive machine (Instron, Buckinghamshire, UK) will be used to load the taper and the Talysurf used to validate the results. Developing an algorithm to measure wear at all contact surfaces can help to understand the evolution of wear throughout the implant as different taper designs may affect the bearing surface wear (Nassif et al. 2014; Brock et al. 2015). Wear at bearing surfaces are as critical as they may also release wear debris which would lead to metallosis (Bergiers et al. 2019; Sharplin et al. 2018). Computational analysis can help to improve and increase the longevity of the implants by investigating different parameters of the implant such as design, surgical techniques and materials as it is less expensive and time-consuming.

5. References

1. Abdo, Jamil. 2015. 'Materials Sliding Wear Model Based on Energy Dissipation', *Mechanics of Advanced Materials and Structures*, 22: 298-304.
2. Affatato, Saverio, W Leardini, Anneli Jedenmalm, O Ruggeri, and A Toni. 2007. 'Larger diameter bearings reduce wear in metal-on-metal hip implants', *Clinical Orthopaedics and Related Research*®, 456: 153-58.
3. Ashkanfar, Ariyan, David J Langton, and Thomas J Joyce. 2017. 'A large taper mismatch is one of the key factors behind high wear rates and failure at the taper junction of total hip replacements: A finite element wear analysis', *Journal of the mechanical behavior of biomedical materials*, 69: 257-66.
4. Bergiers, S., H. Hothi, R. Richards, J. Henckel, and A. Hart. 2019. 'Quantifying the bearing surface wear of retrieved hip replacements', *Biosurface and Biotribology*, 5: 28-33.
5. Brock, Timothy M, Raghavendra Sidaginamale, Steven Rushton, Antoni VF Nargol, John G Bowsher, Christina Savisaar, Tom J Joyce, David J Deehan, James K Lord, and David J Langton. 2015. 'Shorter, rough trunnion surfaces are associated with higher taper wear rates than longer, smooth trunnion surfaces in a

- contemporary large head metal-on-metal total hip arthroplasty system', *Journal of Orthopaedic Research*, 33: 1868-74.
6. Buly, Robert L., Michael H. Huo, Eduardo Salvati, William Brien, and Manjula Bansal. 1992. 'Titanium wear debris in failed cemented total hip arthroplasty: An analysis of 71 cases', *The Journal of Arthroplasty*, 7: 315-23.
 7. Crawford, R. W., and D. W. Murray. 1997. 'Total hip replacement: indications for surgery and risk factors for failure', *Annals of the Rheumatic Diseases*, 56: 455.
 8. English, Russell, Ariyan Ashkanfar, and Glynn Rothwell. 2015. 'A computational approach to fretting wear prediction at the head–stem taper junction of total hip replacements', *Wear*, 338-339: 210-20.
 9. Evans, Jonathan T, Jonathan P Evans, Robert W Walker, Ashley W Blom, Michael R Whitehouse, and Adrian Sayers. 2019. 'How long does a hip replacement last? A systematic review and meta-analysis of case series and national registry reports with more than 15 years of follow-up', *The Lancet*, 393: 647-54.
 10. Fouvry, S., T. Liskiewicz, Ph Kapsa, S. Hannel, and E. Sauger. 2003. 'An energy description of wear mechanisms and its applications to oscillating sliding contacts', *Wear*, 255: 287-98.
 11. Hallan, Geir, Stein A. Lie, and Leif I. Havelin. 2006. 'High wear rates and extensive osteolysis in 3 types of uncemented total hip arthroplasty: A review of the PCA, the Harris Galante and the Profile/Tri-Lock Plus arthroplasties with a minimum of 12 years median follow-up in 96 hips', *Acta Orthopaedica*, 77: 575-84.
 12. Holcomb, William R, Michael G Miller, and Mack D Rubley. 2012. 'Importance of Comprehensive Hip Strengthening', *Strength & Conditioning Journal*, 34: 16-19.
 13. Hua, Zikai, Pingchuan Dou, Haili Jia, Fei Tang, Xiaojing Wang, Xin Xiong, Leiming Gao, Xiuling Huang, and Zhongmin Jin. 2019. 'Wear Test Apparatus for Friction and Wear Evaluation Hip Prostheses', *Frontiers in Mechanical Engineering*, 5.
 14. Langton, D. J., R. Sidaginamale, J. K. Lord, A. V. F. Nargol, and T. J. Joyce. 2012. 'Taper junction failure in large-diameter metal-on-metal bearings', *Bone & joint research*, 1: 56-63.
 15. Langton, DJ, SS Jameson, TJ Joyce, NJ Hallab, S Natu, and AVF Nargol. 2010. 'Early failure of metal-on-metal bearings in hip resurfacing and large-diameter total hip replacement: a consequence of excess wear', *The Journal of bone and joint surgery. British volume*, 92: 38-46.
 16. Man, Kenny, Lin-Hua Jiang, Richard Foster, and Xuebin B Yang. 2017. 'Immunological Responses to Total Hip Arthroplasty', *Journal of Functional Biomaterials*, 8: 33.
 17. Moharrami, N., D. J. Langton, O. Sayginer, and S. J. Bull. 2013. 'Why does titanium alloy wear cobalt chrome alloy despite lower bulk hardness: A nanoindentation study?', *Thin Solid Films*, 549: 79-86.
 18. Nassif, Nader A, Danyal H Nawabi, Kirsten Stoner, Marcella Elpers, Timothy Wright, and Douglas E Padgett. 2014. 'Taper design affects failure of large-head metal-on-metal total hip replacements', *Clinical Orthopaedics and Related Research*, 472: 564-71.
 19. Ramesh, Vikram, Julien van Kuilenburg, and Wessel W. Wits. 2019. 'Experimental Analysis and Wear Prediction Model for Unfilled Polymer–Polymer Sliding Contacts', *Tribology Transactions*, 62: 176-88.
 20. Salem, Khaled Hamed, Norbert Lindner, Markus Tingart, and Alyaa Daa Elmoghazy. 2019. 'Severe metallosis-related osteolysis as a cause of failure after total knee replacement', *Journal of Clinical Orthopaedics and Trauma*.
 21. Sharplin, Paul, Michael C. Wyatt, Alastair Rothwell, Chris Frampton, and Gary Hooper. 2018. 'Which is the best bearing surface for primary total hip replacement? A New Zealand Joint Registry study', *HIP International*, 28: 352-62.
 22. Sipek, KT, ME Lyvers, and MT Mathew. 2018. 'Failure Causes in Total Hip Replacements: A review', *Austin J Orthopade & Rheumatol*, 5:1064.
 23. Teoh, S. H. 2003. '9.01 - Failure in Biomaterials.' in I. Milne, R. O. Ritchie and B. Karihaloo (eds.), *Comprehensive Structural Integrity* (Pergamon: Oxford).
 24. Zmitrowicz, Alfred. 2006. 'Wear patterns and laws of wear-a review', *JOURNAL OF THEORETICAL AND APPLIED MECHANICS*, 44: 219-53.

Appendix III: Poster Presentations



A Computational Approach for Wear Prediction in Total Hip Replacements

Shawn Ming Song Toh, Ariyan Ashkanfar, Russell English, Glynn Rothwell
 School of Engineering, Liverpool John Moores University
 Byrom Street, Liverpool, L3 3AF, UK

Abstract

A total hip replacement (THR) is a revolutionary treatment when a hip joint becomes severely damaged. Wear is known as one of the main reasons for THR failure. In this study, an in-house fretting wear algorithm has been further developed to investigate the wear damage that occurs on bearing surfaces of THRs. The proposed method utilises an energy wear law and a 3D finite element model to predict bearing surface wear of THRs and determine linear and volumetric wear rates that could occur over time. The results obtained are consistent with those found in previous literature and the wear patterns shown are comparable to available conventional polyethylene liners. This method can be used to further aid in the design and clinical technique to reduce wear rate in THRs.

Introduction

THR is a revolutionary treatment over the last decades for people who have lost their natural hip functionality due to diseases such as osteoarthritis. A THR normally consists of 4 parts: acetabular cup, bearing liner, femoral head and femoral stem.

According to the National Joint Registry 2019:

In 2018, ~92,000 Replacement procedures
 Since 2003, ~1 million Replacement procedures

Current lifespan ~15 years ~8% failed <15years
 ~11.5% yearly patients aged <55

Wear is one of the main reasons for premature failure in THRs and can cause a multitude of failures such as aseptic loosening, dislocation, infection or metallosis. Aseptic loosening itself accounts for ~45% of revisions

Current experimental techniques to investigate wear damage in THRs:



- ✓ Time consuming
- ✓ Complicated
- ✓ Expensive

Computational analysis:
 ✓ Lower Cost
 ✓ Lower run time
 ✓ Detailed solutions

Computational analysis has led to the understanding of:
 1. Different Design and material variations
 2. Manufacturing tolerances
 3. Surgical Techniques

Aim

To develop a general computational wear model using FEA to quantify and predict the extent of wear damage occurring in a THR.

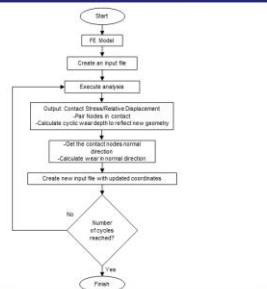
Minimise wear.
 Improve the wear characteristics of prosthesis design.

References

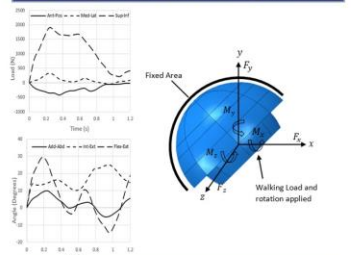
J. J. Callaghan, D. R. Peterson, R. C. Johnston, and T. D. Brown, "Clinical biomechanics of wear in total hip arthroplasty," *The Iowa orthopaedic journal*, vol. 23, p. 1, 2003.
 J. C. Falcho, P. R. Fernandes, L. Eça, and J. Folgado, "Computational hip joint simulator for wear and heat generation," *Journal of Biomechanics*, vol. 40, no. 11, pp. 2358-2366, 2007.
 M. Ali, M. Al-Hajjar, S. Partridge, S. Williams, J. Fisher, and L. M. Jennings, "Influence of hip joint simulator design and mechanics on the wear and creep of metal-on-polyethylene bearings," *Proceedings of the Institution of Mechanical Engineers, Part H: Journal of Engineering in Medicine*, vol. 250, no. 5, pp. 389-392, 2016, doi: 10.1177/0954411916650454.
 R. M. Trommer et al., "Multi-Scale Evaluation of Wear in UHMWPE Metal Hip Implants Tested in a Hip Joint Simulator," *Biotechnology*, vol. 4, pp. 1-11, 2015/12/01/ 2015, doi: https://doi.org/10.1016/j.biotri.2015.08.001.
 Toh, S. M. S., A. Ashkanfar, R. English and G. Rothwell (2021). "Computational method for bearing surface wear prediction in total hip replacements." *Journal of the Mechanical Behavior of Biomedical Materials* 119: 104507.

Methodology

Outline of Python Algorithm



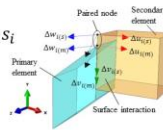
FE Loading, Rotations, and Boundary Conditions



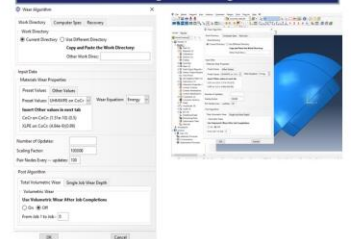
Dissipated Energy Wear Law and implementation

$$W_d = \sum_{j=1}^{(N/\beta)} \beta \sum_{i=1}^n \alpha \tau_i s_i$$

W_d = linear wear depth
 s_i = relative displacement
 τ_i = contact shear stress
 α = energy wear coefficient
 β = wear scaling factor

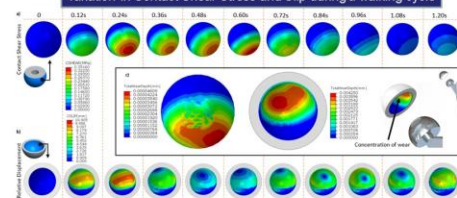


Wear Algorithm Plug-in

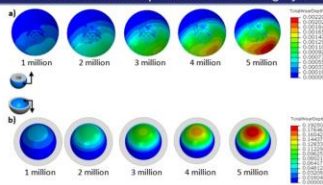


Results

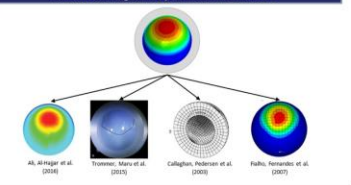
Variation in Contact Shear Stress and Slip during a walking cycle



Evolution of Wear up to 5 million walking cycles



Validation against previous literature



Evolution of Wear up to 5 million walking cycles for different body weights

